UNIVERSITY OF CALGARY

Characterization of Non-Distillable Crude and Refined Oil Fractions for Asphaltene Precipitation Modeling

by

Jane Chioma Okafor

A THESIS
SUBMITTED TO THE FACULTY OF GRADUATE STUDIES
IN PARTIAL FULFILMENT OF THE REQUIREMENTS FOR THE
DEGREE OF MASTER OF SCIENCE

DEPARTMENT OF CHEMICAL AND PETROLEUM ENGINEERING

CALGARY, ALBERTA
January, 2014

UNIVERSITY OF CALGARY

FACULTY OF GRADUATE STUDIES

The undersigned certify that they have read, and recommend to the Faculty of Graduate Studies for acceptance, a thesis entitled "Characterization of Non-Distillable Crude and Refined Oil Fractions for Asphaltene Precipitation Modeling" submitted by Jane Chioma Okafor in partial fulfilment of the requirements of the degree of Master of Science.

Supervisor, Dr. Harvey William Yarranton
Department of Chemical and Petroleum Engineering

Dr. Gordon R. Moore
Department of Chemical and Petroleum Engineering

Dr. Kunal Karan
Department of Chemical and Petroleum Engineering

Dr. Edward Ghent
Department of Geosciences

Date

Abstract

Asphaltenes are the heaviest and most polar components of crude oils and they can precipitate during the production and processing of crude oil, increasing the risk of deposition and fouling. For example, during refining when native and reacted streams are blended and the blend can be unstable versus asphaltene precipitation. Simple and reliable methods are needed to characterize these streams and to predict the conditions at which precipitation occurs.

One approach for predicting the stability of these blends is the Modified Regular Solution Model (RSM) which has been successfully applied to model asphaltene precipitation in upstream fluids and their blends. Input parameters to the regular solution model are the mole fractions, molar volume, and solubility parameters of the pseudo-components making up the crude oil and the *n*-alkane used in the mixture. Few data are available for some of these pseudo-components such as saturates, aromatics, and resins (SAR). Also, the effect of feedstock processing such as thermal cracking and hydrocracking on the component properties is not known.

The main objective of this work is to characterize the non-distillable (SAR) fractions of native and reacted fluids and develop property correlations as inputs to the RSM. Molecular weights, density and refractive index were measured for saturates, aromatics and resins whereas the solubility parameter of saturates and aromatics were back-calculated from fitting asphaltene solubility measurement in these solvents with the Modified Regular Solution Model. In addition, property correlations between the model inputs and the refractive index were sought because it is a reliable indicator property, easy to measure, and proven to relate to valuable properties.

The SAR fractions were found to form non-ideal solutions in the solvents used in this study, toluene and heptane. Excess volume mixing rules for the density and refractive index of SAR fractions and solvents were experimentally identified. A correlation was developed for the binary interaction parameter that quantifies the excess properties. This correlation was used to determine the density and refractive index of samples for which a direct measurement was not possible (solid, high viscosity, limited sample volume) and only mixture data were available.

The refractive index was found to correlate to density of these fractions even at elevated temperatures. Although cracking changed the properties of the SAR fractions, the correlations applied to both native and reacted materials.

Asphaltene solubility was measured in solutions containing toluene, heptane, saturates or aromatics. New methods were developed to measure asphaltene precipitation yields in low volume solutions containing a SAR fraction. Solubility parameters of the SAR fractions were calculated from RSM modeling of asphaltene yield data from these solutions. The back-calculated solubility parameters were correlated to both refractive index and density for the unreacted and thermally cracked oil fractions.

Overall, a set of methods were developed to determine the molecular weight, density, refractive index, and solubility parameter of limited amounts of SAR fractions from native and reacted streams. A dataset was collected for a variety of samples and a set of correlations was developed to determine these properties from a limited set of measurements. The data and correlations are a key part of the characterization of refinery blends for regular solution modeling.

Acknowledgements

My profound thanks and gratitude goes to my Supervisor, Dr. Harvey W. Yarranton, for giving me the opportunity to achieve this feat. He trusted me every step of the way and saw the capabilities and promise in me, my work even when I was convinced otherwise. For continually guiding and encouraging me through my programme and providing a relaxed yet challenging work environment. I have learnt valuable life lessons from him because I was empowered to try my options, make my decisions, make my mistakes, learn and improve while being aware of his availability to review my progress and make treasured inputs. My work/data always took a turn for the best once Harvey has made his inputs. I sincerely appreciate his patience, understanding and trust.

I would also want to thank the members of my examining committee Dr. Gordon R. Moore, Dr. Kunal Karan and Dr. Edward Dale Ghent for taking the time to participate in the conclusion of my graduate programme. I am thankful to the Department of Chemical and Petroleum Engineering, Faculty of Graduate studies and the University of Calgary for this once in a lifetime opportunity. I am thankful to Shell Global solutions for funding the research and providing valuable feedbacks that encouraged success in this work.

The Asphaltene and Emulsion/Heavy Oil Properties and Processing Research group has been a welcoming home on campus for the last couple of years and I am very grateful. I am lucky to have worked with and learned from the diverse crop of intellectuals in this team especially Elaine Baydak and Diana Ortiz. Diana Ortiz was instrumental to my getting a grip on my research work and never faltered in her support. I am grateful for her insights, contributions and warmth. Elaine made working in this team a whole lot more interesting. Thank you for the support, encouragement, smiles, goodwill, cookbooks and friendship. I am sure that I will miss this team.

To crown it all, I am indebted to my husband, Nworah Okafor, because without his unwavering support, encouragement and understanding, these years would have been frustrating. Thank you for being a pillar for me and our daughters.

To Nworah, you've been my backbone.

To our girls, Adaora & Kaeto, for making this journey worth it all. Love you lots.

And to my Mom, for your immense support.

You have inspired and trusted me and I owe it all to you.

.

Table of Contents

List of Tables

List of Figures

List of Symbols, Abbreviations and Nomenclature

A	Coefficient in VPO calibration equation
A	Fitting Parameter for Equation 4.5
C	Solute concentration
c	Fitting Parameter for Equation 4.5
C	A constant in London dispersion equation
d	Fitting Parameter for Equation 4.5
E	Energy of vapourization
f	Density Meter correction term
f_A	Fractional yield
F_{RI}	$\left(\frac{n^2-1}{n^2+2}\right)$.
h	Planck's constant
H	Heptane volume fraction
K	VPO calibration constant
KA	Density Meter constant
KB	Density Meter constant
M	Molecular Weight
m	Mass
n	Refractive index
N_a	Avogadro's number
R	Refraction
r	Distance between molecules
RSM	Regular Solution Model
SP	Solubility Parameter
V	Voltage
v	Electron frequency

v	Mass specific volume
V	Total volume
v_m	Molar volume
w	Component mass fraction
x	Mole fraction

Greek Symbols

α	Coefficient of expansion
φ	Intermolecular potential energy function
α	Polarizability
β	Shape Parameter of the Gamma Distribution
β_{12}	Binary interaction parameter
δ	Solubility parameter
ε_0	Permittivity of a vacuum
ρ	Density
ϕ	Volume fraction

Subscripts

$_A$	Asphaltenes
aro	Aromatics
m	Monomer
mix	Mixture
$_N$	Normalized
s	Solvent
sat	Saturates

Superscripts

°	Initial
h	Heavy liquid phase
l	Light liquid phase

ppt	Precipitated
s	Solution
vap	Vapourization

Chapter One: Introduction

As world reserves of conventional crude oils dwindle, the production and processing of heavy oils and bitumen are gaining prominence and refineries are being adapted to process heavy oil and bitumen alongside conventional oils. Heavy oil and bitumen are more challenging fluids to produce and process because they have high asphaltene contents relative to conventional oils. Asphaltenes are the heaviest and most polar fraction of crude oil; defined as the fraction of crude oil that is insoluble in aliphatic compounds, but soluble in aromatic solvents (Speight, 2007; Andersen, 2008). Asphaltenes contribute to the high viscosity (and low API gravity) of heavy oils and are known to flocculate and precipitate from petroleum upon changes of temperature, pressure and composition as a glass-like phase.

Asphaltene precipitation and deposition has threatened the economic recovery of oil, shut down operations, and increased the cost of production in the oil industry all around the world. During petroleum production, asphaltenes precipitation has caused porosity and permeability decline, and plugged wells and surface facilities due to pressure decline as the petroleum flows to the surface. The processing of asphaltenic oil in refinery operations causes storage capacity loss, equipment fouling, catalyst deactivation, along with various process, and control problems (Piyarat, *et al.*, 2003).

Heavy oils and bitumen usually require thermal stimulation or dissolution with solvents for recovery and processing. These operational practices could cause asphaltene precipitation leading to deposition in the reservoir and fouling in well bores and surface facilities. In refinery operations, process streams undergo changes in temperature and pressure and are often blended with other streams to obtain desired properties or compositions that optimize product value and minimize fouling. A continuing concern is instability, in terms of asphaltene precipitation, when streams are blended. The introduction of heavy oil feedstocks may worsen this issue.

These asphaltene related problems are sources of economic losses in the oil industry and a better understanding of asphaltene behaviour is required in order to avoid operational problems (Birdi, 2008). Understanding the phase behaviour of crude oils (along with asphaltene precipitation) is an important tool to determine effective parameters for optimization of production and processing of heavy oils. Simple and reliable methods are needed to characterize crude oils and to predict the conditions at which precipitation occurs (Buckley *et al.*, 1998).

Numerous models have been proposed to predict asphaltene precipitation. These models fall into two categories: 1) colloidal theory and 2) thermodynamic models. These models have different assumptions and limitations (Haitham *et al.,* 2004). In this work, a thermodynamic model is applied using the regular solution theory. The regular solution approach has been successfully applied to predict asphaltene precipitation in upstream processes both for diluted heavy oils and depressurized conventional oils (Yarranton and Masliyah 1996; Alboudwarej *et al.,* 2003; Akbarzadeh *et al.,* 2005). It has also proven successful in predicting the stability, in terms of asphaltene precipitation, of blended crude oils (Tharanivasan *et al.,* 2009). Hence the regular solution approach is a natural starting point for modeling the stability of refinery (downstream) streams.

Downstream fluids could consist of light ends (volatile streams characterized by distillation curve, gas chromatography) and non-volatile materials characterized by SARA (saturates, aromatics, resins and asphaltene) fractionation. Refinery streams could also contain reacted materials with altered chemistry. For example, asphaltenes exposed to high temperature treatment crack or break into smaller molecular structures. Hydro-processed asphaltenes show a decrease in molecular weight and increase in polarity corresponding to changes in chemical structure (Buch *et al.,* 2003; Groenzin *et al.,* 2007). Other crude oil fractions are also altered as their constituents react or their reaction products become part of the given fraction. Therefore, the property correlations developed for fractions of native petroleum almost certainly will not apply to reacted refinery streams. Hence, a characterization methodology for reacted materials and the data to support it are required.

1.1 Objectives of the Present Thesis

Oil characterization involves dividing the crude oil or reacted stream into a set of components that represent the property distributions within the fluid. Typically, the characterization is based on a boiling curve obtained for the distillable fraction of the fluid. Heavy oils have a significant non-distillable fraction which will be characterized based on SARA (saturates, aromatics, resins, and asphaltenes) analysis. The properties relevant for regular solution modeling of asphaltene precipitation are the molar volume and solubility parameter of each component or pseudo-component. While molar volumes can be determined relatively easily from measured molecular weights and densities, solubility parameters must be determined from modeling asphaltene solubility data. Therefore, it is desirable to find a correlation of solubility parameter to an easily measured property. Buckley *et al.*, 1998 showed that the solubility parameter of many components correlates to their refractive index. Therefore, refractive index was selected as a potential correlating parameter. The main objectives of this thesis are then: 1) to determine the molar volume, refractive index, and solubility parameter of saturates, aromatics, and resins (SAR) from native oils and reacted streams; 2) to develop a correlation for the solubility parameter of the SAR fractions of these fluids.

Specific objectives of this work are as follows:

1. Determine the molecular weight, density, and refractive index of SAR fractions:
    a. Fractionate the non-volatile fractions of a variety of downstream and native fluids into saturates, aromatics, resins and asphaltenes (SARA);
    b. Measure the molecular weight, density and refractive index of the SAR fractions.

2. Determine the solubility parameters of SAR fractions:
    a. Measure asphaltene precipitation yields for one base case asphaltene in solutions of heptane and toluene;
    b. Determine the molar volume and solubility parameter distribution of the base case asphaltenes by modeling the precipitation data with a regular solution model;
    c. Measure base case asphaltene precipitation yields in solutions of saturates/ toluene or n-heptane/aromatics;

d. Determine the solubility parameter of the saturates and aromatics by fitting the above yield data with the regular solution model.

3. Develop a correlation of the solubility parameter of saturates and aromatics to their refractive index. Examine the relationship of refractive index and density and develop a correlation of refractive index to density and, if possible, solubility parameter to density.

1.2 Thesis Structure

This thesis is organized into eight chapters. Chapter 2 reviews petroleum chemistry with a focus on heavy oils and bitumen. A brief background to heavy oil refining is presented and the effects of refining processes on the nature of feedstock are discussed. Phase behaviour models for asphaltene precipitation modeling are also reviewed.

Chapter 3 presents the experimental methods used in this thesis including the precipitation of asphaltenes from crude oil, solids removal, the determination of asphaltene solubility in *n*-heptane/toluene, saturates/toluene and *n*-heptane/aromatics mixtures. The SARA fractionation procedure and the methods used to measure density, molecular weights and refractive indexes of these fractions are explained.

Chapter 4 describes the modified regular solution model used to model asphaltene phase behaviour in upstream fluids. Previously developed property correlations are presented (Akbarzadeh *et al.*, 2005; Barrera *et al*, 2013). Finally, a description of a typical application of the model to predict asphaltene precipitation from diluted heavy oil is presented. The heavy oil application is presented to demonstrate the role of the saturate and aromatic properties. In this thesis, the model is only used for solutions of asphaltenes in solvents (including aromatics and saturates).

Chapter 5 presents the molecular weight, density, and refractive index of the saturates, aromatics, and resin samples characterized for this thesis. The excess volumes and excess refractive index are determined for mixtures of SAR fractions and heptane and toluene. The correlations between

density and refractive index and their excess properties are examined. Finally, the effect of temperature on the refractive index and density of saturates and aromatics is discussed.

Chapter 6 outlines an alternative methodology for estimating fractional asphaltene yields from refractive index measurements of supernatants from solubility experiments. Previously developed correlations to account for the excess volumes and refractive index were applied. The results are compared with a gravimetric method.

Chapter 7 presents the application of the modified regular solution model to determine the solubility parameter of the saturate and aromatic fractions based on gravimetric asphaltene solubility measurements in solutions of saturates/toluene and n-heptane/aromatics. The solubility parameters are used to establish a correlation between solubility parameter and refractive index. A correlation to density is also investigated. The effect of reaction on the solubility properties of the fractions is also discussed.

Chapter 8 summarizes the findings of this thesis and makes recommendations for continuation of this study and some modifications needed for possible future work.

Chapter Two: Literature Review

This chapter provides an understanding of petroleum chemistry with a focus on heavy oils and bitumen. Fluid characterization based on distillation and solubility fractionation is presented. Asphaltene structure and self-association models are introduced for an insight into asphaltene phase behaviour in crude oil systems. Phase behaviour modeling approaches are outlined with a focus on regular solution theory. Finally, changes in oil chemistry resulting from feedstock refining are discussed.

2.1 Petroleum Chemistry

Petroleum/crude oils are naturally occurring, complex mixtures of hydrocarbons with varying amounts of sulfur, oxygen and nitrogen, as well as trace amounts of metals such as nickel and vanadium. Chemical and physical compositions vary with the origin and age of the crude oil (Speight, 2007). Crude oil can be thought of as a distribution of paraffinic, naphthenic and aromatic species of increasing molecular weight and complexity with the largest and most complex being the asphaltenes. The proportions of the constituents in different crude oils vary and the physical properties also vary accordingly.

Crude oil can be classified or characterized in different ways; for example, by its physical properties (*e.g.*, specific gravity, viscosity), recovery methods, elemental composition (amount of carbon, hydrogen, nitrogen, sulphur), carbon distribution, boiling point distillation curve, nature of residue after distillation (*e.g.*, paraffinic, naphthenic, aromatic, asphaltic), or solubility class (*e.g.*, amount of saturates, aromatics, resins, and asphaltenes).

2.1.1 Classification

Petroleum is classified as conventional oil, heavy oil and bitumen based on physical properties (viscosity and API gravity) and recovery methods, as follows (Speight, 2001, 2007)

- Conventional oil exists as free-flowing liquid at reservoir conditions and can be recovered by methods relying on processes such as natural pressure and physical lift (pumping). Conventional oils are usually rich in low-boiling constituents and waxy molecules with viscosities less than 10^2 mPa.s at ambient temperature and API gravity higher than 30°.
- Heavy oils have higher viscosity (10^2–10^5 mPa.s) and lower gravity (20^o to 10^o API) than conventional oils. They have lower mobility at reservoir conditions and their primary recovery usually requires thermal stimulation of the reservoir (enhanced oil recovery). In contrast to conventional oils, heavy oils are darker in colour or black.
- Extra heavy oils or bitumen are extremely viscous hydrocarbon materials which cannot be recovered by either conventional or enhanced oil recovery methods. These heavy-asphaltic crude oils occur in near-solid state, are incapable of flow at reservoir conditions and are generally recovered by mining operations and in-situ recovery methods. Their viscosities are higher than 10^5 mPa.s and their gravity is less than 10^o API.

Whereas conventional crude oils are rich in low boiling and paraffinic compounds, heavy crude oils have greater amounts of high boiling and asphalt-like molecules, are more aromatic, and contain larger amounts of heteroatoms. The hydrocarbon content of petroleum can be as high as 97% by weight in conventional crude oils or as low as 50% by weight or less in heavy oils and bitumen (Speight, 2007). The non-hydrocarbon constituents tend to concentrate in the higher-boiling fractions of the crude oil.

2.1.2 Characterization

For effective design and optimization of crude oil processing, adequate characterization of the fluid is essential for phase behaviour modeling. Characterization is intended to represent the distribution of properties within the crude oil and entails the division of the complex multi-component crude oil into various pure components and pseudo-components of known or correlated properties. Analytically determining the composition of all pure components in crude

oil is impractical so the general procedure is to segregate the constituents according to molecular size and molecular type (Speight, 2001).

The most common compositional representation of crude oils is to lump components into groups of similar properties (pseudo-components) based on their chemical composition (such as H/C content, carbon distribution, heteroatom content), physical properties (such as boiling point, density, molecular weights, viscosity, refractive index) and chemical-function families (as in Paraffins, Naphthenes and Aromatics - PNA, Saturates, Aromatics, Resins and Asphaltenes – SARA), (Riazi, 2005). Techniques that have been employed to separate crude oil into fractions or pseudo-components include gas chromatography, distillation, adsorption chromatography (*e.g.*, PNA, SARA), mass spectrometry, solvent treatments, chemical methods (Speight, 2001, 2007). The choice of fractionation method depends on the nature and composition of the crude oil, the effectiveness of the process, its compatibility with the other separation procedures to be employed (Speight, 2001), and the required fractions or pseudo-components properties.

Typically, separation of the light and volatile constituents of crude oil (N_2, He, H_2S, C_1- *n*C_5) can be achieved with gas chromatography and distillation. However, as the volatility decreases and the complexity of the constituents increase with increasing molecular weight, it becomes very difficult to apply these techniques to higher boiling petroleum constituents (Speight, 2007). Other techniques are applied to characterise the heavier components. The characterisation techniques used for this thesis are outline below.

2.1.2.1 Distillation Methods

In refineries, conventional oils are typically characterised using distillation where the constituents are separated into fractions, or *distillation cuts*, based primarily on their differences in vapour pressure or boiling points. The vapour pressure of a compound is inversely proportional to its boiling point, molecular weight, aromaticity and polarity. Therefore, over a boiling point range, similar constituents (in terms of volatility) are separated from the oil and collected as distillation cuts. The properties of these pseudo-components can be measured. Distillation curves which are plots of boiling temperature versus volume of distillates present a

distribution of the species in a particular crude oil by their volatilities. Distillation can be performed at atmospheric pressure or at reduced pressure depending on the type of crude oil.

Crude oils boil over a range of temperatures from about 20 to above 344^{o}C, beyond which thermal decomposition (cracking) occurs (Kaes, 2000). Compounds boiling above approximately 350^{o}C are called residuum and are removed from the bottom of the atmospheric distillation column and sent to the vacuum distillation column (Speight, 2007). Vacuum distillation is usually adapted to obtain higher-boiling distillates from the residuum at lower temperatures and reduced pressure without the risk of decomposition. The minimum obtainable pressure for vacuum distillation is around 3.5 to 7 kPa. The highest temperature that can be measured at this pressure for most crude oils is in the range of 496 to 526°C when corrected to atmospheric pressure (Kaes, 2000; Wiehe, 2008). Vacuum distillation is also applied to heavier oils.

The distribution of the various compound types throughout the petroleum vary with type of crude (Speight, 2007), but for a given family of hydrocarbons, the molecular weights, complexity, density, aromaticity and polarity increase monotonically with increasing boiling points as illustrated in Figure 2.1. Generally, the residuum contains the highest concentrations of high-molecular weight organic compounds (with sulphur, nitrogen, oxygen, metals and other nonhydrogen species), as well as high-molecular weight hydrocarbons, including condensed-ring aromatics (Mitchell *et al.*, 1973). The higher boiling distillation cuts also contain a broader distribution of components with corresponding properties. However, for practical reasons, distillation cuts are commonly treated as pseudo-components each with a unique boiling point, molecular weight, density, refractive index and critical properties.

Other key characterization parameters (*e.g.*, critical properties, solubility parameters, etc.) of the distillable fractions required for modeling fluid behaviour can be correlated to the measured properties. Critical properties can be estimated using Vetere-Watson, Lee–Kesler or Riazi–Dauber correlations (Riazi, 2005). The solubility parameter can be calculated through its definition with the enthalpy of vaporization which in turn is correlated to the critical properties.

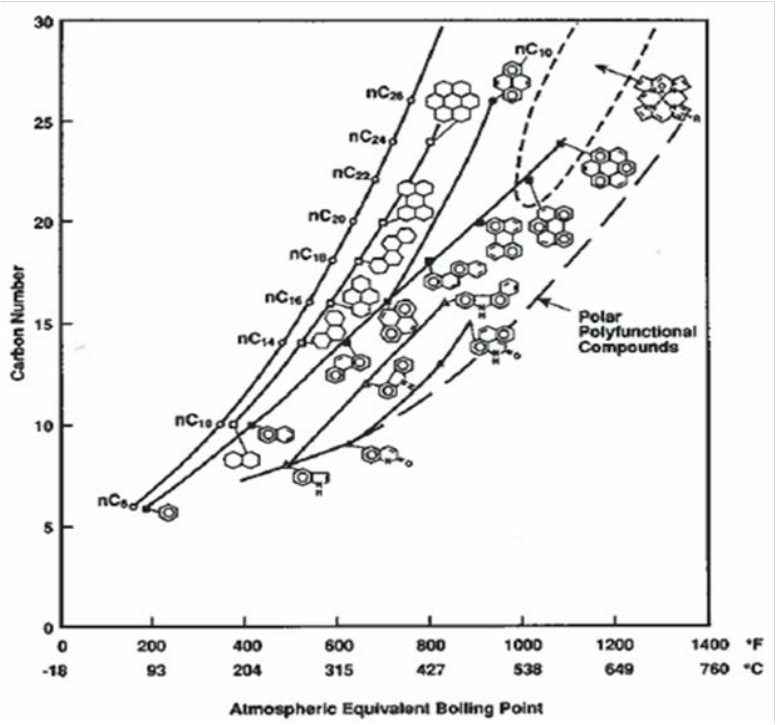

Figure 2.1: Evolutions of molecular weights and structures as a function of the boiling point (Merdrignac and Espinat, 2007)

Heavy oil and bitumen cannot be fully characterized by distillation because these fluids contain large amount of high molar mass components that decompose before they boil. The non-distillable fractions of heavy oils and bitumen can make up as much as 60% by weight of the original oil, which limits the characterization of heavy oils by distillation alone due to the inability to determine properties of higher-boiling cuts (Speight, 2007). Even with vacuum distillation, a significant fraction of the oil (about 50 wt %) remain as residual fraction that does not boil (Peramanu *et al.,* 1999). Therefore, these high-boiling distillates and heavy feedstocks are often characterized according to their molecular weight distribution (gel permeation chromatography), chemical family, or solubility classes (adsorption chromatography) (Speight, 2007). The most common methodology to characterize the heavy oils and bitumen is based on solubility classes.

2.1.2.2 Solubility Based Methods

These methodologies are based on the affinity of petroleum components to solvents and adsorbents and separates petroleum into groups of molecules with similar solubility. A typical solubility-based characterization method is SARA fractionation which is a systematic extraction that separates the crude oil into saturates, aromatics, resins, and asphaltenes (SARA) fractions following the ASTM D2007 method, Figure 2.2.

Heavy oils and bitumen in this thesis were characterized using SARA analysis. This method involves the initial separation of asphaltenes from oil before contacting the feedstock with the adsorbents. Asphaltenes are a true solubility class and include all the materials that are insoluble in a paraffinic hydrocarbon (*i.e.*, *n*-pentane or *n*-heptane), but soluble in an aromatic hydrocarbon such as toluene. The remaining SAR (maltenes) fractions are adsorption classes. Saturates are not adsorbed on polar adsorbents and are recovered with *n*-pentane as the initial eluent from a silica gel/attapulgus clay adsorption column. Aromatic compounds are adsorbed on a column packed with silica gel and are eluted using a mixture of *n*-pentane/toluene and by Soxhlet extraction with toluene. Resins are adsorbed on an attapulgus clay-packed column and are eluted with a mixture of acetone/toluene. SARA fractionation is discussed in more detail in Chapter 3. A schematic of the procedure is shown in Figure 2.2. A typical SARA analysis for heavy oils and bitumen is shown in Figure 2.3. The asphaltene and resin contents of each heavy oil and bitumen exceeds 40 wt/wt %, significantly higher than in conventional oils.

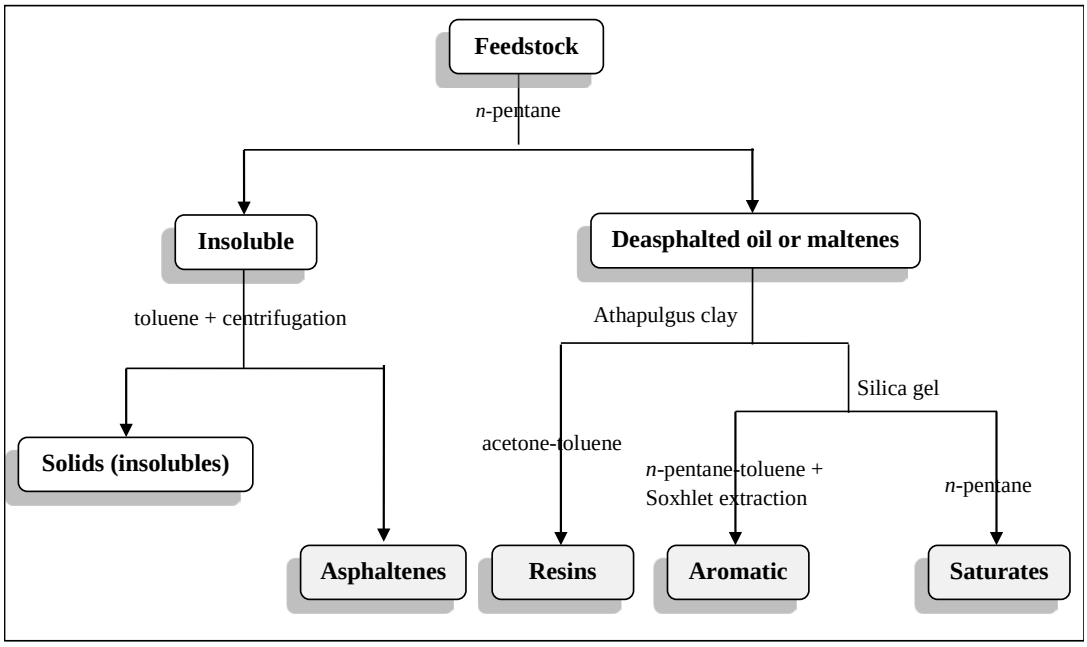

Figure 2.2: ASTM D2007 SARA fractionation procedure.

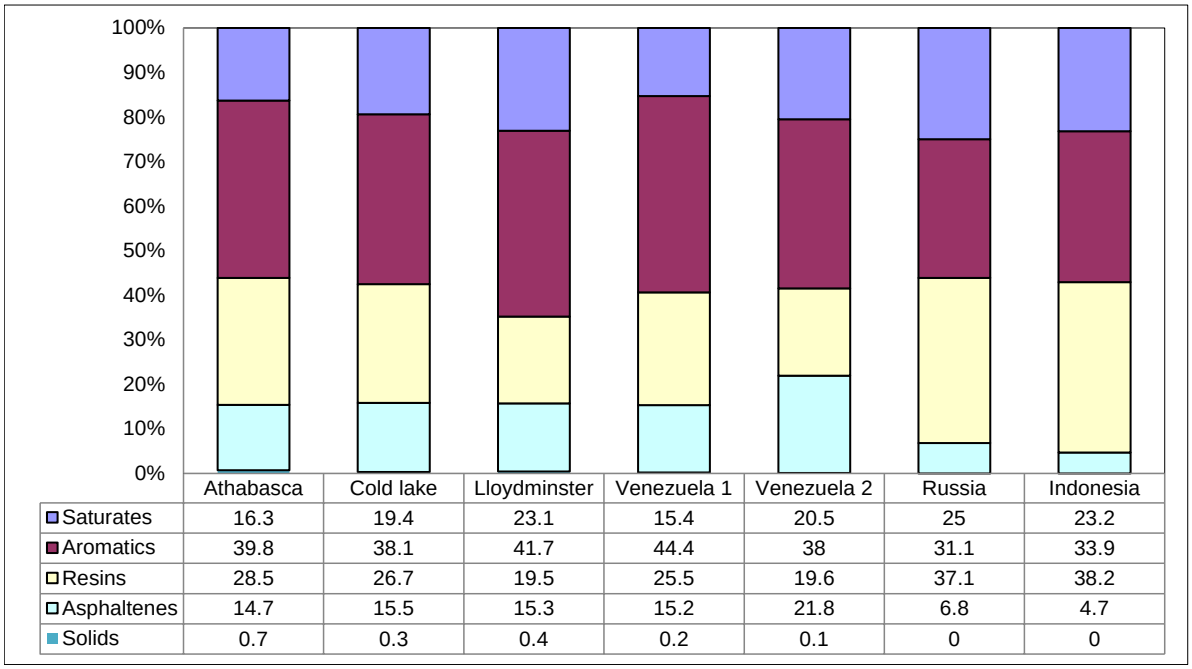

	Athabasca	Cold lake	Lloydminster	Venezuela 1	Venezuela 2	Russia	Indonesia
Saturates	16.3	19.4	23.1	15.4	20.5	25	23.2
Aromatics	39.8	38.1	41.7	44.4	38	31.1	33.9
Resins	28.5	26.7	19.5	25.5	19.6	37.1	38.2
Asphaltenes	14.7	15.5	15.3	15.2	21.8	6.8	4.7
Solids	0.7	0.3	0.4	0.2	0.1	0	0

Figure 2.3: Composition of different heavy oils and bitumen based on SARA fractionation (Ortiz, 2009).

2.1.3 SARA Fractions

Since this thesis focuses on SARA fractions, their properties are discussed in more detail below, particularly the asphaltenes. Asphaltenes are of interest because they are known to self-associate and precipitate out of solution with variations in temperature, pressure and chemical composition of surrounding fluids. Asphaltene deposition is an operational and economic concern in the oil industry because these physical changes are associated with different stages of crude oil production and refining operations. Deposition may occur in the oil reservoir due to pressure variations, injection of solvents or heat causing the blocking of pores, production lines and possible loss of well. In the refinery, during the thermal and thermo-chemical processing of the heavy residues of oil, asphaltenes act as coke precursors leading to equipment losses and deactivation of catalysts (Speight, 2001).

Saturates:

The saturate fraction consists of paraffins and cycloparaffins (Speight, 2001) and is the least polar of the SARA fractions. The single-ring naphthenes, or cycloparaffins, present in petroleum are primarily alkyl-substituted cyclopentanes and cyclohexanes. The alkyl groups are usually short-chained, with methyl, ethyl and isopropyl groups being the predominant substitutes. Generally, naphthene fractions containing more condensed rings have higher molar mass. The molar mass of saturates range from 300 to 600 g/mol. Their densities are in the range 820 to 900 kg/m³. The reported solubility parameter for saturates range from 15 to 16 $MPa^{1/2}$, (Akbarzadeh *et al*, 2004), the lowest value of all the SARA fractions. Lighter oils contain saturates with lower average molar mass, density, and solubility parameter.

Aromatics:

The aromatic fraction consists of compounds containing an aromatic ring and varies from mono-aromatics (containing one benzene ring in a molecule) to di-aromatics (substituted naphthalene) to tri-aromatics (substituted phenanthrene). Higher condensed ring systems, such as tetraaromatics or pentaaroamitcs, are less prevalent than the lower ring systems. In general, higher molar mass aromatics of each type have more condensed ring naphthenes attached to the aromatic ring (Speight, 2001). The molar mass of aromatics is in the range of 300 to 800 g/mol

and their density is approximately 1000 kg/m³. Aromatics are more polar than saturates and their solubility parameters range from 19 to 20 $MPa^{1/2}$ (Akbarzadeh *et al*, 2004).

Resins:

Resins are red to brown coloured, semi-solid and very sticky. They are regarded as materials soluble in whichever hydrocarbon (*n*-pentane or *n*-heptane) is used for the separation of asphaltenes but cannot be extracted from surface-active materials (attapulgus clay) by *n*-pentane or *n*-heptane (Speight, 2007). Resin molecules are essentially large aromatics consisting of naphthenic and benzenic ring structures with long paraffinic side chains and some short paraffinic bridges (Speight, 1994). Resins may also contain esters as well as terminal carbonyl groups (Chang and Fogler, 1994). Resins have higher molar mass, greater polarity and lower hydrogen-to-carbon (H/C) ratios than aromatics (Yarranton, 1997). The molar mass of resins range from 700 to 1300 g/mol. The density of resins is approximately 1050 kg/m³ and their solubility parameter is approximately 20 $(MPa)^{1/2}$ (Akbarzadeh *et al*, 2004).

Asphaltenes:

As stated earlier, asphaltenes are defined as the fraction from a crude oil insoluble in aliphatic compounds (such as pentane and heptane), but soluble in aromatic compounds (*e.g.*, benzene and toluene). They are heterocompounds and are the most polar fraction of crude oil. They are dark brown to black friable solids that have no definite melting point and usually decompose on heating leaving a coke residue. Asphaltenes are a complex mixture of compounds and have proven difficult to characterize.

Chemically and structurally, asphaltenes can be considered as large resins. However, asphaltenes have lower H/C content than resins indicating that they are more aromatic (Speight, 2007). In general, asphaltenes consist of condensed aromatic nuclei with alkyl and cycloalkyl (naphthenic) substituents, containing heteroatoms (*i.e.*, sulfur, nitrogen and oxygen) scattered throughout the hydrocarbon systems. With increasing molar mass of the asphaltene fraction, both aromaticity and the proportion of the heteroatoms increase (Speight, 2007). The elemental composition of asphaltenes from different sources shows that the amounts of carbon and hydrogen usually vary

in a narrow range, with a hydrogen-to-carbon atomic ratio of 1.15 ± 0.05%, although values outside of this range are possible. Heteroatom concentration varies notably with oxygen content varying from 0.3% to 4.9%, sulphur content ranging from 0.3% to 10.3% and nitrogen content varying from 0.6% to 3.3% (Speight, 2007). Asphaltenes have the highest polarity among the SARA fractions.

The density of asphaltenes is in the range of 1100 to 1200 kg/m³. Reported molar masses of asphaltenes range from 1000 to 2,000,000 g/mol depending on the measurement technique (Speight, 2001). The high apparent molar masses have been attributed to asphaltene self-association. The average monomer molar mass of asphaltenes is in the order of 1000 to 2000 g/mol (Alboudwarej, 2003). The solubility parameter for asphaltenes is approximately 21 $MPa^{1/2}$ (Akbarzadeh, 2002).

Aromatics, resins and asphaltene monomers can be considered as a continuum of polynuclear aromatics with progressively increasing polarity, molar mass and heteroatom content (Agrawala, 2001; Yarranton, 2005). However, a significant difference between asphaltenes and the other aromatics is that significant fractions of the asphaltenes self-associate.

2.1.3.1 Asphaltene Structure

Before examining self-association, asphaltene molecular structure is reviewed. The detailed structural characterization of asphaltenes is difficult to achieve because of the complexity of the fractions and limitations of analytical techniques (Merdrignac and Espinat 2007). A single molecular model may not be representative of the structure of asphaltenes because it cannot represent the large range of characteristics and locations of the functional groups nor will it be consistent with field observations of property variations in asphaltene subfractions (Speight, 1994). Nonetheless, two types of structures have been postulated to represent asphaltene molecules: continental and archipelagos.

The continental or island molecular model resembles a relatively flat disk-like molecule and consists of a core aromatic cluster with a large number of fused rings linked to aliphatic bridges

as shown in Figure 2.4. This pericondensed structure has a central cluster of aromatic groups, with perhaps > 10 rings, and alkyl chains at the periphery. This model is based on x-ray diffraction measurements on a series of solid asphaltenes (Dickie *et al.*, 1967). Continental-type models have been used in molecular modeling studies to demonstrate the formation of asphaltene aggregates by stacking of their aromatic regions.

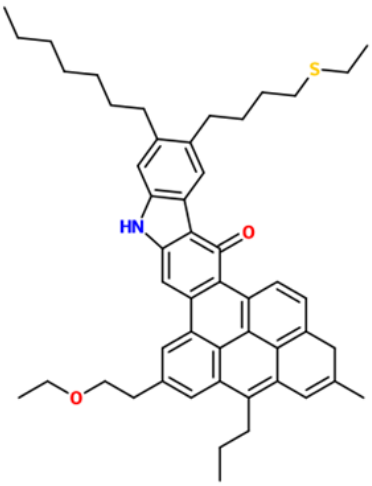

Figure 2.4: Continental structure of asphaltene molecule (adapted from Kuznicki *et al*., 2008).

The archipelago model (Figure 2.5) represents an asphaltene structure with small aromatic groups linked by aliphatic chains. This model is supported by results from pyrolysis, oxidation, thermal degradation and small angle neutron scattering analyses. These techniques showed that aromatic groups present in asphaltenes contain one to four aromatic rings and are linked by aliphatic bridges up to 24 carbons long (Sheremata *et al*., 2004).

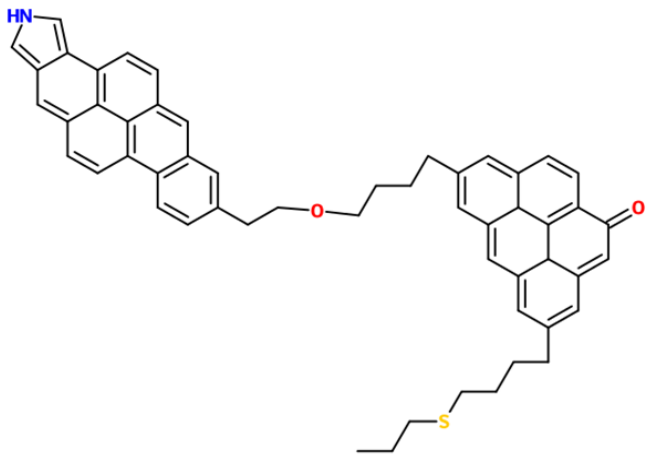

Figure 2.5: Archipelago structure of asphaltene molecule (adapted from Kuznicki *et al.*, 2008).

2.2 Asphaltene Self-Association

Asphaltenes in solution form molecular aggregates of colloidal dimension (Yarranton, 2005) even at very low concentrations. Asphaltene self-association has been established from molecular weight measurements, surface and interfacial tensions (IFT) measurements (Mohamed *et al.*,1999), small angle x-ray scattering (SAXS) (Xu *et al.*, 1995), and small angle neutron scattering (SANS) (Ravey *et al.*, 1988). The exact mechanism of association has not been established; proposed causes of asphaltene interaction include aromatic π-π stacking, hydrogen bonding, van der Waals forces, acid-base interactions, or a combination of the different mechanisms (Speight, 2007; Wiehe, 2008; Gray *et al.*, 2011)

According to x-ray measurements of solid asphaltenes, their aromatic sheets tend to stack one on top of the other to a maximum of five. π-π bonding between these aromatic ring systems is the most commonly posed mechanism for asphaltene association (Yen *et al.*, 1961; Speight, 1994; Andersen, 2008). Since heteroatoms or saturated ring structures are present in the asphaltene molecules, the sheets tend to bend preventing a close approach and creating an amorphous structure. However, there is no evidence that π-π stacking is the main interaction involved in asphaltene aggregation in solution (Gray *et al.*, 2011). The van der Waals forces provide a large contribution to the energy of the aggregates near the equilibrium intermolecular distance

(Murgich, 2002). Ionic associations (i.e, acid-base interactions) also represent a strong interaction driving asphaltene aggregation (Gray *et al.,* 2011). Intermolecular hydrogen bonds can be formed between the OH, NH and COOH functional groups present in asphaltenes. The importance of this mechanism depends on the arrangement and size of the molecules because, in large molecules, the hydrogen bonding sites can be sterically hindered (Andersen, 2008). Each of these interactions is relatively weak in isolation, but Gray *et al.* (2011) suggest that a collective supramolecular assembly of the noncovalent interactions gives a thermodynamically stabilizing association.

Ultimately, the means by which asphaltenes are dispersed in the petroleum is still debated. The associated asphaltenes have been proposed to exist in crude oil as colloids, reverse micelles, or macromolecules. Each one of these postulates leads to different asphaltene precipitation models. The models are discussed briefly below.

2.2.1 Colloidal Model

This model proposes that associated asphaltenes consist of stacks of aromatic sheets (colloids) held together by π-π bonding and that aromatic hydrocarbons of lower molecular weight such as resins adsorb, or simply surround these colloidal structure. The surrounding layer acts as a peptizing agent and maintains the asphaltenes as a colloidal dispersion within the crude oil. Changes in system temperature, pressure and composition cause resin desorption and generate attraction forces between the asphaltene molecules, creating larger structures that precipitate depending on their size (Pfeiffer, 1940; Speight, 1994). The asphaltene colloidal model follows from the continental structure of asphaltene monomers and is consistent by SANS and SAXS measurements, showing that associated asphaltenes consist of stacked aromatic sheets held together by π-π bonding (Yen *et al.*, 1961; Dickie *et al.*, 1967; Ravey *et al.*, 1988; Spiecker, 2001).

Koots and Speight (1975) investigated the role of resins in a crude oil by performing a series of tests based on the dissolution of asphaltenes in various crude oil fractions. The results confirmed that petroleum asphaltenes are not soluble in their corresponding resin-free oil fractions. It was

only possible to bring about dissolution of the asphaltenes by the addition of the corresponding resins. However, this observation does not distinguish between dissolution versus dispersion of the asphaltenes in the presence of resins. Furthermore, aromatic solvents such as toluene are equally or more effective at dissolving or dispersing asphaltenes.

While the colloidal model is the prevalent view of asphaltenes in crude oils, it is not consistent with the step-wise aggregation observed in molecular weight versus concentration data. Nor has this model been linked to a predictive asphaltene phase behaviour model.

2.2.2 Micellar Model

Huanquan *et al.* (1998) suggested that asphaltenes form reverse micelles rather than stacks of molecules. Micelles and reverse micelles are surfactant aggregates. Micelles are a cluster of surface active molecules in aqueous solution arranged such that the hydrophobic non-polar groups are in the centre of the structure while the hydrophilic polar groups are towards the outer surface in contact with the polar solvent (such as water). Micelles can be considered as a separate phase that forms above a critical micelle concentration (cmc) of a surfactant. The cmc is determined experimentally as a change in the slope of the plot of surface tension for an aqueous solution against the logarithm of the surfactant concentration (Friberg, 2007). Reverse micelles have the inverse structure and occur in oil phase. In reverse micelles where the solvent is now the organic phase, the polar groups are sequestered in the core and the non-polar groups are extended away from the centre.

For the case of asphaltenes, polynuclear aromatic groups with the the lowest solubility in aliphatic compounds would be located in the core, and would be surrounded by chains with lower aromaticity. A composition change or the application of an external potential can disturb the balance of forces between these reverse micelles and cause an irreversible asphaltene flocculation.

However, interfacial tension (Yarranton *et al.,* 2000) and isothermal titration calorimetry (Merino-Garcia *et al.,* 2007) studies indicate that the “micellar” model may not apply to

asphaltene association. Yarranton *et al.* (2000) observed no experimental indications of a critical micelle concentration for asphaltenes in toluene solutions at the concentrations studied (down to 2 g/L) and that interfacial tension did not stabilize upon aggregation as would be expected with micelles. They noted that asphaltenes associate in a stepwise manner rather than the sudden transition characteristic of micelles. Merino-Garcia et al., (2007) confirmed that the energy changes observed with dilution were consistent with step-wise aggregatation.

2.2.3 Oligomerization Model

This model assumes that asphaltenes association is analogous to polymerization except that aggregates are held together by dispersion forces (van der Waals) rather than covalent bonds. Asphaltenes are treated as free molecules in solution that contain multiple active sites (heteroatoms or aromatic clusters) through which they can interact with other similar molecules to form aggregates (Agrawala and Yarranton, 2001). Some molecules may have multiple sites that can link with other molecules and hence act as propagators in an oligomerization-like reaction. Other molecules may have a single active site and can be treated as terminators. Yet other molecules may be inert (Yarranton *et al.,* 2007). Hirschberg *et al.* **(**1984) proposed that in crude oil the polymerization is blocked (reduced) by the association of asphaltenes with similar, but less polar hetero-components, such as resins.

Unlike colloids, the size of the macromolecular aggregates is expected to increase with asphaltene concentration as observed with molar mass measurements with vapour pressure osmometry (Agrawala *et al.*, 2001). Further details about the oligomerization model are available from recent studies on asphaltene association (Agrawala 2001; Yarranton, 2005) and asphaltene property distributions (Barrera, 2012). It is possible that the colloidal, macromolecular, and micellar models are all correct for different asphaltene molecules or for different conditions (Yarranton, 2005).

2.3 Asphaltene Phase Behaviour Modelling

In some applications, it is necessary only to determine if a fluid is stable relative to asphaltene precipitation; for example, when blending streams in a refinery. Various stability indices can be used for this purpose (Wiehe *et al.*, 2000; Starks *et al.*, 2003). In other cases, it is desirable to accurately predict the full range of phase behaviour for a crude oil including asphaltene precipitation; for example, depressurized offshore oils and solvent-assisted thermal recovery processes. Understanding the conditions which favour precipitation, onset point, and possible amounts of precipitated materials will help to reduce the operational problems and costs associated with processing heavy oils. This thesis focuses on phase behavior models.

The proposed asphaltene association models have led to two different types of models for asphaltene precipitation predictions: colloidal and thermodynamic models. Colloidal theory considers asphaltenes to be solid-like particles that are suspended in the crude oil and stabilized by the resin molecules (Wu *et al.*, 1998). The resins are assumed to partition between the asphaltene particles and the asphaltene-free part of the crude oil. The model considers precipitation a physical separation that occurs when the resins are stripped off, allowing the asphaltene cores to flocculate into macroscopic particles. Precipitation models based on this approach are not predictive and have only been tested on limited data. Most colloidal models predict that asphaltene precipitation is irreversible which is not the case.

Thermodynamic models assume that asphaltenes self-associate into macromolecules that are part of a continuous mixture (crude oil) and that they remain in solution. This view is consistent with the oligomer concept. Asphaltene precipitation is then considered as a reversible chemical separation (Hirschberg *et al.*, 1984); that is, a liquid-liquid or solid-liquid equilibrium. To date, the thermodynamic approaches have proven the most successful in modeling asphaltene phase behavior (Ting *et al.*, 2003; Akbarzadeh *et al.*, 2005). Thermodynamic approaches for asphaltene precipitation fall into two categories: the regular-solution based models and the equation of state based models. A thermodynamic model based on the regular solution theory is used in this thesis and only these models are reviewed here.

2.3.1 Regular Solution Based Models

Regular solution models relate the activity coefficient of each component to its molar volume and solubility parameter (see Chapter 4 for details). Regular solution models have proven the most successful for fitting and predicting asphaltene precipitation (Andersen and Speight, 1999). Hirschberg *et al.* (1984) was the first to apply the regular solution theory to asphaltene precipitation from crude oils. They considered asphaltenes as monodisperse polymeric molecules dissolved in the crude oil and that their solubility in reservoir crude oil is pressure, temperature and composition dependent. Crude oils were considered a mixture of two liquid phases (asphaltene and solvents) in equilibrium. At the onset of asphaltene precipitation, only asphaltene or *asphalt* (asphaltene and resins) were allowed to partition to the heavy liquid phase. They used a combination of a vapour/liquid model and a liquid/liquid model in that work. Using a compositional model based on the Soave equation of state, first the liquid-phase composition was calculated assuming no asphalt precipitation. The amount of asphaltene/asphalt precipitated from the liquid phase was then calculated using the modified Flory-Huggins theory (Flory, 1953; Huggins, 1941) assuming this precipitation did not change the vapour/liquid equilibrium (VLE).

Kawanaka *et al.* (1991) considered asphaltenes as polydisperse polymers with a broad distribution of molecular weight. They incorporated entropy of mixing based on the Scott and Magat theory (Scott *et al*., 1945; Scott, 1945). They assumed solid-liquid equilibrium between asphaltene and the deasphalted oil in crude oil systems. They also assumed that asphaltenes behaved as heterogeneous polymers, in which case different fractions of the asphaltene may be specified according to their molecular weights. Inputs for the model were composition of the light phase and asphaltene properties. The continuous molecular-weight distribution function of asphaltene was represented by the gamma distribution function. The choice of gamma function was arbitrary as other equally versatile distribution functions could also be used.

This model has been modified through the years to improve its predictive capability. Yarranton and Masliyah (1996) modeled asphaltene precipitation in solvents by treating asphaltenes as a mixture of components of different density and molar mass using a distribution function. In that work, they assumed solid-liquid equilibrium between an asphaltene rich phase and a light liquid

phase and also incorporated Flory-Huggins entropy of mixing term. They developed correlations based on molar mass for the two key model parameters, molar volume and solubility parameter, required for the solubility calculations.

Alboudwarej *et al.* (2003) and Akbarzadeh *et al.* (2004, 2005) extended Yarranton and Masliyah's model to asphaltene precipitation from several different heavy oils and bitumen over a range of temperatures and pressure. A liquid-liquid equilibrium was assumed with only the asphaltenes partitioning to the dense phase. The input parameters for the model were mole fraction, molar volume, and solubility parameter for each component. Heavy oils and bitumen were divided into four main pseudo-components, corresponding to the SARA fractions. Whereas saturates, aromatics and resins were treated as single pseudo-components, the asphaltenes were assumed to be a continuum of aggregates with a molar mass distribution. They developed correlations for the molar volumes and solubility parameters of the pseudo-components, based on solubility, density and molar mass measurements. This model was used in this thesis and a detailed description is provided in Chapter 4.

While progress has been made with the regular solution model for modeling asphaltene precipitation in upstream fluids and their blends (Tharanivasan *et al.*, 2009), a major challenge to the predictability of the model has been the uncertainty of fluid characterization from different streams, particularly reacted streams. An objective of this thesis is to adapt the regular solution based characterization and modeling methodology previously developed for upstream native petroleum to downstream fluids.

2.4 Solubility Parameter Correlations

In the above models, correlations were developed for the solubility parameters and molar volumes of both the pure components and the pseudo-components (such as saturates, aromatics, resins, and asphaltenes). Zuo *et al*. (2010) correlated solubility parameters to densities for live oils at elevated temperatures and pressures. Fossen et al. (2005) correlated Hildebrand and Hansen solubility parameters to IR and NIR spectra through use of multivariate data analysis.

Others have recommended use of different Equations of State methods for solubility parameter calculations (Nikookar *et al*., 2008; Ting *et al*., 2003). Wiehe *et al.* (2000, 2008) introduced the concept of two-dimensional solubility parameters for an Oil Compatibility Model.

A correlating parameter of particular interest is the refractive index because the solubility of a component in a solvent may correlate to its refractive index in that solvent (Barton, 1991, Buckley *et al.,* 1998, 2001; Angle *et al.,* 2006). Refractive index also correlates to other physical properties such as density, molecular weight, boiling point, specific gravity, equation of state parameters, critical constants, and transport properties of hydrocarbon systems with high reliability (Castillo *et al.*, 2009; Riazi, 2005; Vargas *et al*., 2009). Refractive index measurements have been used in the modeling of PVT behaviour, surface tension of reservoir fluids, wetting alterations in reservoirs, and asphaltene precipitation (Evdokimov *et al.,* 2007).

Refractive index, *n*, is the ratio of the speed of light through vacuum to its speed through a fluid:

$$n = \frac{\text{velocity of light in vacuum}}{\text{velocity of light in substance}} \qquad (2.1)$$

Generally, the reflection of light through a medium/substance varies with wavelength of the light and the polarizability and composition of the medium. The connection between refractive index and solubility parameter is through polarizability. The polarizability of a molecule describes its electron distribution change in response to an external electric field or as induced by interactions with other molecules. Induced polarizability is related to the refractive index through the *Lorentz-Lorenz* model (Chartier, 2005; Riazi, 2005) given by:

$$\alpha = F_{RI}\frac{3MW}{4\pi N_a \rho} \qquad (2.2)$$

where α is polarizability, N_a is Avogadro's number, ρ is density, MW is molecular weight, and F_{RI} is fractional refractive index given by $\left(\frac{n^2-1}{n^2+2}\right)$.

For hydrocarbon and crude oil systems, where polar interactions are weak, the interaction energy between the molecules is dominated by the London dispersion forces and is related to polarizability as follows (Hirschfelder, 1964; Israelachvilli, 2001):

$$\varphi = -\frac{3}{4}\frac{h\nu\alpha^2}{(4\pi\varepsilon_0)^2 r^6} = -C\left(\alpha^2\right) \qquad (2.3)$$

where φ is intermolecular potential energy function, α is polarizability, h is Planck's constant, ν is electron frequency, ε_0 is permittivity of a vacuum, r is the distance between molecules and C is a constant.

The internal energy for a volume of fluid (cohesive energy density) also depends on the interaction energy, and the Hildebrand solubility parameter is in turn a function of the cohesive energy density (Barton, 1985):

$$\delta = \left(\frac{\Delta E}{v_m}\right)^{1/2} \qquad (2.4)$$

where δ is the solubility parameter, ΔE is the internal energy of vapourization, and v_m is the molar volume. The ratio of internal energy to molar volume is the cohesive energy density. Hence, the solubility parameter is a function of polarizability and therefore of the refractive index.

The solubility parameters of asphaltenes have been correlated to their refractive index (Buckley *et al.*, 1998; Angle *et al.*, 2006). In those studies, it was assumed that asphaltene solubility in crude oil systems is controlled by the London van der Waals attraction between the molecules (Buckley *et al.*, 1998; Wiehe, 2008). Buckley *et al.* (1998, 2001) observed that, for a series of paraffinic and aromatic hydrocarbons (non-polar compounds), the following linear correlation of the solubility parameter to refractive index, F_{RI}, exists, as also illustrated in Figure 2.6:

$$\delta = 52.042F_{RI} + 2.904 \qquad (2.5)$$

They eliminated the need to estimate solubility parameters from fitting experimental solubility data by calculating the solubility parameters of crude oil and asphaltene precipitation onset mixtures with measured refractive indexes using Equation 2.5. The extension of this correlation to modeling asphaltene precipitation from crude oil systems was based on the assumptions that crude oils are mixtures of mostly non-polar hydrocarbons. However, the complexity of crude oils

evident in the chemistry and composition of their fractions (pseudo-components) suggest that this assumption could be an over-simplification.

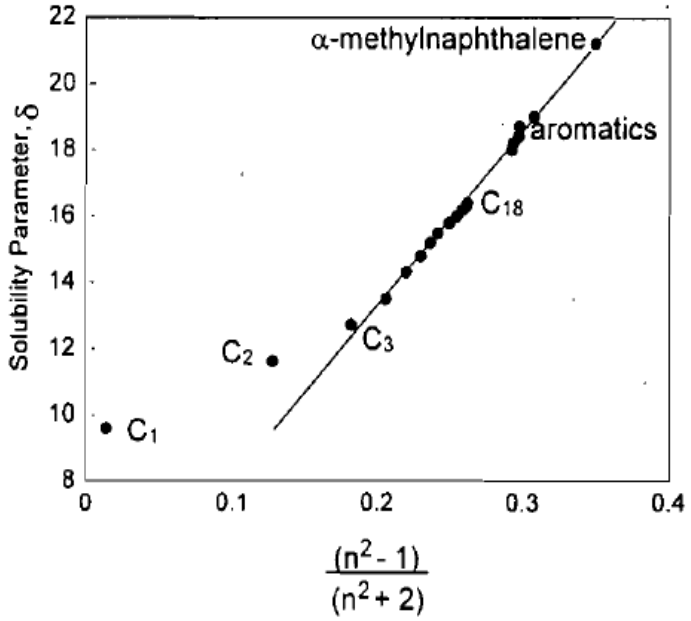

Figure 2.6: Solubility parameter of non-polar molecules a linear function of F_{RI} (Wang and Buckley, 2001).

Angle *et al.* (2006) adopted the arguments Buckley *et al*. used to study the onset of asphaltene precipitation in crude oils. The crude oils were considered to consist of two lumped pseudo-components, asphaltenes and deasphalted oils. They investigated the kinetics of asphaltene precipitation as a function of time and initial oil concentration by studying two systems:

i) partially deasphalted oils in heptol and

ii) heavy oils, bitumen and asphaltenes dissolved in toluene.

Measured physical properties such as density and refractive index were correlated with the calculated Hildebrand solubility parameters of the mixtures. For mixtures of heavy oils, asphaltenes and solvents, they derived the following relationship between the solubility parameter of the mixture, δ_{mix} ($MPa^{0.5}$), and F_{RI}:

$$\delta_{mix} = 47.37F_{RI} + 4.08 \qquad (2.6)$$

Angle *et al.* (2006) also linearly correlated F_{RI} versus density for data of non-polar linear alkanes (C_5-C_{10}), toluene, bitumen, heavy oils, asphaltenes and maltenes at various concentrations as follows:

$$F_{RI}^{22^0C} = 0.02 + 0.309\rho^{22^0C} \qquad (2.7)$$

They suggest that the correlations are material-independent as long as the solvents are similarly nonpolar and the measuring temperature remains at 22°C.

As noted above, the refractive index is a good indicator of the ability of the oil to maintain a stable dispersion of asphaltenes (Wang *et al.*, 2001) and can also be accurately measured using conventional refractometers. However, the refractive index of the heavy crude oils, bitumen, asphaltenes and resins are outside the range of application of the refractometers. Hence to measure the refractive index of these opaque and viscous samples (ASTM D1747), the materials are diluted with light solvents. From the composition of the solution, the refractive index of the pure solvent and that of the solution, refractive index of the viscous material can be estimated (Riazi, 2005) by extrapolation if a simple volumetric mixing rule is applied. However, it is not obvious that mixtures of heavy oil fractions and solvents follow a volumetric mixing rule. Details of the mixing rules (regular solution or excess volume of mixing) are provided in Chapter 5.

2.5 Refining Processes

Refining processes separate crude oil into fractions which are subsequently converted/upgraded into various useful fuel products (*e.g.* petroleum gases, gasoline, diesel, kerosene), petrochemical feedstock and non-fuel products (*e.g.* solvents, waxes, lubricants, asphalt). Refining can generally be divided into separation (desalting, distillation, deasphalting), conversion (coking, catalytic cracking, hydrocracking), and finishing (hydrotreating, hydrogenation) processes (Riazi, 2005; Speight, 2007). Typically, the most desirable refinery products are the lower-boiling naphtha, gasoline, jet fuel, kerosene, and diesel fuel. The feedstock(s) processed by any

refinery determines its products yields and quality as well as the configuration of the refinery facilities. Conventional oils have greater yields of these valuable products whereas heavy oils and bitumen yield higher-boiling products that need to be converted into valuable lower-boiling products (Speight, 2007), increasing the complexity and cost of refining heavy oils and bitumen.

Typically, crude oil refining starts with desalting which dehydrates the crude to remove contaminants such as water-soluble minerals, salts and entrained solids that accompany the crude oil from the reservoir to the wellhead during recovery operation (Speight, 2007). To mitigate such operational problems as deposition and fouling, corrosion and catalysts poisoning, these contaminants need to be removed prior to introducing the crude to the main units. Desalting is a water-washing process which separates water-soluble and dense materials. Using heat and electric fields in the desalter, the brine solution and sediments are separated from the crude oil. The desalter is conveniently placed in the middle of the preheat train and operates best at 120 to 150°C (Kaes, 2000).

After desalting, the crude oil continues through the preheat train where it is heated to the desired distillation column inlet temperature (typically 330 to 380°C), depending on the crude composition (Kaes, 2000). The furnace outlet stream is fed directly into the fractionation column where it is separated into a number of fractions, each having a particular boiling temperature range (Haslego, 2010). At the top of the column, away from the furnace and exposed to cooler temperatures, a mixture of gases (C_3/C_4) and liquid naphtha (gasoline) is collected. Other draw-offs include heavy naphtha (boiling in the range of 150 to 205°C), kerosene (205 to 260°C), gas oils (260 to 400°C), and residue. Residue from the atmospheric crude distillation column is pumped to the vacuum distillation column where it is distilled at sub-atmospheric temperature to recover additional distillates, vacuum gas oils, and lubricating oils (Kaes, 2000; Haslego, 2010; Speight, 2007). Gas oil fractions (light and heavy) and vacuum residue undergo further treatment (hydrocracking, catalytic cracking, delayed coking and hydro processing) to produce lighter fractions which are eventually used for blending the final diesel products.

Cracking reactions break down large and complex organic molecules into simpler molecules by breaking carbon-carbon bonds at elevated temperatures (thermal cracking) or using catalysts (catalytic cracking and hydrocracking).

Thermal cracking is the simplest cracking process and entails the decomposition of the higher-boiling materials into lower-boiling (gasoline, gas oil) products at elevated temperatures of 455 to 540°C and pressure of 480 to 6700 kPa (Speight, 2007). Other products of the process are some highly volatile gases and non-volatile coke. In practice, the feedstocks for thermal cracking are the residuum from atmospheric and/or vacuum distillation of crude and heavier virgin oils. The cracked products and degree of cracking (conversion) for any feedstock are dependent on process temperature, residence time, and pressure. Three major applications of thermal cracking in the refineries are viscosity reduction (visbreaking), thermal gas oil production, and coking (Haslego, 2010).

Cataltyic cracking has progressively displaced thermal cracking for distillate oils conversion because it converts a substantial part of gas oils (>50%) to lower-boiling products and has better yields of higher-octane gasoline. Conversion is achieved by contacting gas oils with an active catalyst under suitable conditions of temperature, residence time and pressure (Speight, 2007). It is a low pressure (135 to 240 kPa), high temperature (483 to 552°C) operation (Kaes, 2000). The natural and synthetic clays (pellets, beads or powder) catalysts used can be arranged in fixed or fluidized beds. Most refineries use the fluidized bed catalytic cracking (FCC) units which have the advantage of enhanced contacting between catalysts and feed, reduced residence time, and less catalyst deactivation due to deposition of carbonaceous materials.

Hydrocracking is a hydrogenation process that complements the catalytic cracking with the added advantage of higher conversions, better distillate quality, removal of sulphur and nitrogen compounds, and a reduction in the amount of coke produced. The operating conditions in the hydrocracker are severe (6900 to 13800 kPa and 316 to 455°C). Hydrocracking feed stocks include diesel fuel, atmospheric and vacuum

gas oils, FCC cycle oils, coker cycle oils, and residual oils. The strategy is to crack the feedstock into lighter products and to saturate olefinic and aromatic compounds with hydrogen. Aromatic rings are very stable and would ordinarily not crack with standard catalytic cracking processes (Kaes, 2000). Hydrocracking reactors use fixed beds of catalysts (a mixture silica-alumina and rare-earth metals) which give both hydrogenation and cracking activity (Kaes, 2000). The hydrogen consumption of this process is high and requires a refinery to have additional hydrogen production capabilities.

The lighter fractions produced from cracking processes are further refined to improve products quality and meet specifications using chemical processes such as hydrotreating, reforming, isomerization, alkylation, and polymerization. .

Refining processes for extra heavy oils and bitumen may differ depending on the capabilities of the receiving refinery. Usually, these feedstocks need upgrading primarily to reduce the viscosity, remove constituents such as asphaltenes and heteroatoms, or "break down" the complex molecules into simpler and lower-boiling molecules. The limitation of processing these heavy feedstocks is often associated with the higher molecular weight constituents (asphaltenes) that contain the majority of the heteroatoms and are responsible for high yields of thermal and catalytic cokes (Speight, 2007). Surface upgrading processes include deasphalting, thermal cracking, catalytic cracking, delayed coking, and hydrogenation.

Thermal and catalytic cracking processes were described previously. Coking processes involve thermally cracking the heavy fractions (in the furnace) to produce lighter fractions (*e.g.* gasoline, fuel gas) and petroleum coke. In *delayed coking*, a severe form of thermal cracking, the coking reactions take place in a controlled environment (Kaes, 2000) to produce large amounts of petroleum coke. The aim is to produce a maximum of cracking products (distillates) whereby the heavy residue becomes so impoverished in hydrogen that it forms coke (Haslego, 2010).

The distillates from the hydrocracking, catalytic cracking and delayed coking processes of heavy oils and bitumen are good feedstock for conventional refineries. These distillates tend to be

unstable and need to be mildly hydrotreated if being pumped through pipelines to distant refineries. In cases where heavy oils or bitumen have already been upgraded to synthetic crude oil, the majority of the conversion and hydrotreating have already occurred. In most Alberta oil sands operations, fractionation, coking, and hydrocracking processes are used to improve the transportability and refining properties of extra heavy oils and bitumen.

Solvent deasphalting processes use an alkane (preferable C_3 to C_6) to precipitate asphaltenes from vacuum distillation residue at high solvent to oil ratio (typically > 4:1). A solvent deasphalting unit produces deasphalted oil (DAO), used as feedstock for a fluid catalytic cracking or hydrocracking unit, and the asphaltic residue used to produce asphalt or as a blend stock for heavy fuel oil (Speight, 2007; Wiehe, 2008). To maintain a liquid regime in the unit, operating conditions are 38 to 82°C and 2000 to 2800 kPa. Lately, deasphalting processes have been used in oil sands processes to obtain a product suitable for transportation and processing in a conventional refinery.

While currently most refining processes are performed at the surface, oil can also be partially processed in the reservoir. *In situ* upgrading with injected cataysts is an active area of research (Pereira *et al.,* 2013). *In-situ* combustion involves burning some of the in situ crude oil with injected air to sweep a bank of unreacted oil to the producers. Thermal cracking can take place near the combustion zone. Steam injection can also achieve temperatures at which the oil will slightly crack when the residence time of the steam in the reservoir reaches months and years. *In situ* electrical heating to upgrade bitumen has been tested in a field pilot (Vermeulen and McGee, 2000; Rassenfoss, 2012). Solvent based and solvent assisted processes such as VAPEX, ES-SAGD, and N-SOLV can partially deasphalt the bitumen before it is produced.

All of these surface and *in situ* reactive processes alter the chemistry of the petroleum feeds. For example, refinery streams from conversion processes contain more light components than native heavy oils and a more elaborate characterization methodology than SARA is required to ascertain the consequent changes that occurred to the constituents. Studies on asphaltenes from hydrocracked streams of thermal processes (Buch *et al.,* 2003; Groenzin *et al.,* 2007; S. Zhao *et*

al., 2007; Asaoka *et al.*, 1983) show that as the cracking temperatures increased, the molecular weights, number of aromatic rings as well as solubility of the asphaltenes decreased. It is expected that cracking would reduce the number of fused ring systems per molecule by cleaving alkyl side chains and rearranging aromatic rings. Similar property changes are also observed with thermal cracked asphaltenes (Lababidi, *et al.*, 2013).

These studies have focused mainly on asphaltenes constituents because of the problematic nature of these fractions during crude oil production and refining. However, as with asphaltenes, the structure and properties of saturates, aromatics and resins can be affected by thermal or hydro-processing. Thermogravimetric analysis of atmospheric and vacuum residue and their SARA fractions indicate that aromatic and resin fractions undergo cracking reactions from 320 to 480°C (Alvarez *et al.,* 2010; Huaser *et al.,* 2013). Saturates are not usually present in vacuum residues since they are completely volatilized at high temperatures (Hauser *et al.,* 2013). Nonetheless, some changes in saturate properties can be expected since some reaction products will fall into the saturate solubility class. It is necessary to determine how much the saturate, aromatic, and resin (SAR) properties change from native to reacted samples.

The regular solution approach has been successfully used to model asphaltene precipitation from upstream/native heavy oils (Buckley *et al.*, 1998; Alboudwarej *et al.*, 2003; Akbarzadeh *et al.*, 2005; Angle *et al.*, 2006 Tharanivasan *et al.*, 2010). However, for partially reacted/refinery streams, the chemistry and properties of the pseudo-components are expected to change. Therefore, fluids from downstream processes need to be fully characterized to verify whether or not previously developed correlations still apply.

Chapter Three: Experimental Methods

This chapter describes the characterization methodologies applied to the crude oil samples. It also describes the experimental methods for measuring the properties of the non-distillable fractions and solubility measurements of the saturate, aromatic and asphaltene fractions. The materials and apparatus are described and the experimental procedures are discussed.

3.1 Materials

Ten crude oil samples were characterized for this project. All the samples were supplied by Shell Global Solutions and are listed in Table 3.1. Of the native samples, three were dead bitumen, one was a bitumen diluted with unknown solvents, and one was the bottoms product from a vacuum distillation of a bitumen. The *in situ* samples were obtained from a thermal process and were partially cracked. The HOSbottoms sample was the bottoms product from a heavy oil stripper located after a hydrocracking process. One sample was of unknown origin and reaction history.

Table 3.1: Bitumen and crude oil samples used for this thesis.

Native Bitumen	*In Situ* Thermocracked Bitumen	Hydrocracked Bitumen	Unknown Origin
Arabian	26845-38	HOSBottoms	27-168-179
WC-B-CI	27034-113	-	-
WC-B-B2	27034-87	-	-
WC-DB-A2	-	-	-
WC-VB-B2	-	-	-

Technical grade (EMD) *n*-heptane, *n*-pentane, toluene and acetone were purchased from VWR International, LLC. These solvents were used for asphaltene precipitation, solids removal and SARA fractionation. SARA molecular weight measurements were carried out with Omnisolv high purity toluene (99.99%) obtained from VWR; sucrose octaacetate (98%), octacosane (99%)

and polystyrene standard (99%) were obtained from Sigma-Aldrich Chemical Company. Analytical solvents (Omnisolv toluene and Omnisolv heptane) used for solubility experiments, density measurements and refractive index measurements were purchased from VWR. Reverse osmosis water was provided by the University of Calgary water plant.

3.2 Characterization Methodology Materials

SARA fraction properties are to be determined for the heavier fraction of a crude oil which cannot be characterized directly from a GC analysis. Prior to isolation of the heavier feedstock into saturates, aromatics, resins and asphaltenes, the volatile components of a dead crude oil were removed by distillation; only distillation residua (bottoms) were used in this study.

3.2.1 Distillation

The advanced distillation curve, ADC, performed at atmospheric pressure was used to obtain the residua. The distillations were performed in a separate project at the University of Calgary (Ortiz, 2013) and therefore the methods are only briefly summarized below.

ADC was designed by Bruno (2006) and is an improved procedure from the standard ASTM D86 method. ADC allows the measurement of boiling points in the bulk of the fluid which corresponds to thermodynamic state points (normal boiling points). Accurate measurements of the volume of the condensed vapors are also obtained when material is collected above ~8 vol%, which is the minimum measurement of the ADC distillation. The distillation ends at a defined temperature before the crude oil cracks; in this case, the temperature was set at 300^{o}C. The ADC apparatus used in this work was obtained from the National Institute of Standards (NIST). The procedure is described in more detail elsewhere (Bruno, 2006; Ortiz, 2013)

Note, the 27034-113 and WC-B-C1 oil samples contained some residual water which was removed prior to distillation. The procedure used was similar to the ADC distillation but with the temperature controller set to 120^{o}C.

3.2.2 SARA Fractionation

SARA fractionation was performed using a modified ASTM D4124 procedure. SARA fractionation includes the following two main steps:

1. separation of alkane-insoluble asphaltenes and alkane-soluble maltenes with excess of n-alkane (*n*-pentane or *n*-heptane);
2. liquid chromatographic separation of maltenes into saturate, aromatic, and resin fractions.

The procedure is shown schematically in Figure 3.1 and each step is discussed in detail below.

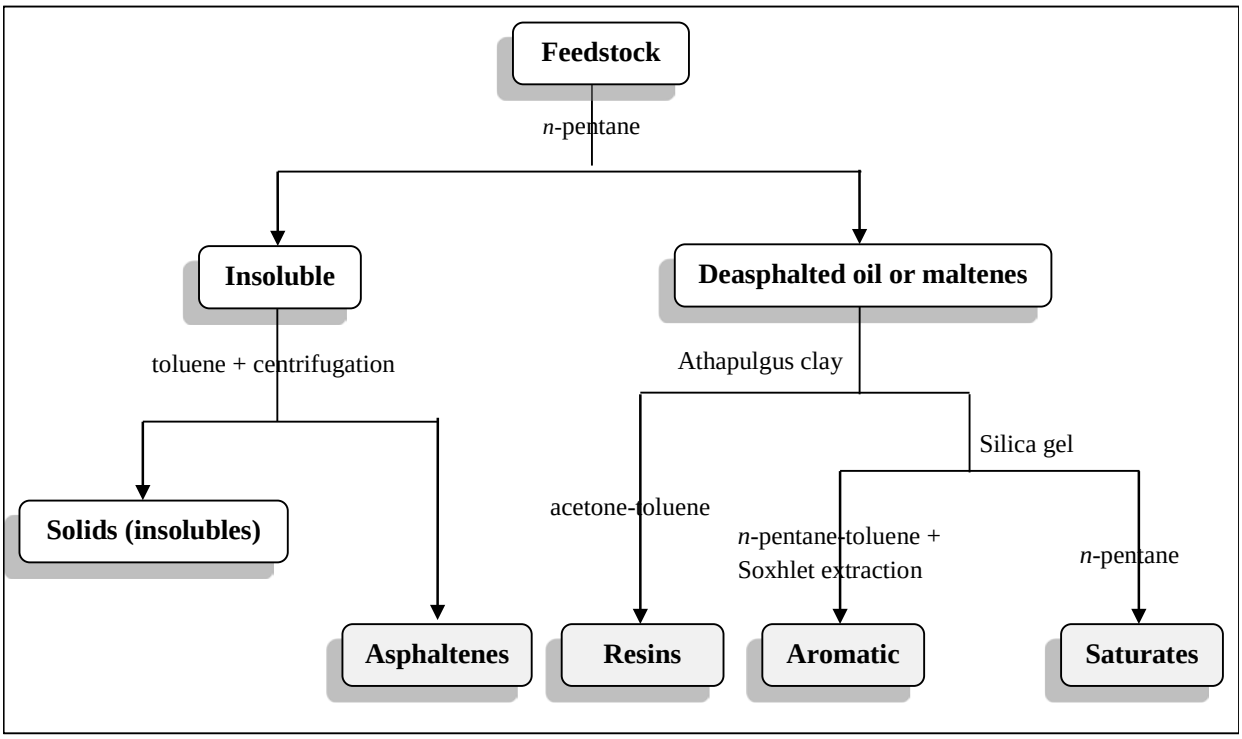

Figure 3.1: Schematic of SARA fractionation procedure

3.2.2.1 Asphaltene Precipitation from Bitumen/Heavy Oil

Asphaltenes were extracted from bitumen or heavy oil by mixing a ratio of 1 g of oil to 40 ml of *n*-alkane (typically 40 g of oil to 1600 ml of *n*-alkane). To ensure adequate mixing, the mixture

was sonicated in an ultrasonic bath for 60 minutes at room temperature and left to settle undisturbed for a total contact time of 24 hours. The supernatant of the mixture was filtered through Whatman #2, 24 cm diameter filter paper until approximately 25% of the solution (precipitant) remained in the beaker.

Then 10% of the original *n*-alkane volume was added to precipitant in the beaker and sonicated for 45 minutes. The mixture was left to settle overnight for a contact time of approximately 18 hours. The remaining mixture was filtered through the same filter paper. The filter cake was washed using 25 mL of *n*-alkane each time at least three times per day over five days or until the effluent from the filter was almost colorless. The filter cake was dried in a closed fume hood until the weight of the filter did not change significantly. The dry filter cake consisted of asphaltenes and inorganic solids which were collected with the precipitated asphaltenes. The material extracted with n-heptane is termed "C_7-asphaltenes+solids" and that extracted with n-pentane is referred to as "C_5-asphaltenes+solids". Asphaltenes+solids yields were reported as the mass of asphaltenes recovered after the washing and drying stages divided by the original mass of crude oil or residue used.

The filtrate consists of maltenes and *n*-alkanes. The maltenes were recovered by evaporating the *n*-alkane in a rotary evaporator. Roto-evaporation of *n*-heptane requires vacuum conditions and temperature between 40 to 60°C whereas *n*-pentane recovery generally does not require vacuum and the temperature should not exceed 50ºC. The maltenes were then placed in a fume hood and dried until the weight did not change significantly. Dried maltenes were labelled "C_5-maltenes" and "C_7-maltenes" according to the *n*-alkane used in the procedure.

Note, only C_5-maltenes were separated into saturates, aromatics, and resins because the liquid chromatography method is a standardized procedure designed for C_5-maltenes. The asphaltenes used for property measurements in this project were the *n*-heptane precipitate asphaltenes because the focus was on the self-associating components which are believed to be concentrated in the C_7-asphaltenes.

3.2.2.2 Solids Removal from Asphaltenes

The "solids" that co-precipitate with the asphaltenes include mineral material like sand, clay, and ash, as well as adsorbed organics. In the case of downstream samples, solids may include traces of catalysts and other solids present in different stages and coke, all produced during the refining of crude oil. These solids do not affect the onset or percentage of precipitated asphaltenes (Mitchell *et al.*, 1973, Alboudwarej *et al*., 2003).

Solids were removed from asphaltenes by using a previously established centrifugation technique (Sztukowski and Yarranton, 2005). A solution of approximately 10 g/L of C_7-asphaltenes+solids in toluene was prepared at room temperature; usually 2.0 g of asphaltene in 200 mL of technical toluene. The mixture was sonicated in an ultrasonic bath for 20 minutes or until all asphaltenes were dissolved, and then the solution was settled for 60 minutes. The mixture was divided into centrifuge tubes and centrifuged at 4000 rpm for 6 minutes. The supernatant (solids-free asphaltene solution) was decanted into a beaker and set into the fume hood to dry for 4 days or until constant weight, and then solids-free asphaltenes were recovered and stored in a jar. The non-asphaltenic solids, corresponding to the remaining material in the centrifuge tubes, were dried and weighed to calculate the solids content as the mass of solids divided by the mass of the original asphaltene sample. The asphaltenes extracted with *n*-heptane and treated with toluene to remove solids are termed "C_7-asphaltenes".

3.2.2.3 Chromatographic/Adsorption Separation of Saturates, Aromatics and Resins

The chromatographic/adsorption separation apparatus includes two glass columns connected in series. In the first column, resins are adsorbed onto activated Attapulgus clay. In the second column, aromatics are adsorbed onto silica gel. The saturates elute through both columns. The adsorbed resins and aromatics are then eluted separately with appropriate solvents. The maltenes used for the adsorption separation were the C_5-maltenes.

For a typical SAR fractionation, approximately 300 g of Attapulgus clay and 250 g of silica gel were activated in an oven at 150^0C and full vacuum overnight (or more) for packing the

columns. The lower column was packed with 200 g of silica gel and topped with 50 g of clay. Two upper columns were packed with 100g of clay each. The packings were tapped with rubber mallet to tightly and evenly pack the adsorbents. Glass wool was placed at the top of the columns to diffuse the eluent/sample flows. To begin a separation, one of the upper columns was connected to the lower column with clamps and the entire apparatus was held vertical.

Two (2) 200 g/L solutions of C_5-maltenes in pentane, typically 5 g maltenes in 25 ml of *n*-pentane, were prepared and sonicated until homogenous. To collect the saturate fraction, the upper column was first wet with 25 mL of *n*-pentane and then the diluted maltene solution was poured through it. 480 mL of *n*-pentane was gradually run through the column from a separatory funnel for full elution. The first upper column was detached, the second upper column was attached to the same lower column, and the same procedure was repeated. Then, the columns were separated. By definition, the saturates are the material that elutes through both columns.

Aromatics adsorb on the lower column packed with silica gel and were eluted using a mixture of of *n*-pentane-toluene (200 mL:200 mL). The elutions were performed with the upper and lower columns connected and a total of 800 mL of each solvent were used for each upper column. Using the Soxhlet apparatus, the residual aromatics in the lower column were recovered by refluxing toluene through the silica gel.

The resins adsorb on the upper column packed with pre-activated clay. To collect the resin fraction, the two upper columns were connected and the resins were eluted twice with a mixture of acetone-toluene (200 mL:200 mL).

Solvents were recovered from each of the eluted fractions in a roto-vaporator. Then, each recovered SAR fraction was weighed and the SARA composition of the sample determined.

The SARA compositions of the samples characterized for this thesis are presented in Table 3.2.

Table 3.2: SARA analysis of the heavy oils/bitumen characterised for this thesis.

Sample	wt%			
	Saturates	**Aromatics**	**Resins**	**Asphaltenes***
WC-B-B2	17.1	44.0	19.4	19.4
Arabian	35.3	41.2	15.6	7.8
WC-DB-A2	21.1	44.9	23.4	10.6
WC-B-C1	14.7	45.0	21.2	19.1
WC-VB-B2	5.3	37.4	20.1	37.2
27168179	46.4	31.5	17.2	4.8
26845-38	17.6	46.5	20.7	15.2
27034-87	21.1	52.2	15.2	11.5
27034113	21.3	49.6	19.8	9.2
HOSB	19.7	47.3	17.3	15.7

* C_5-asphalthenes

3.3 Property Measurements

The properties determined for the SARA fractions were molecular weight, density, refractive index and solubility properties. The apparatus and experimental procedures are outlined below.

3.3.1 Molecular Weight Measurement

Vapor Pressure Osmometry (VPO) was used to measure asphaltene molecular weight. The method is based on the change in vapour pressure when a solute is added to a solvent. Two separate thermistors are set in a chamber saturated with pure solvent vapor. By means of syringes, droplets of the solvent are placed on one of the thermistors and droplets of the solution (known concentration of solute in the same solvent) are placed on the other thermistor. Since the solution has a lower vapour pressure than the solvent, solvent from the chamber atmosphere condenses into the solution. The heat of condensation warms the solution droplets until the

vapour pressure is the same as that of the surroundings. The temperature/voltage difference is measured and recorded.

Theoretically, the solvent droplets on the other thermistor are in equilibrium with the solvent in the chamber. In reality, however, convection and other effects cause minute disturbances in the system, the effects of which can be minimized by subtracting the voltage of the solvent thermistor from that of the solution thermistor (Klaus H.A *et al*, 1995). The voltage difference is related to the molecular weight of the solute, M_2, as follows (Peramanu *et al*., 1999):

$$\frac{\Delta V}{C_2} = K\left(\frac{1}{M_2} + A_1 C_2 + A_2 {C_2}^2 + ...\right) \qquad (3.1)$$

where ΔV is the voltage difference between the thermistors, C_2 is the solute concentration, K is the proportionality constant, and A_1 and A_2 are coefficients arising from the non-ideal behavior of the solution. Note that the voltage reading includes a correction for the blank run reading (when only solvent is added to both thermisters) as follows:

$$\Delta V = \Delta V_{meas} - \Delta V_{blank} \qquad (3.2)$$

where the subscripts *meas* and *blank* indicate the measurement run and the blank run, respectively.

In most cases, at low concentrations, most of the higher order terms become negligible, and Equation 3.1 reduces to:

$$\frac{\Delta V}{C_2} = K\left(\frac{1}{M_2} + A_1 C_2\right) \qquad (3.3)$$

For the calibration, the molecular weight of the solute is known, and the proportionality constant, *K*, was calculated by extrapolation in a plot of $\Delta V/C_2$ versus C_2 to zero concentration. For a non-ideal solution, the molecular weight of an unknown solute is also calculated from the intercept of a plot of $\Delta V/C_2$ versus C_2 this time solving for M_2.

For an ideal system however, the second term in Equation 3.3 is zero and $\Delta V/C_2$ is constant. In this case, the molecular weight is determined from the average $\Delta V/C_2$ as follows:

$$M_2 = \frac{K}{\left(\Delta V / C_2\right)} \qquad (3.4)$$

The use of the ideal and non-ideal calculations is discussed in Chapter 5.

Procedure

The molecular weights of the SAR fractions were measured using a Jupiter Model 833 Vapor Pressure Osmometer with toluene as the solvent at 50°C. This instrument has a detection limit of $5x10^{-5}$ mol/L when used with toluene or chloroform. The instrument was calibrated with sucrose octaacetate (679 g/mol) as solute and octacosane (395 g/mol) was used to check the calibration.

The first step in preparing for a VPO run was to clean the chamber assembly. Five solutions of the sample ranging from 2 g/L to 20 g/L (depending on the expected MW of the sample) were prepared (typically 2 to 10g/L for saturates and aromatics and 2 to 20 g/L for resins). Prior to running the samples, a blank control run with pure solvent (toluene) in both syringes was done. The voltage output on the panel was adjusted to get a reading between 0 and 5 on the meter for the blank run. The voltage output readings were taken at 5 minutes intervals (typically for at least four constant values) and the average value taken. Then, one of the solvent syringes was replaced by a sample syringe filled with the most dilute solution. Drops of the solvent and solution were placed on the thermistor within the chamber. The voltage reading was recorded after stabilization (5 minutes). Four or more readings were taken for the same concentration and the average calculated.

During the molecular weight measurements, there were slight fluctuations in the voltage at any given condition, likely caused by slight variations in local temperature and atmospheric pressure. Therefore, two readings were taken at each concentration to obtain an accurate voltage response for that concentration. The measured molecular weight of octacosane was within 3% of the correct value. The repeatability of the molecular weight measurements was approximately ±12% for all the samples.

3.3.2 Density Measurements

Densities were measured at 20°C and atmospheric pressure with an Anton Paar DMA 4500M density meter. The measurement is based on the oscillating U-tube method. The sample introduced into the U-shaped borosilicate glass tube is excited to vibrate at its characteristic frequency. The characteristic frequency changes depending on the density of the sample. The density is calculated from the quotient of the period of oscillation of the U-tube and the reference oscillator:

$$density = KA \times Q^2 \times f_1 - KB \times f_2 \qquad (3.5)$$

where *KA, KB* are apparatus constants, Q is quotient of the period of oscillation of the U-tube divided by the period of oscillation of the reference oscillator, f_1 and f_2 are corrections terms for temperature, viscosity and non-linearity. The product of the constants and the correction factors were determined by calibration over a range of temperatures and pressures. Reverse osmosis water and air were used for the calibration.

The instrument precision was ±0.00001 g/cm³ with an accuracy of ±0.00005 g/cm^3. The major source of error in density measurements are gas bubbles in the measuring cell but the DMA 4500M density meter is equipped with automatic bubble detection and a visual inspection of the measuring cell using a real time camera with zoom function (U-View). Measurements can also be performed at different temperatures using one sample input without the concern of evaporation losses/leaks in the U-tube. Densities of saturates and aromatics were also measured at 40^{o}C and 60^{o}C.

Procedure

The saturate and aromatic densities were measured directly and also were calculated indirectly from the densities of mixtures of the given fraction in toluene or heptane. The repeatability of the direct density measurements were ±0.83 kg/m³ and ±0.94 kg/m³ for saturates and aromatics respectively. Resin and asphaltene densities could not be measured directly and were only measured in solutions of toluene. Concentrations ranging from 2 up to 60 g/L (typically 20 g/L) were used for resins and asphaltenes density measurements. Density values were extrapolated

from the binary mixtures' densities by assuming either regular or excess volume solutions are formed. The densities calculated indirectly from solutions have additional uncertainties in the measurement from concentration errors. The repeatability of the indirect densities (calculated assuming no excess volume of mixing) was found to be ±5.8 kg/m³ for resins and ±23 kg/m³ for asphaltenes.

If the mixture of a SARA component and solvent forms a regular solution, the density of the solution is given by:

$$\frac{1}{\rho_{mix}} = \frac{w_1}{\rho_1} + \frac{w_2}{\rho_2} \tag{3.6}$$

where ρ_{mix}, ρ_1, and ρ_2 are the mixture, solvent, and SARA component density (kg/m³), respectively, and w_1 is the SARA component mass fraction. The density of SARA component can be determined indirectly from a plot of the specific volume (the inverse of the mixture density) versus the component mass fraction, as follows:

$$\rho_2 = \frac{1}{S + I} \tag{3.7}$$

where *S* and *I* are the slope and intercept respectively in the specific volume plot.

If the mixture does not form a regular solution; that is, there is an excess volume of mixing, then the mixture density can be expressed as follows:

$$\frac{1}{\rho_{mix}} = \frac{w_1}{\rho_1} + \frac{w_2}{\rho_2} - w_S w_2 \left(\frac{1}{\rho_1} + \frac{1}{\rho_2} \right) \beta_{12} \tag{3.8}$$

where β_{12} is a binary interaction parameter between the SARA component and the solvent. The last term in the expression is the excess volume of mixing. The use of the regular solution and excess volume mixing rules is discussed in Chapter 5. In this case, either the interaction parameter or the density of a component can be determined from a rearrangement of Eq. 3.8.

3.3.3 Refractive Index Measurement

The refractive indexes of SARA fractions were measured with an Anton Paar Abbemat HP refractometer with a sodium D lamp at a reference temperature of 20°C and a wavelength of 589.3 nm. The apparatus includes a measuring prism made of a glass of a high refractive index (YAG -Yttrium-Aluminum-Garnet). The refractometer is designed to be used with samples with lower refractive index than the prism. A liquid sample in contact with the prism is illuminated by an LED and the critical angle of the total reflection at 589.3 nm sodium D wavelength is measured with a high-resolution sensor array. The refractive index (n_D) is calculated from this value. The instrument has an accuracy of 0.00002 nD.

To measure the refractive index of a liquid sample, it was placed on the measuring (refractive) prism and covered with a lid. Some time was usually required for the sample to attain the prism temperature and to obtain a constant reading. Constant readings were taken 5 seconds after temperature equilibration (typically 30 seconds for light/volatile samples and 60 seconds for viscous samples). The measuring prism was cleaned with solvent (toluene or acetone) and dried before another sample was applied.

Rather than using the refractive index directly, most mixing rules and correlations are based on a function of the refractive index, FRI, given by:

$$FRI = \frac{n_D^2 - 1}{n_D^2 + 2} \tag{3.9}$$

Therefore, all of the measured refractive indices were converted to FRI and only FRI are reported unless otherwise indicated.

The saturate and aromatic FRI were determined from direct measurements of the refractive index and also were calculated indirectly from the FRI of mixtures of the given fraction (2 to 20 g/L) in toluene or heptane. Very viscous saturates and aromatics were warmed up to 60^{o}C in a water bath prior to measurements to facilitate sample placement. The repeatability of the FRI from direct measurements was ±0.00036 and ±0.00025 for saturates and aromatics, respectively. Resin

and asphaltene refractive indices could not be measured directly and were only measured indirectly in solutions of toluene. The FRI calculated indirectly from solutions have additional uncertainties in the measurement from concentration errors. The repeatability of the indirect FRI (calculated assuming regular solution behavior) was found to be ±0.0043 for saturates and aromatics, ±0.0043 for resins, and ±0.0058 for asphaltenes Measurements were taken for all fractions at 20°C and additional measurements were performed for some saturates and aromatics at 40°C and 60°C.

The FRI of a mixture is often taken as the volume average of the FRI of the components, which for a binary mixture is given by:

$$FRI_{mix} = \phi_1 FRI_1 + \phi_2 FRI_2 \tag{3.10}$$

where ϕ is volume fraction. Some mixtures did not follow this rule and were fitted with an analogy to the excess volume mixing rule given by:

$$FRI_{mix} = \phi_1 FRI_1 + \phi_2 FRI_2 - \phi_1 \phi_2 (FRI_1 + FRI_2)\beta_{12}^{*} \tag{3.11}$$

where β_{12}^{*} is the binary interaction parameter for the refractive index. The use of these mixing rules is discussed in Chapter 5.

3.3.4 Asphaltene Solubility Measurements

Asphaltene precipitation (solubility) measurements were performed in mixtures of 10 g/L of asphaltenes in toluene/*n*-alkane, saturates/toluene and aromatics/*n*-heptane, and mixtures of bitumen and *n*-alkane. These experiments were mass-based and all measurements were taken at 21°C and atmospheric pressure.

3.3.4.1 Asphaltene Precipitation Measurements in Heptol

Typical heptane/toluene (heptol) ratios range from 0.4 to 1.0 (vol/vol). To perform a standard solubility experiment, the required mass of C_7 asphaltenes (*e.g.* 0.1g) was first dissolved in the specified mass of toluene by sonicating for 20 minutes. The appropriate amount of *n*-heptane was then added and the mixture was sonicated for 45 minutes and left to settle for 24 hours. The

mass of the solution vials were monitored to account for evaporation losses. After 24 hours, the mixture solution was centrifuged at 4000 rpm for 6 minutes to separate supernatant and precipitant. The supernatant was collected into marked vials with fine plastic pipettes (for refractive index measurements of the soluble asphaltene fraction). The vials were sealed with Teflon tapes to reduce evaporation losses.

Refractive index readings for the soluble asphaltene fraction were taken 5 seconds after temperature equilibration and at 30 seconds. These FRI measurements were used to determine asphaltene yields using a new procedure as will be described in Chapter 6. Note the refractive index of the solvents (*e.g.* toluene/*n*-alkane, saturates/toluene and aromatics/*n*-heptane) were either measured directly or estimated using the refractive index and volume fraction of the individual constituents for every solubility measurement.

The sediments (precipitated asphaltenes) at the bottom of the vials were washed with the same solvent (heptol) mixtures, sonicated for 5 minutes and centrifuged at 4000 rpm for 6 minutes. Subsequent supernatants (from washing) were decanted with plastic pipette and discarded. Washing was repeated until the supernatant was colourless. The recovered asphaltenes were dried in an oven under vacuum at 60^0C until the weight was constant. Gravimetic asphaltene precipitation yields were calculated as the mass of precipitated asphaltenes divided by the initial mass of asphaltenes. The data are reported as an asphaltene solubility curve, a plot of the yield of precipitated asphaltenes versus the mass fraction of the poor solvent. The repeatability for this experiment was ±3 wt% yield.

3.3.4.2 Asphaltene Precipitation in Saturates/Toluene or Aromatics/n-Heptane

The solubility experiments for saturates and aromatics required a few adjustment to the standard asphaltene-heptol experiments. The model solvents consisted of saturates/toluene and aromatics/*n*-heptane. While maintaining the concentration of the solutions at 10g/L, the total solvent volume were adjusted to < 2mL to accommodate the low available volumes of the saturate and aromatic fractions. The procedure for the experiments involving saturates/toluene

was almost the same as described above; however, the total solvent volume was 1 to 2 mL (for approximately 0.01 to 0.02g asphaltenes) and precipitants were washed with only heptane.

Asphaltene solubility measurements in aromatics/*n*-heptane required further modifications because it was not possible to dissolve asphaltenes in the aromatic fractions at room temperature. Therefore, the mixing temperature and time were increased to enable dissolution. A precipitation method was used instead. Typical *n*-heptane /aromatics ratios used were 0.5 to 0.9 (vol/vol) with the total solvent volume of $\leq$ 2 mL (for approximately 0.02 g asphaltenes). To perform the solubility experiment involving aromatics, the specified mass of asphaltenes was added to required mass of aromatics. The corresponding mass of *n*-heptane was then added. The mixture was sonicated in a 60ºC water bath for upwards of 90 minutes (until the asphaltenes were dissolved) for proper mixing. Once the asphaltene was dissolved in the solvents, the solution was allowed to cool to room temperature and settle for 24 hours. After 24 hours, the total mass of the solution was recorded to account for heptane losses. The solution was then centrifuged, the supernatant collected and refractive index of supernatant measured as discussed previously. Washing of the precipitated asphaltene-solvent mixture was carried out using a solution of 90 vol% *n*-heptane and 10 vol% toluene because washing with an aromatics-heptane mixture failed to remove entrained aromatics and gave apparent yields above 100%. The recovered asphaltenes were dried and fractional yield calculated. The yields in all cases were all determined on a solids-free asphaltenes. The repeatability of the yields was ±7 wt% and ±8 wt% for saturates and aromatics, respectively.

One concern with using the “precipitation method” versus the “solubility method” is a hysteresis between the two measurements as observed by Yarranton and Masliyah (1996). Therefore, the two methods were compared for solutions of asphaltenes in toluene/*n*-heptane, Figure 3.2. At the conditions of the tests performed in this thesis, the hysteresis is small (approximately 2 wt% yield). Therefore, the precipitation method was accepted as an alternative to the standard solubility method for asphaltene solubility measurements in aromatics/ *n*-heptane for the purposes of this thesis.

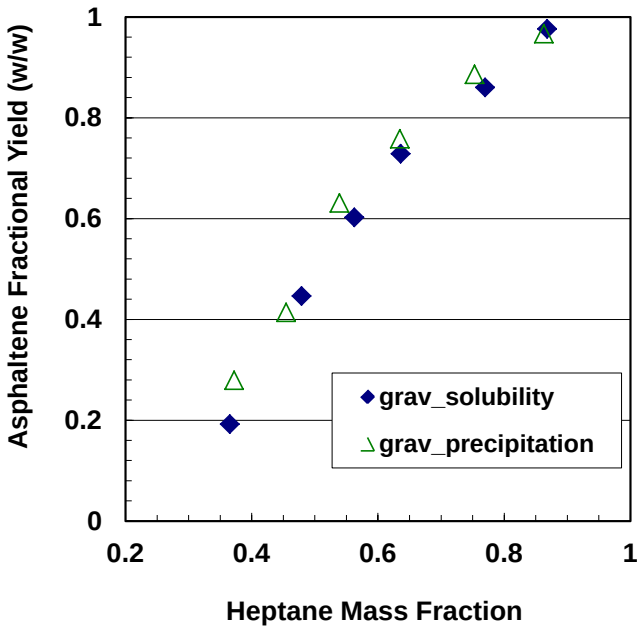

Figure 3.2: A comparison of the precipitation and solubility methods for asphaltene gravimetric yield measurements for solutions of 10 g/L asphaltenes in *n*-heptane and toluene.

Chapter Four: The Modified Regular Solution Model

Asphaltene precipitation modeling for this thesis is based on a previously developed regular solution approach. This chapter outlines the model and presents previously developed property correlations. The modifications made to the model (and property correlations) for this thesis will be presented in Chapter 7. The full model for diluted heavy oils is presented to illustrate the role of the saturate, aromatic, and resin solubiltity parameters. Only precipitation of asphaltenes from solutions including combinations of toluene, heptane, saturates, and aromatics are modeled in this thesis.

4.1 Modified Regular Solution Model

Hirschberg et al. (1984) modified regular solution theory for asphaltene solubility in mixtures to include an enthalpy contribution from Scatchard-Hildebrand solubility theory and a Flory-Huggins entropic contribution from the difference in molecular sizes. In the modified regular solution model, further refined by others (Alboudwarej *et al.*, 2003; Akbarzadeh *et al.*, 2005; Yarranton *et al.*, 2007), a liquid-liquid equilibrium is assumed to exist between the heavy liquid phase (asphaltene-rich phase including asphaltenes and resins) and the light liquid phase (solvent-rich phase including all components). The equilibrium ratio, K_i^{hl}, for any given component is given by:

$$K_i^{hl} = \frac{x_i^h}{x_i^l} = exp\left\{ \begin{array}{l} \frac{v_i^h}{v_m^h} - \frac{v_i^l}{v_m^l} + ln\left(\frac{v_i^l}{v_m^l}\right) - ln\left(\frac{v_i^h}{v_m^h}\right) + \\ \frac{v_i^l}{RT}\left(\delta_i^l - \delta_m^l\right)^2 - \frac{v_i^h}{RT}\left(\delta_i^h - \delta_m^h\right)^2 \end{array} \right\} \qquad (4.1)$$

where x_i^h and x_i^l are the heavy and light liquid phase mole fractions, R is the universal gas constant, T is temperature, v_i and δ_i are the molar volume and solubility parameter of component i in either the light liquid phase (l) or the heavy liquid phase (h), and v_m and δ_m are the molar volume and solubility parameter of either the light liquid phase or the heavy liquid phase. Once the equilibrium ratios are known, the phase equilibrium is determined using standard techniques (Rijkers and Heidemann, 1986; Alboudwarej *et al.*, 2003). Note, in the phase equilibrium

calculations, it was assumed that only asphaltenes and resins partitioned to the heavy phase. To use this model, the mole fraction, molar volume, and solubility parameter of each component (or pseudo-component in the mixture must be specified.

4.2 Fluid Characterization

Characterization entails the division of fluids into pure components (the solvents) and pseudo-components, and then assigning properties to each component. The fluid systems of interest in this thesis are:

a) solvent diluted crude/heavy oils
b) asphaltene in solvents (pure solvents, saturates, aromatics)

For heavy oil, the oil is divided into pseudo-components based on a SARA analysis (saturates, aromatics, resins, and asphaltenes). The SARA analysis provides mass fractions. The mole fractions of the components and pseudo-components are determined from the masses of the solvent and bitumen, the SARA analysis, and the measured or estimated molar masses. The characaterization of the asphaltenes and properties of n-alkane solvents and the SARA fractions are described below.

4.2.1 Asphaltene and Resin Characterization

Saturates, aromatics, and resins are each treated as a single pseudo-component. However, it has proven necessary to divide the asphaltene fraction into several pseudo-components in order to accurately predict yields. The asphaltenes are considered to be macromolecular aggregates of monodisperse asphaltene monomers. Therefore, asphaltenes are further divided in fractions of different molecular weight using a Gamma function:

$$f(M) = \frac{1}{\Gamma(\beta)}\left[\frac{\beta}{\left(\overline{M} - M_m\right)}\right]^{\beta}\left(M - M_m\right)^{\beta-1}\exp\left[\frac{\beta(M_m - M)}{(\overline{M} - M_m)}\right] \qquad (4.2)$$

where M_m and $\overline{M}$ are the monomer molecular weight and the average molecular weight of asphaltenes, $f(M)$ is the mass frequency of the given molecular weight, and β is a parameter which determines the shape of distribution. The asphaltenes were discretized into 30 sub-

fractions ranging up to 30,000 g/mol. The monomer molecular weight is taken as 1,800 g/mol and the average molecular weight is measured using vapour-pressure osmometry method for asphaltenes in solvents or used as a fitting parameter for asphaltenes in crude oil. The recommended values for β are from 2 to 4. More details of the asphaltene discretization from the gamma function can be found in Alboudwarej *et al.* (2003) and Akbarzadeh *et al*. (2004).

The density of each asphaltene pseudo-component is determined from the following correlation (Barrera *et al.*, 2012):

$$\rho=1100+100\left(1-\exp\left(-\frac{M}{3850}\right)\right) \tag{4.3}$$

where ρ is the density (kg/m³) and M is the molecular weight (g/mol) of the asphaltene cut at 10g/L asphaltene concentration. The molecular weight of an asphaltene pseudo-component is the associated molecular weight (rM_m) of that pseudo-component as determined from the gamma distribution. r is the average aggregation number. The molar volume of an asphaltene pseudo-component is simply the ratio of the molecular weight to the density:

$$v = \frac{1000M}{\rho} \tag{4.4}$$

where v is the molar volume (cm^3/mol) of an asphaltene sub-fraction.

The solubility parameter of each asphaltene pseudo-component is determined from the following correlation (Barrera *et al*., 2012):

$$\delta = \left(A\rho\left(cMW^{d}\right)\right)^{1/2} \tag{4.5}$$

where δ is the solubility parameter expressed in $MPa^{0.5}$, A is approximately equal to the monomer heat of vaporization (kJ/g) and is given by:

$$A = \left(-7.5\times10^{-4}T + 0.579\right) \tag{4.6}$$

and c and d are parameters specific to the asphaltene source. Parameter d is set to 0.0495 and c must be tuned based on asphaltene yield data. Both the molar volume and the solubility parameter of the asphaltenes were assumed to be independent of pressure.

It was assumed that resins did not self-associate and the measured molecular weight was taken to be a constant. Since the asphaltene and resin monomers are a continuum of polynuclear aromatics, the property correlations developed for the asphaltenes were also used for the resins.

4.2.2 Saturates and Aromatics Properties

Molecular weights and densities were measured for saturates and aromatics from each bitumen or heavy oil. However, if the molar volumes of the individual saturate and aromatic fractions are unavailable, average molar masses and densities from Table 4.1 can be used. Akbarzadeh *et al*. (2005) demonstrated that using the average values of density, molar mass, and solubility parameter for the saturate, aromatic and resin fractions, rather than individual values for each oil, did not introduce significant error to the model predictions.

Table 4.1: Average molecular weight, density and solubility parameter for saturates, aromatics and resins.

Fraction	Molecular Weight at 50°C (g/mol)	Density at 23°C (kg/m^3)	Solubility Parameter at 23°C ($MPa^{0.5}$)
saturates	460	880	15.9
aromatics	522	990	20.2
resins	1040	1044	19.6

Akbarzadeh *et al.,* 2005 also developed the following correlations to predict the change in density (and therefore molar volume) with temperature:

$$\rho_{sat} = 1078.96 - 0.6379T \quad (4.7)$$

$$\rho_{aro} = 1184.47 - 0.5942T \quad (4.8)$$

where ρ_{sat} and ρ_{aro} are the densities of Athabasca saturates and aromatics in kg/m^3, respectively, and T is the temperature in K.

The solubility parameters of saturates and aromatics were determined by Akbarzadeh et al, 2005 by fitting the model to asphaltene solubility data for mixtures of asphaltenes and solvents. They developed the following correlations for the solubility parameters of saturates and aromatics:

$$\delta_{sat} = 22.381 - 0.0222T \tag{4.9}$$

$$\delta_{aro} = 26.333 - 0.0204T \tag{4.10}$$

where δ_{sat} and δ_{aro} are the solubility parameters of saturates and aromatics in $MPa^{0.5}$ and T the temperature in Kelvin. The saturate and aromatic densities and solubility parameters are assumed to be independent of pressure.

4.2.3 Solvent Properties

The molar masses and densities of the pure components are known or can be determined using well-established Hankinson-Brobst-Thomson (HBT) method (Reid *et al.*, 1987). Solubility parameters for the solvents at 25°C were calculated as follows (Tharanivasan et al, 2007):

$$\delta_{25°C} = \left(\frac{\Delta H^{vap*}_{25°C} - 298.15R}{v_{25°}} \right)^{1/2} \tag{4.11}$$

where δ is the solubility parameter in $MPa^{0.5}$, ΔH^{vap*} is the molar heat of vaporization (J/mol), R is the universal gas constant in J/molK, v is the molar volume in cm^3/mol, and subscript 25°C indicates that the property is determined at 25°C. For n-alkanes, the heat of vaporizations were determined from the following correlations:

Carbon Number ≤ 4:

$$\Delta H^{vap*}_{25°C} = 3492.8 + 276.54M + 0.52400M^2 \tag{4.12}$$

Carbon Number ≥ 5:

$$\Delta H^{vap*}_{25°C} = 103.65 + 368.7M - 0.06030M^2 \tag{4.13}$$

Note that ΔH^{vap*} is slightly different than the actual heat of vaporization but fits the solubility parameters at 25°C from the CRC Handbook of Solubility Parameters (Barton, 1991) to within 0.01 $MPa^{0.5}$.

It was assumed that pressure only affected the molar volume and therefore the solubility parameter at any pressure is given by:

$$\delta_{25°,P} = \delta_{25°C}\left(\frac{v_{25°C}}{v}\right)^{1/2} \tag{4.14}$$

The effect of temperature is accounted for using an expression developed for n-alkanes by Akbarzadeh *et al.*, 2005.

$$\delta = \delta_{25°C}\left(\frac{v_{25°C}}{v}\right)^{1/2} - 0.0232(T - 298.15) \tag{4.15}$$

4.3 Model Implementation

The application of the modified regular solution model to predict the onset and amount of asphaltene precipitation from diluted heavy oils or bitumen is summarized in the following algorithm (Akbarzadeh *et al*., 2005):

1. Obtain the SARA analysis of the oil sample. Normalized fluid composition is calculated based on the solvent-heavy oil dilution ratio and the amount of SARA fractions (wt %). Note heavy oil-solvent mixtures are divided into solvents and SARA fractions.
2. Calculate the liquid molar volumes and solubility parameters of the relevant *n*-alkane(s) as described in Section 4.2.3.
3. If the SARA properties (molar mass and density) are not available, use the average properties presented in Table 4.1. Calculate the densities of saturates and aromatics at temperatures other than 23°C from Equations 4.7 and 4.8, respectively. Estimate solubility parameters of saturates and aromatics at other temperatures from Equations 4.9 and 4.10, respectively.
4. Subdivide asphaltenes into sub-fractions using the gamma distribution, Equation 4.2. The parameters required for the gamma function are average molar mass of asphaltenes (measured) and the shape factor β. With a given asphaltene average molar mass and shape factor, the molar mass of each asphaltene sub-fraction is calculated as the arithmetic average of the highest and lowest molar mass of that particular sub-fraction.

5. Determine density and solubility parameters of asphaltene (and resin) sub-fractions from the calculated molar masses using Equation 4.3 and 4.5, respectively.
6. Perform equilibrium calculations using Equation 4.1 and standard techniques (Rijkers and Heidemann, 1986; Alboudwarej *et al*., 2003). A bisection method is used for model convergence.
7. Calculate the amount of asphaltene precipitation at desired conditions (temperature, pressure, solvent mass fraction).
8. Check the accuracy of model predictions with experimental data if available. If necessary, adjust the average asphaltene molar mass to obtain a better fit.

To fit asphaltene-solvents solubility data with the model, all the model parameters are fixed except the average aggregation number, r and the shape factor, parameter β of molecular weight distribution. In the case of asphaltenes in pure solvents, the average aggregation number can be determined from the average measured molecular weight using the vapour pressure osmometer (Yarranton *et al.,* 2007). A β value of 2.5 is recommended. An example of the model predictions for asphaltenes in solutions of toluene and n-heptane is provided in Figure 4.1.

Unlike the asphaltene-solvent systems, the average molar mass of the asphaltenes cannot be measured in a mixture like crude oil. Therefore, the average associated molar mass of the asphaltenes must be estimated, that is the average aggregation number is used as a fitting parameter to match the asphaltene yield from a crude oil diluted with n-alkane. Thereafter, the average associated molar mass is fixed. A β value of 3.5 is recommended for crude /heavy oil systems. An example of the model fit (n-heptane) and predictions (other n-alkanes) for n-alkane diluted bitumen is provided in Figure 4.2.

This proposed asphaltene precipitation model is valid for heavy oils and bitumen diluted with liquid *n*-pentane and higher carbon number alkanes at temperatures from 0 to 100°C and pressures up to 7MPa. Since the model is based on property correlations determined for only this range of conditions and because only a liquid–liquid phase transition is considered, caution is recommended in extrapolating beyond these conditions.

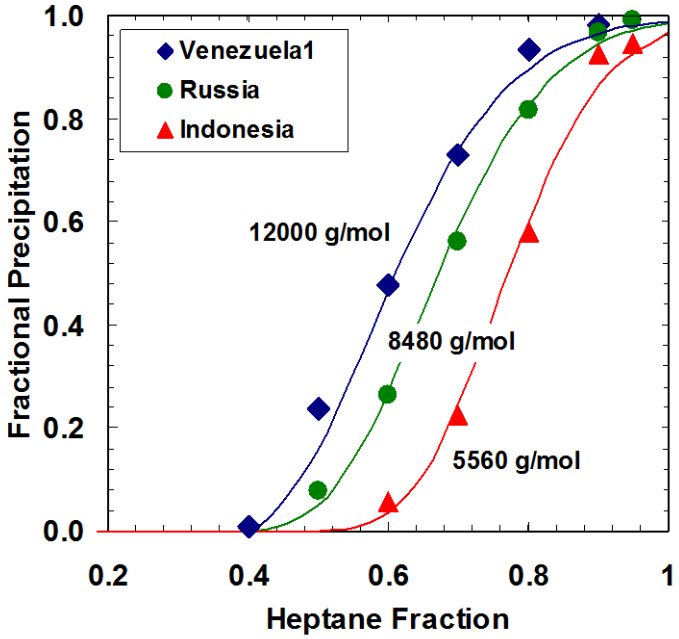

Figure 4.1: Asphaltene precipitation from solutions of asphaltenes in toluene and n-heptane. Symbols are data (Akbarzadeh *et al*., 2004); lines are regular solution model.

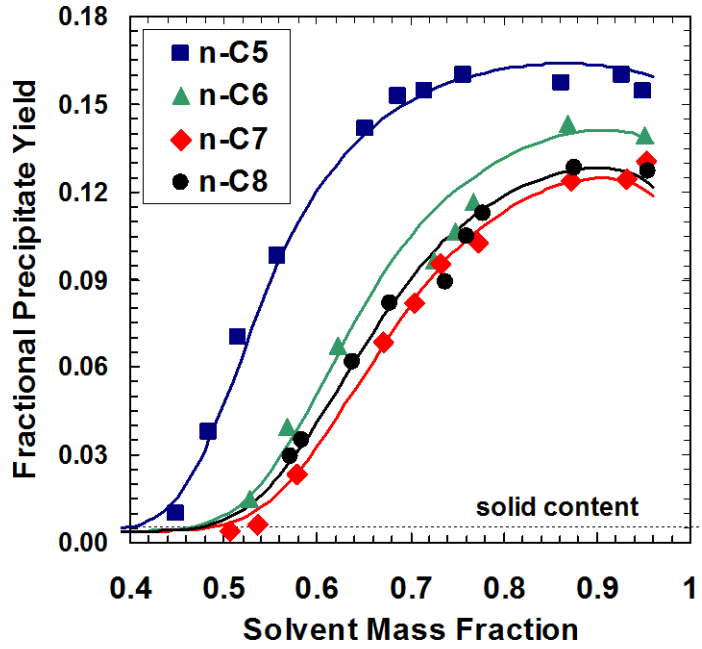

Figure 4.2: Asphaltene precipitation from Lloyminster heavy oil diluted with n-alkanes). Symbols are data (Akbarzadeh *et al*., 2004); lines are regular solution model.

Chapter Five: Molecular Weight, Density, and Refractive Index of Saturates, Aromatics, and Resins

In this chapter, the properties of saturate, aromatics, and resins (SAR) required as inputs for the modified regular solution model presented in Chapter 4 are determined; that is molecular weight, and density. Refractive index is also considered since it has potential as a correlating parameter for solubility parameters. The density and refractive index of some asphaltene samples were also measured to test a proposed correlation of FRI to density. Fractions from native crude oils, thermocracked samples, and hydrocracked samples are evaluated. While the measurement techniques were described in Chapter 3, some analysis is required to determine the properties from the data and is presented here. The effect of temperature on density and refractive index is examined. Correlations are developed to relate refractive index to density. Finally, the effect of thermo- and hydrocracking on the SAR properties is discussed briefly.

5.1 Interpretation of Measurements

5.1.1 Molecular Weight

SAR fractions molecular weights were measured in toluene at 50°C using a vapour pressure osmometer (VPO). As was discussed in Chapter 3, the measured voltage difference in the VPO is related to the molecular weight, M_2, of the solute as follows:

$$\frac{\Delta V}{C_2} = K\left(\frac{1}{M_2} + A_1 C_2\right) \tag{5.1}$$

In some cases, the higher order term (A_1) is negligible. Two issues were encountered when interpreting the data. First, the data were scattered and the magnitude of A_1 was sometimes obscured by the scatter. Second, self-association is known to occur in the asphaltenes and may occur in the resins as well. Therefore, the effects of the higher order term must be distinguished from the effects of self-association.

To determine the magnitude of A_1, the $\Delta V/C_2$ term was plotted versus C_2 for of all of the saturate fractions together and all of the aromatic fractions together to better discern any common trend

in A_1, Figure 5.1a and 5.1b respectively. Resins will be considered later because they may self-associate. In general, the saturate fractions and aromatic fractions each follow a common trend particularly at higher concentrations were the data are more reliable. Data at concentrations at or below 2 g/L were generally unreliable because the signal was within the noise of the measurements, Figure 5.2. Excluding the data at or below 2 g/L, the average slopes were found to be 0.13 mV/(g/L)² and 0.09 mV/(g/L)² for saturates and aromatics, respectively. These slopes were then were used to fit the VPO data and to determine molecular weight from the intercepts. Example of the fitted VPO data are provided in Figure 5.3. The VPO responses ($\Delta V/C_2$ versus C_2 plots) for the other saturate and aromatic fractions used in this thesis are presented in Appendix B. The molecular weights calculated from the intercepts are provided in Table 5.1. Based on the scatter in the data, the molecular weights are precise to ±34 g/mol and ±50 g/mol for saturates and aromatics, respectively.

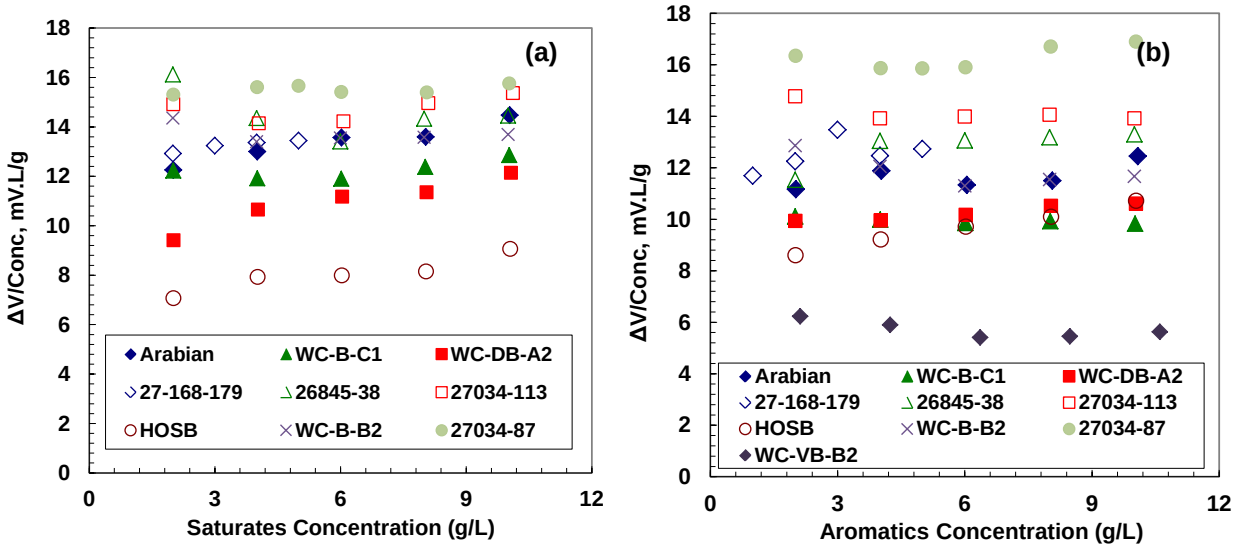

Figure 5.1: VPO measurements for saturates (a) and aromatics (b) in toluene at 50°C.

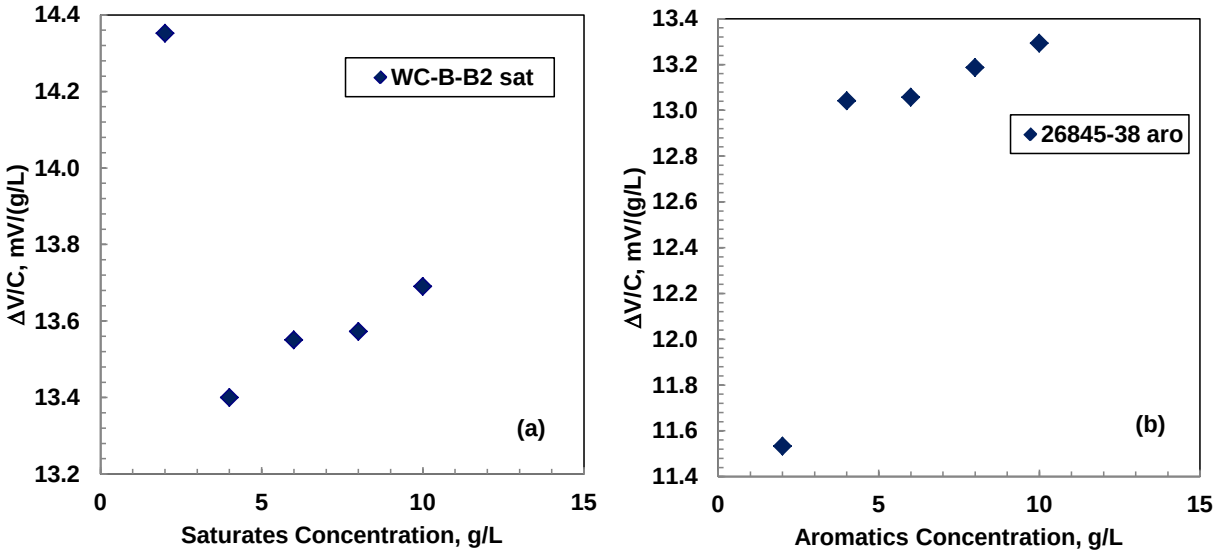

Figure 5.2: VPO measurements for saturates from WC-B-B2 (a) and aromatics from 26845-38 (b) samples in toluene at 50°C.

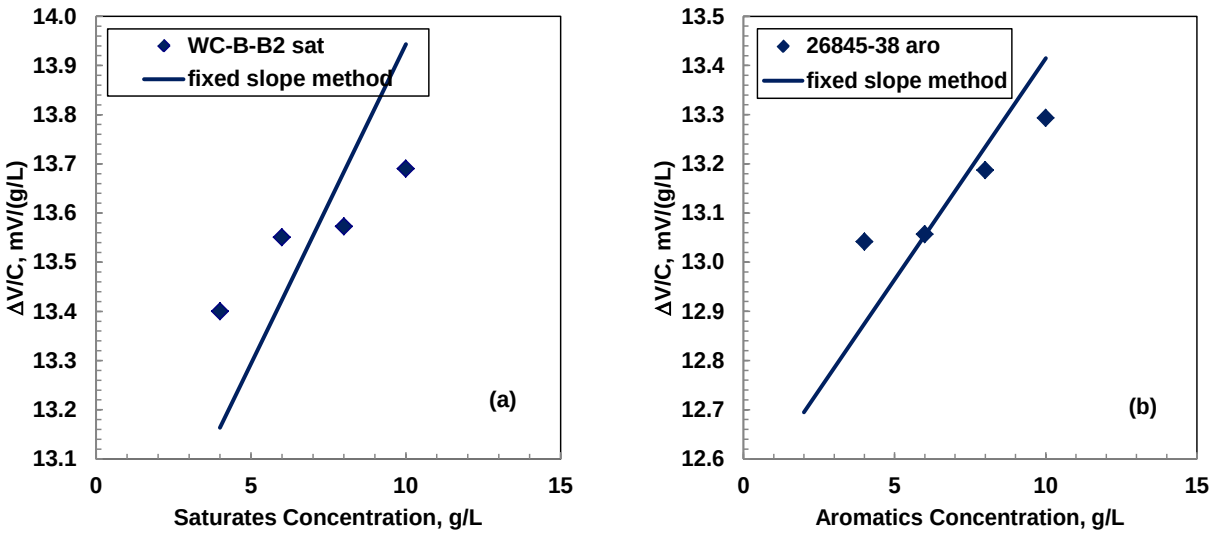

Figure 5.3: Fitting of VPO measurements for WC-B-B2 saturates (a) and 26845-38 aromatics (b) samples in toluene at 50°C. The average slopes of 0.13 mV/(g/L)^2 and 0.09 mV/(g/L)^2 were used for the saturates and aromatics, respectively.

Table 5.1: Molecular weight of saturates, aromatics, and resins measured in toluene at 50°C (A_1 = 0.13 mV/(g/L)² for saturates, 0.09 mV/(g/L)² for aromatics, and zero for resins).

Sample	Saturate Molecular Weight (g/mol)	Aromatic Molecular Weight (g/mol)	Resin Molecular Weight (g/mol)
Native Crude Oils			
WC-B-B2	370	440	990
Arabian	360	410	1000
WC-DB-A2	440	470	1050
WC-B-C1	400	480	1280
WC-VB-B2	-	930	1400
Thermocracked Samples			
27-168-179	370	390	830
26845-38	360	380	880
27034-113	330	340	830
27034-87	320	300	-
Hydrocracked Samples			
HOS Bottoms	600	480	670

The VPO measurements for the resins did not exhibit a consistent trend, Figure 5.4. The response could be a combined effect of the higher order term and self-association. Given the relatively small slope for the aromatic fractions, it was assumed that the second order term was negligible and A_1 was set to zero. Since any trends could not be distinguished from scatter in the data (particularly at low concentrations), it was further assumed that self-association in the resins was negligible. The resin molecular weights were determined from the average VPO response rather than the intercept. Individual plots of the VPO measurements for the resins are presented in Appendix B. The resin molecular weights are reported in Table 5.1.

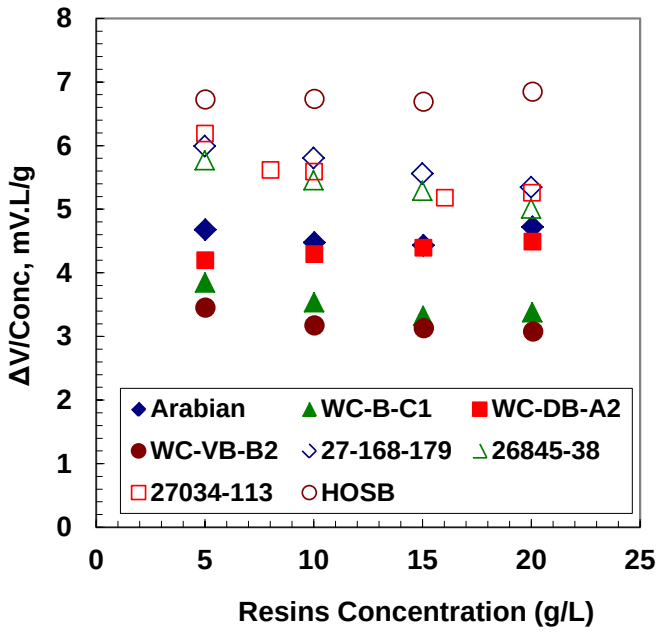

Figure 5.4: VPO measurements for resin fractions in toluene at 50 °C.

5.1.2 Density at 20°C and Atmospheric Pressure

The densities of saturates, aromatics, and resins were measured at 20°C and atmospheric pressure. The density of the saturates and aromatics could be measured directly but the resins were too viscous for a direct measurement. Instead, the resin densities were determined indirectly from the densities of solutions of resins in toluene. To interpret the data, it is necessary to determine the magnitude, if any, of the excess volumes of these solutions. To do so, the excess volumes were first determined for solutions of saturates and aromatics in toluene and heptane. Then, a correlation was developed to predict the excess volumes of solutions of any SAR fraction in a solvent. The correlation can also be used to estimate densities for small samples where dilution with a solvent is necessary to achieve the necessary volume for the measurement.

Recall that for a regular solution, the density of the solution is given by:

$$\frac{1}{\rho_{mix}} = \frac{w_1}{\rho_1} + \frac{w_2}{\rho_2} \qquad (5.2)$$

where ρ_{mix}, ρ_1 and ρ_2 are the mixture, solvent, and solute density (kg/m³), respectively, and w_2 is the solute mass fraction. If the mixture does not form a regular solution, that is, there is an excess volume of mixing, then the mixture density can be expressed as follows:

$$\frac{1}{\rho_{mix}} = \frac{w_1}{\rho_1} + \frac{w_2}{\rho_2} - w_1 w_2 \left(\frac{1}{\rho_1} + \frac{1}{\rho_2} \right) \beta_{12} \tag{5.3}$$

where β_{12} is a binary interaction parameter between the solute and the solvent. The last term in the expression is the excess volume of mixing. Therefore, the simplest visual representation is to plot the specific volume (inverse density) versus mass fraction of the solvent or solute. The specific volumes of a regular solution will plot linearly.

When only low solute concentrations are considered, the solutions can appear to be regular even when there are significant excess volumes of mixing. Consider a solution of saturates in toluene, Figure 5.5. At low saturate contents, the solution appears to be regular, Figure 5.5a. However, when the directly measured saturate density is included, it is apparent that the solutions expand upon mixing, Figure 5.5b. Similar behaviour is observed for saturates in heptane, Figure 5.6. Figures 5.7a and 5.7b show that solutions of aromatics in toluene and heptane, respectively, also have non-zero excess volumes of mixing.

The densities and binary interaction parameters for the mixtures with saturates are given in Table 5.2 and for mixtures with aromatics in Table 5.3. Regular solution extrapolation of densities from solutions of saturates in toluene underestimated the density of the fractions by approximately 10 kg/m^3 (AARD of 1%), whereas extrapolations from solutions of saturates in heptane overestimated the values by 18 kg/m^3 (AARD of 2%). Regular solutions density extrapolation from binary solutions of aromatics in toluene produced better estimates (AARD of 0.8%) compared to the estimations from solutions in heptane (AARD of 3.5%). Therefore, toluene was selected as the solvent of choice for density extrapolations for viscous and semi-solid samples.

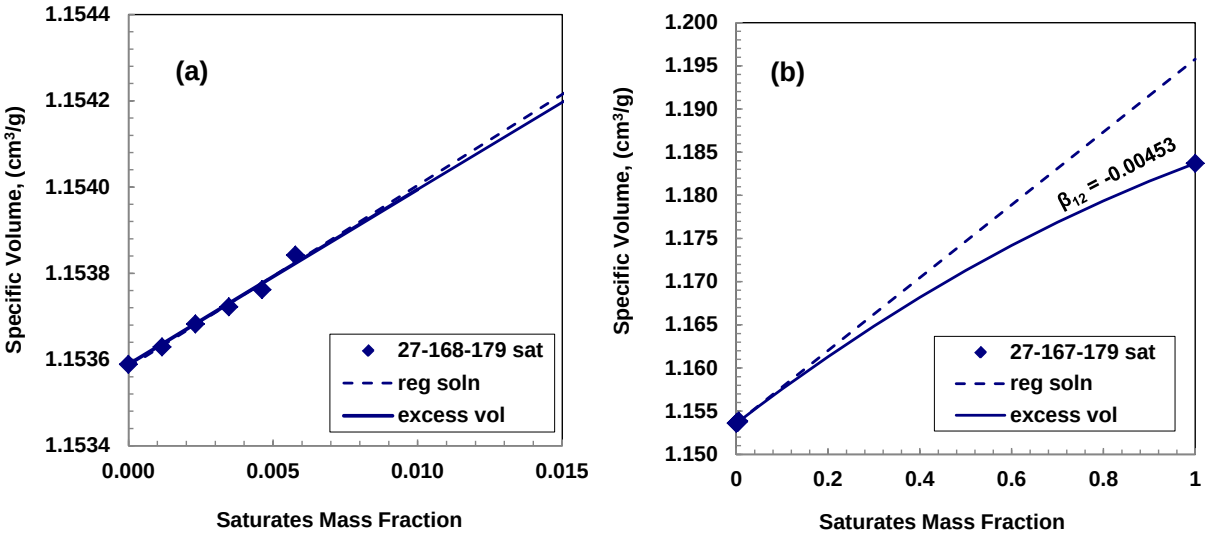

Figure 5.5: Density measurements of 27-168-179 saturates in toluene: a) expanded scale at low saturate mass fractions; b) full scale including the direct density measurement of the saturate and the regular solution extrapolation. The binary interaction parameter used to fit this data is -0.00453.

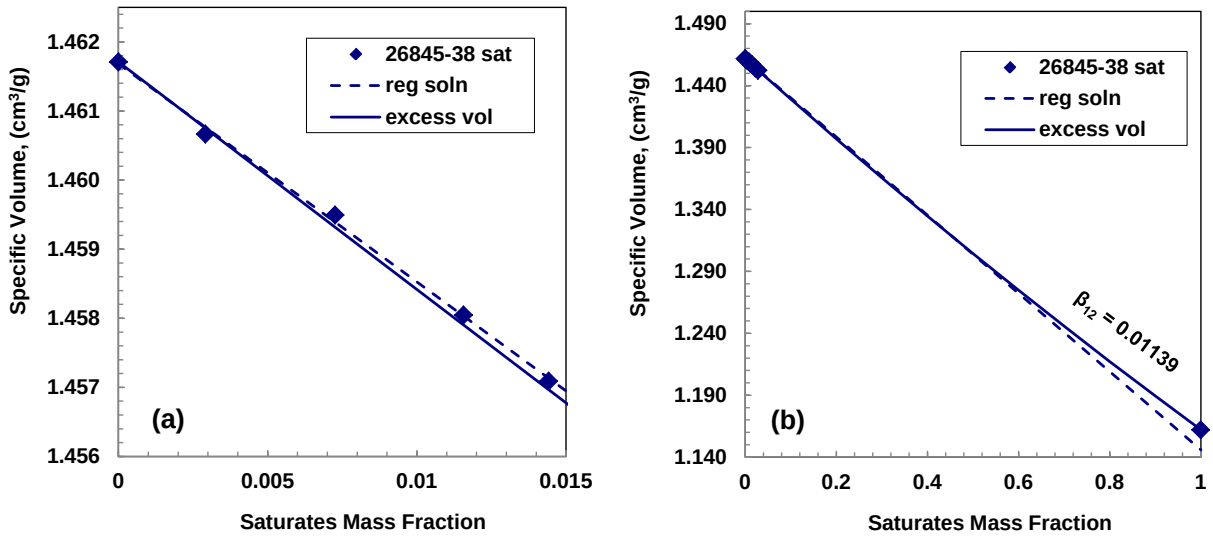

Figure 5.6: Density measurements of 26845-38 saturates in heptane: a) expanded scale at low saturate mass fractions; b) full scale including the direct density measurement of the saturate and the regular solution extrapolation. The binary interaction parameter used to fit this data is +0.01139.

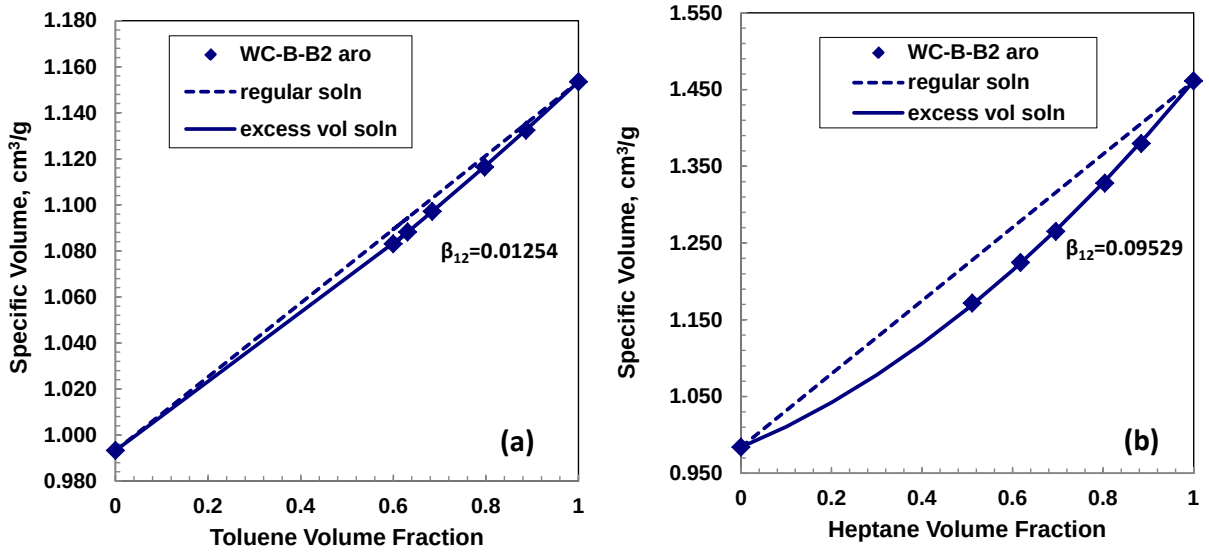

Figure 5.7: Density measurements for WC-B-B2 aromatics mixed with: a) toluene and b) heptane.

Table 5.2: Density of saturates at 20°C, density extrapolated incorrectly assuming regular solution behaviour, and binary interaction parameters fitted to measured density data.

Sample	Solvent	Direct Density (kg/m³)	Density Regular Solution (kg/m³)	β_{12}
WC-B-B2	toluene	887.1	870.3	-0.0096
Arabian	toluene	826.7	816.2	-0.0057
WC-DB-A2	toluene	888.2	881.0	-0.0034
27-168-179	toluene	844.8	836.3	-0.0045
26845-38	toluene	860.6	854.0	-0.0037
27034-87	toluene	847.8	833.8	-0.0076
HOSB	toluene	876.9	869.8	-0.0038
WC-B-B2	heptane	887.1	915.0	+0.0138
27-168-179	heptane	844.8	865.4	+0.0111
26845-38	heptane	860.6	872.7	+0.0114

Table 5.3: Density of aromatics at 20°C, density extrapolated incorrectly assuming regular solution behaviour, and binary interaction parameters fitted to measured density data.

Sample	Solvent	Direct Density (kg/m^3)	Density Regular Solution (kg/m^3)	β_{12}
WC-B-B2	toluene	1005.9	1011.5	0.0031
Arabian	toluene	978.5	982.2	-0.0002
WC-DB-A2	toluene	1002.9	1011.8	0.0032
27-168-179	toluene	969.7	973.4	0.0017
26845-38	toluene	1008.7	1017.2	0.0037
27034-87	toluene	1028.1	1033.2	0.0004
HOSB	toluene	1033.8	1048.1	0.0046
26845-38	heptane	1008.3	1046.7	0.0154
27-168-179	heptane	970.6	1002.5	0.0154

Saryazdi et al., (2012) found that the excess volumes of binary hydrocarbon mixtures correlate to the normalized difference between the mass specific volumes of the two components, defined as:

$$v_N = \frac{2|v_1 - v_2|}{v_1 + v_2} \tag{5.4}$$

where v_1 and v_2 are the mass specific volumes (inverse of density) of the two components. Figure 5.8 shows that the β_{12} of mixtures of components from the same chemical family all increased linearly on the same trend line with increasing normalized specific volume difference. Although there was some scatter, the β_{12} of mixtures of components from different chemical families all appeared to group on another similar trend line. Note that the trends lines accommodate both expansion and shrinkage depending on the magnitude of v_N.

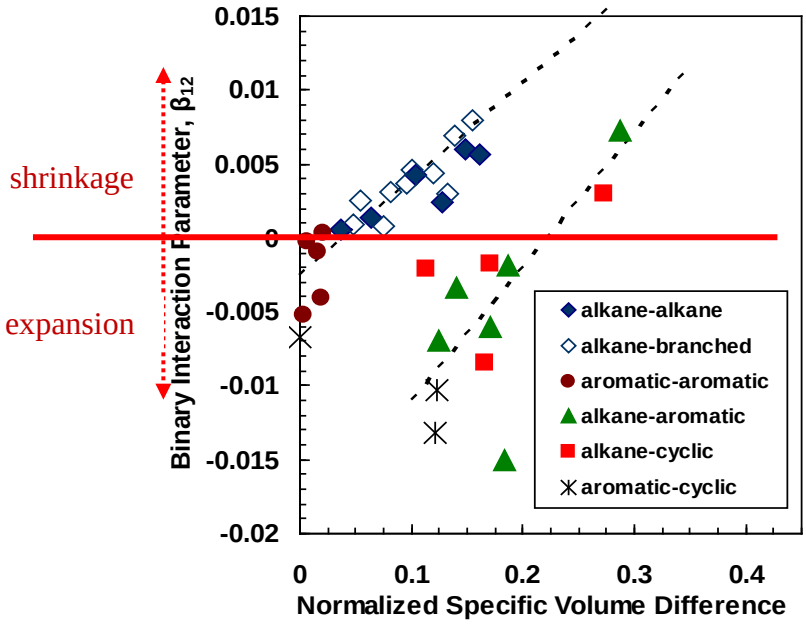

Figure 5.8: Binary interaction parameters of the excess volume on mixing of binary mixtures of pure hydrocarbons correlated to the normalized specific volume difference between them (Adapted from Saryazdi, 2012).

The data from the petroleum fractions in solvents were intermediate compared with pure hydrocarbons from same and different families, Figure 5.9. The petroleum fractions have mixed chemistry and it is not surprising that they fall between the two trends. Since the binary interaction parameters for pseudo-binary mixtures of saturates and aromatics with toluene and heptane followed a clear trend when plotted against v_N, Figure 5.10, the trend was fitted with the following expression:

$$\beta_{12} = -0.00754 + 0.05635\left(1 - \exp\left\{-1.5 v_N\right\}\right) \tag{5.5}$$

The correlation fits the majority of the data to ±0.0020.

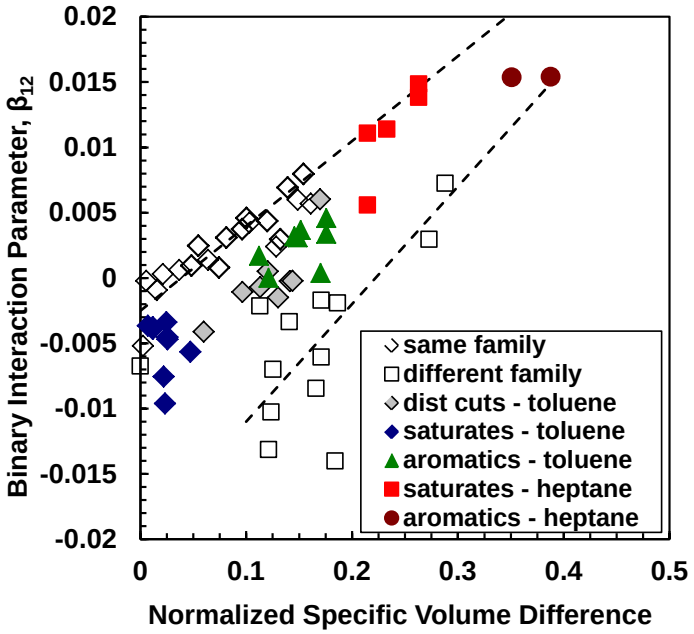

Figure 5.9: Binary interaction parameters of the excess volume on mixing of pseudo-binary mixtures saturate and aromatic with toluene and heptane versus normalized specific volume difference compared to the excess volume of pure hydrocarbons.

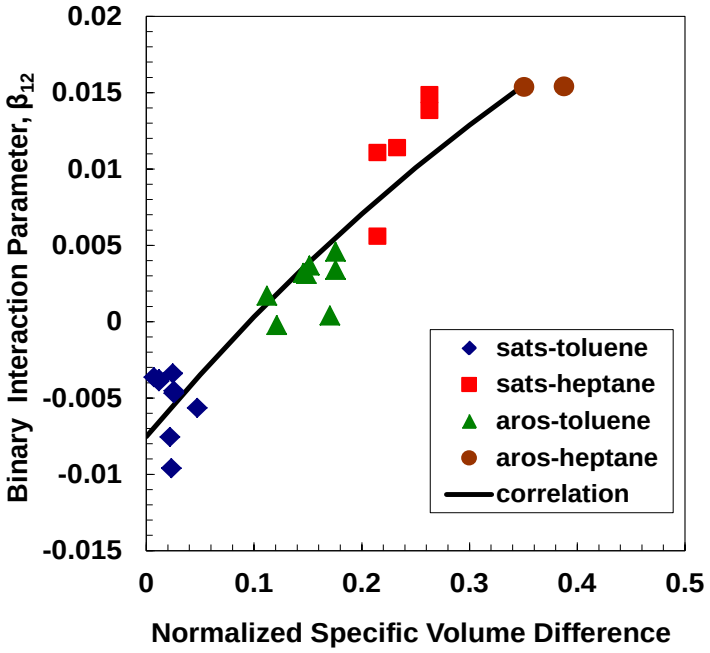

Figure 5.10: Binary interaction parameters of the excess volume on mixing of pseudo-binary mixtures saturate and aromatic with toluene and heptane correlated to the normalized specific volume difference.

Equation 5.5 was used to estimate the binary interaction parameters for solutions of resins in toluene. The density based on the regular solution mixing rule, the correlated binary interaction parameters, and the density based on fitting with Equation 5.3 are provided in Table 5.4. The densities based on the excess volume mixing rule are consistently about 19 kg/m³ less than the densities determined from the regular solution mixing rule. Note the β_{12} values of all of the samples except HOSB are all within 0.0006 of an average value of 0.0077. Values outside this range may indicate experimental error or that the sample has been significantly reacted.

Table 5.4: Density of resins at 20°C determined with regular solution mixing rule and with the excess volume mixing rule, Equation 5.3, and the correlated binary interaction parameters.

Sample	Solvent	Density Regular Solution (kg/m³)	Density Excess Volume Rule (kg/m³)	Correlated β_{12}
WC-B-B2	toluene	1074.4	1054.4	0.0079
Arabian	toluene	1066.1	1051.5	0.0075
WC-DB-A2	toluene	1066.5	1047.6	0.0075
WC-B-C1	toluene	1064.2	1045.0	0.0073
WC-VB-B2	toluene	1059.7	1041.0	0.0071
27-168-179	toluene	1063.6	1044.1	0.0073
26845-38	toluene	1081.7	1062.8	0.0083
27034-87	toluene	1073.1	1053.6	0.0079
27034-113	toluene	1081.6	1058.0	0.0083
HOSB	toluene	1098.2	1072.3	0.0092

Asphaltenes were not the focus of this thesis but some data were collected as a preliminary study. The density based on the regular solution mixing rule, the correlated binary interaction parameters (Equation 5.5), and the density based on fitting with Equation 5.3 are provided in Table 5.5. The densities based on the excess volume mixing rule are on average 39 kg/m³ less than the densities determined from the regular solution mixing rule.

Table 5.5: Density of asphaltenes at 20°C determined with regular solution mixing rule and with the excess volume mixing rule, Equation 5.3, and the correlated binary interaction parameters.

Sample	Solvent	Density Regular Solution (kg/m^3)	Density Excess Volume (kg/m^3)	Correlated β_{12}
27-168-179	toluene	1194.1	1152.0	0.0138
26845-38	toluene	1210.7	1170.9	0.0145
WC-B-B2	toluene	1184.7	1148.0	0.0134
WC-B-C1	toluene	1179.0	1140.3	0.0132

A summary of the measured densities (saturates and aromatics) and excess volume extrapolated densities (resins) used for this thesis is provided in Table 5.6. Note that SARA fractionation of the vacuum distillation residue sample (WC-VB-B2) did not produce enough saturate fractions for characterization.

Table 5.6: Densities of the SAR fractions.

Sample	Saturates (kg/m^3)	Aromatics (kg/m^3)	Resins (kg/m^3)
WC-B-B2	887.1	1005.9	1054.4
Arabian	826.7	978.5	1047.7
WC-DB-A2	888.2	1002.9	1047.6
WC-B-C1	877.4	1001.6	1045.0
WC-VB-B2		1016.5	1041.0
27168179	844.8	969.7	1045.3
26845-38	860.6	1008.7	1062.8
27034-87	847.8	1028.1	1053.6
27034113	841.4	1008.3	1059.0
HOSB	876.9	1033.8	1072.3

5.1.3 Refractive Index at 20°C and Atmospheric Pressure

The refractive indexes of saturates, aromatics, and resins were measured at 20°C and atmospheric pressure. Rather than using the refractive index directly, most mixing rules and correlations are based on a function of the refractive index, FRI, given by:

$$FRI = \frac{n_D^2 - 1}{n_D^2 + 2} \tag{5.6}$$

Therefore, all of the measured refractive indices were converted to FRI and only FRI are reported unless otherwise indicated.

Recall that, ideally, the FRI of a mixture is given by:

$$FRI_{mix} = \phi_1 FRI_1 + \phi_2 FRI_2 \tag{5.7}$$

where ϕ is volume fraction. Some mixtures did not follow this rule and were fitted with an analogy to the excess volume mixing rule given by:

$$FRI_{mix} = \phi_1 FRI_1 + \phi_2 FRI_2 - \phi_1 \phi_2 (FRI_1 + FRI_2) \beta_{12}^* \tag{5.8}$$

where β^*_{12} is the binary interaction parameter for the refractive index.

Solutions of combinations of heptane and toluene were found to follow the volume average mixing rule, Figure 5.11. However, solutions of saturates and aromatics in toluene and heptane followed the excess volume mixing rule, Figure 5.12. As with density, extrapolations based on the regular solution rule could lead to significant errors, Figure 5.13 and Figure 5.14. The refractive indexes from the volume average and excess volume mixing rules as well as the binary interaction parameters are summarized in Tables 5.7 and 5.8 for saturates and aromatics, respectively.

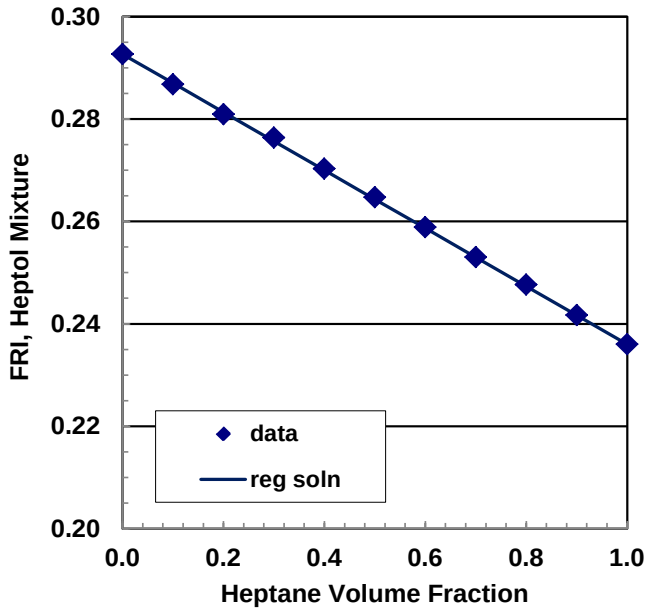

Figure 5.11: FRI of solutions of heptane and toluene at 20°C.

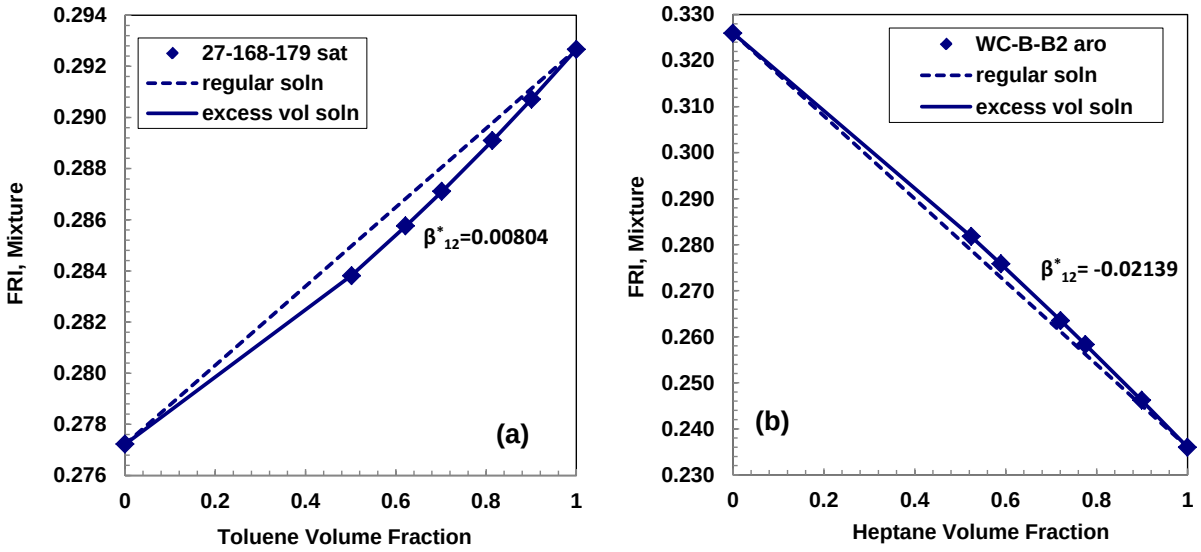

Figure 5.12: FRI at 20°C of mixtures of: a) 27-168-179 saturates in toluene and b) WC-B-B2 aromatics in heptane.

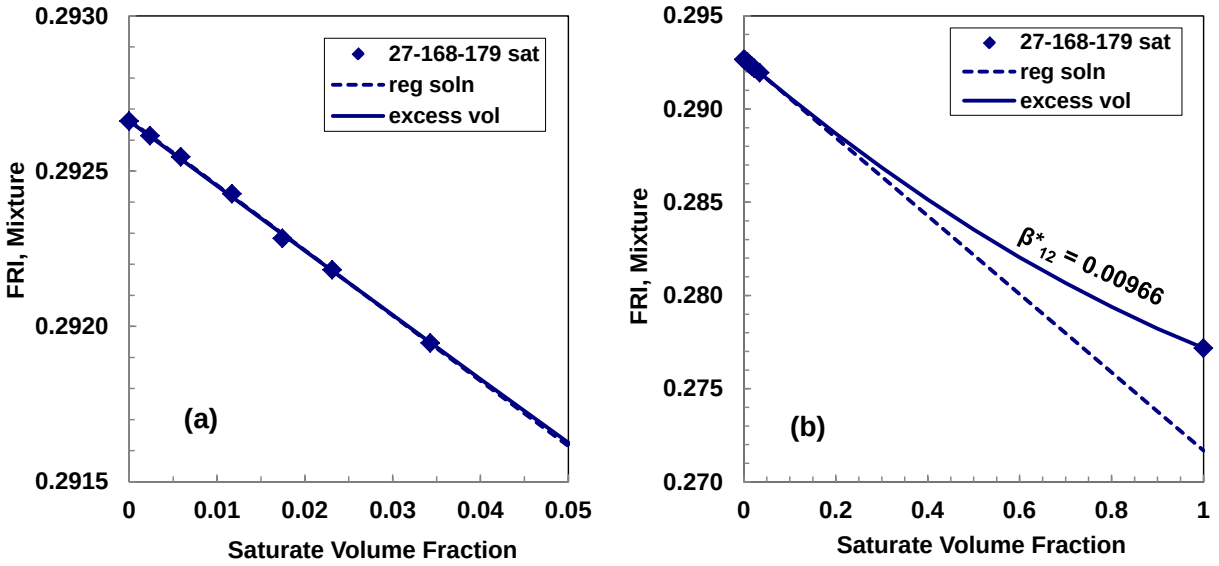

Figure 5.13: FRI of 27-168-179 saturates in toluene: a) expanded scale at low saturate volume fractions; b) full scale including the directly measured FRI of the saturate.

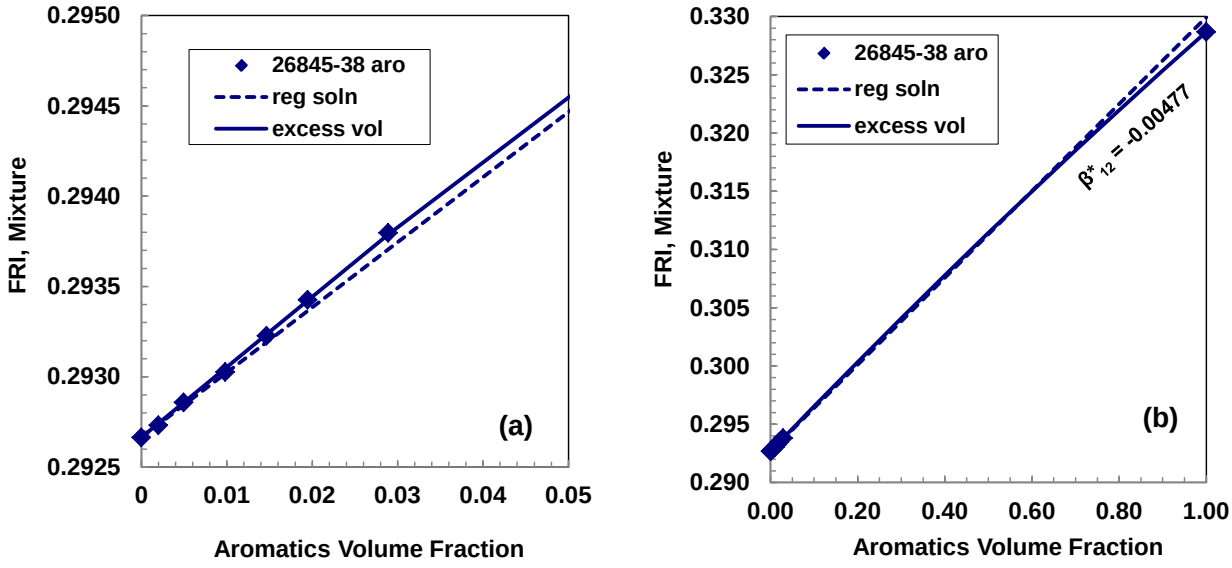

Figure 5.14: FRI of 26845-38 aromatics in toluene: a) expanded scale at low saturate volume fractions; b) full scale including the directly measured FRI of the aromatic.

Table 5.7: Refractive index and FRI of saturates at 20°C, FRI extrapolated incorrectly from the regular solution mixing rule, and binary interaction parameters fitted to FRI data.

Sample	Solvent	FRI Measured	FRI Reg Soln	β_{12}
WC-B-B2	toluene	0.28388	0.28057	0.0054
Arabian	toluene	0.27286	0.26737	0.0002
WC-DB-A2	toluene	0.28634	0.28248	0.0067
27-168-179	toluene	0.27717	0.27265	0.0081
26845-38	toluene	0.28008	0.27574	0.0078
27034-87	toluene	0.27962	0.27055	0.0123
HOSB	toluene	0.28600	0.28073	0.0080
WC-B-B2	heptane	0.28569	0.29303	-0.0138
27-168-179	heptane	0.27705	0.28477	-0.0149
26845-38	heptane	0.28008	0.28684	-0.0134
26845-38	heptane	0.28008	0.28587	-0.0110

Table 5.8: Refractive index and FRI of aromatics at 20°C, FRI extrapolated incorrectly from the regular solution mixing rule, and binary interaction parameters fitted to FRI data.

Sample	Solvent	FRI Measured	FRI Reg Soln	β_{12}
WC-B-B2	toluene	0.32602	0.32909	-0.0037
Arabian	toluene	0.32022	0.32339	-0.0005
WC-DB-A2	toluene	0.32529	0.32886	-0.0055
27-168-179	toluene	0.31949	0.31992	0.0016
26845-38	toluene	0.32869	0.32993	-0.0048
27034-87	toluene	0.33794	0.34174	-0.0045
HOSB	toluene	0.34446	0.35112	-0.0061
WC-B-B2	heptane	0.32596	0.33255	-0.0214
27-168-179	heptane	0.31968	0.33100	-0.0174
26845-38	heptane	0.32874	0.34274	-0.0209

Similar to the approach taken for density, the binary interaction parameters for the FRI were correlated based on the normalized difference between the FRI of the two components in the mixture, defined as:

$$FRI_N = \frac{2\left|FRI_1 - FRI_2\right|}{FRI_1 + FRI_2} \tag{5.9}$$

The binary interaction parameters for pseudo-binary mixtures of saturates and aromatics with toluene and heptane followed a clear trend when plotted versus FRI_N, Figure 5.15. The trend was fitted with the following expression:

$$\beta_{12}^{*} = 0.01699 - 0.04561\left(1 - \exp\left\{-5.71 FRI_N\right\}\right) \tag{5.10}$$

The correlation fit the majority of the data to ±0.0026. Note that the trend only applies to SARA fractions with solvents. For example, the β_{12}^{*} for solutions of heptane and toluene is zero and is not on the same trend as the SARA fractions.

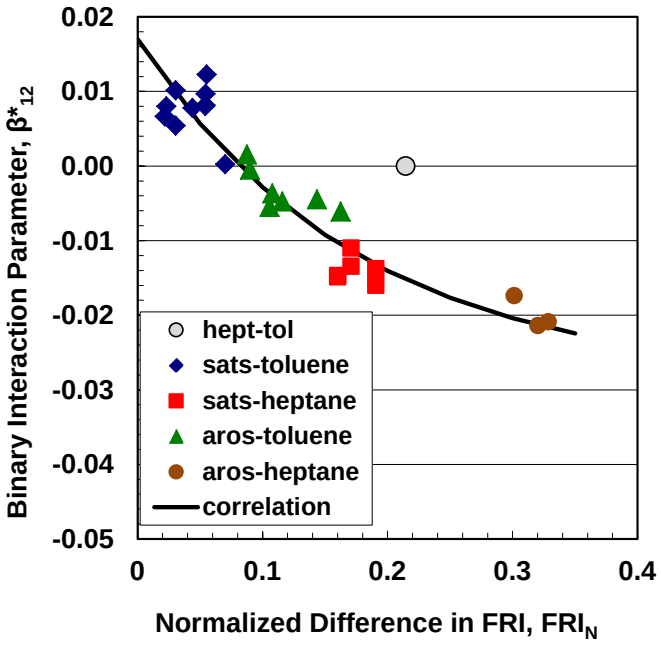

Figure 5.15: Relationship to normalized FRI of binary interaction parameters for the FRI of saturate and aromatic pseudo-binary mixtures with toluene and heptane.

The correlation was used to estimate the binary interaction parameters for solutions of resins and asphaltenes in toluene. From Figure 5.16 and 5.17, it was observed that at low dilutions, the assumption of regular mixing behaviour or non-ideal mixing behaviour appeared to be insignificant, but the final extrapolation values suggested otherwise. FRI based on the regular solution mixing rule, the correlated binary interaction parameters, and the FRI based on fitting with Equation 5.10 are provided in Table 5.9 and 5.10 for resins and asphaltenes respectively. The FRI based on the excess volume mixing rule were consistently about 0.007 less than the FRI determined from the regular solution mixing rule for resins and 0.015 less for asphaltenes. Correlated β^*_{12} values of all of the resin samples except HOSB are within 0.0012 of an average value of 0.0097.

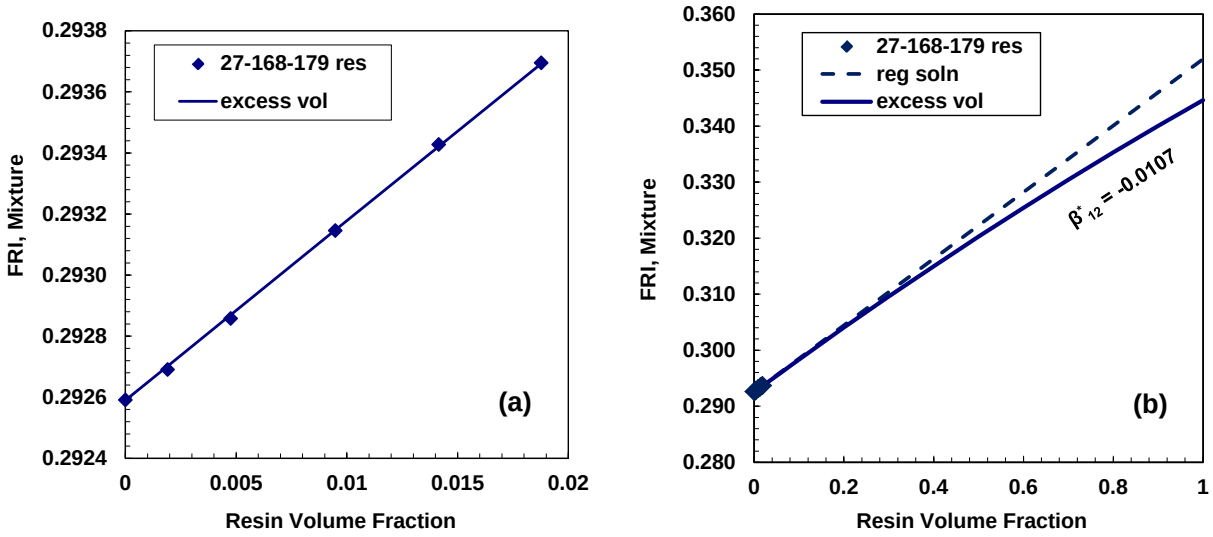

Figure 5.16: FRI of 27-168-179 resins in toluene: a) expanded scale at low resin volume fractions; b) full scale including the extrapolated FRI of the resins.

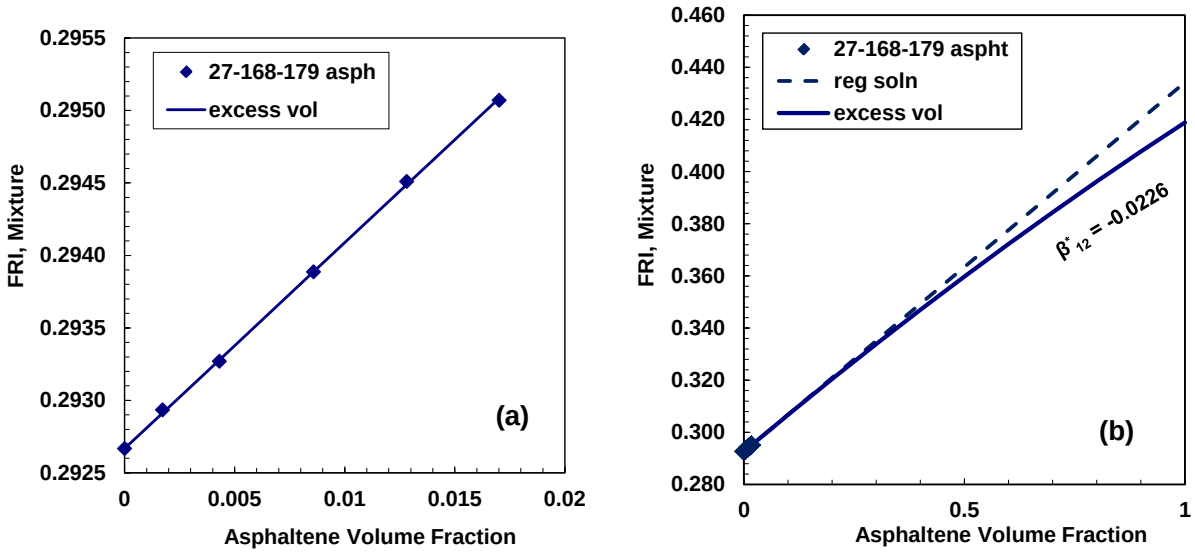

Figure 5.17: FRI of 27-168-179 asphaltenes in toluene: a) expanded scale at low asphaltenes volume fractions; b) full scale including the extrapolated FRI of the asphaltenes

Table 5.9: FRI of resins at 20°C determined with regular solution mixing rule and with excess volume mixing rule, Equation 5.10, and the correlated binary interaction parameters.

Sample	Solvent	FRI Reg Soln	FRI Excess Vol	Correlated β_{12}^{*}
WC-B-B2	toluene	0.34457	0.33798	-0.0088
Arabian	toluene	0.35310	0.34602	-0.0109
WC-DB-A2	toluene	0.34759	0.34052	-0.0095
WC-B-C1	toluene	0.34442	0.33729	-0.0086
WC-VB-B2	toluene	0.34438	0.33749	-0.0087
27-168-179	toluene	0.35196	0.34505	-0.0106
26845-38	toluene	0.35142	0.34459	-0.0105
27034-87	toluene	0.34763	0.34086	-0.0096
27034-113	toluene	0.35150	0.34439	-0.0105
HOSB	toluene	0.37306	0.36563	-0.0151

Table 5.10: FRI of asphaltenes at 20°C determined with regular solution mixing rule and with excess volume mixing rule, Equation 5.10, and the correlated binary interaction parameters.

Sample	Solvent	FRI Reg Soln	FRI Excess Vol	Correlated β_{12}^{*}
WC-B-B2	toluene	0.40432	0.38923	-0.0198
WC-B-C1	toluene	0.39485	0.38080	-0.0185
27-168-179	toluene	0.43503	0.41966	-0.0225
26845-38	toluene	0.42496	0.41113	-0.0218
27034-87	toluene	0.41791	0.40616	-0.0214

The measured FRI (saturates and aromatics) and excess volume extrapolated FRI (resins) values used for this thesis are shown in Table 5.11.

Table 5.11: A summary of the FRI values for the characterized SAR fractions

Sample	Saturates	Aromatics	Resins
WC-B-B2	0.2839	0.3259	0.3383
Arabian	0.2729	0.3202	0.3523
WC-DB-A2	0.2863	0.3253	0.3405
WC-B-C1	0.2838	0.3248	0.3373
WC-VB-B2	-	0.3300	0.3375
27168179	0.2772	0.3195	0.3398
26845-38	0.2801	0.3287	0.3446
27034-87	0.2769	0.3379	0.3409
27034-113	0.2759	0.3307	0.3444
HOSB	0.2860	0.3445	0.3656

5.2 Effect of Temperature on Density and Refractive Index

The effect of temperature on saturate and aromatic density and refractive index was determined from measurements at 20°C, 40°C and 60°C. Both specific volume (or density) and FRI were found to be linearly related to temperature for both saturate and aromatic fractions, Figure 5.18. For density, the relationship to temperature can be expressed in terms of coefficient of thermal expansion, α_V, defined as:

$$\alpha_V = \frac{1}{v}\left(\frac{dv}{dT}\right) \tag{5.11}$$

which can be rearranged to obtain:

$$v = v_o \exp(\alpha_V T) \tag{5.12}$$

Since density is the reciprocal of the specific volume, Equation 5.12 is equivalent to:

$$\rho = \rho_o \exp(-\alpha_V T) \tag{5.13}$$

For $\alpha_V T$ <<1, Equation 5.12 can be expressed as follows:

$$v = v_o(1+\alpha_V T) = A + BT \tag{5.14}$$

where v is specific volume in cm^3/g and T is temperature in °C, A and B are the intercept and slope, and subscript $_0$ is for reference or initial value. Hence, the linear trend in Figure 5.18 indicates that α_V is a constant, at least over the temperature range of the data.

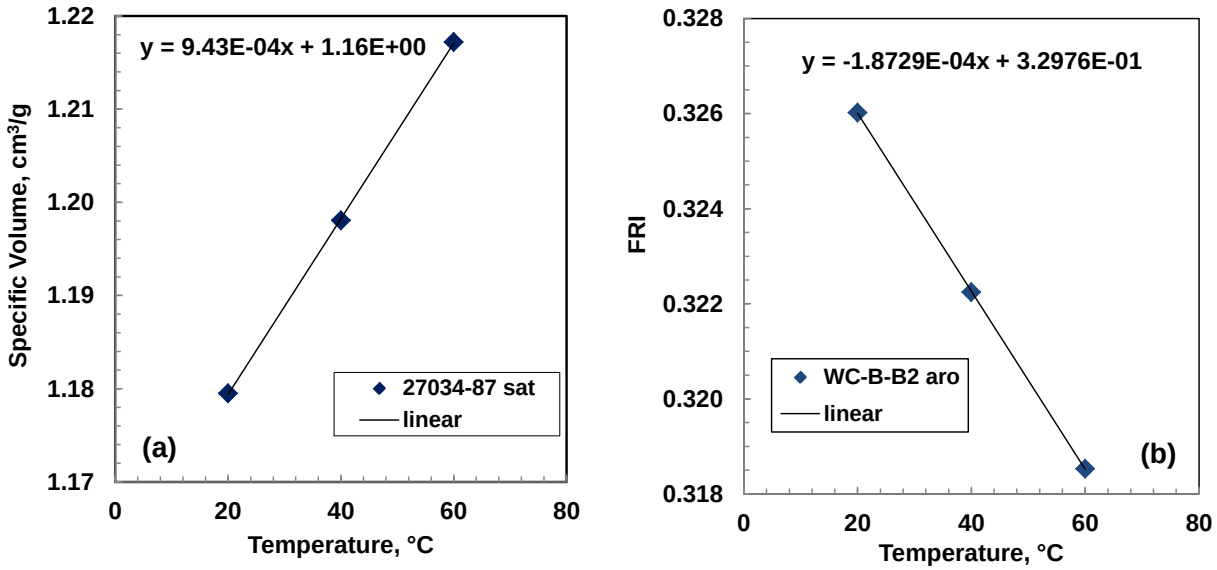

Figure 5.18: Temperature is linearly related to: a) the specific volume of 27034-87 saturates and b) the FRI of WC-B-B2 aromatics.

The thermal expansion coefficients were calculated for each dataset using Equation 5.14., Appendix B, and are provided in Table 5.12. These coefficients were found to correlate linearly to the specific volume at 20°C, Figure 5.19 and the correlations are given by:

$$\alpha_{V,sat} = -0.00079116 + 0.0013488 v_{20} \tag{5.15}$$

$$\alpha_{V,aro} = -0.0004627 + 0.0011372 v_{20} \tag{5.16}$$

where v_{20} is specific volume (cm^3/g) at 20°C. Eqns 5.15 and 5.16 can also be expressed in terms of density as follows:

$$\alpha_{V,sat} = -0.00079116 + \frac{0.0013488}{\rho_{20}} \tag{5.17}$$

$$\alpha_{V,aro} = -0.0004627 + \frac{0.0011372}{\rho_{20}} \tag{5.18}$$

Hence, the density of saturates and aromatics at any temperature and atmospheric pressure (as long as they remain in the liquid state) can be related to the density measured at 20°C as follows:

$$\rho = \rho_{20} \exp(-\alpha_{V,X} (T - 20°C)) \tag{5.19}$$

where ρ_{20} is density (g/cm^3) at 20°C and $\alpha_{V,X}$ is thermal expansion coefficient for saturates or aromatics. The correlation, Equation 5.19, fit the experimental data with an AARD of 0.05% as shown in Figure 5.20.

Table 5.12: Thermal expansion coefficients calculated from slopes and v_{20} for each saturate and aromatics using Equation 5.14.

	Saturates			***Aromatics***		
Sample	v_{20}	**B(slope)**	α_v	v_{20}	**B(slope)**	α_v
WC-B-B2	1.1273	0.00082	0.00073	0.9944	0.00067	0.00068
Arabian	1.2097	0.00102	0.00084	1.0219	0.00071	0.00069
WC-B-C1	1.1398	0.00085	0.00075	0.9984	0.00067	0.00067
WC-DB-A2	1.1258	0.00082	0.00072	0.9971	0.00065	0.00066
WC-VB-B2	-	-	-	0.9838	0.00063	0.00064
27-168-179	1.1829	0.00096	0.00081	-	-	-
27034-113	1.1883	0.00096	0.00080	0.9917	0.00069	0.00070
27034-87	1.1795	0.00094	0.00080	0.9726	0.00067	0.00069
HOSB	1.1404	0.00082	0.00072	0.9673	0.00061	0.00063

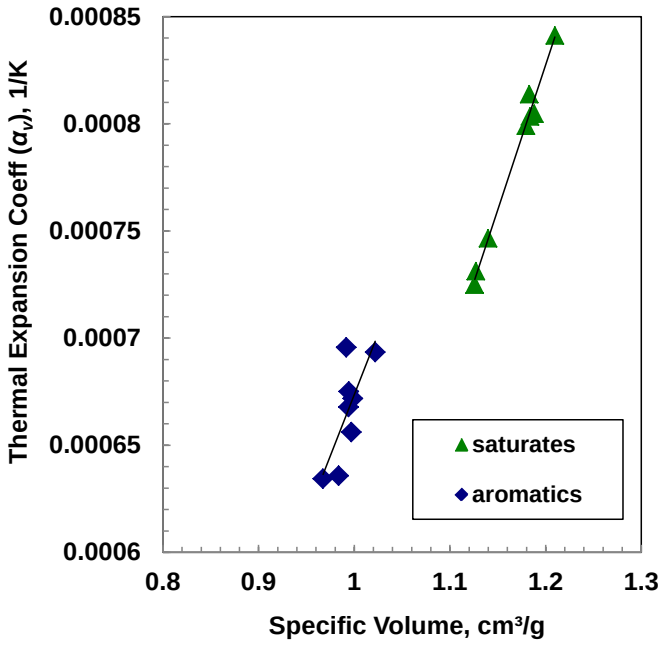

Figure 5.19: Thermal expansion coefficient versus specific volume for saturates and aromatics.

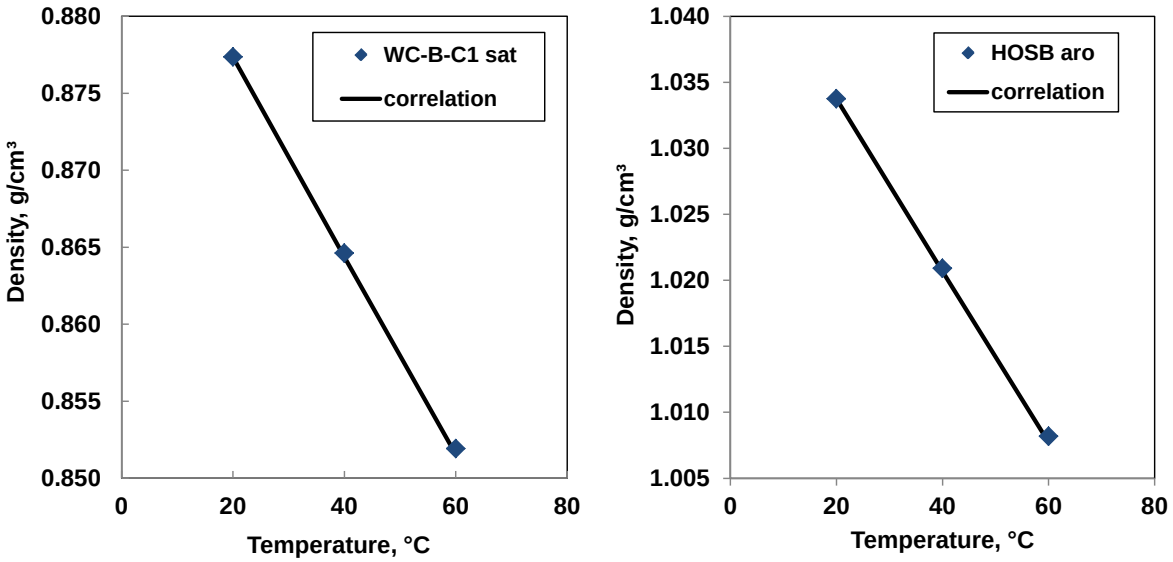

Figure 5.20: Density estimation for: a) WC-B-C1 saturates and b) HOSBottoms aromatics using the correlation of Equation 5.19.

The refractive index of a material, like its density, changes with temperature. The magnitude of the change depends on the wavelength and the type of material the light passes through. The effect of wavelength on the refractive index is not significant for this thesis because all measurements were made using the same wavelength and the same measuring prism. However, the refractive index will change with temperature as the density of the fluid changes. The derivative of the refractive index with temperature has been determined experimentally (Subedi *et al*., 2006) and for a pure component has been shown to relate to the thermal expansion coefficient of the fluid (Li et al., 1994). Since FRI and density are linearly related for the temperature range examined in this thesis, an analogous thermal coefficient can be defined for FRI as follows:

$$\alpha_{FRI} = \frac{1}{FRI}\left(\frac{dFRI}{dT}\right) \tag{5.20}$$

where α_{FRI} is thermal FRI coefficient, *FRI* is a standard function of refractive index and *T* is temperature in °C. The thermal FRI coefficient is also constant over the temperature range of the data. The following correlations for α_{FRI} were developed as described for the thermal expansion coefficient:

$$\alpha_{FRI(s)} = -0.0028273 + 0.0076062 FRI_{20} \tag{5.21}$$

$$\alpha_{FRI(a)} = -0.0011164 + 0.0016398 FRI_{20} \tag{5.22}$$

where subscript *s* and *a* are for saturates and aromatics respectively. Hence, the FRI of saturates and aromatics at any temperature and atmospheric pressure (as long as they remain in the liquid state) can be related to the FRI measured at 20°C as follows:

$$FRI = FRI_{20} \exp(\alpha_{FRI(X)}(T - 20°C)) \tag{5.23}$$

where FRI_{20} is the FRI at 20°C and $\alpha_{FRI(X)}$ is thermal FRI coefficient for saturates or aromatics. Values of calculated thermal FRI coefficients are given in Table 5.13. The FRI above 20°C were estimated with an AARD of 0.04% with the exception of HOSB and 27-168-179 saturates. These samples are consistent outliers through this thesis and this behavior could be tied to their reaction history.

Table 5.13: Thermal FRI coefficients calculated from slopes and FRI_{20} for each saturate and aromatics using Equation 5.20.

	Saturates			*Aromatics*		
Sample	FRI_{20}	**B(slope)**	α_{FRI}	FRI_{20}	**B(slope)**	α_{FRI}
WC-B-B2	0.28579	-0.00019	-0.00065	0.32602	-0.00019	-0.00057
Arabian	0.27286	-0.00020	-0.00074	0.32022	-0.00019	-0.00060
WC-B-C1	0.28381	-0.00019	-0.00067	0.32475	-0.00019	-0.00058
WC-DB-A2	0.28635	-0.00018	-0.00065	0.32529	-0.00018	-0.00056
WC-VB-B2	-	-	-	0.32999	-0.00019	-0.00058
27-168-179	0.27708	-0.00020	-0.00074	-	-	-
27034-113	0.27563	-0.00020	-0.00073	0.33070	-0.00020	-0.00059
27034-87	0.27692	-0.00020	-0.00072	0.33794	-0.00020	-0.00058
HOSB	0.28600	-0.00022	-0.00075	0.34448	-0.00018	-0.00053

5.3 Relationship between Refractive Index and Density

Recall that the refractive index is related to density through the Lorentz-Lorenz formula:

$$FRI = \left(\frac{n_D^2 - 1}{n_D^2 + 2}\right) = \frac{4\pi\alpha N}{3}\left(\frac{\rho}{MW}\right) \tag{5.24}$$

or

$$FRI = R_m\left(\frac{\rho}{MW}\right) \tag{5.25}$$

where α is the polarizability of the media, n_D is the refractive index, N_A is Avogadro's number and R_m is the molar refraction.

Iglesias-Otero *et al.*, 2008; Vargas *et al.*, 2009) rearranged Eq. 5.25 as follows:

$$R_m = \left(\frac{FRI}{\rho} \right) MW \tag{5.26}$$

and demonstrated that when the molar refractions of different pure hydrocarbons are plotted with respect to their molecular weights a common linear trend with a slope equal to approximately 1/3 is obtained, Figure 5.21. This is referred to as the one-third rule (Varga *et al.*, 2010). The one-third rule indicates that the FRI of any pure component is approximately 1/3 of its density (in g/cm³). In other words, the effects of changing molecular weight and polarizability cancel out of the Lorentz-Lorenz relationship. The one-third rule was found to apply to crude oil systems as well (Varga *et al.*, 2010).

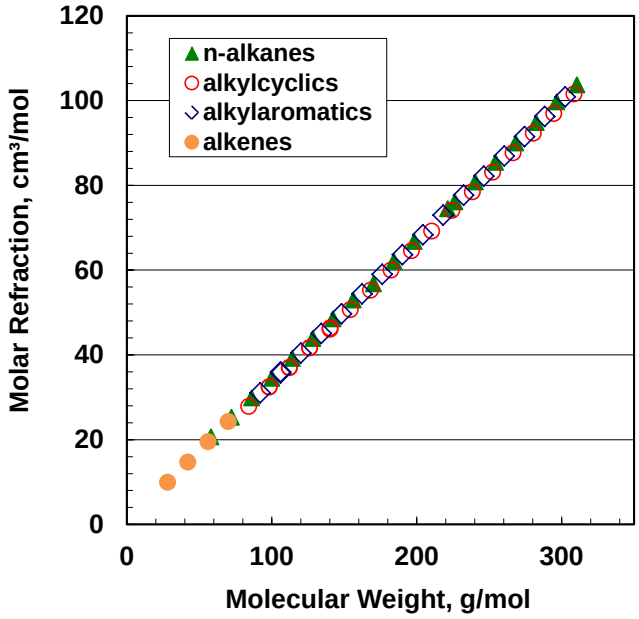

Figure 5.21: Molar refraction as a linear function of the molecular weights for different pure hydrocarbons (based on data from NIST standard reference database).

For saturates, aromatics, and resins, the average ratio of FRI to density ranged from 0.3210 to 0.3410 with an average of 0.3265. The one-third rule was used to predict the FRI_{20} of saturates, aromatics, resins, and asphaltenes from their measured densities, Figure 5.22. The one-third rule predicted the FRI with an AARD of 2.4%, 2.0%, 2.7% and 3.6% for saturates, aromatics, resins and asphaltenes respectively. Since the molar refraction is nearly independent of temperature and

pressure (Varga *et al.*, 2010), the one-third rule was still applicable to the saturate and aromatic fractions at higher temperatures, Figure 5.23 with an AARD of 2%.

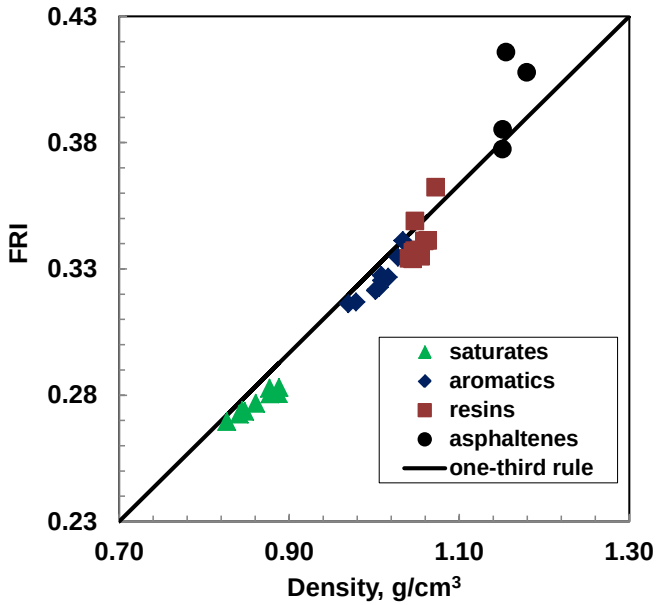

Figure 5.22: Comparison of the measured FRI for SARA fractions from different crude oil samples at 20°C (symbols) to the predictions using the one-third rule (line).

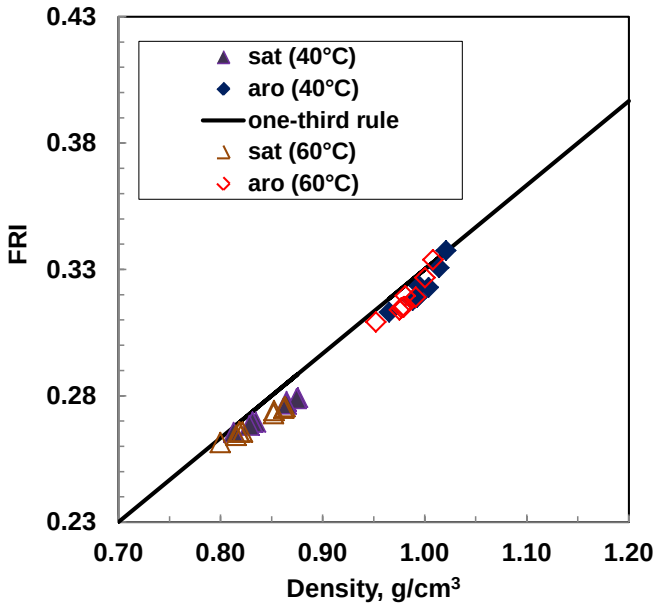

Figure 5.23: Comparison of the measured FRI for saturate and aromatic fractions from different crude oil samples at 40 and 60°C (symbols) to the predictions using the one-third rule (line).

The one-third rule is a robust general correlation for FRI. However, FRI for a given chemical family can also be correlated to density, Figure 5.24a. Figure 5.24b shows that saturates and aromatics are similar to the alkylcyclic and alkylaromatic families. A more accurate relationship for FRI can be obtained specifically for SARA fractions by correlating FRI to density as follows:

$$FRI_{20} = 0.5141 - 0.7745\rho + 0.5843\rho^2 \qquad (5.27)$$

where FRI_{20} is FRI at 20°C and ρ is density in g/cm^3. Equation 5.27 predicts the FRI with an AARD of 0.3% for saturates, 0.8% for aromatics, 1.7% for resins and 2.9% for asphaltenes. FRI predictions using the Equation 5.27 are more accurate than using the one-third rule especially for the least polar fractions.

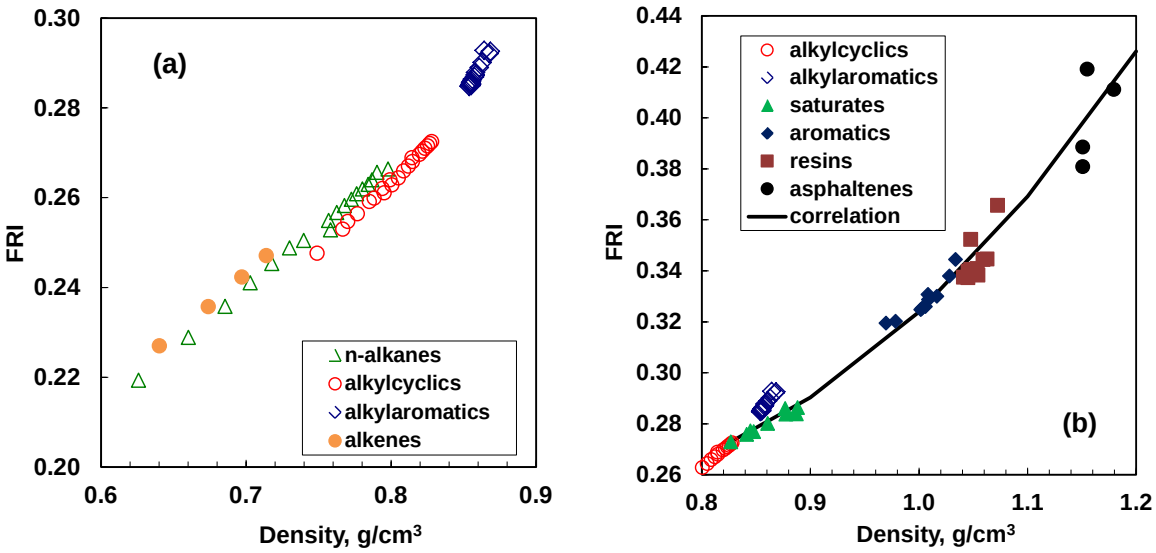

Figure 5.24: Relationship between density and the function of the refractive index, FRI for a) pure hydrocarbons and b) SARA fractions

The relationship between FRI and density extend to their thermal coefficients, Figure 5.25, and their binary interaction parameters for excess properties, Figure 5.26. The thermal coefficients were observed to be linearly related to each other as follows:

$$\alpha_{FRI} = 0.00013 - 1.05546\alpha_V \qquad (5.28)$$

The binary interaction parameters for FRI were approximately equal to the negative of the interaction parameters of the densities. As expected from the inverse relationship between specific volume and FRI, shrinkage corresponds to a positive deviation of FRI.

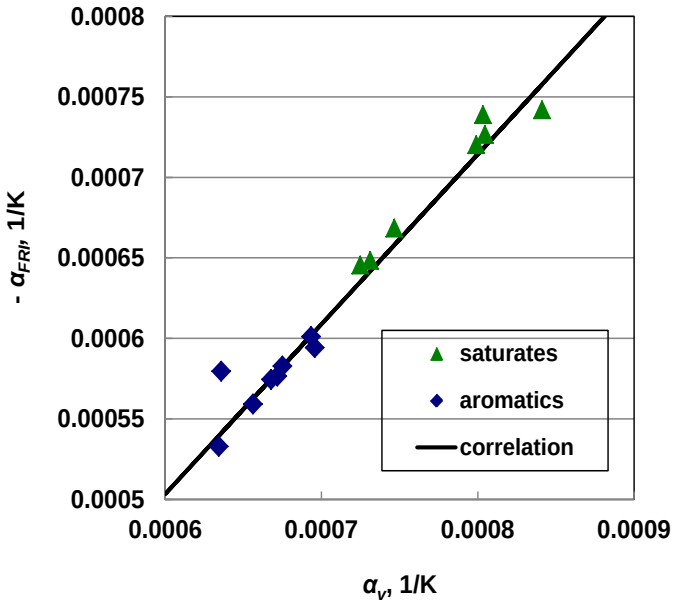

Figure 5.25: Correlation of the thermal expansion coefficient to the thermal FRI coefficient for saturate and aromatic fractions.

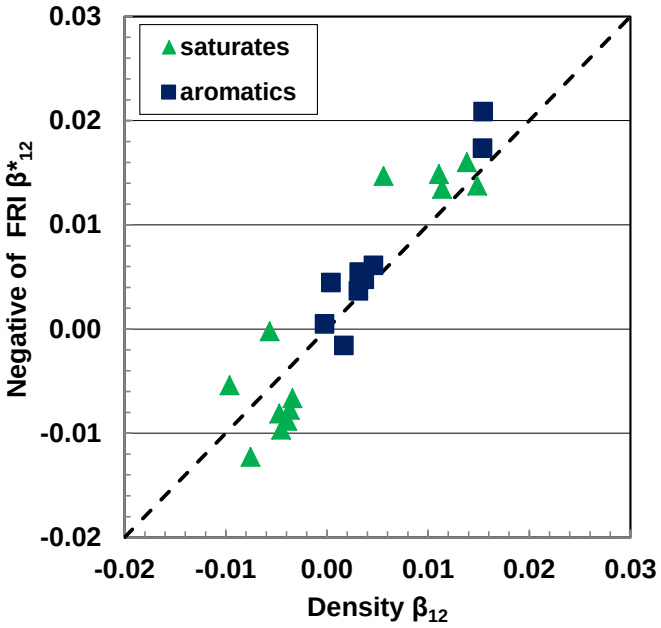

Figure 5.26: Correlation of binary interaction parameters for FRI and density.

In summary, we now have correlations between FRI and density, their thermal coefficients, and their excess properties. Therefore, FRI or density can be predicted as a function of temperature given a single measurement of either of the variables. Similarly, the excess properties of one can be predicted from the other. As an example, the FRI of the saturate and aromatic fractions were predicted at 20°C from the measured densities at 20°C using Equation 5.27. The FRI at 40 and 60°C were then predicted using Equations 5.21 and 5.22. This method fit the experimental FRI_{40} and FRI_{60} data with an AARD of < 1% in both cases. In contrast, the one-third rule applied at these temperatures fit the experimental data with an AARD of approximately 2%.

5.4 Effect of Cracking on SAR Fraction Properties

Although the dataset is limited, some preliminary observations on the effects of thermo-cracking and hydrocracking are made. The molecular weight and density (at 20°C) data for the saturates, aromatics, and resins are summarized in Figures 5.27 and 5.28, respectively. Since FRI and density are closely correlated, the FRI data are not considered here. Recall that the samples are classified as follows:

- Unreacted (native): WC-B-B2, Arabian, WC-DB-A2, WC-B-C1, WC-VB-B2
- Unknown: 27-168-179
- Thermocracked: 26845-38, 27034-87, 27-034-113
- Hydrocracked: HOSB

The feedstock for the cracked samples was a WC-B-B2 bitumen.

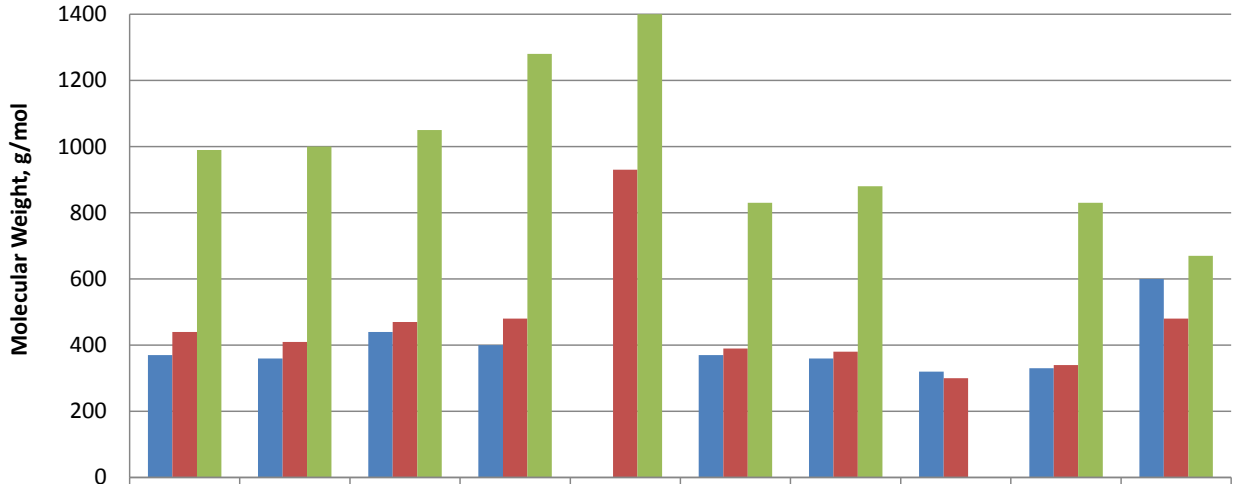

	WC-B-B2	Arabian	WC-DB-A2	WC-B-C1	WC-VB-B2	27168179	26845-38	27034-87	27034113	HOSB
Saturates	370	360	440	400		370	360	320	330	600
Aromatics	440	410	470	480	930	390	380	300	340	480
Resins	990	1000	1050	1280	1400	830	880		830	670

Figure 5.27: Molecular weight of saturates, aromatics, and resins measured in toluene at 50°C.

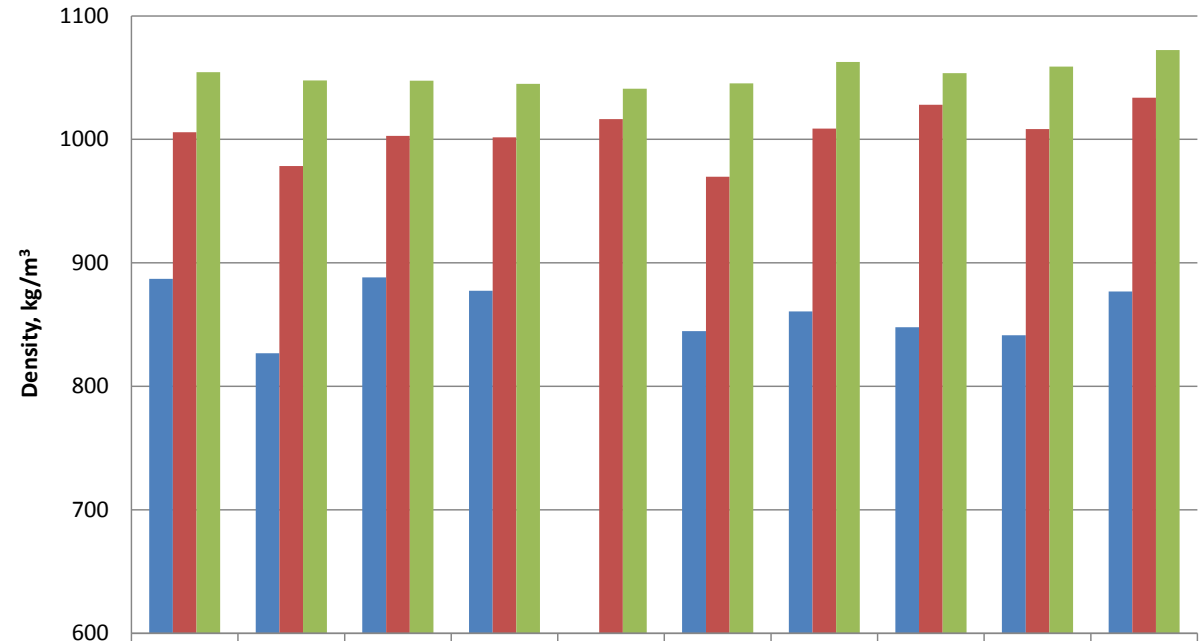

	WC-B-B2	Arabian	WC-DB-A2	WC-B-C1	WC-VB-B2	27168179	26845-38	27034-87	27034113	HOSB
Saturates	887.1	826.7	888.2	877.4		844.8	860.6	847.8	841.4	876.9
Aromatics	1005.9	978.5	1002.9	1001.6	1016.5	969.7	1008.7	1028.1	1008.3	1033.8
Resins	1054.4	1047.7	1047.6	1045	1041	1045.3	1062.8	1053.6	1059	1072.3

Figure 5.28: Density of saturate, aromatic, and resins samples at 20°C.

Thermocracking reduces the molecular weight of each fraction. It decreases the density of the saturates but has little impact on the density of the aromatics and resins. Thermal processes are expected to decrease the average molecular weight of the fractions due to cracking. This effect will be most pronounced in the saturates and aromatics because the smaller molecules created by cracking tend to accumulate in these fractions. The density of the saturates decreases in accordance with the lower molecular weight. The effect on the density of the aromatic, resin and asphaltene fractions is more complex because, although they become smaller, they also become more polar as the paraffinic fragments are stripped from the aromatic ring structures. These two effects oppose each other and therefore the density changes relatively little and may even increase.

The hydrocracked HOSB sample exhibits higher molecular weight saturates but lower molecular weight aromatic and resin fractions than the feedstock. It is likely the lightest saturates were removed in the distillation prior to the HOSB separation. The density of the aromatic and resins fractions increases relative to the feedstock. It is likely that the extent of reaction was significant enough that the density increase from the increase in polarity due to side chain removal more than compensated for the decrease in density expected with smaller molecules.

Of significance here is that, despite the changes in chemical structure from both thermocracking and hydrocracking, the relationship between FRI and density remained consistent. Hence, there is some promise that correlations for solubility parameters can be developed for the reacted materials that will allow the regular solution approach to be applied.

Chapter Six: Asphaltene Content and Yield Determination from Refractive Index Measurements

The determination of solubility parameters for saturate and aromatic fractions involves the measurement of asphaltene yields, and several grams of each fraction are required for accurate results. Since it is time consuming to obtain these fractions, it is desirable to measure the yields at low masses and volumes. Gravimetric measurements involving saturates also require washing the precipitate with the saturate fraction, a process which can consume a large amount of saturates. Therefore, an alternative method is desired. One option is to measure the volume fraction of asphaltenes that remain in solution (in the supernatant) using the refractive index of the solution, and then calculate the yield from a mass balance. This approach would require less of the saturate or aromatic fraction but could suffer from a propagation of errors when determining the volume fraction. This chapter present the low volume FRI method and tests the accuracy of this approach. Note, that all of the samples considered in Chapter 5 were evaluated in Chapter 6 except for the Arabian sample. Wax drop out was observed for the Arabian sample at 20°C which invalidated the experiments.

6.1 Approach

The objective is to determine the fractional yield of precipitated asphaltenes from solvents systems which is defined as follows:

$$f_A = \frac{m_A^{ppt}}{m_A^o} = \frac{m_A^o - m_A^s}{m_A^o} \tag{6.1}$$

where f_A is the fractional yield, $m_A{}^{ppt}$ is the mass of precipitated asphaltenes, $m_A{}^{\circ}$ is the initial measured mass of asphaltenes and $m_A{}^{s}$ is the mass of asphaltenes remaining in solution. See Chapter 3 for details of asphaltene solubility measurements. The initial mass of asphaltenes is a controlled variable. Gravimetric methods measure the mass of precipitate directly. Here, the intention is to measure the mass of asphaltenes in solution which can be determined from the measured volume fraction as follows:

$$m_A^s = \frac{\phi_A V_S \rho_A}{1-\phi_A} \tag{6.2}$$

where ϕ_A is the volume fraction of asphaltenes, V_S is the volume of solvents, and ρ_A is the asphaltene density. The volume fraction is to be determined from FRI measurements.

As discussed in Chapter 5, the FRI of a mixture is often taken as the volume average of the FRI of the components, which for a binary mixture is given by:

$$FRI_{mix} = \phi_1 FRI_1 + \phi_2 FRI_2 \tag{6.3}$$

where ϕ is volume fraction and subscripts *1, 2,* and *mix* refer to the two components of the mixture and the mixture itself. If the FRI of a mixture FRI follows this "ideal" volume average mixing rule, the volume fractions of the constituents in a binary mixture can be determined as follows:

$$\phi_1 = \left(\frac{FRI_{mix} - FRI_2}{FRI_1 - FRI_2} \right) \tag{6.4}$$

For binary mixtures that do not form regular solutions, the FRI of these mixtures could be fitted with the following "non-ideal" mixing rule:

$$FRI_{mix} = \phi_1 FRI_1 + \phi_2 FRI_2 - \phi_1 \phi_2 (FRI_1 + FRI_2) \beta_{12}^* \tag{6.5}$$

The volume fraction of a component in the excess volume binary mixture is found from the solution of the following quadratic equation:

$$\beta_{12}^* \phi_1^2 + \left[\left(\frac{FRI_1 - FRI_2}{FRI_1 + FRI_2} \right) - \beta_{12}^* \right] \phi_1 + \left(\frac{FRI_2 - FRI_{mix}}{FRI_1 + FRI_2} \right) = 0 \tag{6.6}$$

Note for asphaltenes in a mixed solvent, the FRI of the asphaltenes (FRI_1) and of the mixed solvent (FRI_2) are required. The FRI of the solvent mixture can be determined from Equation 6.3 or 6.5. The refractive indices and densities were measured as described in Chapter 5. Asphaltene precipitation (solubility) measurements were performed as described in Chapter 3.

6.2 Refractive Index of Solvent Mixtures

Asphaltene yields were determined in solutions of heptane and toluene, saturates and toluene, or heptane and aromatics. The FRI of the asphaltene-free solvent mixtures are required before determining the asphaltene concentration. As discussed in Chapter 5, solutions of toluene and heptanes were found to follow the volume averaging (regular solution) mixing rule. FRI calculated with the volume average mixing rule were compared with the measured FRI and the average absolute deviation (AAD) was 0.00029 and the average absolute relative deviation (AARD) was 0.1%, approximately within the accuracy of the measurements. Therefore, the volume averaging FRI method was used to determine the FRI of solutions of heptane and toluene.

Mixtures of SARA fractions with a solvent were found to deviate from the volume average mixing rule (Chapter 5), but could be fitted with the excess volume mixing rule. The β^*_{12} used for the SARA fractions were determined Equation 5.10. The calculated β^*_{12} for 27-168-179 saturates/toluene was 0.00482 and -0.02129 for WC-B-B2 aromatics/heptane. FRI calculated with both the volume averaging and excess volume mixing rules were compared with the measured FRI for 27-168-179 saturates in toluene and WC-B-B2 aromatics in heptane. The average deviations between the calculated and measured FRI are given in Table 6.1. The error of 0.00034 occurs for 27-168-179 saturates because the β^*_{12} from the correlation is not exactly the same as the actual β^*_{12} from fitting the experimental FRI data for this sample. The deviations of 0.00001 and 0.00034 are representative of the best and worst cases, respectively, observed with this method. The accuracy of the excess volume method is superior to that of the regular solution method and therefore it is recommended for all solutions involving SARA fractions.

Table 6.1: Deviation between measured FRI and the calculated FRI of solutes in solvents using the regular solution mixing rule and excess volume mixing rule.

Sample	Volume Average Rule		Excess Volume Rule	
	AAD	%AARD	AAD	%AARD
27-167-178 saturate/toluene	0.00086	0.3	0.00034	0.1
WC-B-B2 aromatics/heptane	0.00230	1.0	0.00002	<0.1

6.3 Asphaltene Contents in Heptol Mixtures

As a first step, asphaltene volume fractions were determined at conditions where all of the asphaltenes remained in solution (no precipitation); that is, with pseudo-ternary solutions of asphaltenes in heptane and toluene at heptane contents below 50 vol%. The gravimetric asphaltene content is simply the mass of asphaltenes added divided by the mass of the solution. The FRI of the heptane/toluene mixed solvent was calculated using the volume averaging mixing rule. The refractive indexes of the asphaltenes were calculated from FRI data of asphaltenes in toluene using two methods: 1) volume averaging; 2) excess volume mixing rules.

The experimental solubility data for WC-B-B2 and 26845-38 C_7 asphaltenes at heptane contents below 50 vol% are presented in Figures 6.1 and 6.2. The numbers in the legend represent the heptane content for each data set. Figure 6.1 (a) shows the calculated asphaltene volume fractions against the gravimetric volume fractions assuming a volume average mixing rule for the FRI of the heptol/asphaltene pseudo-binary. Figure 6.1 (b) shows the same data except that the excess volume mixing was used for the FRI of the heptol/asphaltenes pseudobinary. In this case, the FRI and densities of the asphaltenes were calculated using excess volume mixing rules. Estimated β^*_{12} for the asphaltene-heptol solutions ranged from -0.021 to -0.024. In Figure 6.1 (b), asphaltenes from 26845-38 at 40 vol% heptane deviated from an otherwise linear trend. This could be attributed to onset of asphaltene precipitation for this sample.

The average deviations between the calculated and measured volume fractions are reported in Table 6.2. There appears to be a systematic deviation to low volume fractions with the FRI method. Although there is a lower average error when using the volume average mixing rule, the results are more scattered than with the excess volume rule. The data cluster on a consistent linear trend with the excess volume rule, Figure 6.1 (b). It appears that the non-ideal interaction between asphaltenes and the heptol must be accounted for to determine consistent volume fractions. However, the systematic error must still be addressed.

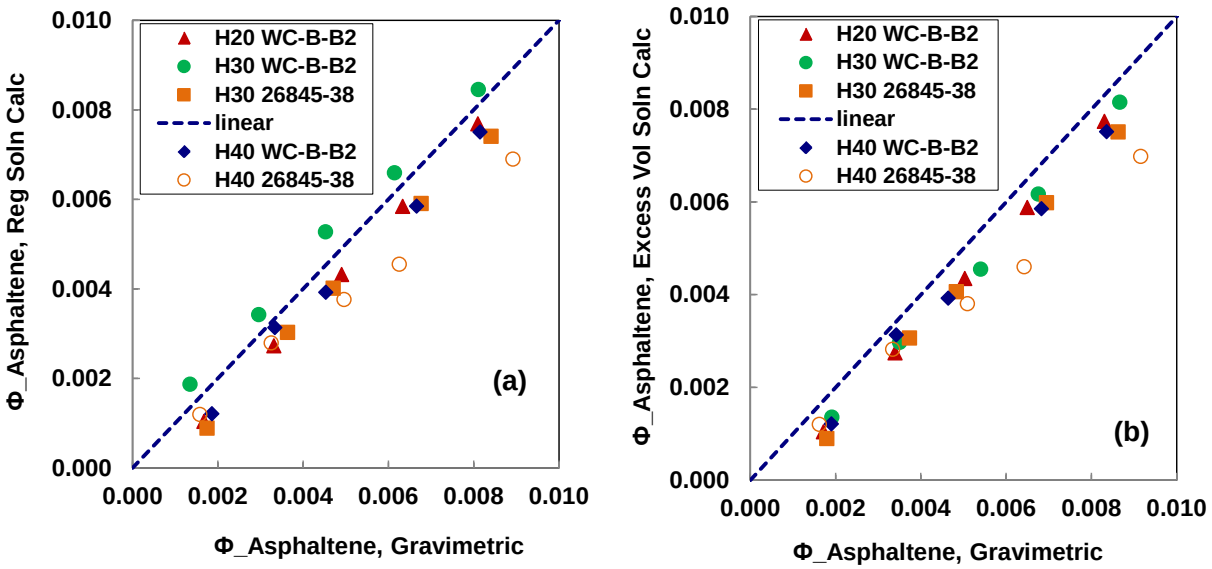

Figure 6.1: Measured asphaltene volume fractions compared to asphaltene gravimetric volume fractions assuming (a) regular solution mixing rule and (b) excess volume solution mixing rule for asphaltenes FRI, densities and interaction with heptol. The numbers in the legend are the vol% of heptane in the solvent mixture.

Table 6.2: Average deviations between the calculated and measured volume fractions for WC-B-B2 and 26845-38 asphaltenes in heptol at all heptol ratios measured.

	Regular Solution	Excess Vol. Solution
AAD	0.00072	0.00082
%AARD	17.67	19.15

It was observed that the asphaltene content calculations are very sensitive to the FRI of the heptol. Interestingly, the introduction of a small non- ideality for the heptol (β^*_{12} = 0.00080) fit all the asphaltene/heptol data quite well, Figure 6.2 (AARD of 6.3%). This small excess volume has negligible effect on the fitting of the FRI data of the mixture of heptane and toluene. It seems likely that there is a small excess volume of mixing for solutions of heptane and toluene. While accounting for this excess volume provided accurate volume fractions, the sensitivity of the FRI method to small non-idealities is a potential concern.

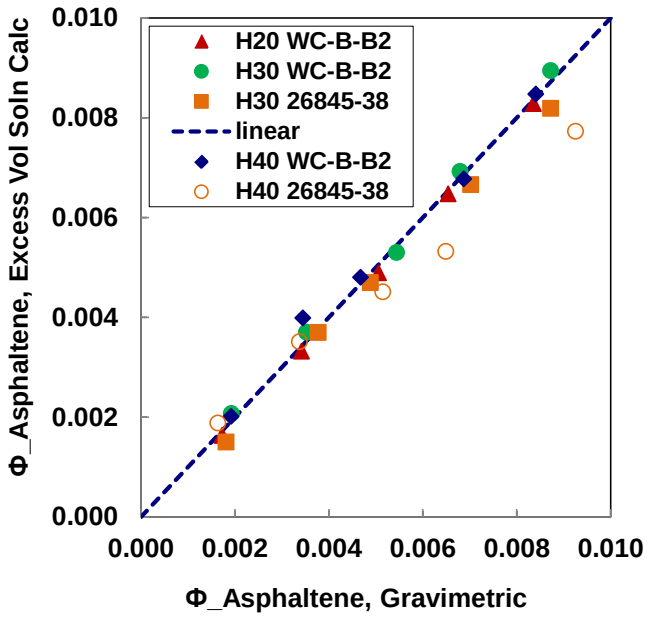

Figure 6.2: Measured asphaltene volume fractions compared to asphaltene gravimetric volume fractions assuming excess volume solution mixing rule for heptol mixtures and asphaltene-heptol mixtures.

The volume fractions calculated from FRI with the excess volume solution mixing behaviour (for all the mixtures) are compared with the gravimetric measurements (all at 10 g/L) in Table 6.3. The concentration of 10 g/L was selected because the asphaltene solubility measurements used to determine solubility parameters are performed at this concentration. The β^*_{12} used for the heptol mixtures was set to 0.00080 whereas β^*_{12} (-0.021 to -0.024) for asphaltene-heptol mixtures was estimated with Equation 5.10. Asphaltene densities and FRI using excess volume

extrapolations are 1.1509g/cm^3 and 0.38971 for WC-B-B2 and 1.1794g/cm^3 and 0.40995 for 26845-38. Excluding the measurements for the sample 26845-38 at 40 vol% heptane (with possible onsets of asphaltene precipitation), the AAD and %AARD were 0.00024 and 2.74, respectively.

Table 6.3: Asphaltene gravimetric volume fractions compared to the volume fractions estimated from FRI of solutions at approximately 10 g/L assuming excess volume of mixing behaviour for all the mixtures (heptane-toluene and asphaltene-heptol)

Solution/Sample	Vol. Fraction Gravimetric	Vol. Fraction Excess vol	Deviation	AARD%
H20 WC-B-B2	0.00830	0.00828	-0.00003	0.31
H30 WC-B-B2	0.00866	0.00883	0.00017	1.94
H40 WC-B-B2	0.00835	0.00826	-0.00010	1.15
H30 26845-38	0.00863	0.00798	-0.00065	7.55
H40 26845-38	0.00916	0.00763	-0.00153	16.72

6.4 Asphaltene Yield Measurements

The second step was to determine asphaltene yields at conditions where asphaltenes do precipitate: that is, in solutions of heptol at heptane content above 50 vol% (from FRI of the separated supernatant). Yields calculated with the FRI method results were compared those from the gravimetric method. Both the volume averaging and excess volume mixing rules for asphaltene/heptol mixtures were evaluated for the FRI method. Note that in this case, FRI of heptol mixtures were either measured directly or calculated using Equation 5.10 with β^*_{12} of 0.00080 in the cases were direct measurements were unavailable.

The methods were assessed for “high” masses of asphaltenes (0.10 g in 10 cm³ of solvent) and “low” masses (0.02 g in 2 cm³ of solvent). The gravimetric method is expected to be precise to ± 0.02 w/w asphaltene yield at high masses but less precise at low yields. Gravimetric methods are sensitive to washing procedures and small mass measurement errors at low masses. The FRI

method may be sensitive to small errors in FRI measurements (for example if solvent evaporation alters the FRI of the solvent). The excess volume FRI method also depends on the accuracy of the binary interaction parameter correlation. It could also be sensitive to any changes in the soluble asphaltene composition or asphaltene self-association that may occur during precipitation. Therefore, low mass gravimetric and FRI based yields are compared with high mass gravimetric based yields for WC-B-B2 asphaltenes in Figure 6.3. Both the low mass gravimetric method and the volume average FRI method underestimated the yields, particularly near the onset of precipitation. The excess volume FRI method was generally within 0.1 w/w (approximately 10% deviation at high yields) of the high mass gravimetric yield. Hence, the excess volume FRI method appears to be the best approach for low mass yield measurements.

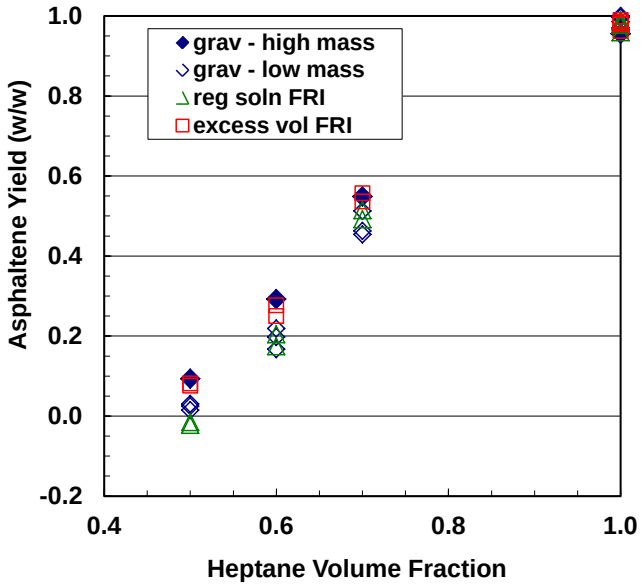

Figure 6.3: Fractional WC-B-B2 asphaltene yields in heptol solutions at 21°C.

Due to limited amounts of sample, only low mass measurements were evaluated for three other asphaltene samples, Figure 6.4. All three methods capture the shift in onset from approximately 0.4 to 0.5 to 0.6 heptol ratio for the 26845-38, WC-B-C1 and 27-168-179 asphaltenes, respectively. In general, the measurements are within 0.2 w/w yield of each other and the excess volume mixing rule gives the highest yields. Based on the WC-B-B2 data, these are likely the most accurate yields.

Note that the FRI yield estimated at the highest precipitant volume fraction match the gravimetric yields. These solubility measurements were done in ≥ 0.9 heptane volume fraction and therefore were least affected by the error introduced with the β_{12}^{*} estimations. Also, the mass of precipitate was highest at this condition and therefore the mass errors were minimized for the gravimetric method.

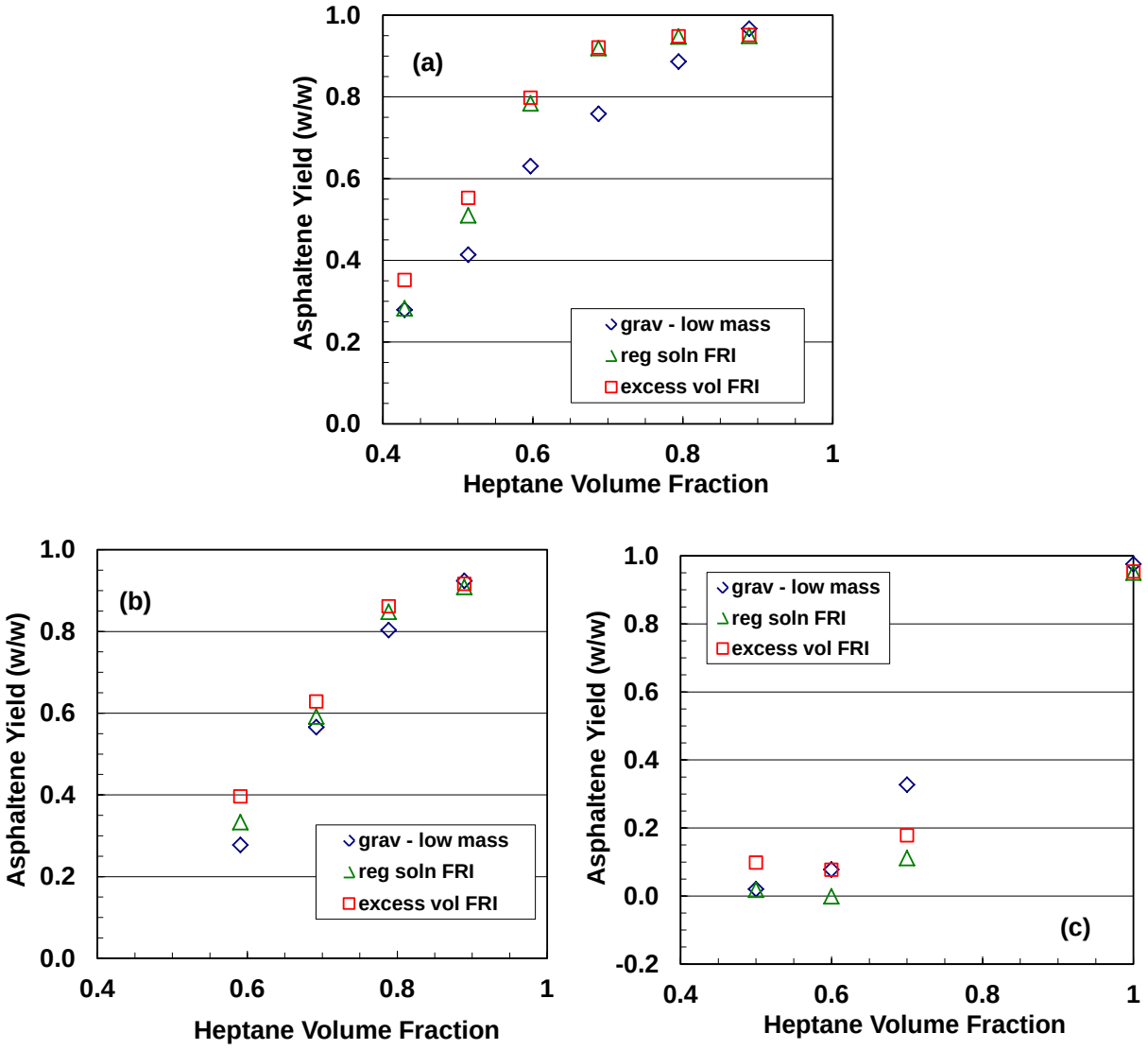

Figure 6.4: Fractional asphaltene yields in heptol solutions at 21°C: a) 26845-38 asphaltenes; b) WC-B-C1 asphaltenes; c) 27-168-179 asphaltenes.

6.5 Saturates and Aromatics Solubility Measurements

Recall that the main objective of this work is to determine saturate and aromatic solubility parameters from asphaltene yield measurements. Asphaltene yields were determined from solutions of toluene/saturates or aromatics/heptane using both the gravimetric method and the volume averaging or excess volume FRI methods. The binary interaction parameters applied in the excess volume FRI measurements were either those β_{12}^{*} values used to fit previous FRI data or were estimated from the correlation (Equation 5.10) when fitted values were not available.The methods were assessed on "low" masses (≤ 0.02 g of asphaltenes in 2 cm³ of solvent). Asphaltene solubility measurements were performed using only WC-B-B2 C_7-asphaltenes.

6.5.1 Asphaltene Yield Measurements with Saturate as Precipitant

Unlike the previous results for asphaltene in heptol solutions, the FRI based yields were lower than the low mass gravimetric yields, Figure 6.5. The problem appears to be the sensitivity of the FRI method to the binary interaction parameter between the saturates and toluene, β_{12}^{*}.

For example, Figures 6.6 and 6.7 show the effect of using the correlated versus the fitted β_{12}^{*} on the calculated yields. In Figure 6.6, the correlation provides a better yield prediction while in Figure 6.7 the fitted value is better. Nonetheless, all of the yields calculated from FRI data are lower than the gravimetric yields. Figures 6.6 and 6.7 present the best and worst case scenarios for the sensitivity of FRI based measurements to the value of β^{*}_{12}. Given the sensitivity to the interaction parameters for these pseudo-ternary mixtures, the gravimetric method is recommended.

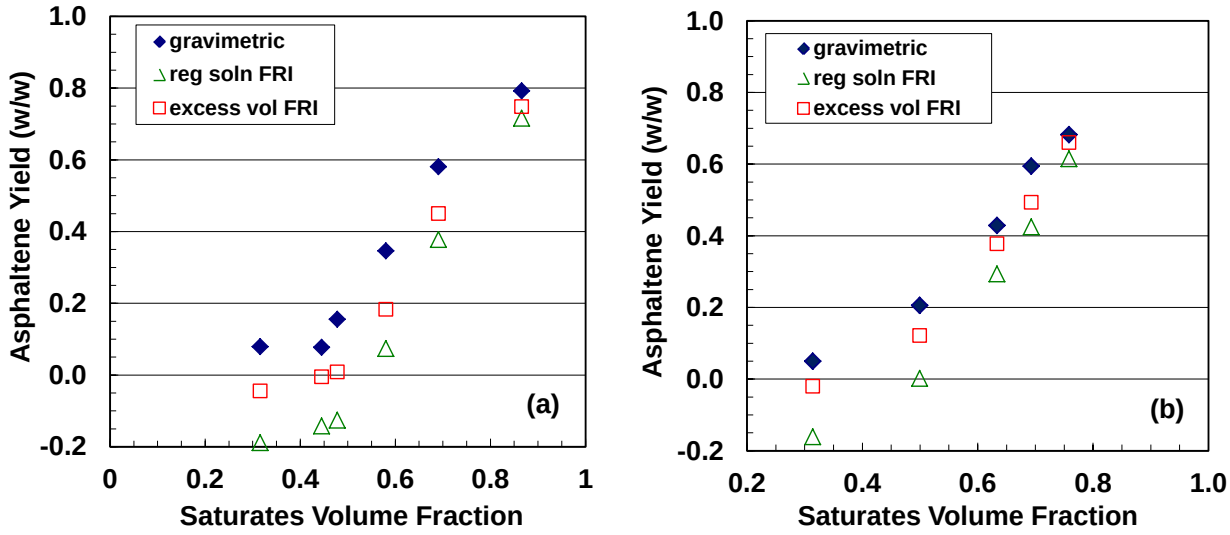

Figure 6.5: Fractional asphaltene yields in saturates/toluene solutions at 21°C for: a) 26845-38 saturates; b) WC-DB-A2 saturates.

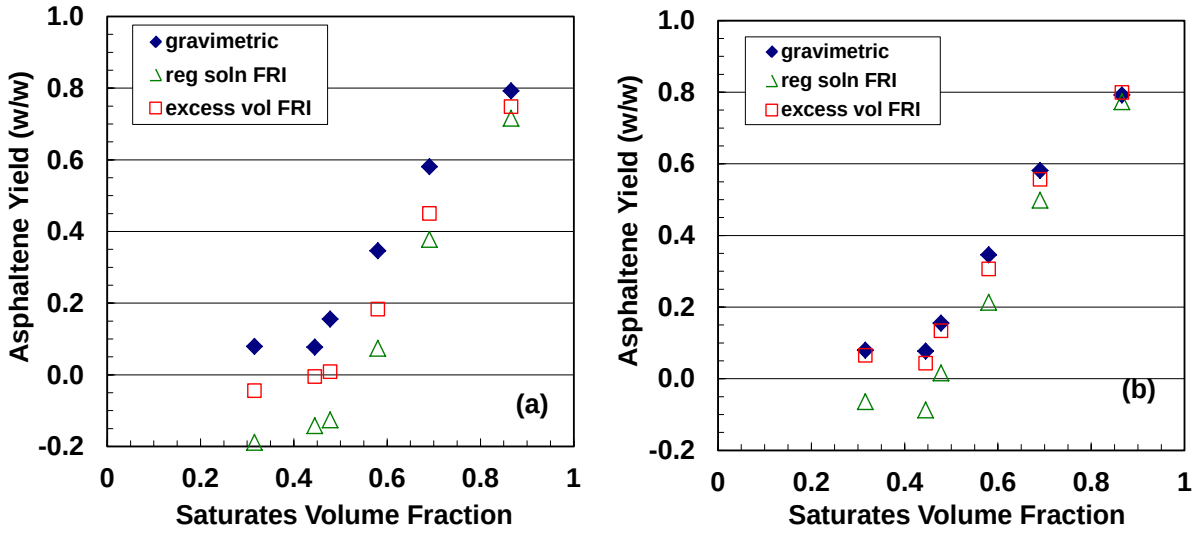

Figure 6.6: The effect of β^*_{12} on the asphaltene yield from solutions of 26845-38 saturates and toluene at 21°C: a) β^*_{12} of 0.0078 from fitting saturate/toluene FRI data; b) β^*_{12} of 0.0069 from correlation, Eq. 5.10.

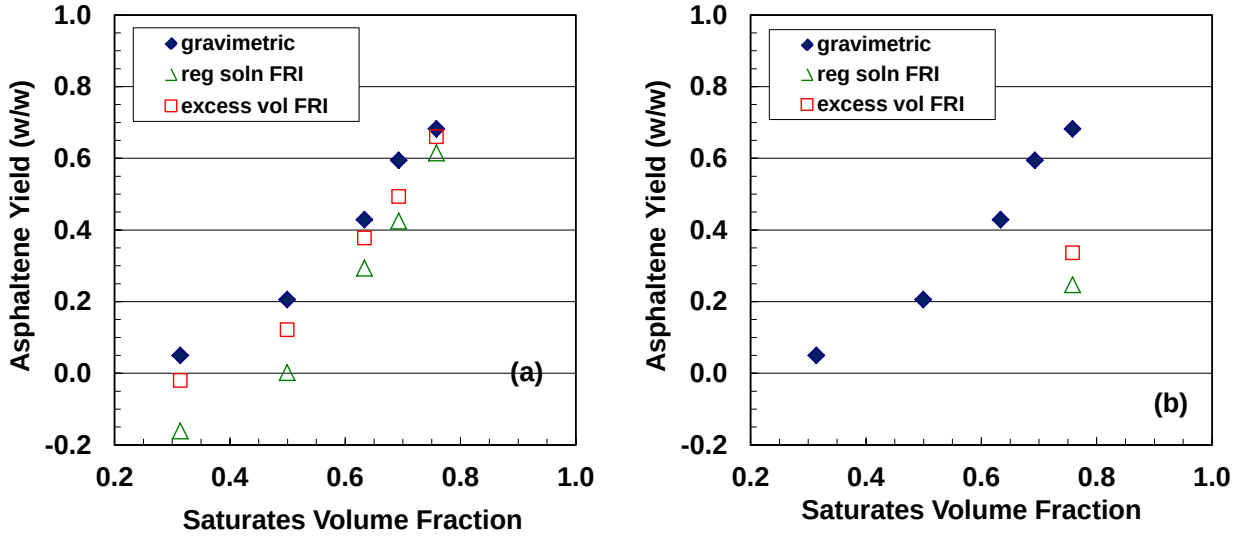

Figure 6.7: The effect of β^*_{12} on the asphaltene yield from solutions of WC-DB-A2 saturates and toluene at 21°C: a) β^*_{12} of 0.0067 from fitting saturate/toluene FRI data; b) β^*_{12} of 0.0116 from the correlation, Eq. 5.10. Note, most of the FRI method points for (b) are far below zero.

Figure 6.8 shows the gravimetric based asphaltene yields from all of the solutions of saturates and toluene. Most of the yields follow a consistent trend. The hydrotreated sample (HOSB) and 27-168-179 (of unknown reaction history) do not follow this trend. The HOSB saturates had a significantly higher molecular weight than the other saturates and therefore a change in solubility parameter is not surprising. The 27-168-179 saturate properties were not significantly different than the other saturates. Since the history of this sample is unknown, it was not possible to determine why these saturates give a different yield.

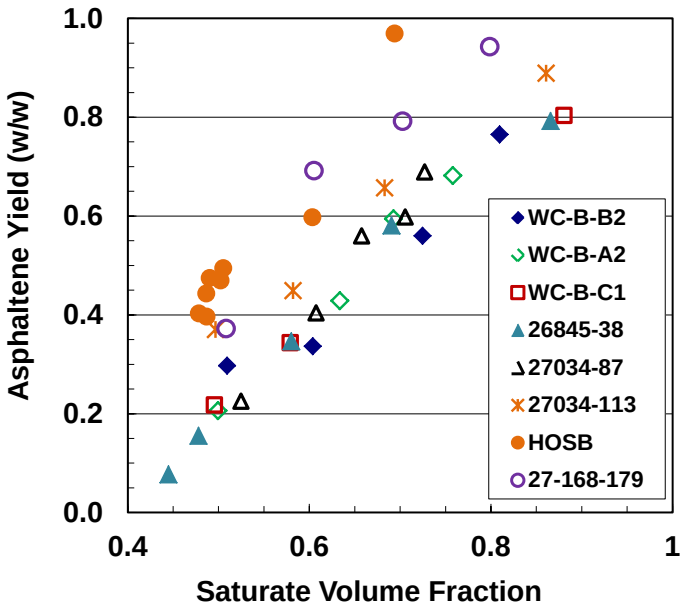

Figure 6.8: Fractional asphaltene yields in saturates/toluene solutions at 21°C for WC-B-B2 asphaltenes using different saturate fractions as precipitants.

6.5.2 Asphaltene Yield Measurements with Aromatics as Solvent

As was observed for the solutions with saturates, the FRI based yields were lower than the gravimetric yields but with more scatter and higher error bars especially at lower precipitant volume fractions, Figure 6.9 and 6.10. Therefore, only the gravimetric based yields were used from this point on.

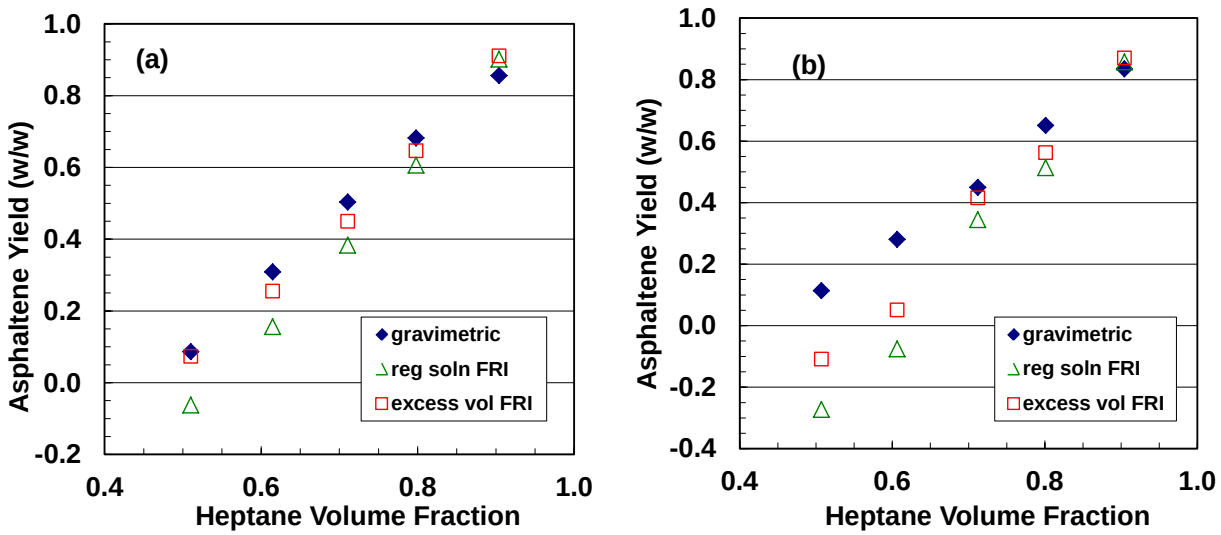

Figure 6.9: Fractional asphaltene yields in aromatics/heptane solutions at 21°C for: a) WC-B-B2 aromatics; b) WC-B-C1 aromatics.

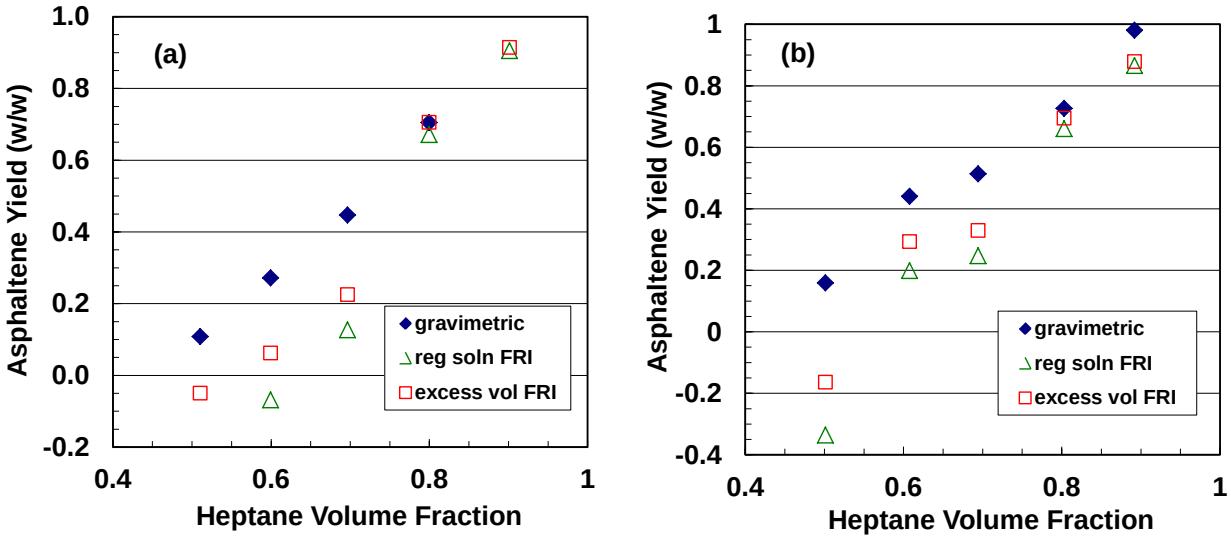

Figure 6.10: Fractional asphaltene yields in aromatics/heptane solutions at 21°C for: a) 26845-38 aromatics; b) WC-DB-A2 aromatics

The gravimetric asphaltene yields for solutions of aromatics and heptane all followed a consistent trend, Figure 6.11, although WC-DB-A2 and HOSB data had more scatter than the others. Likewise to their saturates solubility properties, 27-168-179 aromatics deviate from an otherwise consistent trend.

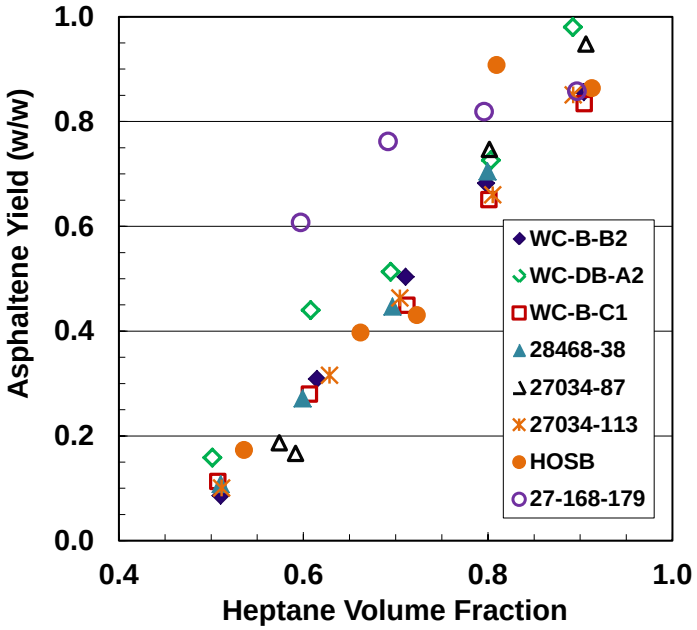

Figure 6.11: Fractional asphaltene yields in aromatics/heptane solutions at 21°C for WC-B-B2 asphaltenes using different aromatic fractions as solvent.

6.6 Summary

For pseudo-ternary solutions of asphaltenes in a pure solvent mixture, the FRI based methods for asphaltene yield are an alternative to the cumbersome gravimetric experiments. Any excess volumes must be accounted for in the yield calculation including small excess volumes in the mixed solvent itself. The FRI method is particular well suited for experiments where low masses are required. The method was not accurate for pseudo-ternaries involving saturates and aromatics. It is likely that the accumulation of error from the excess volumes and possible ternary interactions in the excess volumes was too significant for accurate yield calculations.

Chapter Seven: Saturates and Aromatics Solubility Parameters

The solubility parameters of saturates and aromatics cannot be measured directly but rather are determined by fitting a regular solution model to solubility measurements involving these fractions. In this chapter, the regular solution model described in Chapter 4 is fitted to the gravimetric solubility measurements from Chapter 6 of asphaltenes in solutions of toluene/saturates and aromatics/heptane. Since the asphaltene, heptane, and toluene properties are known and the saturate and aromatic molar volumes are also known, the solubility parameters of saturates and aromatics can be determined from the model fitting. The correlation between solubility parameter and the refractive index is also explored.

7.1 Modeling Asphaltene Yield Data with Regular Solution Model

As discussed in Chapter 4, the inputs to the regular solution model are the molar volume and solubility parameter for each component or pseudo-component. In this case, the components are: toluene, n-heptane, saturates, aromatics, and the asphaltene pseudo-components. All of the properties are known except the saturate and aromatic solubility parameters. The known properties are presented first and then the fitting of the unknown solubility parameters is discussed.

7.1.1 Solvent Properties

The molecular weight, density, molar volumes, and solubility parameters of toluene and n-heptane at 21°C are provided in Table 7.1. The densities and solubility parameters were calculated as discussed in Chapter 4.

Table 7.1: Properties of *n*-heptane and toluene at 23°C.

Solvent	Molecular Weight (g/mol)	Density (g/cm^3)	Molar Volume (cm^3/mol)	Solubility Parameter ($MPa^{1/2}$)
n-heptane	100	0.6814	147.1	15.2
toluene	92	0.8660	106.4	18.3

7.1.2 Asphaltenes Property Distributions

Only WC-B-B2 C_7_asphaltenes were used for the solubility measurements of the saturate/aromatics model systems in this thesis. Therefore, the required asphaltene pseudo-component properties are the molecular weight, density distribution, solubility parameter distributions of the WC-B-B2 asphaltenes. These distributions were determined previously by Barrera *et al.* (2012).

Two WC-B-B2 asphaltene samples (A1 and A2) were used in this work and their average molecular weights were 4500 and 5000 g/mol, respectively. In both cases, the molecular weight distribution was determined with a Gamma function using a monomer molecular weight of 800 g/mol, a maximum molecular weight of 30000 g/mol. The shape factor was set based on model predictions for WC-B-B2 asphaltenes in solutions of heptane and toluene, Figure 7.1. The average asphaltene molecular weight was set to 4500 and 5000 g/mol for the two respective samples, and only the shape factor, β, was adjusted. A β of 1.5 was found to provide the best fit of asphaltene yield data in both cases. Note that the model predicted the slightly higher yields expected with the slightly higher molecular weight asphaltenes.

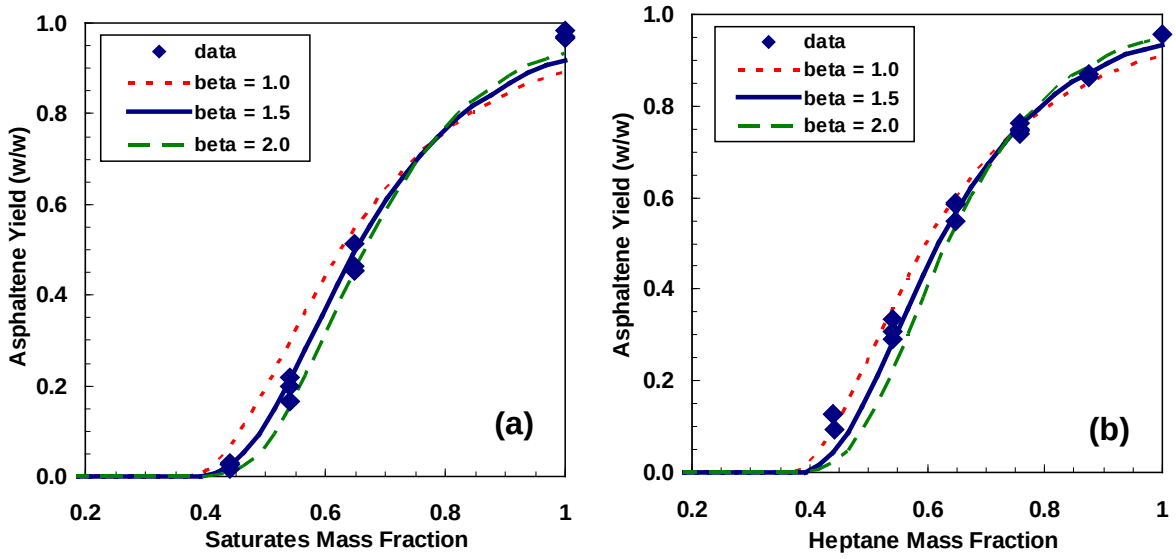

Figure 7.1: Effect of shape factor, β, on regular solution model fit of WC-B-B2 asphaltene yield in solutions of *n*-heptane and toluene (10 g/L asphaltenes, 21°C, 1 atm) for: 1) 4500 g/mol asphaltenes., A1; b) 5000 g/mol asphaltenes, A2.

The distributions were then divided into 30 asphaltene pseudo-components representing equal increments of molecular weight. The density and solubility of each asphaltene pseudo-component was determined from the correlations presented in Chapter 4 (Equations 4.3 and 4.5, respectively). The value of parameter *c* in the solubility parameter correlation (Equation 4.5) was found to be 0.0126 for WC-B-B2 asphaltenes based on fitting yield data from asphaltenes in solutions of heptane and toluene (Barrera, 2012). The properties of the asphaltene pseudo-components for the 5000 g/mol sample are summarized in Table 7.2.

Note, since the asphaltene molecular weight distribution represents nano-aggregates not individual molecules, the distribution can change with changes in temperature or composition. The temperature dependence is accounted for with a correlation of average molecular weight to temperature (not required for this work which was conducted only at 23°C). The compositional dependence has been found to be negligible except when there are significant changes in the ratio of resins to asphaltenes (Akbarzadeh *et al*, 2005, Yarranton and Fox, 2007). Therefore, the asphaltene property distributions were assumed to be unaffected by the presence of saturates and aromatics.

Table 7.2: Properties of 5000 g/mol WC-B-B2 asphaltene pseudo-components at 23°C.

Asphaltene Subfraction	Mass Fraction	Molar Mass (g/mol)	Density (g/cm^3)	Molar Volume (cm^3/mol)	Solubility Parameter ($MPa^{0.5}$)
1	0.03039	1000	1.123	1225	19.4
2	0.09587	1966	1.140	2055	19.8
3	0.13188	2932	1.153	2871	20.1
4	0.13930	3898	1.164	3678	20.3
5	0.12926	4864	1.172	4481	20.5
6	0.11107	5830	1.178	5280	20.6
7	0.09069	6796	1.183	6079	20.7
8	0.07140	7762	1.187	6878	20.8
9	0.05471	8728	1.190	7676	20.9
10	0.04105	9694	1.192	8476	21.0
11	0.03028	10660	1.194	9276	21.0
12	0.02203	11626	1.195	10077	21.1
13	0.01585	12592	1.196	10879	21.2
14	0.01129	13558	1.197	11682	21.2
15	0.00797	14524	1.198	12485	21.2
16	0.00559	15490	1.198	13289	21.3
17	0.00390	16456	1.199	14094	21.3
18	0.00270	17422	1.199	14899	21.3
19	0.00186	18388	1.199	15705	21.4
20	0.00128	19354	1.199	16511	21.4
21	0.00088	20320	1.199	17317	21.4
22	0.00060	21286	1.200	18124	21.4
23	0.00041	22252	1.200	18931	21.5
24	0.00027	23218	1.200	19738	21.5
25	0.00019	24184	1.200	20545	21.5
26	0.00012	25150	1.200	21352	21.5
27	0.00008	26116	1.200	22160	21.6
28	0.00006	27082	1.200	22967	21.6
29	0.00004	28048	1.200	23775	21.6
30	0.00003	29014	1.200	24582	21.6

7.1.3 Saturate and Aromatic Molar Volumes

Molar volume is simply the ratio of molecular weight to density. The molecular weights and densities were measured as described in Chapter 5 and are reported with the molar volumes in Tables 7.3 and 7.4 for saturates and aromatics, respectively. Recall that the WC-VB-B2 sample has insufficient saturates for characterization measurements.

Table 7.3: Properties of saturates at 21°C.

Saturate	Molecular Weight (g/mol)	Density (g/cm^3)	Molar Volume (cm^3/mol)	Solubility Parameter ($Mpa^{0.5}$)
Native Crude Oils				
WC-B-B2	370	0.8871	417.1	16.6
WC-DB-A2	440	0.8882	495.4	16.7
WC-B-C1	400	0.8774	455.9	16.7
Thermocracked Samples				
27034-113	330	0.8415	392.1	16.1
27034-87	320	0.8478	377.4	16.3
26845-38	360	0.8606	418.3	16.5
Hydrocracked Samples				
HOS Bottoms	600	0.8769	684.2	15.8
Unknown Sample				
27-168-179	370	0.8448	438.0	15.7

Table 7.4: Properties of aromatics at 21°C.

Aromatics	Molecular Weight (g/mol)	Density (g/cm^3)	Molar Volume (cm^3/mol)	Solubility Parameter ($Mpa^{0.5}$)
Native Crude Oils				
WC-B-B2	440	1.0059	437.4	20.8
WC-DB-A2	470	1.0029	468.6	20.8
WC-B-C1	480	1.0016	479.2	20.8
WC-VB-B2	930	1.0165	914.9	20.8
Thermocracked Samples				
27034-113	340	1.0083	337.2	20.8
27034-87	300	1.0281	291.8	20.6
26845-38	380	1.0087	376.7	21.0
Hydrocracked Samples				
HOS Bottoms	480	1.0338	464.3	20.8
Unknown Sample				
27-168-179	390	0.9697	402.2	19.2

7.1.4 Saturates Solubility Parameters

The saturate solubility parameters were determined from asphaltene solubility data in solutions of saturates and toluene. For each saturate, gravimetric asphaltene yields were measured as described in Chapter 3. The data for all of the saturates are shown in Figure 7.2. The data for the native and least reacted saturates follow the same trend indicating that their solubility parameters are similar. Note the relatively high scatter at low yields were the measurements that are least accurate (limits of gravimetric yield).

To model these data, the only remaining unknown is the solubility parameter of the saturate fractions. The saturate solubility parameter was adjusted to fit the yield data (with $\beta = 1.5$), as shown in Figure 7.3. Any obvious outliers were eliminated and the best fit was selected by

inspection with more weight given to the higher yield data. The solubility parameters determined with this method are precise to ±0.1 $MPa^{0.5}$. The fitting for each saturate is presented in Appendix B. The calculated saturate solubility parameters are given in Table 7.3.

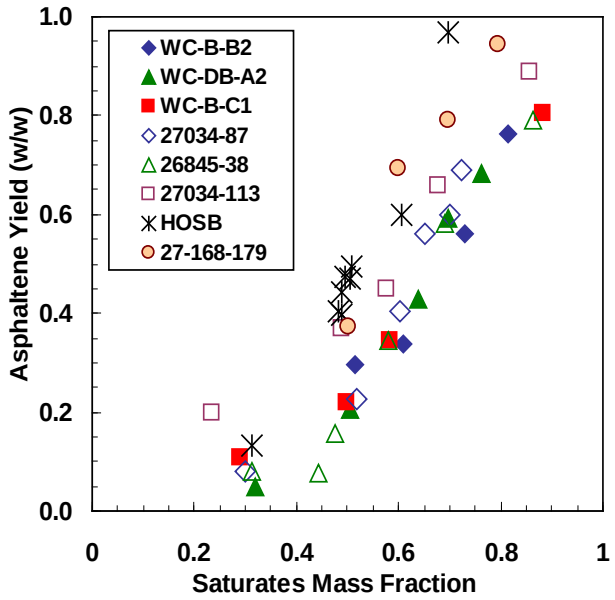

Figure 7.2: Solubility of 10 g/L of WC-B-B2 asphaltenes in solutions of toluene and various saturates at 21°C and 1 atm.

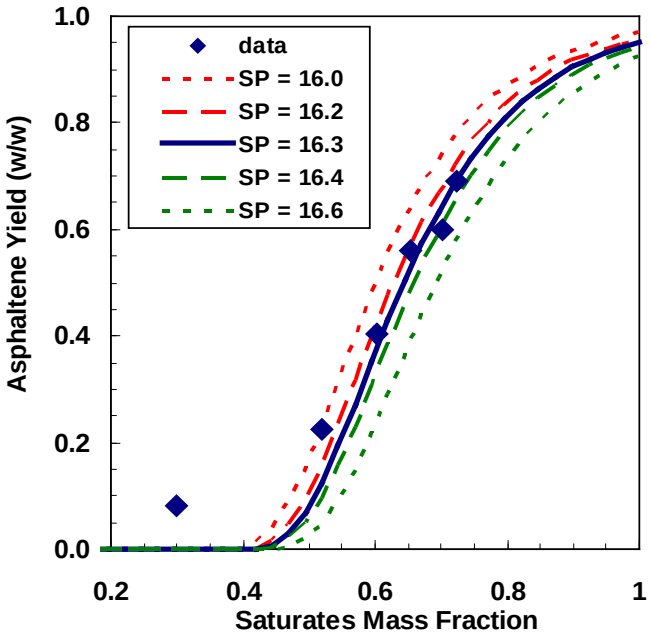

Figure 7.3: Determination of solubility parameter for 27034-87 saturates from yields of WC-B-B2 asphaltenes in toluene and the saturates. The solubility parameter is determined to be 16.3 ±0.1MPA$^{0.5}$.

The native saturates (from three different Western Canadian sources) had similar asphaltene yield curves, Figure 7.4a, and had almost identical solubility parameters (16.7 ± 0.1 MPa$^{0.5}$). These values are higher than the average solubility parameter of 15.9 MPa$^{0.5}$ suggested by Tharanivasan, 2012. The difference is partly caused by the update to the asphaltene characterization (the old characterization gives a solubility parameter of 16.4 MPa$^{0.5}$ for these data). However, most of the difference can be attributed to more extensive data; the previous values were based on a very limited dataset. Note, the model generally fits the yields above 0.3 w/w. The deviations at low yields are likely due to experimental error but a deficiency in the model cannot be ruled out.

The saturates recovered from *in-situ* processes have experienced some thermal cracking and the yield curves are shifted to the left, Figure 7.4b. In other words, less saturates are required to precipitate asphaltenes indicating that they have become poorer solvents for asphaltenes. Their solubility parameters are lower than the native asphaltenes, ranging from 16.1 to 16.5 MPa$^{0.5}$.

Compared to native samples, saturates from thermally cracked oils have lower densities, molecular weights, and solubility parameters (approximately 40 g/cm³, 60 g/mol, and 0.4 $MPa^{0.5}$ lower, respectively). These property changes suggest that thermal cracking may lead to an accumulation of relatively smaller paraffins (cracked off side chains) in the saturates.

The HOSB sample was hydrocracked and these saturates are a significantly poorer solvent for asphaltenes, Figure 7.5, with a solubility parameter of 15.8 $MPa^{0.5}$ (similar to that of heptane). The solubility parameter is similar to that of heptane even though the HOSB saturates have higher molecular weight and density than the native saturates. Higher molecular weight and density with low solubility parameter suggest that these saturates are enriched with naphthenic components.

Although no information is provided on the history of 27-168-179 fraction, its density and molecular weights are similar to the thermally cracked samples (especially 26845-38). However, its solubility parameter is significantly lower than those of both native samples and thermally cracked samples, Figure 7.5, but similar to that of the hydrocracked (HOSB) sample. The low molecular weight, density, and solubility parameter suggest that this sample has been extensively thermally cracked or hydrotreated and is enriched in relatively small paraffins.

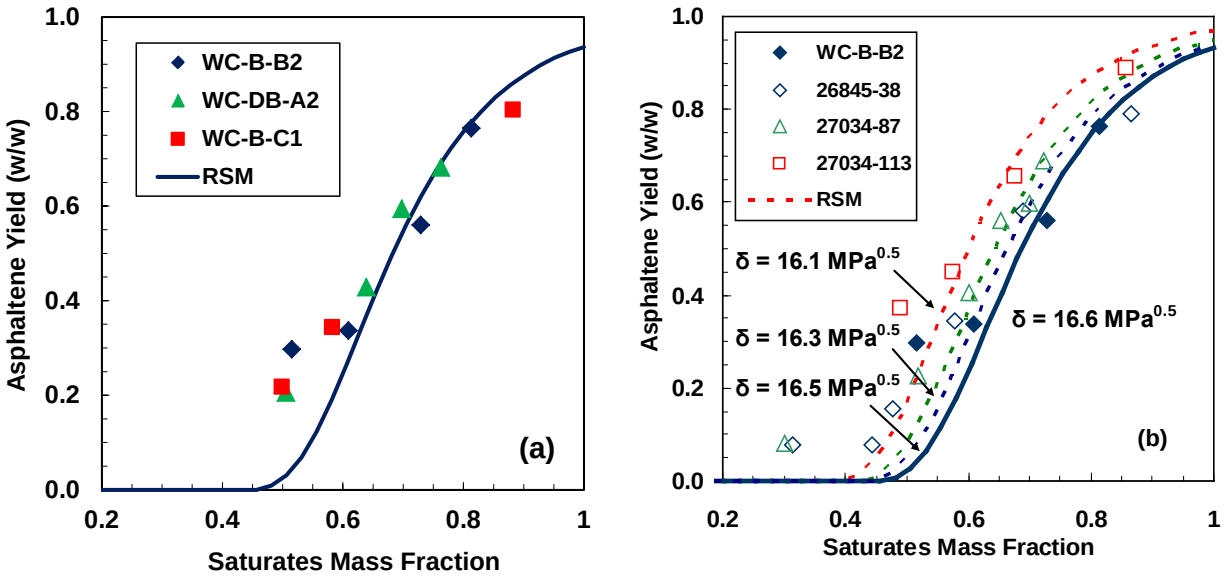

Figure 7.4: Asphaltene precipitation from solutions of asphaltenes in toluene/saturates at 21°C fit with regular solution model using: a) saturates from native oils with an average solubility parameter of 16.6 $MPa^{0.5}$; b) saturates from native WC-B-B2 bitumen and thermally cracked oils.

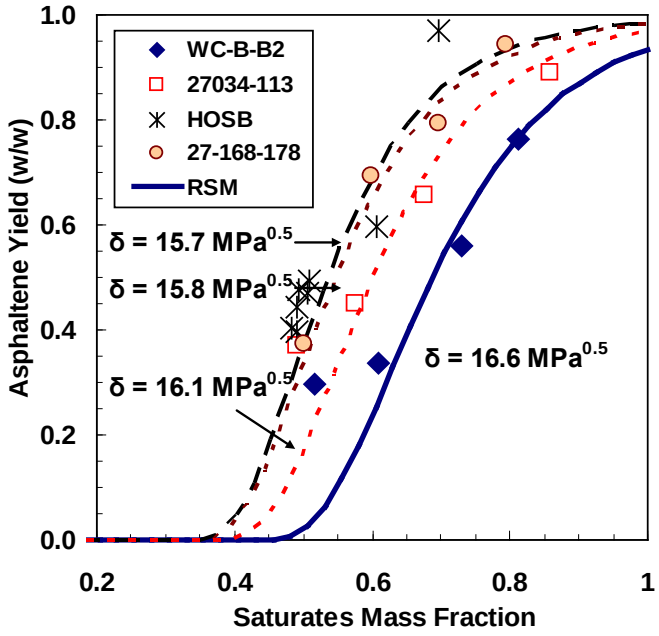

Figure 7.5: Asphaltene precipitation from solutions of asphaltenes in toluene/saturates at 21°C fit with regular solution model; comparison of saturates from native WC-B-B2, thermally cracked 27034-113, hydrocracked HOSB, and unknown 27-168-179 oil samples.

7.1.5 Aromatics Solubility Parameters

The yield data for all of the solutions with aromatics are shown in Figure 7.6. The data for most of the aromatics follow the same trend indicating that their solubility parameters are similar. As described for the saturates data, the aromatics solubility parameter was adjusted to fit the yield data (with $\beta = 1.5$), as shown in Figure 7.7. The solubility parameters determined with this method are precise to ±0.2 $MPa^{0.5}$. The fitting for each aromatic is presented in Appendix B. The calculated aromatic solubility parameters are given in Table 7.4.

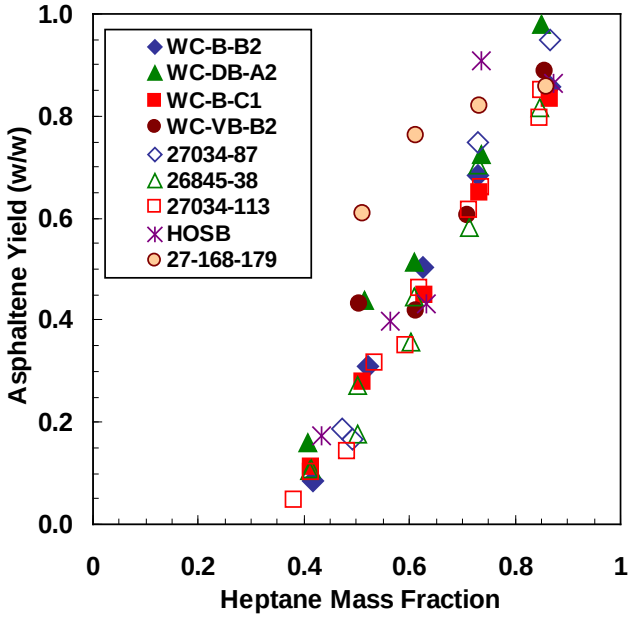

Figure 7.6: Solubility of 10 g/L of WC-B-B2 asphaltenes in solutions of heptane and various aromatics at 21°C and 1 atm.

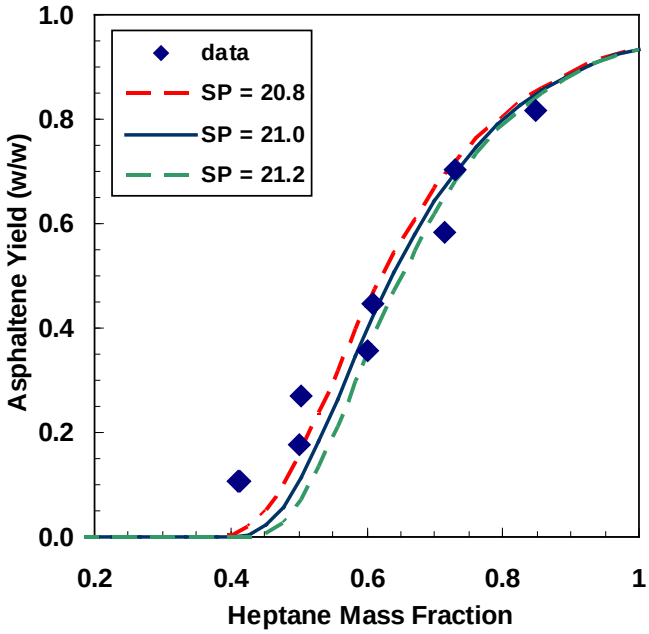

Figure 7.7: Determination of solubility parameter for 26845-38 aromatics from yields of WC-B-B2 asphaltenes in heptane and the aromatics. The solubility parameter is determined to be 21.0 ±0.2MPA$^{0.5}$.

The native aromatics had similar asphaltene yield curves, Figure 7.8a, and had similar solubility parameters (20.8 ±0.2 MPa$^{0.5}$). This value is lower than the average of 20.3 MPa$^{0.5}$ from Tharanivasan, 2012 for the same reasons as noted with the saturates. Note that while the density and molecular weight of the aromatics from the vacuum residue (WC-VB-B2) are higher than the source oil (consistent with removal of light components), the solubility parameter was not altered beyond the precision of the measurement.

The aromatics recovered from *in-situ* processes produce the same yield curves as native aromatics, Figure 7.8b, and have similar solubility parameters (20.8 ±0.2 MPa$^{0.5}$). Compared to native samples, aromatics from thermally cracked oils have lower molecular weights (approximately 50 g/mol lower), slightly higher densities, and similar solubility parameters. These property changes suggest that while thermal cracking has altered the aromatics, the overall impact on solubility parameter is negligible. Similarly, while the HOSB aromatics are denser than native aromatics, they provide the same solubility for asphaltenes, Figure 7.9. The HOSB

solubility parameter was unchanged from its source aromatics (20.8 $MPa^{0.5}$ for HOSB aromatics versus 20.8 $MPa^{0.5}$ for WC-B-B2 aromatics).

The 27-168-179 aromatics are an outlier and were the least effective solvent for the asphaltenes, Figure 7.9, with the lowest solubility parameter of all the aromatics (19.2 $MPa^{0.5}$). The density and molecular weight of these aromatics are similar to the other samples. Without knowing the history of this sample, it is not possible to determine why its aromatics are so different than those of the other samples.

.

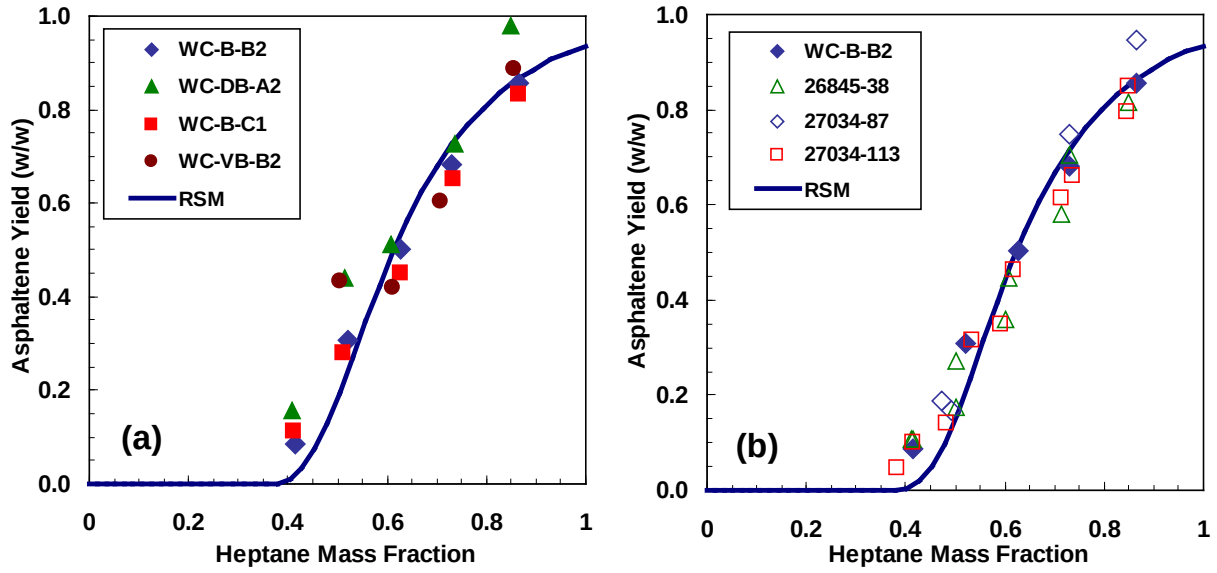

Figure 7.8: Asphaltene precipitation from solutions of asphaltenes in aromatics and *n*-heptane at 21°C fit with regular solution model: a) aromatics from native oils; b) aromatics from native WC-B-B2 bitumen and thermally cracked oils. The aromatic solubility parameter used in the fits shown here was 20.8 $MPa^{0.5}$.

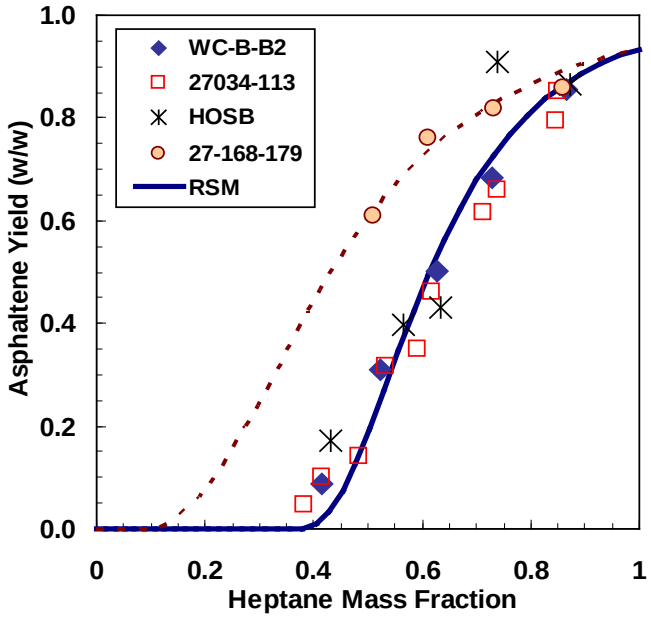

Figure 7.9: Asphaltene precipitation from solutions of asphaltenes in aromatics/*n*-heptane at 21°C fit with regular solution model: comparison of aromatics from native WC-B-B2, thermally cracked 27034-113, hydrocracked HOSB, and unknown 27-168-179 oil samples.

7.2 Solubility Parameter Correlations

7.2.1 Solubility Parameter and Refractive Index

Recall that Buckley *et al.*, 2001 had shown that the refractive index is linearly related to solubility parameter for a series of paraffinic hydrocarbons from methane to eicosane and for aromatics including benzene, toluene, ethylbenzene, *o*-xylene, styrene and *α*- methylnaphthalene. Figure 7.10a shows that Buckley et al.'s correlation is a good approximation for much of the hydrocarbon data but deviates significantly for molecules with long alkyl chains (high carbon number paraffins and alkylaromatics). The correlation fits the aromatic solubility parameters with an AARD of 3.1% but the saturates with an AARD of only 7.7%. If only the native aromatic and saturates are considered, the AARD are 4.4% and 6.3%, respectively. The correlation does not perform well for the saturates, probably because they include some long alkyl chains.

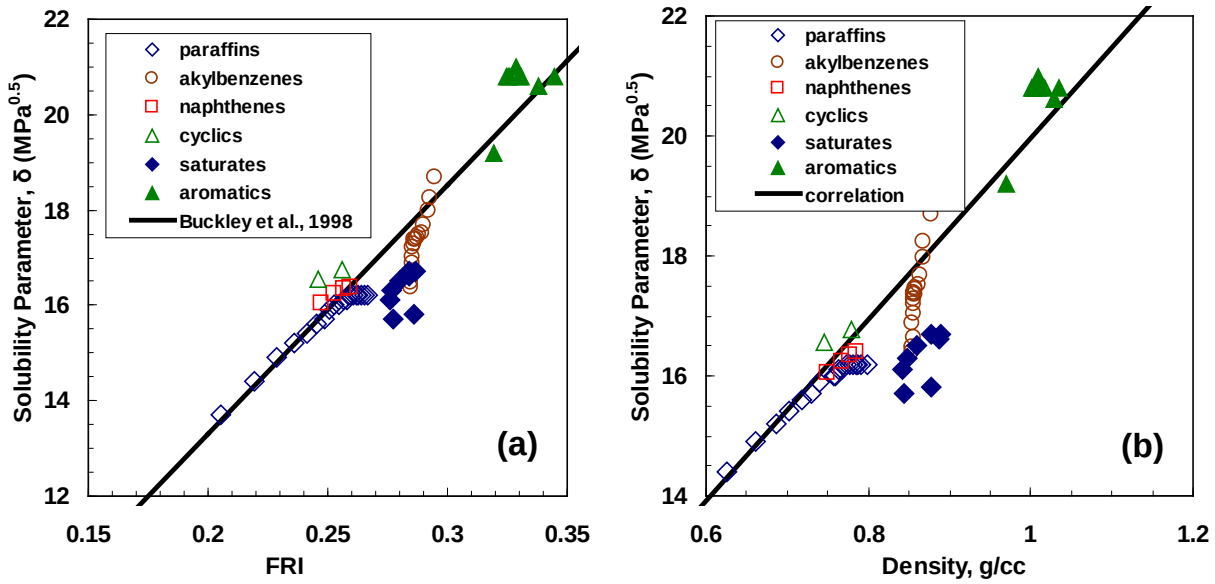

Figure 7.10: The relationship between solubility parameter and F_{RI} (a) and density (b) for a series of pure hydrocarbons plus saturate and aromatic fractions.

A better correlation may be possible if the chemistry of the components were accounted for; for example, by introducing H/C ratio or Watson K factor into the correlation. The correlation would also be strengthened by including data for resins and asphaltenes. However, such data are not presently available. In the meantime, the correlation between solubility parameter and FRI is examined in more detail in Figure 7.11a. The following preliminary correlation fits the data for the native saturate and aromatic cuts with an AARD of 0.9%, and fit the thermally cracked saturates and aromatics with an AARD of 0.9% and 2.6% respectively:

$$\delta = 94.2F_{RI} - 10.0 \qquad (7.1)$$

where δ is the solubility parameter in $MPa^{0.5}$ and F_{RI} is a fractional function of the refractive index. The more reacted saturates and aromatics shift towards lower solubility parameters and higher FRI. A better correlation may be possible if an indicator for the extent of reaction, such as H/C ratio, were included; however, such data are not yet available. Note the extrapolation of the correlation to resins and asphaltenes may be misleading because the chemistry of the fractions is not accounted for.

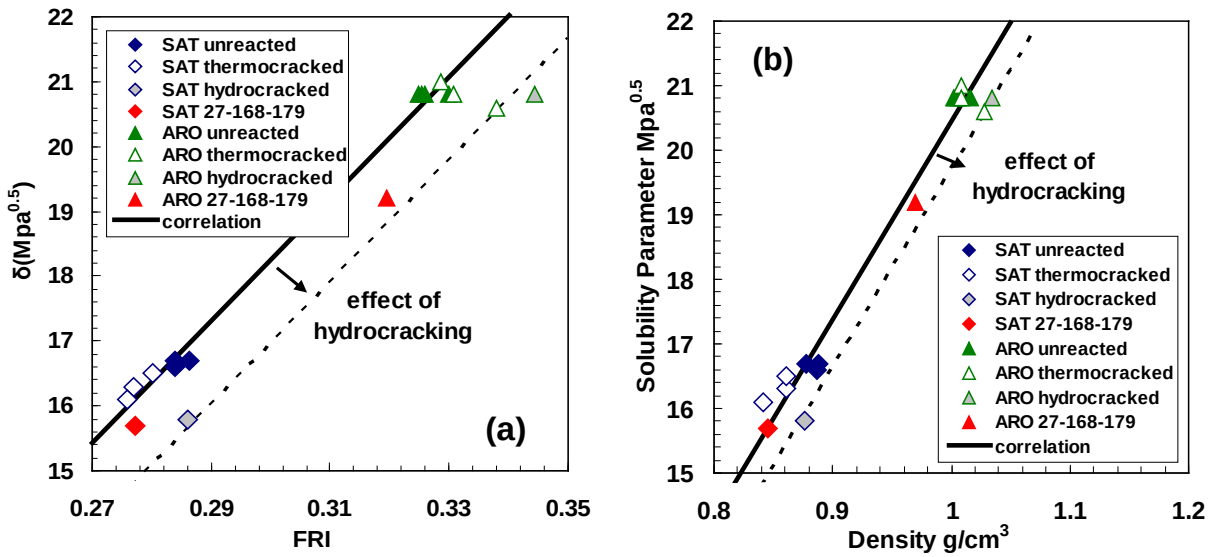

Figure 7.11: The relationship between solubility parameter and F_{RI} (a) and density (b) for saturate and aromatic fractions only.

Since FRI correlates to density, it seems likely that solubility parameters would also correlate to density. Figures 7.10b and 7.11b demonstrate that the solubility parameters do indeed correlate to density with the same strengths and weaknesses of the correlation to FRI. The following equation was fit to the saturate and aromatic data of Figure 7.11b:

$$\delta = 30.7\rho - 10.26 \qquad (7.2)$$

The correlation fits the aromatic and saturate solubility parameters with an AARD of 1.7% and 2.0%, respectively. If only the native aromatic and saturates are considered, the AARD are 1.1% and 1.4%, respectively. Hence, either FRI or density can be used as a correlating parameter for solubility parameters. All of the above correlations are only intended to demonstrate trends and identify pathways for future research. Since the chemistry of the fractions is not accounted for, any extrapolation to other fractions or to reacted materials is not recommended.

Chapter Eight: Conclusions and Recommendation

The principal objective of this thesis was to characterize the non-distillable fractions of native and reacted heavy oils for regular solution modeling of asphaltene precipitation. Relevant inputs for the model required molecular weight, density and solubility parameter for the fractions. Since solubility parameters are not measured directly and require lengthy experimental procedure and modeling to estimate them, it is desirable to develop a correlation between solubility parameter and other easily measured and reliable properties such as density and refractive index.

8.1 Conclusions

Based on the characterization studies performed in this thesis, the following conclusions are made:

1. The SAR fractions exhibit excess volume of mixing in solution with solvents. Depending on the nature of the solvent and similarity of the solute to the solvent, the solution either shrank or expanded on mixing. A binary interaction parameter was introduced to account for the excess volume behaviour for density and refractive index measurements. The interaction parameter was correlated to the normalized specific volume or refractive index difference between the SAR fraction and the solvent.

2. As is expected, the density and refractive index of SAR fractions decrease with increased temperatures. The effect of temperature could be accounted for with temperature independent thermal coefficients. Density was correlated to refractive index and the thermal expansion coefficient was correlated to the refractive index thermal coefficient. Therefore, given a single measurement of either of the variables, both the FRI and density of the fractions can be predicted as a function of temperature.

3. Thermocracking processes are expected to decrease the average molecular weight and density of the fractions. A decrease in the molecular weight and density was observed

only for saturate fractions. The molecular weight of aromatics and resin also decreased but their density did not. Aromatics and resins are complex pseudo-components and become more polar with the stripping of paraffinic side chains. The increase in polarity combined with a decrease in size might result in a relatively small change or even an increase in density.

4. An alternative methodology for asphaltene yield determination using the refractive index (FRI) of the supernatant from solubility measurements was developed. The concentration of soluble asphaltenes was determined from the FRI and the fractional precipitation determined from a mass balance. This methodology is well suited for low volume measurements. For pseudo-ternary solutions of asphaltenes in a pure solvent mixture, the FRI based methods for asphaltene yield are an alternative to the cumbersome gravimetric experiments. However, the FRI based methods are not well suited for pseudo-ternary mixtures involving saturates and aromatics. The accumulated effect of excess volumes and ternary interactions introduced too much error for a reliable measurement.

5. The solubility parameter of saturates and aromatics were determined from regular solution modeling of asphaltene yields from solution including a solvent and either a saturate or aromatic. The solubility parameter of saturates were higher than the previously reported average for these fractions. The observed difference is due primarily to an extensive data set used in this work and an update to the asphaltene characterization. The solubility (and solubility parameter) of saturate fractions decreases with increased reaction or cracking. Surprisingly, the solubility properties of aromatic fractions appear unchanged with reaction.

6. Solubility parameters of unreacted and mildly thermally cracked saturate and aromatic fractions were correlated to their refractive index and density within experimental error. The hydrocracked and highly thermocracked saturates and aromatics shift towards lower solubility parameters and higher FRI.

8.2 Recommendations

1. There is still potential to improve the refractive index (FRI) methods for solubility measurements involving saturates and aromatics. Focus should be placed on the design of the experiments especially in the measurements with aromatics as solvents. In this work, there were concerns about aromatics entrainment in the precipitated asphaltenes and the effect of entrainment on the calculated yields. In designing the experiments, emphasis should be placed on the optimum solvent mixture for washing the precipitate.

2. Density and refractive index measurements on a greater variety of petroleum fractions is recommended with which to improve the versatility and applicability of the excess volume correlations.

3. The correlation between solubility parameter and refractive index (and density) is promising and should be built upon to include other petroleum fractions. The chemistry (H/C ratio) of these fractions or the degree of reaction need to be accounted for since other properties measured exhibit behaviour consistent with alteration in chemical nature due to processing.

References

Agrawala, M., *Measurement and Modeling of Asphaltene Association*, MSc Thesis, Department of Chemical and Petroleum Engineering, University of Calgary, Alberta, Canada. 2001.

Agrawala, M., Yarranton, H. W., *An Asphaltene Association Model Analogous to Linear Polymerization.* Industrial and Engineering Chemistry Research. 40, 4664-4672, 2001.

Akbarzadeh, K., *A New Thermodynamic Model for Predicting Asphaltene Precipitation at Various Conditions,* Ph.D. Thesis, Shiraz University, Iran, January 2002.

Akbarzadeh, K., Alboudwarej, H., Svrcek, W.Y. and Yarranton, H.W., *A Generalized Regular Solution Model for Asphaltene Precipitation from n-Alkane Diluted Heavy Oils and Bitumens*. Fluid Phase Equilibria 232 (1-2): 159-170. 2005.

Akbarzadeh, K., Ayatollahi, S., Moshfeghian, M., Alboudwarej, H. and Yarranton, H.W., *Estimation of SARA fraction properties with the SRK EOS*, Journal of Canadian Petroleum Technology Vol. 43(9), 31-39. 2004.

Akbarzadeh, K., Dhillon, A., Svrcek, W.Y. and Yarranton, H.W., *Methodology for the Characterization and Modeling of Asphaltene Precipitation from Heavy Oils Diluted with n-Alkanes*, Energy and Fuels 18(5): 1434-1441. 2004.

Alboudwarej, H., *Asphaltene Deposition in Flowing Systems*, Ph.D. Thesis, Department of Chemical and Petroleum Engineering., University of Calgary, AB, Canada, 2003.

Alboudwarej, H.,Akbarzadeh, K., Beck, J., Svrcek, W.Y., Yarranton, H.W., *Regular Solution Model for Asphaltene Precipitation from Bitumen and Solvents*, AiChE Journal, Vol. 49 (11), 2948-2956, 2003.

Altgelt, K.H., Boduszynski, M.M., *Composition and Analysis of Heavy Petroleum Fractions*, Marcel Dekker, New York, NY, 1994.

Alvarez, E., Marroquin, G., Trejo, F., Centeno, G., Ancheyta, J. and Diaz, J.A.I., *Pyrolysis Kinetics of Atmospheric Residue and its SARA Fractions*, Fuel 90, 3602–3607, 2011.

Andersen, S. I. and Speight, J. G., *Thermodynamic Models for Asphaltene Solubility and Precipitation*, Journal of Petroleum Science and Engineering 22, 53-66, 1999.

Andersen, S. I., *Association of Petroleum Asphaltenes and the Effect on Solution Properties*, Handbook of Surface and Colloid Chemistry, 3rd Edition, Chapter 18, Birdi, K. S., Ed. CRC Press Taylor and Francis Group. Boca Raton, Florida. 2008.

Andersen, S.I. and Stenby, E.I., *Thermodynamics of Asphaltenes Precipitation and Dissolution Investigation of Temperature and Solvent Effects*, Fuel Science & Technology Int'l, Vol. 14 (1 &2), 261-287, 1996.

Angle, C. W., Long, Y., Hamza, H., Lue, L., *Precipitation of asphaltenes from solvent-diluted heavy oil and thermodynamic properties of solvent-diluted heavy oil solutions*, Fuel 85, Issue 4, 492-506, 2006.

Asaoka, S., Nakata, S., Shiroto, Y. and Takeuchi, C., *Asphaltene Cracking in Catalytic Hydrotreating of Heavy Oils. 2: Study of Changes in Asphaltene Structure during Catalytic Hydroprocessing*, Industrial and Engineering Chemistry Process Design Development 22 (2), 242-248, 1983.

ASTM Standards: D86,*"Standard Test Method for Distillation of Petroleum Products at Atmospheric Pressure"*; D1160, "*Standard Test Method for Distillation of Petroleum Products at Reduced Pressure*"; D1747, *"Standard Test Method for Refractive Index of Viscous Materials"*; D4124, *"Standard Test Method for Separation of Asphalt into Four Fractions"*; D2007, *"Standard Test Method for Characteristic Groups in Rubber Extender and Processing Oils and Other Petroleum-Derived Oils by the Clay-Gel Absorption*

Chromatographic Method", ASTM International, West Conshohocken, PA, USA, www.astm.org.

Badre, S., Goncalves, C. C., Norinaga, K., Gustavson, G. and Mullins, O. C., *Molecular Size and Weight of Asphaltene and Asphaltene Solubility Fractions from Coals, Crude oils and Bitumen, Fuel 85*, 1-11, 2006.

Barrera, D.M., *Determination and Application of Asphaltene Property Distributions for Native and Refined Crude Oils*, MSc Thesis, Department of Chemical and Petroleum Engineering, University of Calgary, AB Canada, 2012.

Barton A.F., *Handbook of Solubility Parameters and other Cohesion Parameters,* Boca Raton, FL: CRC Press; 1991 p. 139–215.

Bruno, T.J., *Improvement in the Measurement of Distillation Curves. 1. A Composition-Explicit Approach,* Industrial and Engineering Chemistry Research 45, 4371 – 4380, 2006.

Buch L., Groenzin H., Buenrostro-Gonzalez E., Andersen S.I., Lira-Galeana C. and Mullins O.C., *Molecular Size of Asphaltene Fractions Obtained from Residuum Hydrotreatment*, Fuel 82, 1075-1084, 2003.

Buckley J.S., Hirasaki G.J., Liu Y., Von Drasek S., Wang J.X and Gill B.S., *Asphaltene Precipitation and Solvent Properties of Crude Oils*, et al., Petroleum and Science Technology, 16 (3 & 4), 251-285, 1998.

Buckley J.S., *Predicting the Onset of Asphaltene Precipitation from Refractive Index Measurements,* Energy and Fuels, 13, 328-332, 1999.

Castillo J., Gutierrez H., Ranaudo M. and Villarroel O., *Measurement of the Refractive Index of Crude Oil and Asphaltene Solutions: Onset Flocculation Determination,* Energy & Fuels 24, 492–495, 2010.

Chang, V.L., Fogler, H.S., *Stabilization of Asphaltenes in Aliphatic Solvents using Alkylbenzene-Derived Amphiphiles, 1*: *Effect of the Chemical Structure of Amphiphiles on Asphaltene Stabilization*, Langmuir, 10, (1749), 1994.

Chartier, G., *Introduction to Optics*, Springer Science+Business Media, Inc., 2005

Dickie, J.P., Yen, T.F., *Macrostructures of the asphaltic fractions by various instrumental methods"*, Anal Chemistry 39 (14): 1847-1852. 1967.

Evdokimov I.N., Losev A.P., *Effects of molecular de-aggregation on refractive indices of petroleum-based fluids,* Fuel 86: 2439–2445, 2007.

Flory, P. J. *Principles of Polymer Chemistry.* Cornel University Press, Ithaca, New York. 1953.

Friberg, S. E., *Micellization, Asphaltenes, Heavy Oils and Petroleomics*, Chapter 7, Springer, New York, 2007.

Gray, M.R., Tykwinski, R.R., Stryker, J.M., and Tan, X., *Supramolecular Assembly Model for Aggregation of Petroleum Asphaltenes*, Energy & Fuels 25 (7), 3125-3134, 2011.

Groenzin, H. and Mullins, O.C., *Asphaltene Molecular Size and Weight by Time-Resolved Fluorescence Depolarization,* Asphaltenes, Heavy Oils and Petroleomics, Chapter 2, Springer, New York, 2007.

Haslego, C., *A Students Guide to Refining*, Chemical and Process Engineering Resources, 2010, www.cheresources.com.

Hauser, A., AlHumaidan, F., Al-Rabiah, H., *NMR Investigations on Products from Thermal Decomposition of Kuwaiti Vacuum Residues,* Fuel 113, 506–515, 2013.

Hildebrand, J. H.; Scott, R. L. *Regular Solutions.* Prentice Hall. Englewood Cliffs, New Jersey. 1962.

Hildebrand, J. H.; Scott, R. L. *The Solubility of Non-Electrolytes.* Third Edition. Reinhold Publishing Corp. New York. 1949.

Hirschberg, A., DeJong, L. N. J., Schipper, B. A. and Meijer, J. G., *Influence of Temperature and Pressure on Asphaltene Flocculation,* SPE Journal, 283-293, 1984.

Hirschfelder J.O., Curtiss C.F. and Bird R.B., *Molecular Theory of Gases and Liquids*, John Wiley & Sons, Inc, 1964.

Huanquan P.; Firoozabadi A., *Thermodynamic Micellization Model for Asphaltene Aggregation and Precipitation in Petroleum Fluids,* SPE Production and Facilities, May 1998.

Huggins, M. L. *Solutions of Long Chain Compounds.* The Journal of Chemical Physics. 9 (5), 440, 1941.

Iglesias-Otero, M.A., Troncoso, J., Carballo, E. and Romani, L., *Density and Refractive Index in Mixtures of Ionic Liquids and Organic Solvents: Correlations and Predictions,* Journal of Chemical Thermodynamics 40, 949-956, 2008.

Israelachvili J.N., *Intermolecular and surface forces*, 3rd Edition, New York: Academic Press; 2011.

Kaes, G.L., *Refinery process Modeling*; *A Practical Guide to Steady State Modeling of Petroleum Resources*, 1st Edition, Kaes Enterprises Inc., Colbert, Georgia, 2000.

Kawanaka, S., Park, S.J. and Mansoori, G.A., *Organic Deposition from Reservoir Fluids: A Thermodynamic Predictive Technique,* SPE Reservoir Engineering, 185-192, 1991.

Koots, J.A. and Speight, J.C., *Relation of Petroleum Resins to Asphaltenes,* Fuel Vol. 54, 179-184, 1975.

Kuznicki, T., Masliyah, J. H. and Bhattacharjee, S., *Molecular Dynamics Study of Model Molecules Resembling Asphaltene-like Structures in Aqueous Organic Solvent Systems,* Energy & Fuels 22, 2379-2389, 2008.

Lababidi, H.M.S., Garrouch, A.A., and Mohammed A. Fahim, M.A., *A Fuzzy Heuristic Approach for Predicting Asphaltene Precipitation Potential,* Energy & Fuels 18, 242-250, 2004.

Lababidi, H.M.S., Sabti, H.M., AlHumaidan, F.S., *Changes in Asphaltenes during Thermal Cracking of Residual Oils,* Fuel, 2013.

Li, W.B., Segre, P.N., Gammon, R.W., and Sengers, J.V., *Determination of the Temperature and Concentration Dependence of the Refractive Index of a Liquid Mixture,* The Journal of Chemical Physics, Vol. 101 (6), 5058-5069, 1994.

Merdrignac, I. and Espinat D., *Physicochemical Characterization of Petroleum Fractions: the State of the Art,* Oil & Gas Science and Technology – Rev. IFP, Vol. 62 (1), 7-32, 2007.

Merino-Garcia, D., Murgich, J. and Andersen, S. I., *Asphaltene Self-Association: Modeling and Effect of Fractionation with a Polar Solvent,* Petroleum Science and Technology Vol. 22 (7&8), 735–758, 2004.

Mitchell, D.L. and Speight, J.G., *The Solubility of Asphaltenes in Hydrocarbon Solvents,* Fuel 52, 149-152, 1973.

Mohamed, R.S., Ramos, A.C.S. and Loh, W., *Aggregation Behavior of Two Asphaltene Fractions in Aromatic Solvents,* Energy & Fuels, 13(2), 323 - 327, 1999.

Murgich, J., *Intermolecular Forces in Aggregates of Asphaltenes and Resins,* Petroleum Science & Technology 20 (9 - 10), 983 – 997, 2002.

Nikookar, M., Omidkhah, M. R. and Pazuki, G. R., *Prediction of Density and Solubility Parameter of Heavy Oils and SARA Fractions Using Cubic Equations of State*, Petroleum Science and Technology, 26: 16, 1904-1912, 2008.

Ortiz, D.P., *Effects of Surfactants on Asphaltene Interfacial Films and Stability of Water-in-Oil Emulsions*, MSc Thesis, Department of Chemical and Petroleum Engineering, University of Calgary, 2009.

Ortiz, D.P., Personal Communication, University of Calgary, 2013.

Ortiz, D.P., *Thermodynamics and Fluid Characterization using Trajectory Optimization*, Fluid Phase Equilibria 351, 34 – 42, 2013.

Ovalles, C., Rogel, E., Moir, M., Thomas, L. and Pradhan, A., *Characterization of Heavy Oils, Their Fractions, and Hydrovisbroken Products by the Asphaltene Solubility Fractions Method*, Energy & Fuels 26, 549-556, 2012.

Peramanu, S., Pruden, B.B. and Rahimi, P., *Molecular Weight and Specific Gravity Distributions for Athabasca and Cold Lake Bitumens and Their Saturates, Aromatics, Resin, and Asphaltene Fractions*, Industrial and Engineering Chemistry Research 38, 3121-3130, 1999.

Pereira-Almao, P., Catalysis for Bitumen Upgrading and Hydrogen Production Research Team, University of Calgary, 2013.

Perry, R. H., and D. Green, *Perry's Chemical Engineers' Handbook*, 7th ed., McGraw-Hill, New York, 1997.

Pfeiffer, J. P.; Saal, R. N. J. *Asphaltic Bitumens and Colloid System.* Journal of Physical Chemistry. 44, 139-149, 1940.

Piyarat, W., David, W.J., Gustavo, B. and Fogler, H. S., *Study of Asphaltene Precipitation Using Refractive Index Measurement*, Petroleum Science and Technology 21 (3 - 4), 591 - 613, 2003.

Rassenfoss, S., *Seeking more oil, fewer emissions*, Journal of Petroleum Technology 64 (9), 34–38, 2012.

Ravey, J.C., Ducouret, G. and Espinat, D., *Asphaltene Macrostructure by Small Angle Neutron Scattering*, Fuel 67, 1560 - 1567, 1988.

Reid, R. C., J. M. Prausnitz, and B. E. Poling, *The Properties of Gases & Liquids*, 4th ed., McGraw-Hill, New York, 1989.

Riazi, M.R. and Roomi, Y.A., *Use of Refractive Index in the Estimation of Thermophysical Properties of Hydrocarbons and Petroleum Mixtures,* Industrial and Engineering Chemistry Research 40, 1975-1984, 2001.

Riazi, M.R., *Characterization and Properties of Petroleum Fractions*, 1st Edition, ASTM, West Conshohocken, PA, 2005.

Rijkers, M. P. W., and Heidemann, R. A., *Convergence Behavior of Single-Stage Flash Calculations, Article in Equations of State, Theories and Applications,* K. C. Chao and R. L. Robinson, Jr., eds., ACS Symposium Series 300, Washington, DC, 1986.

Sabbagh, O.,*"An EOS Approach to Modeling Asphaltene Precipitation"*, MSc Thesis, Department of Chemical and Petroleum Engineering, University of Calgary, Alberta, Canada. 2004.

Sadeghi, H.M., Personal communication 2013

Saryazdi, F., *Density Prediction for Mixtures of Heavy Oil and Solvents*, MSc Thesis, Department of Chemical and Petroleum Engineering, University of Calgary, Alberta, Canada. 2012.

Scott, R. L. and Magat, M., *The Thermodynamics of High-Polymer Solutions: I. The Free Energy of Mixing of Solvents and Polymers of Heterogeneous Distribution,* The Journal of Chemical Physics, 172-177, 1945.

Scott, R. L. *The Thermodynamics of High-Polymer Solutions: II. The Solubility and Fractionation of a Polymer of Heterogeneous Distribution,* The Journal of Chemical Physics, 178-187, 1945.

Sheremata, J. M.; Gray, M. R.; Dettman, H. D.; McCaffrey W. C. *Quantitative Molecular Representation and Sequential Optimization of Athabasca Asphaltenes,* Energy & Fuels 18, 1377-1384, 2004.

Speight, J. G., *Chemical and Physical Studies of Petroleum Asphaltenes,* Developments in Petroleum Science, Volume 40, Part A, Yen, T.F.; Chilingarian, G.V. Eds. Elsevier. Amsterdam. 7 - 65, 1994.

Speight, J. G., *Handbook of Petroleum Analysis,* John Wiley & Sons Inc. Hoboken, New Jersey. 2001.

Speight, J. G., *The Chemistry and Technology of Petroleum, 4th* Edition, CRC Press Taylor & Francis Group, Boca Raton, Florida. 2007.

Speight, J.G., *Characterization of Heavy Crude Oils and Petroleum Residues, B.Tissot (Editor),* Edition Technip, Paris, 1984.

Spiecker, P.M., *The Impact of Asphaltene Chemsitry and Solvation on Emulsion and Interfacial Film Formation,* PhD Thesis, North Carolina State University, 2001.

Starks, J.L., and Asomaning, S., *Crude Oil Blending Effects on Asphaltene Stability in Refinery Fouling,* Petroleum Science and Technology, Vol. 21(3 & 4),569– 579, 2003.

Strausz, O.P., Mojelsky, T.W. and Lown, E.M., *The Molecular Structure of Aspha1tene: An Unfolding Story*, Fuel Vol.71, 1355-1363, 1992.

Subedi, D.P., Adhikari, D.R., Joshi, U.M., Poudel, H. N., Niraula, B., *Study of Temperature and Concentration Dependence of Refractive Index of Liquids using a Novel*

Technique, Kathmandu University Journal of Science, Engineering and Technology, Vol. II (1), 2006.

Sztukowski, D.M., Yarranton, H.W., *Oilfield Solids and Water-in-Oil Emulsion Stability*, Journal of Colloid and Interface Science 285, 821–833, 2005.

Tharanivasan A.K, Svrcek W.Y, Yarranton HW, Taylor S.D, Merino-Garcia D and Rahimi P.M., *Measurement and Modeling of Asphaltene Precipitation from Crude Oil Blends,* Energy and Fuels 23(8): 3971-3980, 2009.

Tharanivasan, A.K., *Asphaltene Precipitation from Crude Oil Blends, Conventional Oils, and Oils with Emulsified Water,* PhD Thesis, Department of Chemical and Petroleum Engineering, University of Calgary, Alberta, Canada, 2012.

Ting, P.D., Hirasaki, G.J. and Chapman W.G., *Modeling of Asphaltene Phase Behaviour with the SAFT Equation of State,* Petroleum Science and Technology, Vol. 21 (3 &4), 647-661, 2003.

Vargas, F.M. and Chapman, W.G., *Application of the One-Third Rule in Hydrocarbon and Crude Oil Systems*, Fluid Phase Equilibria 290, 103-108, 2010.

Vargas, F.M., Gonzalez, D.L., Creek, J.L., Wang, J., Buckley, J., Hirasaki, G.J. and Chapman, W.G., *Development of a General Method for Modeling Asphaltene Stability,* Energy & Fuels 23, 1147-1154, 2009.

Vermeulen, F., McGee, B., *In-Situ Electromagnetic Heating for Hydrocarbon Recovery and Environmental Remediation*, Journal of Canadian Petroleum Technology 39 (8), 24–28, 2000.

Wang J.X. and Buckley J.S., *An Experimental Approach to Prediction of Asphaltene Flocculation.* SPE 64994, 179-187, 2001.

Wattana, P., Wojciechowski, D.J., Bolanos, G. and Fogle H.S., *Study of Asphaltene Precipitaion Using Refractive Index Measurement*, Petroleum Science & Technology Vol.21 (3 & 4), 591-613, 2003.

Wiehe I.A. and Kennedy R.J., *Application of the Oil Compatibility Model to Refinery Streams*, Energy & Fuels, Vol. 14 (1), 60-63, 2000.

Wiehe I.A., *Two-Dimensional Solubilty Parameter Mapping of Heavy Oils*, Fuel Science & Technolgy Int'l. 14(1&2), 289-312, 1996.

Wiehe, I.A., *Process Chemistry of Petroleum Macromolecules,* CRC Press Taylor & Francis Group, Boca Raton, Florida. 2008.

Wiehe, l.A.; Liang, K.S., *Asphaltenes, Resins, and Other Petroleum Macromolecules*, Fluid Phase Equilibria, 30, 265-279, 1996.

Wu, J. and Prausnitz J.M., *Molecular Thermodynamic Framework for Asphaltene-Oil Equilibria, AICHE:* Vol. 44, No 5. 1188 – 1199, 1998.

Xu, Y., Koga, Y. and Strausz, O.P., *Characterization of Athabasca Asphaltenes by Small Angle X-ray Scattering*, Fuel, 74(7), 960, 1995.

Yarranton, H. W., Alboudwarej, H. and Jakher, R., *Investigation of Asphaltene Association with Vapor Pressure Osmometry and Interfacial Tension Measurements*, Industrial and Engineering Chemistry Research 39, 2916-2924, 2000.

Yarranton, H.W. and Masliyah, J.H., *Molar Mass Distribution and Solubility Modeling of Asphaltenes,* AICHE, Vol. 42 (12), 3533-3543, 1996.

Yarranton, H.W., *Asphaltene Self-Association*, Journal of Dispersion Science and Technology, 26, 5-8, 2005.

Yarranton, H.W., *Asphaltene Solubility and Asphaltene Stabilized Water-in-Oil Emulsions*, PhD. Thesis, Department of Chemical and Material Engineering, University of Alberta, Edmonton, AB, Canada. 1997.

Yarranton, H.W., Fox W.A. and Svrcek W.Y., *Effects of Resins on Asphaltene Self-Association and Solubility*, The Canadian Journal of Chemical Engineering, Vol. 85, 635-642, 2007.

Yen, T. F., Erdman, J. G. and Pollack, S. S., *Investigation of the Structure of Petroleum Asphaltenes by X-Ray Diffraction*, Analytical Chemistry 33, 1587-1594, 1961.

Zhao, S., Sparks, B.D., Kotlyar, L.S. and Chung, K.H., *Correlation of Processability and Reactivity Data for Residua from Bitumen, Heavy Oils and Conventional Crudes: Characterization of Fractions from Super-critical Pentane Separation As A Guide to Process Selection*, Catalysis Today 125, 122-136, 2007.

Zuo, J.Y., Mullins, O.C., Freed, D. and Zhang, D., *A Simple Relation between Solubility Parameters and Densities for Live Reservoir Fluids*, Journal of Chemical & Engineering Data, 55 (9), 2964–2969, 2010.

Appendix A: Error Analysis Summary

Tables **A.1 to A.14** show the repeatability analyses for the density and refractive index measurements. In most cases, the dataset of repeats for any property, such as density, consisted of pairs of measurements. The mean, μ, for each pair of measurement is given by:

$$\mu = \frac{\sum_{i=1}^{n} y_i}{n} \tag{A.1}$$

where y_i is the experimental measured value and n is the number of measurements or repeats (here n is usually equal 2). The sample variance, s, was calculated based on the variance for all of the pairs of measurements and is given by:

$$s = \sqrt{\frac{\sum_{i=1}^{n} (y_i - \mu)^2}{m-1}} \tag{A.2}$$

where m is the number of variances determined for that property measurement. The variance of the property measurements is then estimated using a Chi-square distribution as follows:

$$\sigma = \sqrt{\frac{\lambda^2 s^2}{(n-1)}} \tag{A.3}$$

where λ^2 is the Chi-square variable (from statistical tables) and σ is the population standard deviation. Finally, the 95% confidence interval (*CI*) for any single measurement is determined as 1.645σ and for pairs of measurements as $(1.645/\sqrt{2})\sigma$. The confidence interval for single measurements is reported in Tables A.1 to A.14.

Deviations between the predicted and measured values are shown in Tables **A.15 to A.41.** Deviations between the predicted value, y_i^* and the experimentally measured value are defined as:

$$dev = y_i^* - y_i \tag{A.4}$$

The Average Absolute Deviation (AAD) of the fits or predictions to the experimental data is given by:

$$AAD = \frac{1}{n}\sum_{1}^{n}\left|y_i^* - y_i\right| \quad \text{(A.5)}$$

and the Absolute Average Relative Deviation is given by:

$$AARD = \frac{1}{n}\sum_{1}^{n}\left|\frac{y_i^* - y_i}{y_i}\right| \quad \text{(A.6)}$$

Table A.1. Repeatability of direct measured densities for saturate fractions:

Saturates	*n*	μ (kg/m^3)	s^2
WC-DB-A2	2	888.2	0.0061
27-168-179	3	844.8	0.1070
27034.87	3	847.8	0.1436
		Average	0.0856
		CI	**0.83 kg/m^3**

Table A.2. Repeatability of direct measured densities for aromatic fractions:

Aromatics	*n*	μ (kg/m^3)	s^2
27-168-179	2	970.1	0.4050
26845-38	2	1008.5	0.0648
27034.87	2	1027.6	0.5940
HOSB	2	1003.8	0.0004
WC-DB-A2	2	1002.9	0.0005
Arabian	2	978.5	0.0012
WC-B-B2	2	1005.8	0.0181
		Average	0.1549
		CI	**0.94 kg/m^3**

Table A.3. Repeatability of indirect densities of resin fractions extrapolated from toluene solutions assuming regular solutions are formed.

Resins	*n*	μ (kg/m^3)	s^2
Arabian	2	1064.8	3.3800
WC-B-C1	2	1063.9	0.2450
27-168-179	2	1061.6	8.4050
		Average	4.0100
		CI	**5.8 kg/m^3**

Table A.4. Repeatability of indirect densities of asphltene fractions extrapolated from toluene solutions assuming regular solutions are formed.

Asphaltenes	*n*	μ (kg/m^3)	s^2
Arabian	2	1179.9	45.52
WC-B-C1	2	1193.9	0.06
27-168-179	2	1219.1	144.38
		Average	63.32
		CI	**23 kg/m^3**

Table A.5. Repeatability of direct measured FRI for saturate fractions:

Saturates	*n*	μ (Expt. FRI)	s^2
WC-B-C1	2	0.28391	1.81E-08
WC-DB-A2	2	0.28636	6.40E-10
26845-38	2	0.28029	9.08E-08
27034-87	2	0.27693	4.86E-10
27034-113	2	0.27574	2.42E-08
27-168-179	2	0.27720	1.23E-09
		Average	2.26E-08
		CI	**0.00036**

Table A.6. Repeatability of direct measured FRI for aromatic fractions:

Aromatics	*n*	μ (Expt. FRI)	s^2
WC-B-B2	2	0.32599	1.51E-09
WC-B-C1	2	0.32493	6.21E-08
WC-DB-A2	2	0.32530	2.60E-10
26845-38	2	0.32872	1.74E-09
27034-87	2	0.27693	4.86E-10
27034-113	2	0.33072	9.37E-10
27-168-179	2	0.31959	1.76E-08
HOSB	2	0.34448	5.79E-10
		Average	1.07E-08
		CI	**0.00025**

Table A.7. Repeatability of indirect FRI of saturates and aromatics extrapolated from toluene and heptane solutions (*) by assuming that regular solutions are formed.

Sat/Arom	*n*	μ (Reg. Soln. FRI)	s^2
WC-B-B2 sat	2	0.28052	4.83E-09
WC-B-B2* sat	2	0.29140	5.31E-06
26845-38* sat	2	0.28635	4.74E-07
27-168-179 sat	2	0.27217	4.61E-07
27-168-179* sat	2	0.28408	9.59E-07
WC-B-B2 aro	2	0.33493	1.13E-05
		Average	3.09E-06
		CI	**0.0043**

Table A.8. Repeatability of indirect FRI of resins extrapolated from toluene solutions by assuming that regular solutions are formed.

Resins	*n*	μ (Reg. Soln. FRI)	s^2
WC-B-B2	2	0.34490	2.24E-07
Arabian	2	0.35459	4.42E-06
WC-B-C1	2	0.34435	1.11E-08
27034-87	2	0.34738	1.22E-07
27-168-179	2	0.35415	9.62E-06
		Average	2.88E-06
		CI	**0.0043**

Table A.9. Repeatability of indirect FRI of asphaltenes extrapolated from toluene solutions by assuming that regular solutions are formed.

Asphaltenes	*n*	μ (Reg Soln. FRI)	s^2
WC-B-B2	3	0.40339	3.29E-06
WC-DB-A2	2	0.40313	3.95E-07
WC-B-C1	2	0.39692	8.60E-06
27034-87	2	0.42047	1.32E-05
27-168-179	2	0.43461	3.46E-07
		Average	5.16E-06
		CI	**0.0058**

Table A.10a. Repeatability of asphaltene solubility measurements (for WC-B-B2 C_7 asphaltenes) in *n*-heptane and toluene (heptol) at 21°C (low masses).

heptol	*n*	μ (wt/wt)	s^2
0.5	3	0.0233	0.00006
0.6	3	0.1941	0.00068
0.7	3	0.4762	0.00100
1	3	0.9741	0.00009
		Average	0.00049
		CI	**0.056 w/w**

Table A.10b. Repeatability of asphaltene solubility measurements (for WC-B-B2 C_7 asphaltenes) in *n*-heptane and toluene (heptol) at 21°C (high masses).

heptol	*n*	μ (wt/wt)	s^2
0.5	2	0.0849	0.00014
0.6	2	0.2903	0.00001
0.7	2	0.5598	0.00025
1	2	0.9488	0.00009
		Average	0.00012
		CI	**0.030 w/w**

Table A.11. Repeatability of asphaltene solubility measurements in saturates and toluene solutions at 21°C.

Saturates	Sat. vol. frac	*n*	μ	s^2
27-168-179	0.80	2	0.91681	0.00068
HOSB	0.49	4	0.42948	0.00101
HOSB	0.51	2	0.48237	0.00015
			Average	0.00061
			CI	**0.071 w/w**

Table A.12. Repeatability of asphaltene solubility measurements in aromatics and hepatne solutions at 21°C.

Aromatics	Heptane vol. frac	*n*	μ	s^2
WC-B-B2	0.6	2	0.2692	0.0005
WC-B-B2	0.7	2	0.5911	0.0000
WC-B-B2	0.8	3	0.6328	0.0002
26845-38	0.5	2	0.1070	0.0000
26845-38	0.6	2	0.2236	0.0023
26845-38	0.7	2	0.4021	0.0020
26845-38	0.8	2	0.6434	0.0038
WC-DB-A2	0.6	2	0.4129	0.0007
WC-DB-A2	0.7	2	0.5026	0.0001
WC-DB-A2	0.8	2	0.6581	0.0046
HOSB	0.8	2	0.8657	0.0018
27034-113	0.8	2	0.6374	0.0005
27034-113	0.9	2	0.8234	0.0007
			Average	0.0013
			CI	**0.079 w/w**

Table A.13. Precision of saturates molecular weight measurements using the fixed slope method

Saturates	*n*	μ (g/mol)	s^2
WC-B-B2	2	365.0	128.0
WC-B-C1	2	399.5	40.5
WC-DB-A2	2	453.0	512.0
Arabian	2	372.5	264.5
26845-38	2	350.5	84.5
27034-87	2	313.5	84.5
27034-113	2	334.0	128.0
27-168-179	2	371.0	8.0
HOSB R1	2	649.5	1012.5
HOSB R2	2	575.0	2.0
		Average	226.5
		CI	**34 g/mol**

Table A.14. Precision of aromatics molecular weight measurements using the fixed slope method

Aromatics	*n*	μ (g/mol)	s^2
WC-DB-A2	2	470.0	2.0
WC-B-C1	2	465.5	684.5
Arabian	2	411.0	8.0
WC-VB-B2 R1	2	931.0	1922.0
WC-VB-B2 R2	2	865.5	1512.5
26845-38	2	372.5	40.5
27034-87 R1	2	308.5	144.5
27034-87 R2	2	293.0	8.0
27034-113	2	329.0	98.0
27-168-179	2	392.5	24.5
HOSB R1	2	*529.0*	1800.0
HOSB R2	2	466.0	2.0
		Average	520.5
		CI	**50 g/mol**

Table A.15. Error analysis of the deviation of saturates measured density values to the extrapolated values assuming regular solution mixing in solvents.

Saturates	Solvent	Measured kg/m^3	Regular Solution kg/m^3	Deviation	%AARD
WC-B-B2	toluene	887.1	870.3	-16.9	1.9
WC-DB-A2	toluene	888.2	881.0	-7.2	0.8
Arabian	toluene	826.7	816.2	-10.4	1.3
26845-38	toluene	860.6	854.0	-6.6	0.8
27034-87	toluene	847.8	833.8	-14.0	1.7
27-168-179	toluene	844.8	836.3	-8.5	1.0
27-168-179 R2	toluene	844.8	836.3	-8.5	1.0
HOSB R1	toluene	876.9	869.6	-7.3	0.8
HOSB R2	toluene	876.9	869.8	-7.1	0.8
			Average	-9.6 kg/m^3	1.1
WC-B-B2	heptane	887.1	915.0	27.9	3.1
WC-B-B2	heptane	887.1	903.5	16.4	1.8
26845-38	heptane	860.6	872.7	12.1	1.4
27-168-179 R1	heptane	844.8	865.4	20.6	2.4
27-168-179 R2	heptane	844.8	855.9	11.1	1.3
			Average	17.6 kg/m^3	2.0

Table A.16. Error analysis of the deviation of aromatics measured density values to the extrapolated values assuming regular solution mixing in solvents

Aromatics	Solvent	Measured kg/m^3	Regular Solution kg/m^3	Deviation	%AARD
WC-B-B2	toluene	1005.9	1011.5	5.7	0.6
WC-DB-A2	toluene	1002.9	1011.8	8.9	0.9
Arabian	toluene	978.5	982.2	3.6	0.4
26845-38	toluene	1008.7	1017.2	8.5	0.8
27034-87	toluene	1028.1	1033.2	5.1	0.5
27-168-179	toluene	969.7	973.4	3.7	0.4
HOSB R1	toluene	1033.8	1048.1	14.3	1.4
HOSB R2	toluene	1033.8	1048.5	14.7	1.4
			Average	8.1	0.8
26845-38	heptane	1008.3	1046.7	38.4	3.8
27-168-179	heptane	970.6	1002.5	31.9	3.3
			Average	35.2	3.5

Table A.17. Error analysis of the deviation of resins extrapolated density values assuming excess volume on mixing in toluene to the regular solution extrapolations.

Resins	Regular Solution kg/m^3	Excess volume kg/m^3	Deviation	%AARD
WC-B-B2	1074.4	1054.4	-20.0	1.9
Arabian R1	1066.1	1051.5	-14.6	1.4
Arabian R2	1063.5	1044.0	-19.5	1.8
WC-DB-A2	1066.5	1047.6	-18.9	1.8
WC-B-C1 R1	1063.5	1044.9	-18.6	1.7
WC-B-C1 R2	1064.2	1045.0	-19.2	1.8
WC-VB-B2	1059.7	1041.0	-18.7	1.8
27-168-179 R1	1059.5	1046.5	-13.0	1.2
27-168-179 R2	1063.6	1044.1	-19.5	1.8
26845-38	1081.7	1062.8	-18.0	1.7
27034-87	1073.1	1053.6	-17.8	1.7
27034-113	1081.6	1058.0	-23.6	2.2
HOSB	1098.2	1072.3	-25.9	2.4
		Average	-19.0	1.8

Table A.18. Error analysis of the deviation of asphaltenes extrapolated density values assuming excess volume on mixing in toluene to the regular solution extrapolations.

Asphaltenes	Regular Solution kg/m^3	Excess volume kg/m^3	Deviation	%AARD
WC-B-B2	1184.7	1148.0	-36.7	3.1
WC-B-C1	1179.0	1140.3	-38.7	3.3
26845-38	1210.7	1170.9	-39.8	3.3
27-168-179	1194.1	1152.0	-42.1	3.5
		Average	-39.3	3.3

Table A.19: Comparison of measured FRI and FRI calculated with regular solution mixing rule for binary mixtures of heptane and toluene.

Heptane Vol%	Measured FRI	Calculated FRI	Deviation	AARD %
0	0.29267			
10	0.28676	0.28700	0.00024	0.1
20	0.28094	0.28133	0.00039	0.1
30	0.27634	0.27567	-0.00067	0.2
40	0.27029	0.27000	-0.00029	0.1
50	0.26472	0.26433	-0.00039	0.1
60	0.25887	0.25867	-0.00021	0.1
70	0.25303	0.25300	-0.00003	0.0
80	0.24765	0.24733	-0.00031	0.1
90	0.24172	0.24167	-0.00006	0.0
100	0.23600			

Table A.20: Measured FRI of pseudo-binary mixtures of 27-168-179 saturates and toluene compared with FRI determined from the regular solution and excess volume solution mixing rules.

Toluene Vol%	Measured FRI	Regular Soln FRI	Deviation	Excess Vol Soln FRI	Deviation
0.0	0.27722				
50.2	0.28381	0.28497	0.00117	0.28428	0.00047
62.2	0.28576	0.28682	0.00106	0.28617	0.00041
70.2	0.28711	0.28806	0.00095	0.28748	0.00037
81.4	0.28910	0.28979	0.00069	0.28937	0.00027
90.1	0.29071	0.29113	0.00042	0.29088	0.00017
100.0	0.29266				

Table A.21: Measured FRI of pseudo-binary mixtures of WC-B-B2 aromatics and heptane compared with FRI determined from the regular solution and excess volume solution mixing rules.

Heptane Vol%	Measured FRI	Regular Soln FRI	Deviation	Excess Vol Soln FRI	Deviation
0.0	0.32596				
52.4	0.28178	0.27878	-0.00300	0.28177	-0.00002
59.0	0.27582	0.27291	-0.00291	0.27580	-0.00002
72.1	0.26349	0.26109	-0.00239	0.26350	0.00001
77.5	0.25831	0.25621	-0.00210	0.25829	-0.00002
89.9	0.24618	0.24506	-0.00111	0.24615	-0.00003
100.0	0.23599				

Table A.22: Comparison of measured densities for saturate fractions at 40 and 60°C to the estimated densities using Equation 5.19.

Saturates	α_v	Temp °C	ρ (g/cm^3)	$\rho^{correlation}$ (g/cm^3)	AD	ARD
WC-B-B2	0.00073	40	0.8745	0.8743	0.0002	0.0002
WC-B-B2	0.00073	60	0.8619	0.8616	0.0003	0.0003
WC-B-C1	0.00075	40	0.8646	0.8644	0.0003	0.0003
WC-B-C1	0.00075	60	0.8519	0.8515	0.0004	0.0004
Arabian	0.00084	40	0.8129	0.8129	0.0000	0.0000
Arabian	0.00084	60	0.7997	0.7993	0.0004	0.0005
WC-DB-A2	0.00073	40	0.8757	0.8754	0.0003	0.0003
WC-DB-A2	0.00073	60	0.8632	0.8628	0.0004	0.0005
27034-87	0.00080	40	0.8347	0.8344	0.0003	0.0004
27034-87	0.00080	60	0.8216	0.8211	0.0004	0.0005
27034-113	0.00081	40	0.8284	0.8280	0.0004	0.0005
27034-113	0.00081	60	0.8153	0.8147	0.0006	0.0008
27-168-179	0.00080	40	0.8315	0.8319	0.0003	0.0004
27-168-179	0.00080	60	0.8187	0.8186	0.0001	0.0001
HOSB	0.00075	40	0.8648	0.8639	0.0009	0.0010
HOSB	0.00075	60	0.8524	0.8511	0.0014	0.0016
					AARD%	0.0498

Table A.23: Comparison of measured densities for aromatic fractions at 40 and 60°C to the estimated densities using Equation 5.19.

Aromatics	α_v	Temp °C	ρ (g/cm^3)	$\rho^{correlation}$ (g/cm^3)	AD	ARD
WC-B-B2	0.00067	40	0.9927	0.9925	0.0002	0.0002
WC-B-B2	0.00067	60	0.9797	0.9794	0.0003	0.0004
WC-B-C1	0.00067	40	0.9884	0.9882	0.0002	0.0002
WC-B-C1	0.00067	60	0.9754	0.9750	0.0004	0.0004
Arabian	0.00070	40	0.9652	0.9649	0.0003	0.0003
Arabian	0.00070	60	0.9521	0.9515	0.0006	0.0006
WC-DB-A2	0.00067	40	0.9901	0.9895	0.0005	0.0006
WC-DB-A2	0.00067	60	0.9773	0.9763	0.0009	0.0009
WC-VB-B2	0.00066	40	1.0038	1.0032	0.0006	0.0006
WC-VB-B2	0.00066	60	0.9913	0.9901	0.0011	0.0011
WC-B-B2*	0.00067	40	0.9924	0.9923	0.0001	0.0001
WC-B-B2*	0.00067	60	0.9792	0.9792	0.0001	0.0001
27034-87	0.00064	40	1.0143	1.0150	0.0007	0.0007
27034-87	0.00064	60	1.0005	1.0020	0.0015	0.0015
27034-113	0.00067	40	0.9946	0.9950	0.0004	0.0004
27034-113	0.00067	60	0.9810	0.9819	0.0008	0.0008
HOSB	0.00064	40	1.0209	1.0207	0.0002	0.0002
HOSB	0.00064	60	1.0082	1.0077	0.0004	0.0004
					AARD%	0.0532

Table A.24: Comparison of measured FRI for saturate fractions at 40 and 60°C to the estimated densities using Equation 5.23.

Saturates	α_{FRI}	Temp °C	FRI	$FRI^{correlation}$	AD	ARD
WC-B-B2	-0.00065	40	0.2821	0.2821	0.00001	0.00002
WC-B-B2	-0.00065	60	0.2784	0.2784	0.00004	0.00014
WC-B-C1	-0.00067	40	0.2800	0.2800	0.00004	0.00015
WC-B-C1	-0.00067	60	0.2762	0.2763	0.00010	0.00036
Arabian	-0.00075	40	0.2688	0.2688	0.00002	0.00006
Arabian	-0.00075	60	0.2648	0.2648	0.00001	0.00005
WC-DB-A2	-0.00065	40	0.2826	0.2827	0.00001	0.00003
WC-DB-A2	-0.00065	60	0.2790	0.2790	0.00005	0.00019
27034-87	-0.00072	40	0.2729	0.2730	0.00006	0.00022
27034-87	-0.00072	60	0.2689	0.2690	0.00011	0.00039
27034-113	-0.00073	40	0.2716	0.2716	0.00004	0.00014
27034-113	-0.00073	60	0.2676	0.2677	0.00007	0.00027
WC-B-B2*	-0.00067	40	0.2800	0.2801	0.00007	0.00024
WC-B-B2*	-0.00067	60	0.2762	0.2764	0.00015	0.00055
27-168-179	-0.00072	40	0.2729	0.2745	0.00151	0.00554
27-168-179	-0.00072	60	0.2690	0.2706	0.00159	0.00593
HOSB	-0.00065	40	0.2811	0.2823	0.00124	0.00441
HOSB	-0.00065	60	0.2774	0.2786	0.00126	0.00454
					AARD%	0.1291

Table A.25: Comparison of measured FRI for aromatic fractions at 40 and 60°C to the estimated densities using Equation 5.23.

Aromatics	α_{FRI}	Temp °C	FRI	$FRI^{correlation}$	AD	ARD
WC-B-B2	-0.00058	40	0.3222	0.3222	0.00001	0.00002
WC-B-B2	-0.00058	60	0.3185	0.3185	0.00001	0.00002
WC-B-C1	-0.00058	40	0.3210	0.3210	0.00002	0.00005
WC-B-C1	-0.00058	60	0.3173	0.3173	0.00001	0.00002
Arabian	-0.00059	40	0.3163	0.3165	0.00012	0.00039
Arabian	-0.00059	60	0.3125	0.3127	0.00021	0.00069
WC-DB-A2	-0.00058	40	0.3217	0.3215	0.00015	0.00046
WC-DB-A2	-0.00058	60	0.3180	0.3178	0.00022	0.00070
WC-VB-B2	-0.00058	40	0.3261	0.3262	0.00007	0.00022
WC-VB-B2	-0.00058	60	0.3223	0.3225	0.00014	0.00044
WC-B-B2*	-0.00058	40	0.3221	0.3221	0.00006	0.00018
WC-B-B2*	-0.00058	60	0.3183	0.3184	0.00010	0.00031
27034-87	-0.00056	40	0.3340	0.3342	0.00018	0.00054
27034-87	-0.00056	60	0.3300	0.3304	0.00038	0.00116
27034-113	-0.00057	40	0.3268	0.3269	0.00017	0.00051
27034-113	-0.00057	60	0.3228	0.3232	0.00035	0.00109
HOSB	-0.00055	40	0.3408	0.3407	0.00007	0.00021
HOSB	-0.00055	60	0.3371	0.3370	0.00017	0.00052
					AARD%	0.0419

Table A.26: Comparison of measured FRI for saturate and aromatic fractions to the estimated FRI using the One-third rule (Varga *et al.*, 2010).

Saturates	(g/cm^3)	FRI_{20}^{exp}	$FRI_{20}^{1/3\text{-rule}}$	AD	ARD
WC-B-B2	0.8871	0.2839	0.2957	0.0118	0.0416
Arabian	0.8267	0.2729	0.2756	0.0027	0.0099
WC-DB-A2	0.8882	0.2863	0.2961	0.0097	0.0340
WC-B-C1	0.8774	0.2838	0.2925	0.0087	0.0305
27-168-179	0.8448	0.2772	0.2816	0.0044	0.0160
26845-38	0.8606	0.2801	0.2869	0.0068	0.0242
27034-87	0.8478	0.2769	0.2826	0.0057	0.0205
27034-113	0.8414	0.2759	0.2805	0.0046	0.0167
HOSB	0.8769	0.2860	0.2923	0.0063	0.0220
				AARD%	2.39
Aromatics					
WC-B-B2	1.0059	0.3259	0.3353	0.0094	0.0288
Arabian	0.9785	0.3202	0.3262	0.0059	0.0186
WC-DB-A2	1.0029	0.3253	0.3343	0.0090	0.0277
WC-B-C1	1.0016	0.3248	0.3339	0.0091	0.0281
WC-VB-B2	1.0165	0.3300	0.3388	0.0088	0.0268
27-168-179	0.9697	0.3195	0.3232	0.0037	0.0117
26845-38	1.0087	0.3287	0.3362	0.0075	0.0230
27034-87	1.0281	0.3379	0.3427	0.0048	0.0141
27034-113	1.0083	0.3307	0.3361	0.0054	0.0162
HOSB	1.0338	0.3445	0.3446	0.0001	0.0004
				AARD%	1.95

Table A.27: Comparison of extrapolated FRI for resin and asphaltene fractions to the estimated FRI using the One-third rule (Varga *et al.*, 2010).

Resins	(g/cm^3)	FRI_{20}^{exp}	$FRI_{20}^{1/3\text{-rule}}$	AD	ARD
WC-B-B2	1.0544	0.3383	0.3515	0.0132	0.0390
Arabian	1.0477	0.3523	0.3492	0.0031	0.0088
WC-DB-A2	1.0476	0.3405	0.3492	0.0087	0.0255
WC-B-C1	1.0450	0.3373	0.3483	0.0110	0.0327
WC-VB-B2	1.0410	0.3375	0.3470	0.0095	0.0282
27168179	1.0453	0.3398	0.3484	0.0086	0.0254
26845-38	1.0628	0.3446	0.3543	0.0097	0.0281
27034-87	1.0536	0.3409	0.3512	0.0103	0.0303
27034113	1.0590	0.3444	0.3530	0.0086	0.0250
HOSB	1.0723	0.3656	0.3574	0.0082	0.0224
				AARD%	2.65
Asphaltenes					
WC-B-B2	1.1509	0.3885	0.3836	0.0049	0.0126
WC-B-C1	1.1508	0.3808	0.3836	0.0028	0.0074
27168179	1.1550	0.4191	0.3850	0.0341	0.0814
26845-38	1.1794	0.4111	0.3931	0.0180	0.0438
				AARD%	3.63

Table A.28: Comparison of measured FRI at 40 and 60°C for saturate fractions to the estimated FRI using the One-third rule (Varga *et al.*, 2010).

Saturates	ρ_{40} (g/cm^3)	FRI_{40}	$FRI_{40}^{1/3\ rule}$	ARD
27034-87	0.8347	0.2729	0.2782	0.0195
Arabian	0.8129	0.2688	0.2710	0.0081
27-168-179*	0.8315	0.2729	0.2772	0.0155
WC-DB-A2	0.8757	0.2826	0.2919	0.0327
HOSB	0.8648	0.2811	0.2883	0.0256
WC-B-B2	0.8745	0.2821	0.2915	0.0334
27-168-179	0.8313	0.2728	0.2771	0.0157
27034-113	0.8284	0.2716	0.2761	0.0167
WC-B-C1	0.8646	0.2800	0.2882	0.0293
			AARD%	**2.18**

	ρ_{60} (g/cm^3)	FRI_{60}	$FRI_{60}^{1/3\ rule}$	ARD
27034-87	0.8216	0.2689	0.2739	0.0183
Arabian	0.7997	0.2648	0.2666	0.0069
27-168-179*	0.8187	0.2690	0.2729	0.0145
WC-DB-A2	0.8632	0.2790	0.2877	0.0315
HOSB	0.8524	0.2774	0.2841	0.0244
WC-B-B2	0.8619	0.2784	0.2873	0.0321
27-168-179	0.8185	0.2689	0.2728	0.0146
27034-113	0.8153	0.2676	0.2718	0.0155
WC-B-C1	0.8519	0.2762	0.2840	0.0280
			AARD%	**2.06**

Table A.29: Comparison of measured FRI at 40 and 60°C for aromatic fractions to the estimated FRI using the One-third rule (Varga *et al.*, 2010).

Aromatics	ρ_{40} (g/cm^3)	FRI_{40}	$FRI_{40}^{1/3\ rule}$	ARD
WC-B-B2	0.9927	0.3222	0.3309	0.0269
27034-87	1.0143	0.3340	0.3381	0.0123
WC-B-B2*	0.9924	0.3221	0.3308	0.0271
Arabian	0.9652	0.3163	0.3217	0.0171
WC-DB-A2	0.9901	0.3217	0.3300	0.0260
HOSB	1.0209	0.3408	0.3403	0.0014
27034-113	0.9946	0.3268	0.3315	0.0147
WC-B-C1	0.9884	0.3210	0.3295	0.0263
WC-VB-B2	1.0038	0.3261	0.3346	0.0260
			AARD%	**1.97**
	ρ_{60} (g/cm^3)	FRI_{60}	$FRI_{60}^{1/3\ rule}$	ARD
WC-B-B2	0.9797	0.3185	0.3266	0.0252
27034-87	1.0005	0.3300	0.3335	0.0105
WC-B-B2*	0.9792	0.3183	0.3264	0.0254
Arabian	0.9521	0.3125	0.3174	0.0155
WC-DB-A2	0.9773	0.3180	0.3258	0.0243
HOSB	1.0082	0.3371	0.3361	0.0032
27034-113	0.9810	0.3228	0.3270	0.0129
WC-B-C1	0.9754	0.3173	0.3251	0.0248
WC-VB-B2	0.9913	0.3223	0.3304	0.0251
			AARD%	**1.85**

Table A.30: Comparison of measured FRI for saturate and aromatic fractions to the estimated FRI using Equation 5.27.

Saturates	(g/cm^3)	FRI_{20}^{exp}	$FRI_{20}^{correlation}$	AD	ARD
WC-B-B2	0.8871	0.2839	0.2869	0.0030	0.0105
Arabian	0.8267	0.2729	0.2732	0.0003	0.0011
WC-DB-A2	0.8882	0.2863	0.2871	0.0008	0.0028
WC-B-C1	0.8774	0.2838	0.2844	0.0006	0.0019
27-168-179	0.8448	0.2772	0.2768	0.0004	0.0013
26845-38	0.8606	0.2801	0.2803	0.0002	0.0009
27034-87	0.8478	0.2769	0.2775	0.0005	0.0019
27034-113	0.8414	0.2759	0.2761	0.0002	0.0009
HOSB	0.8769	0.2860	0.2842	0.0018	0.0062
				AARD%	0.30
Aromatics					
WC-B-B2	1.0059	0.3259	0.3262	0.0003	0.0010
Arabian	0.9785	0.3202	0.3157	0.0045	0.0141
WC-DB-A2	1.0029	0.3253	0.3250	0.0002	0.0008
WC-B-C1	1.0016	0.3248	0.3245	0.0002	0.0007
WC-VB-B2	1.0165	0.3300	0.3306	0.0006	0.0017
27-168-179	0.9697	0.3195	0.3125	0.0070	0.0219
26845-38	1.0087	0.3287	0.3274	0.0013	0.0040
27034-87	1.0281	0.3379	0.3354	0.0025	0.0074
27034-113	1.0083	0.3307	0.3272	0.0035	0.0107
HOSB	1.0338	0.3445	0.3379	0.0066	0.0191
				AARD%	0.81

Table A.31: Comparison of measured FRI for resins and asphaltene fractions to the estimated FRI using Equation 5.27.

Resins	(g/cm^3)	FRI_{20}^{exp}	$FRI_{20}^{correlation}$	AD	ARD
WC-B-B2	1.0544	0.3383	0.3471	0.0088	0.0260
Arabian	1.0477	0.3523	0.3440	0.0083	0.0235
WC-DB-A2	1.0476	0.3405	0.3440	0.0035	0.0102
WC-B-C1	1.0450	0.3373	0.3428	0.0055	0.0164
WC-VB-B2	1.0410	0.3375	0.3410	0.0036	0.0105
27168179	1.0453	0.3398	0.3430	0.0031	0.0092
26845-38	1.0628	0.3446	0.3510	0.0064	0.0185
27034-87	1.0536	0.3409	0.3467	0.0058	0.0171
27034113	1.0590	0.3444	0.3492	0.0048	0.0139
HOSB	1.0723	0.3656	0.3554	0.0102	0.0278
				AARD%	1.73
Asphaltenes					
WC-B-B2	1.1509	0.3885	0.3967	0.0081	0.0209
WC-B-C1	1.1508	0.3808	0.3966	0.0158	0.0415
27168179	1.1550	0.4191	0.3990	0.0201	0.0480
26845-38	1.1794	0.4111	0.4134	0.0023	0.0055
				AARD%	2.90

Table A.32: Comparison of measured FRI at 40 and 60°C for saturate fractions to the estimated FRI values at these temperatures with Equation 5.23 (using FRI_{20} estimated from Equation 5.27).

Saturates	ρ_{20}^{exp}(g/cm^3)	$FRI_{20}^{Equ.5.27}$	$\alpha_{FRI(s)}^{Equ.\ 5.21}$	FRI_{40}^{exp}	$FRI_{40}^{Equ.5.23}$	AD	ARD
27034-87	0.8478	0.27746	-0.00072	0.27289	0.27351	0.00062	0.00226
Arabian	0.8267	0.27314	-0.00075	0.26877	0.26908	0.00031	0.00114
27-168-179*	0.8454	0.27693	-0.00072	0.27294	0.27296	0.00002	0.00007
WC-DB-A2	0.8882	0.28715	-0.00064	0.28264	0.28348	0.00084	0.00296
HOSB	0.8769	0.28424	-0.00067	0.28106	0.28048	0.00058	0.00205
WC-B-B2	0.8871	0.28686	-0.00065	0.28207	0.28318	0.00111	0.00392
27-168-179	0.8448	0.27680	-0.00072	0.27281	0.27283	0.00002	0.00007
27034-113	0.8415	0.27612	-0.00073	0.27160	0.27214	0.00054	0.00199
WC-B-C1	0.8774	0.28435	-0.00066	0.28000	0.28060	0.00060	0.00214
						AARD%	0.18

	FRI_{60}^{exp}	$FRI_{60}^{Equ.5.23}$	AD	ARD
27034-87	0.26894	0.26962	0.00068	0.00252
Arabian	0.26476	0.26507	0.00031	0.00117
27-168-179*	0.26899	0.26906	0.00006	0.00024
WC-DB-A2	0.27895	0.27986	0.00091	0.00325
HOSB	0.27738	0.27678	0.00061	0.00218
WC-B-B2	0.27838	0.27955	0.00117	0.00420
27-168-179	0.26889	0.26892	0.00003	0.00012
27034-113	0.26762	0.26821	0.00059	0.00219
WC-B-C1	0.27622	0.27690	0.00067	0.00243
			AARD%	0.20

Table A.33: Comparison of measured FRI at 40 and 60°C for aromatic fractions to the estimated FRI values at these temperatures with Equation 5.23 (using FRI_{20} estimated from Equation 5.27).

Aromatics	ρ_{20}^{exp}(g/cm^3)	$FRI_{20}^{Equ.5.27}$	$\alpha_{FRI(a)}^{Equ.\ 5.22}$	FRI_{40}^{exp}	$FRI_{40}^{Equ.5.23}$	AD	ARD
WC-B-B2	1.0059	0.32623	-0.00058	0.32224	0.32246	0.00022	0.00068
27034-87	1.0281	0.33544	-0.00057	0.33399	0.33167	0.00232	0.00695
WC-B-B2*	1.0057	0.32616	-0.00058	0.32209	0.32239	0.00029	0.00091
Arabian	0.9785	0.31571	-0.00060	0.31633	0.31195	0.00438	0.01385
WC-DB-A2	1.0029	0.32506	-0.00058	0.32167	0.32129	0.00039	0.00120
HOSB	1.0338	0.33787	-0.00056	0.34077	0.33409	0.00668	0.01961
27034-113	1.0083	0.32722	-0.00058	0.32676	0.32345	0.00330	0.01011
WC-B-C1	1.0016	0.32452	-0.00058	0.32100	0.32075	0.00025	0.00078
WC-VB-B2	1.0165	0.33055	-0.00057	0.32614	0.32677	0.00063	0.00192
						AARD%	0.62

	FRI_{60}^{exp}	$FRI_{60}^{Equ.5.23}$	AD	ARD
WC-B-B2	0.31853	0.31873	0.00020	0.00064
27034-87	0.33005	0.32793	0.00211	0.00641
WC-B-B2*	0.31832	0.31866	0.00033	0.00105
Arabian	0.31252	0.30824	0.00428	0.01370
WC-DB-A2	0.31802	0.31756	0.00046	0.00144
HOSB	0.33714	0.33036	0.00678	0.02012
27034-113	0.32284	0.31972	0.00312	0.00965
WC-B-C1	0.31726	0.31702	0.00024	0.00075
WC-VB-B2	0.32234	0.32304	0.00070	0.00217
			AARD%	0.62

Table A.34: Comparison of the binary interaction parameter from density measurements of saturates and aromatics in solution with toluene or heptane from fitting experimental data to the values calculated from Equation 5.5.

Saturates	solvent	$\beta_{ij}^{exp.\ fit}$	$\beta_{ij}^{Corr\ (Eq.\ 5.5)}$	AD
27-168-179 R1	toluene	-0.0045	-0.0054	0.0009
27-168-179 R2	toluene	-0.0047	-0.0054	0.0007
26845-38	toluene	-0.0037	-0.0069	0.0033
27034-87	toluene	-0.0076	-0.0057	0.0018
WC-B-B2	toluene	-0.0096	-0.0056	0.0040
Arabian	toluene	-0.0057	-0.0037	0.0020
WC-DB-A2	toluene	-0.0034	-0.0055	0.0021
HOSB R1	toluene	-0.0039	-0.0066	0.0027
HOSB R2	toluene	-0.0038	-0.0066	0.0028
27-168-179 R1	heptane	0.0111	0.0080	0.0031
27-168-179 R2	heptane	0.0056	0.0080	0.0024
26845-38	heptane	0.0114	0.0091	0.0023
WC-B-B2 R1	heptane	0.0138	0.0108	0.0030
WC-B-B2 R2	heptane	0.0149	0.0108	0.0040
			AAD	0.0025
Aromatics				
27-168-179	toluene	0.0017	0.0012	0.0005
26845-38	toluene	0.0037	0.0039	0.0002
27034-87	toluene	0.0004	0.0052	0.0048
WC-B-B2	toluene	0.0031	0.0037	0.0006
Arabian	toluene	-0.0002	0.0018	0.0021
WC-DB-A2	toluene	0.0032	0.0035	0.0003
HOSB R1	toluene	0.0046	0.0055	0.0009
HOSB R2	toluene	0.0034	0.0055	0.0021
26845-38	heptane	0.0154	0.0173	0.0019
27-168-179	heptane	0.0154	0.0155	0.0001
			AAD	0.0014

Table A.35: Comparison of the binary interaction parameter from refractive index measurements of saturates and aromatics in solution with toluene or heptane from fitting experimental data to the values calculated from Equation 5.10.

Saturates	solvent	$\beta^*_{ij}{}^{exp.\ fit}$	$\beta^*_{ij}{}^{Corr\ (Eq.\ 5.10)}$	AD
27-168-179 R1	toluene	0.0097	0.0048	0.0048
27-168-179 R2	toluene	0.0081	0.0048	0.0033
26845-38	toluene	0.0078	0.0069	0.0009
27034-87	toluene	0.0123	0.0046	0.0076
WC-B-B2 R1	toluene	0.0054	0.0097	0.0043
Arabian	toluene	0.0002	0.0020	0.0017
WC-DB-A2	toluene	0.0067	0.0116	0.0050
HOSB R1	toluene	0.0080	0.0114	0.0034
27-168-179 R1	heptane	-0.0149	-0.0103	0.0045
27-168-179 R2	heptane	-0.0147	-0.0103	0.0043
26845-38 R1	heptane	-0.0134	-0.0114	0.0020
26845-38 R2	heptane	-0.0110	-0.0114	0.0004
WC-B-B2 R1	heptane	-0.0160	-0.0132	0.0028
WC-B-B2 R2	heptane	-0.0138	-0.0132	0.0005
			AAD	0.0031
Aromatics				
27-168-179	toluene	0.0016	-0.0010	0.0025
26845-38	toluene	-0.0048	-0.0051	0.0003
27034-87	toluene	-0.0045	-0.0085	0.0041
WC-B-B2	toluene	-0.0037	-0.0040	0.0003
Arabian	toluene	-0.0005	-0.0013	0.0008
WC-DB-A2	toluene	-0.0055	-0.0037	0.0018
HOSB	toluene	-0.0061	-0.0106	0.0045
WC-B-B2 R2	heptane	-0.0214	-0.0213	0.0001
26845-38	heptane	-0.0209	-0.0216	0.0007
27-168-179	heptane	-0.0174	-0.0205	0.0031
			AAD	0.0018

Table A.36: Comparison of the model fit solubility parameter to the solubility parameter calculated using Buckley et al. 1998 correlation to FRI.

Saturates	FRI	Sol. Par.^{RSM}	Sol. Par.$^{Buckley'98}$	Dev.	ARD
WC-B-B2	0.2839	16.60	17.68	1.08	0.06493
WC-DB-A2	0.2863	16.70	17.81	1.11	0.06622
WC-B-C1	0.2838	16.70	17.67	0.97	0.05833
27-168-179	0.2772	15.70	17.33	1.63	0.10374
26845-38	0.2801	16.50	17.48	0.98	0.05938
27034-87	0.2769	16.30	17.32	1.02	0.06229
27034-113	0.2759	16.10	17.26	1.16	0.07205
HOSB	0.2860	15.80	17.79	1.99	0.12583
				AARD %	7.66
Aromatics					
WC-B-B2	0.3259	20.80	19.87	-0.93	0.04492
WC-DB-A2	0.3253	20.80	19.83	-0.97	0.04650
WC-B-C1	0.3248	20.80	19.80	-1.00	0.04785
WC-VB-B2	0.3300	20.80	20.08	-0.72	0.03474
27-168-179	0.3195	19.20	19.53	0.33	0.01725
26845-38	0.3287	21.00	20.01	-0.99	0.04717
27034-87	0.3379	20.60	20.49	-0.11	0.00528
27034-113	0.3307	20.80	20.12	-0.68	0.03286
HOSB	0.3445	20.80	20.83	0.03	0.00147
				AARD %	3.09

Table A.37: Comparison of the model fit solubility parameter to the solubility parameter calculated for native saturate and aromatic fractions using the correlation to FRI in Equation 7.1.

Saturates	FRI	Sol. Par.^{RSM}	Sol. Par.$^{Eq.\ 7.1}$	Dev.	ARD
WC-B-B2	0.2839	16.60	16.74	0.14	0.00854
WC-DB-A2	0.2863	16.70	16.97	0.27	0.01639
WC-B-C1	0.2838	16.70	16.74	0.04	0.00211
				AARD %	0.90
Aromatics					
WC-B-B2	0.3259	20.80	20.70	-0.10	0.00472
WC-DB-A2	0.3253	20.80	20.64	-0.16	0.00757
WC-B-C1	0.3248	20.80	20.59	-0.21	0.01001
WC-VB-B2	0.3300	20.80	21.09	0.29	0.01370
				AARD %	0.90

Table A.38: Comparison of the model fit solubility parameter to the solubility parameter calculated for thermally cracked saturate and aromatic fractions using the correlation to FRI in Equation 7.1.

Saturates	FRI	Sol. Par.^{RSM}	Sol. Par.$^{Eq.\ 7.1}$	Dev.	ARD
26845-38	0.2801	16.50	16.38	-0.12	0.00707
27034-87	0.2769	16.30	16.09	-0.21	0.01315
27034-113	0.2759	16.10	15.99	-0.11	0.00712
				AARD %	0.91
Aromatics					
26845-38	0.3287	21.00	20.96	-0.04	0.00180
27034-87	0.3379	20.60	21.83	1.23	0.05992
27034-113	0.3307	20.80	21.16	0.36	0.01711
				AARD %	2.63

Table A.39: Comparison of the model fit solubility parameter to the solubility parameter calculated for native saturate and aromatic fractions using the correlation to density in Equation 7.2.

Saturates	ρ (g/cm^3)	Sol. Par.^{RSM}	Sol. Par.$^{Eq. 7.2}$	Dev.	ARD
WC-B-B2	0.8871	16.60	16.97	0.37	0.02253
WC-B-C1	0.8774	16.70	16.68	-0.02	0.00143
WC-DB-A2	0.8882	16.70	17.01	0.31	0.01843
				AARD %	1.41
Aromatics					
WC-B-B2	1.0059	20.80	20.62	-0.18	0.00860
WC-DB-A2	1.0029	20.80	20.53	-0.27	0.01303
WC-B-C1	1.0016	20.80	20.49	-0.31	0.01495
WC-VB-B2	1.0165	20.80	20.95	0.15	0.00705
				AARD %	1.09

Table A.40: Comparison of the model fit solubility parameter to the solubility parameter calculated for all saturate and aromatic fractions using the correlation to density in Equation 7.2.

Saturates	ρ (g/cm^3)	Sol. Par.^{RSM}	Sol. Par.$^{Eq. 7.2}$	Dev.	ARD
WC-B-B2	0.8871	16.60	16.97	0.37	0.02253
WC-B-C1	0.8774	16.70	16.68	-0.02	0.00143
WC-DB-A2	0.8882	16.70	17.01	0.31	0.01843
27034-87	0.8606	16.30	16.16	-0.14	0.00856
26845-38	0.8606	16.50	16.16	-0.34	0.02058
27034-113	0.8414	16.10	15.57	-0.53	0.03286
27-168-179	0.8448	15.70	15.68	-0.02	0.00157
HOSB	0.8769	15.80	16.66	0.86	0.05448
				AARD %	2.01
Aromatics					
WC-B-B2	1.0059	20.80	20.62	-0.18	0.00860
WC-DB-A2	1.0029	20.80	20.53	-0.27	0.01303
WC-B-C1	1.0016	20.80	20.49	-0.31	0.01495
WC-VB-B2	1.0165	20.80	20.95	0.15	0.00705
26845-38	1.0087	21.00	20.71	-0.29	0.01395
27034-87	1.0281	20.60	21.30	0.70	0.03411
27034-113	1.0083	20.80	20.69	-0.11	0.00506
27-168-179	0.9697	19.20	19.51	0.31	0.01613
HOSB	1.0338	20.80	21.48	0.68	0.03258
				AARD %	1.71

Table A.41: Deviation between measured FRI and the calculated FRI of solutes in solvents using the regular solution mixing rule and the excess volume mixing rule.

27-168-179_Saturates + Toluene

vol frac (tol)	FRI^{exp}	$FRI^{reg\ sol}$	AD	ARD	$FRI^{exc\ vol}$	AD	ARD
0.50	0.28381	0.28497	0.00117	0.00411	0.28429	0.00048	0.00169
0.62	0.28576	0.28682	0.00106	0.00373	0.28618	0.00042	0.00147
0.70	0.28711	0.28806	0.00095	0.00330	0.28748	0.00037	0.00130
0.81	0.28910	0.28979	0.00069	0.00239	0.28937	0.00027	0.00095
0.90	0.29071	0.29113	0.00042	0.00145	0.29088	0.00018	0.00060
		Average	0.00086	0.00299	***Average***	0.00034	0.00120

WC-B-B2_Aromatics + Heptane

vol frac (hep)	FRI^{exp}	$FRI^{reg\ sol}$	AD	ARD	$FRI^{exc\ vol}$	AD	ARD
0.52	0.28178	0.27878	0.00300	0.01065	0.28177	0.00002	0.00006
0.59	0.27582	0.27291	0.00291	0.01056	0.27580	0.00002	0.00006
0.72	0.26349	0.26109	0.00239	0.00908	0.26350	0.00001	0.00005
0.78	0.25831	0.25621	0.00210	0.00814	0.25829	0.00002	0.00007
0.90	0.24618	0.24506	0.00111	0.00453	0.24615	0.00003	0.00012
		Average	0.00230	0.00859	***Average***	0.00002	0.00007

Appendix B: Additional Figures

Figures B.1 to B.18 represent the VPO responses for SARA fractions of samples used in thesis; plots of ΔV/C (mV/(g/L)) vs. Conc. g/L

Figures B.18 to B.33 represent the density measurements (in toluene or heptane solutions) plots for the SARA fractions characterized in this thesis; plots of specific volume (cm^3/g) vs. SARA mass fraction.

Figures B.34 to B52 represent the refractive index measurements (in toluene or heptane solutions) plots for the SARA fractions used in this thesis; plots of FRI vs. SARA volume fraction.

Figures B.53 to B.60 show the slopes and intercepts for individual plots of specific volume (cm^3/g) vs. temperature, T°C for saturates and aromatics; used for thermal expansion coefficients.

Figures B.61 to B.69 show the slopes and intercepts for individual plots of FRI vs. temperature, T°C for saturates and aromatics; used for thermal FRI coefficients.

Figures B.70 to B.78 show results from using the Regular Solution Model to fit aspheltene yield data from solutions of saturates/toluene and aromatics/heptane and the back-calculated solubility parameters.

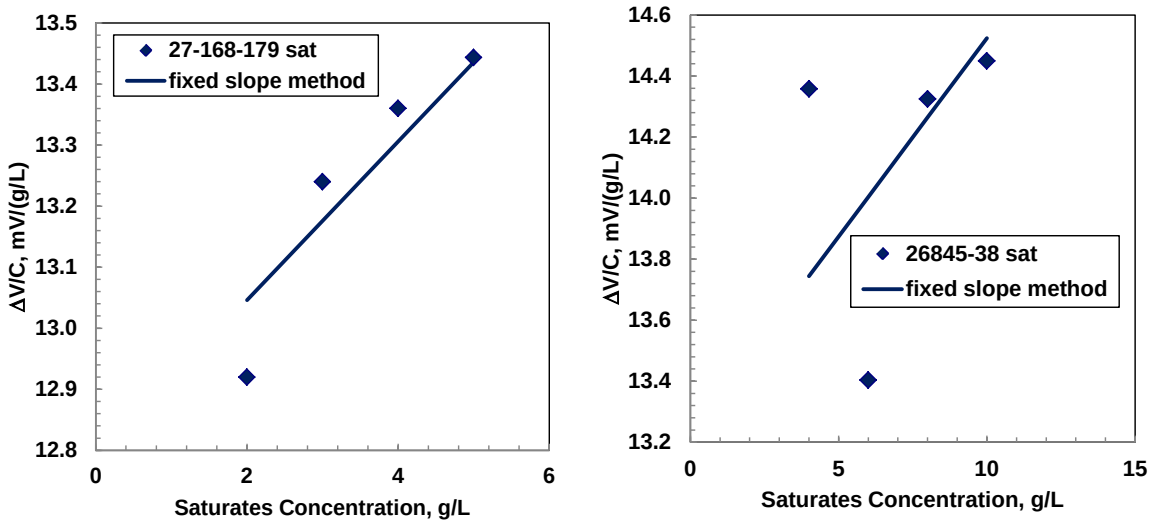

Figure B.1. VPO measurements of voltage difference over concentration for saturates from 27-168-179 & 26845-38 at 50°C.

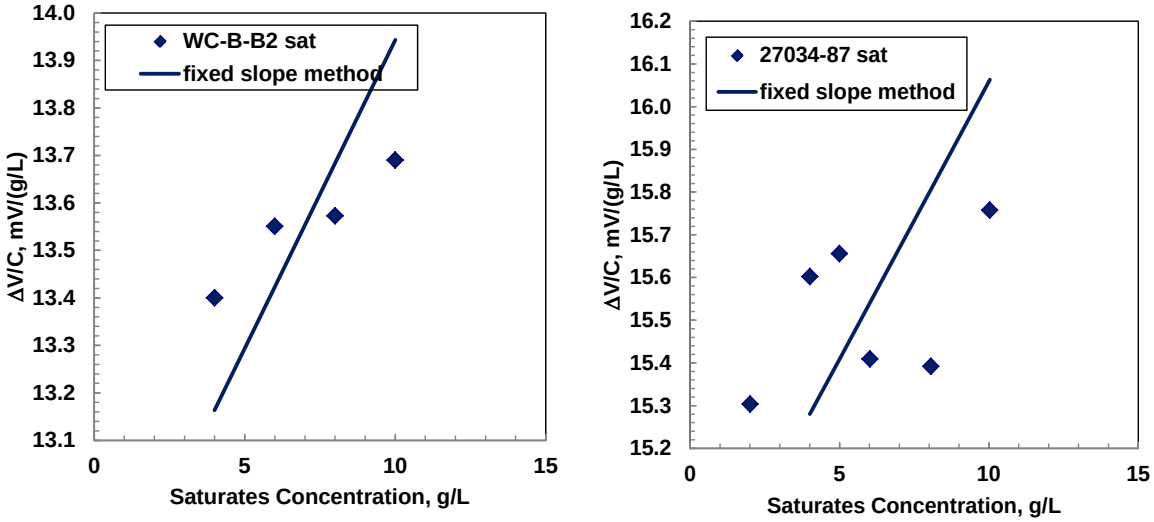

Figure B.2. VPO measurements of voltage difference over concentration for saturates from WC-B-B2 & 27034-87 at 50°C.

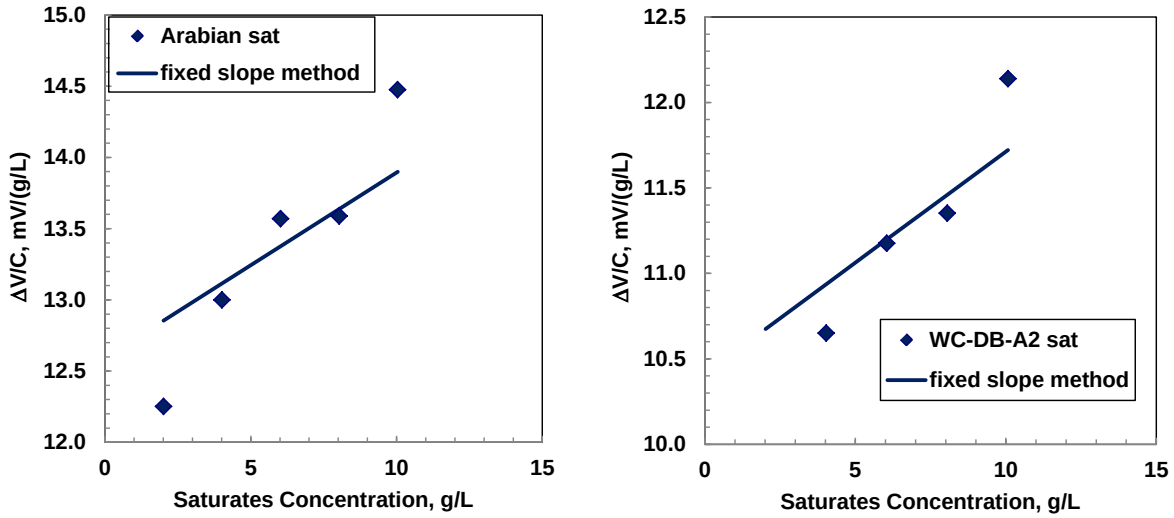

Figure B.3 VPO measurements of voltage difference over concentration for saturates from Arabian & WC-DB-A2 at 50°C

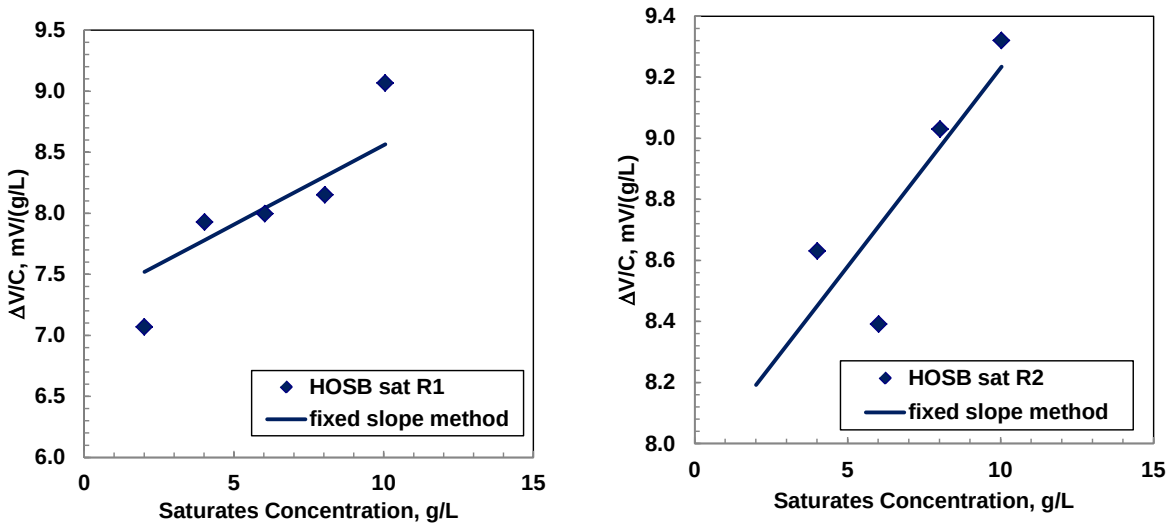

Figure B.4. VPO measurements of voltage difference over concentration for saturates from Heavy Oil Stripper Bottoms (HOSB) at 50°C

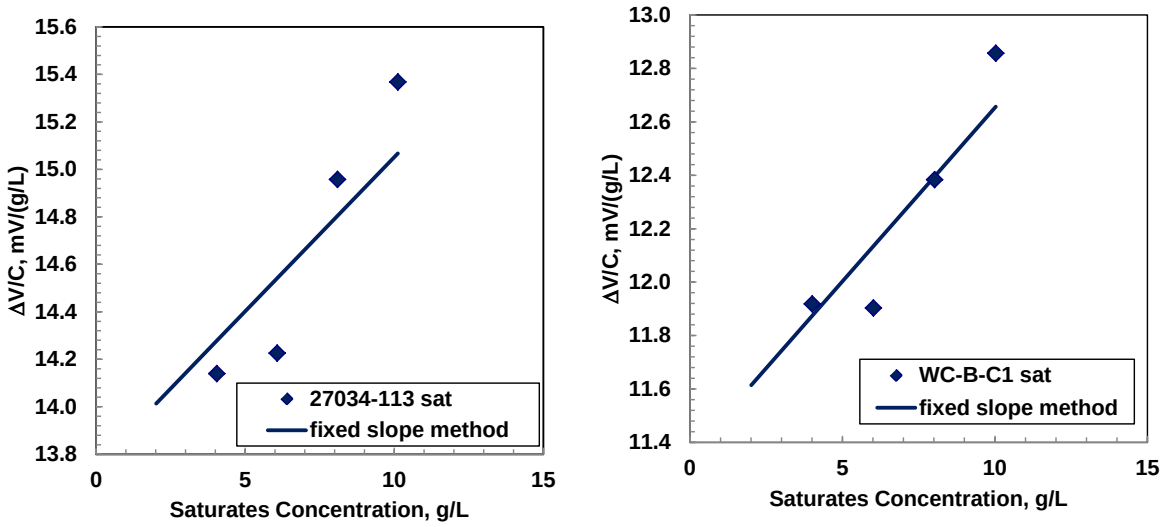

Figure B.5. VPO measurements of voltage difference over concentration for saturates from 27034-113 & WC-B-C1at 50°C

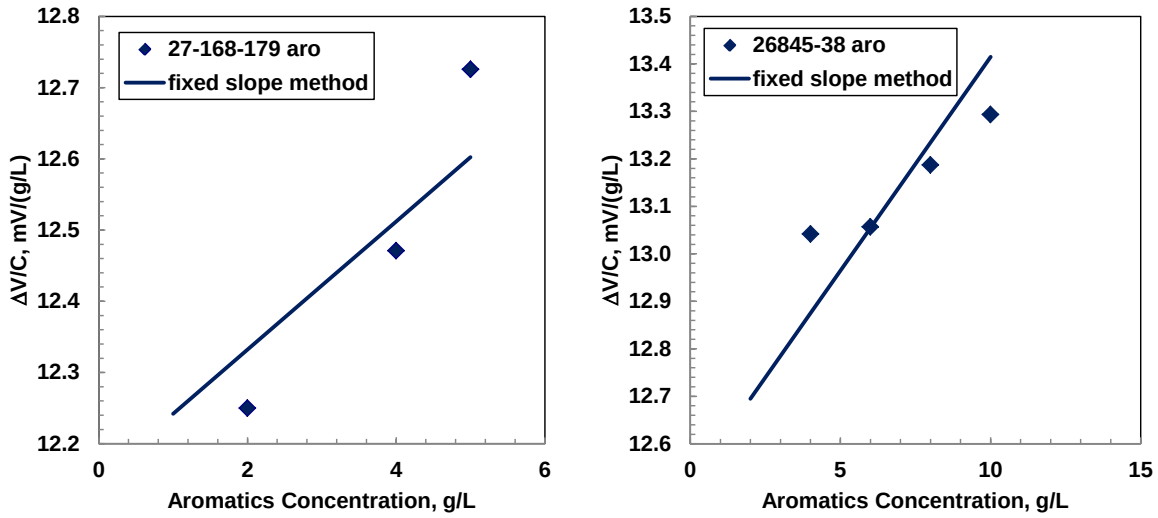

Figure B.6. VPO measurements of voltage difference over concentration for aromatics from 27-168-179 & 26845-38 at 50°C

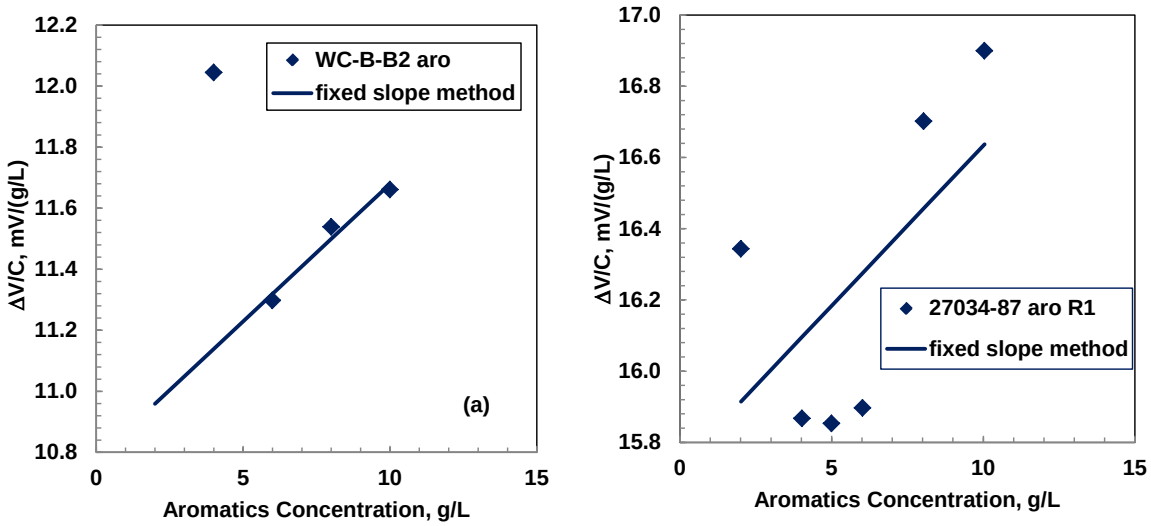

Figure B.7. VPO measurements of voltage difference over concentration for aromatics from WC-B-B2 & 27034-87 at 50°C

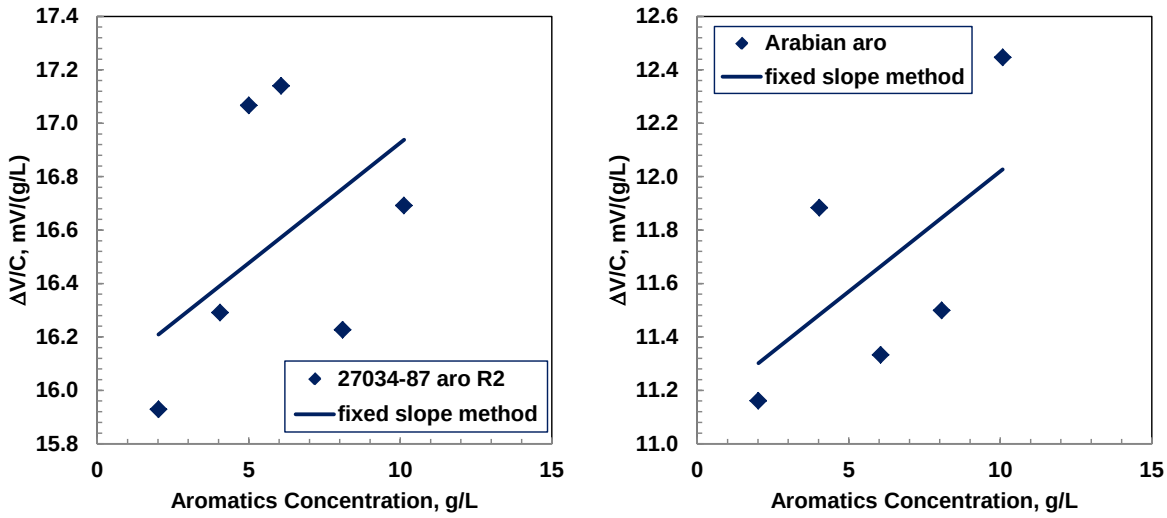

Figure B.8. VPO measurements of voltage difference over concentration for aromatics from 27034-87 & Arabian at 50°C

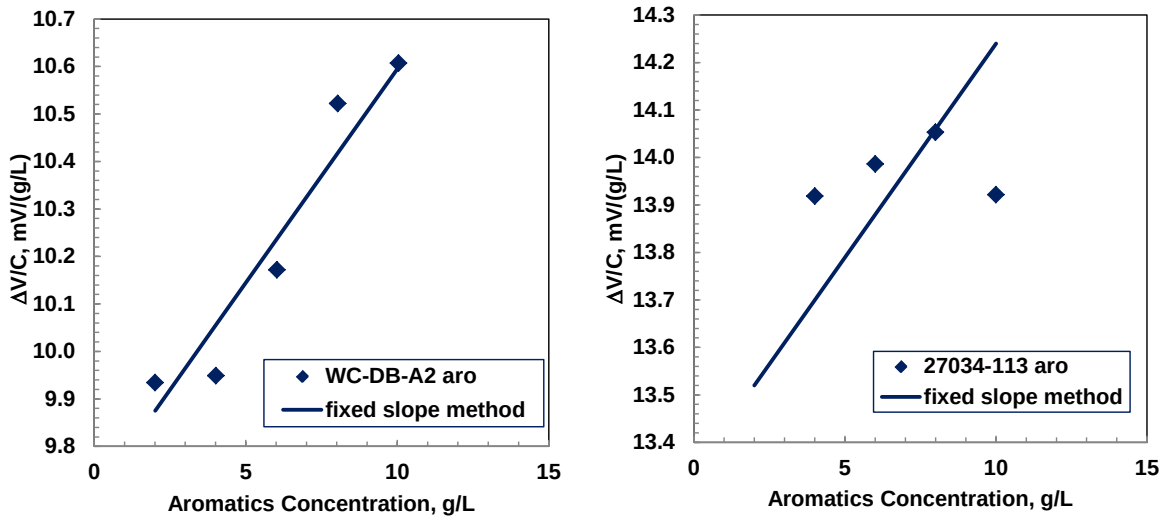

Figure B.9. VPO measurements of voltage difference over concentration for aromatics from WC-DB-A2 & 27034-113 at 50°C

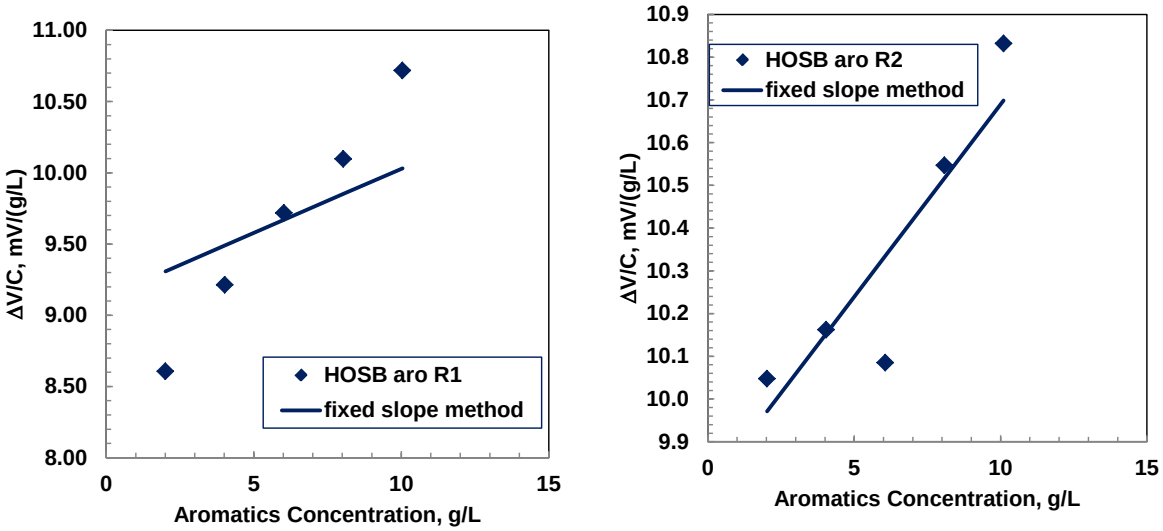

Figure B.10. VPO measurements of voltage difference over concentration for aromatics from HOSB at 50°C

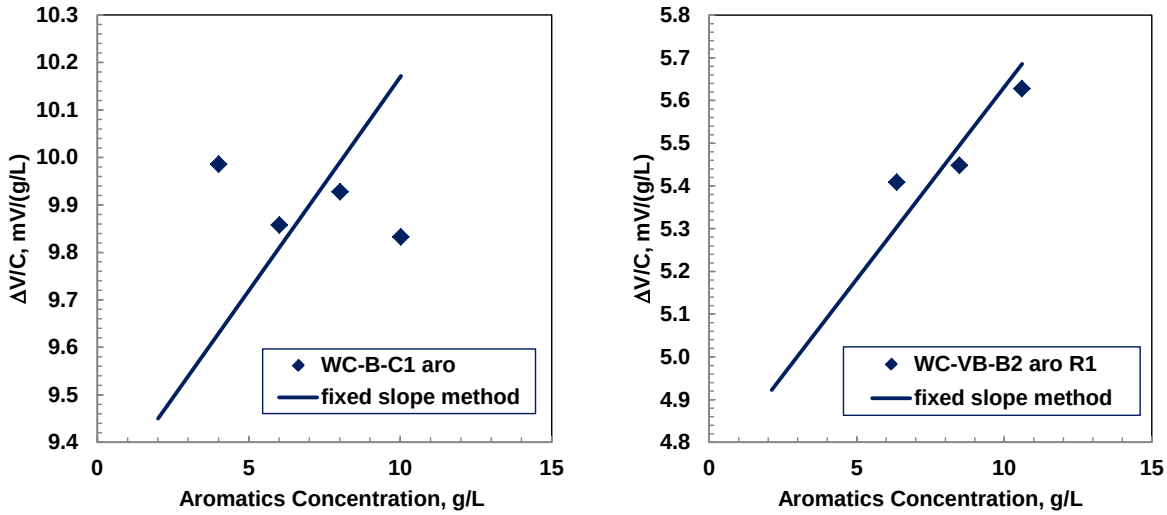

Figure B.11. VPO measurements of voltage difference over concentration for aromatics from WC-B-C1 at 50°C

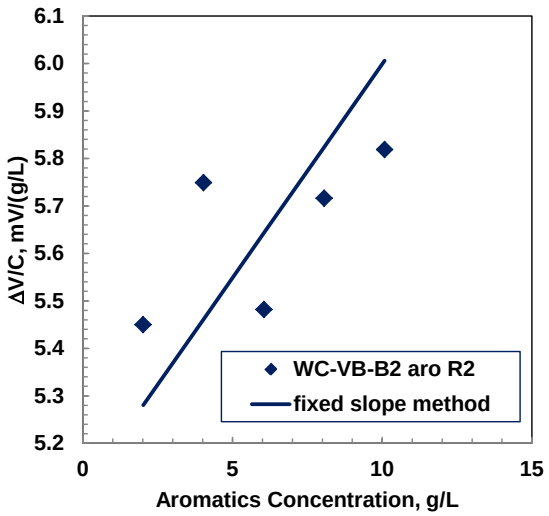

Figure B.12. VPO measurements of voltage difference over concentration for aromatics from WC-VB-B2 at 50°C

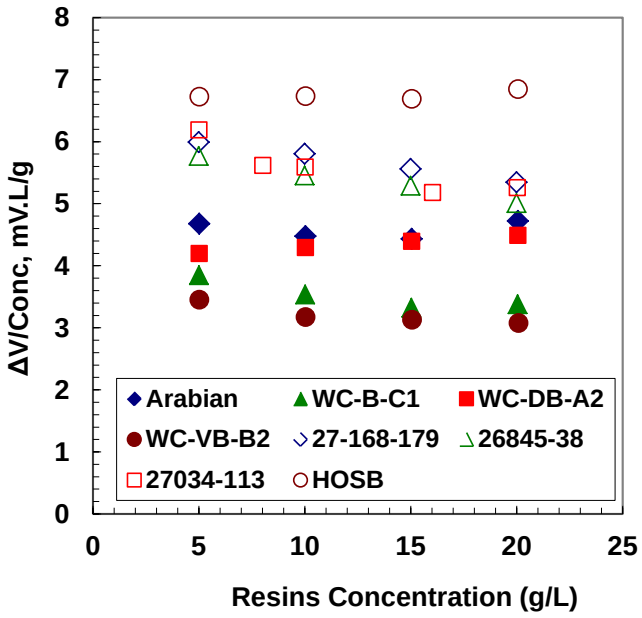

Figure B.13. VPO measurements of voltage difference over concentration for 8 resin fractions at 50°C

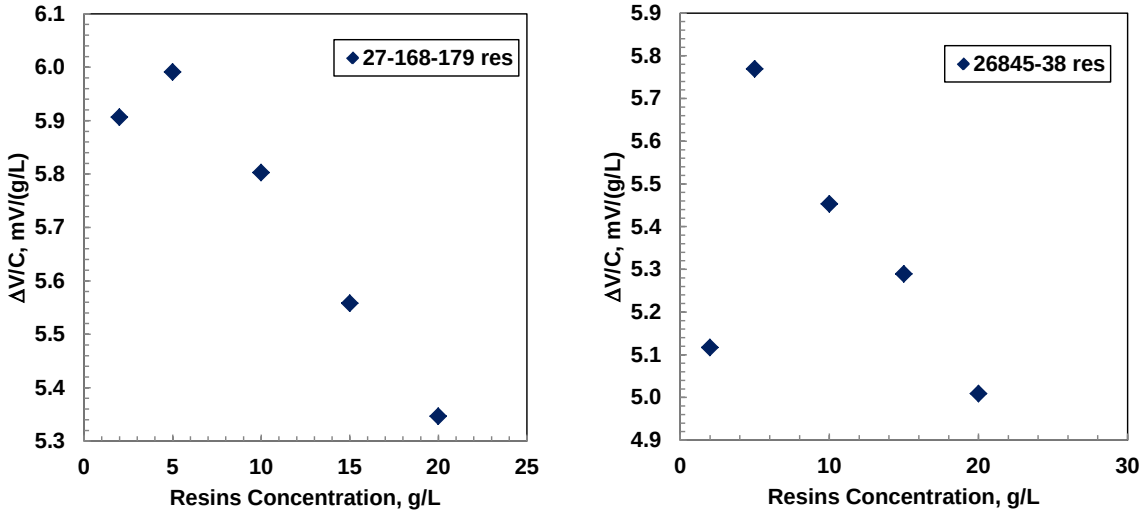

Figure B.14. VPO measurements of voltage difference over concentration for resins from 27-168-179 & 26845-38 at 50°C

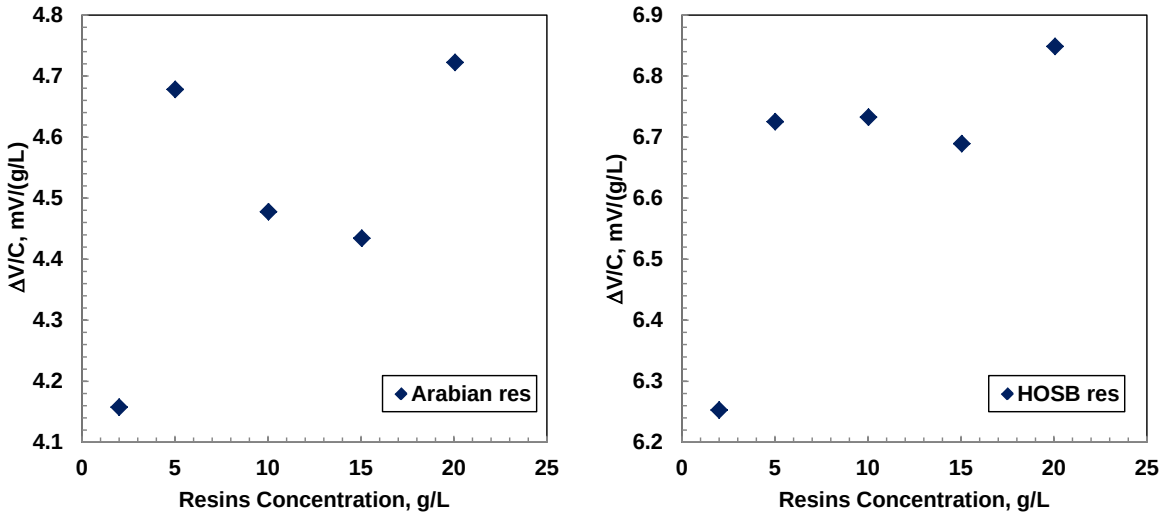

Figure B.15. VPO measurements of voltage difference over concentration for resins from Arabian & HOSB at 50°C

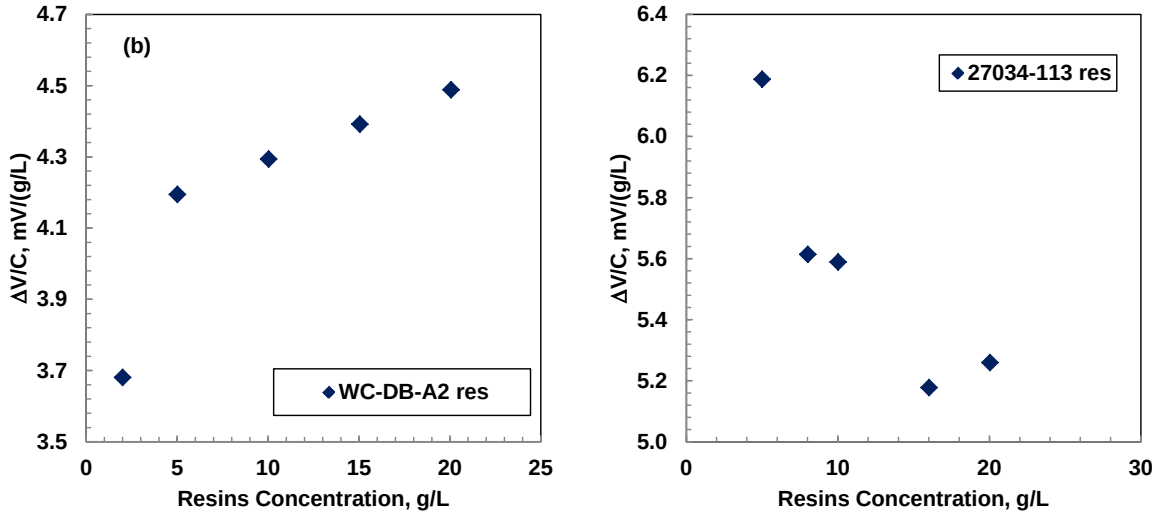

Figure B.16. VPO measurements of voltage difference over concentration for resins from WC-DB-A2 & 27034-113 at 50°C

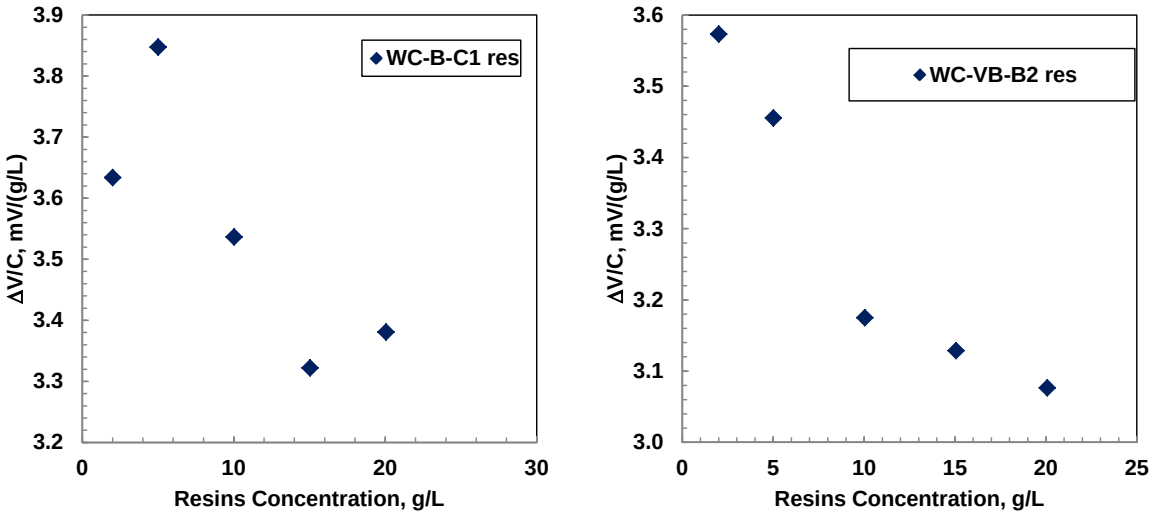

Figure B.17. VPO measurements of voltage difference over concentration for resins from WC-B-C1 & WC-VB-B2 at 50°C

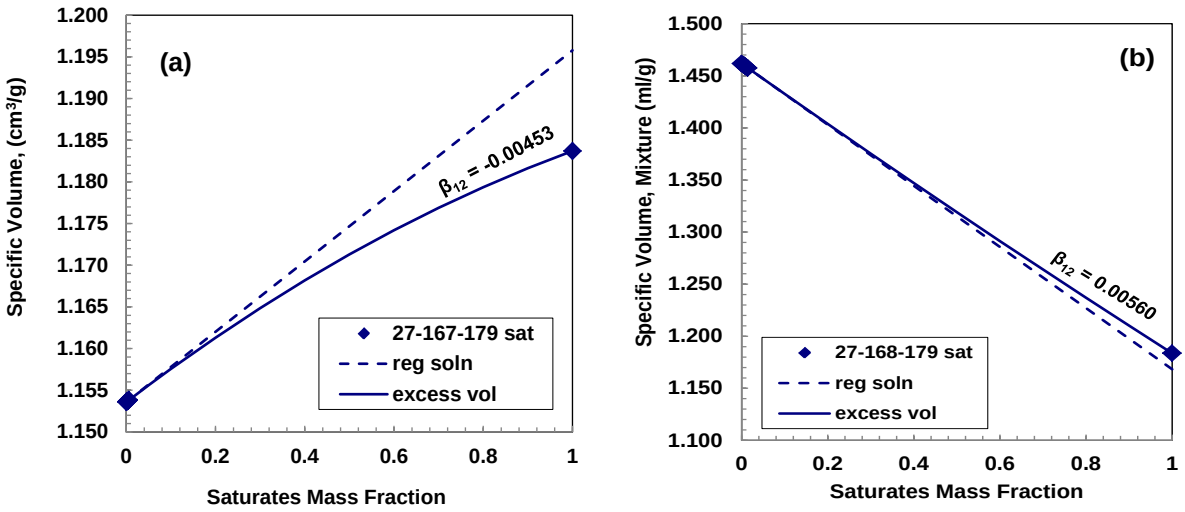

Figure B.18. Density measurements of 27-168-179 saturates in: a) toluene & b) heptane

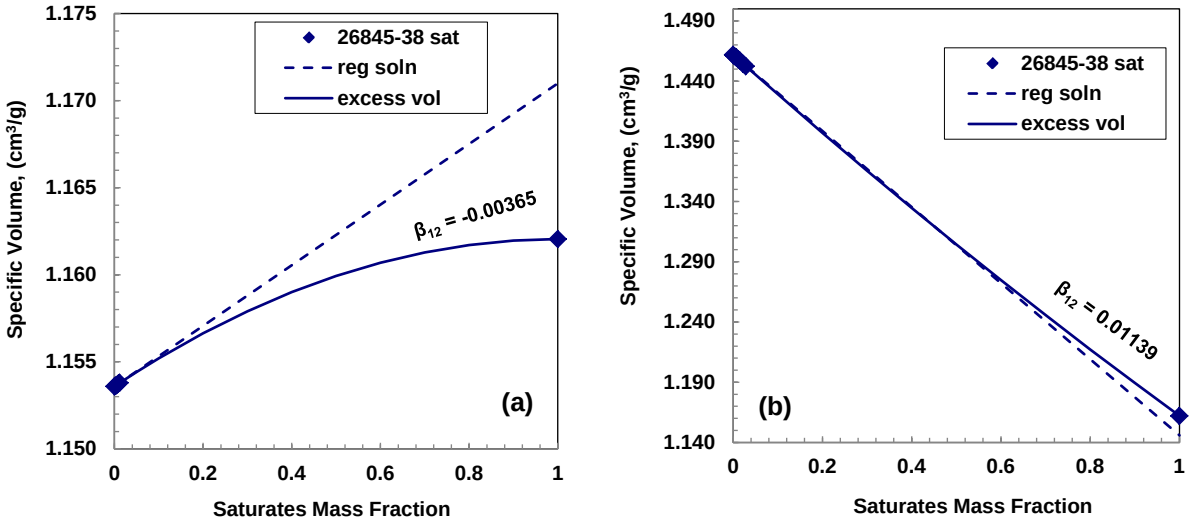

Figure B.19. Density measurements of 26845-38 saturates in: a) toluene b) heptane

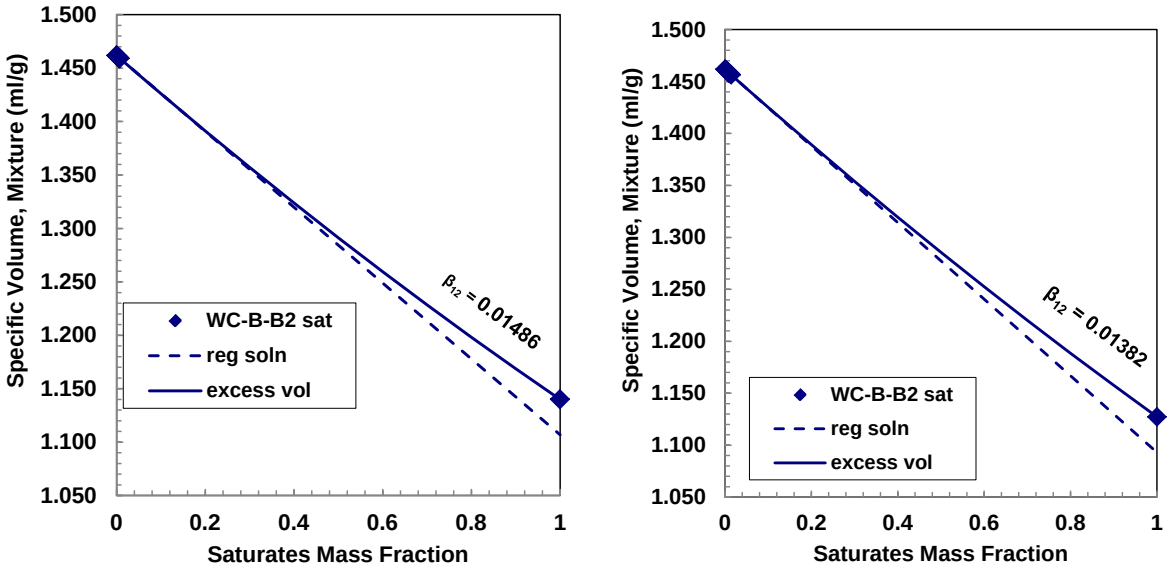

Figure B.20. Density measurements of WC-B-B2 saturates in heptane

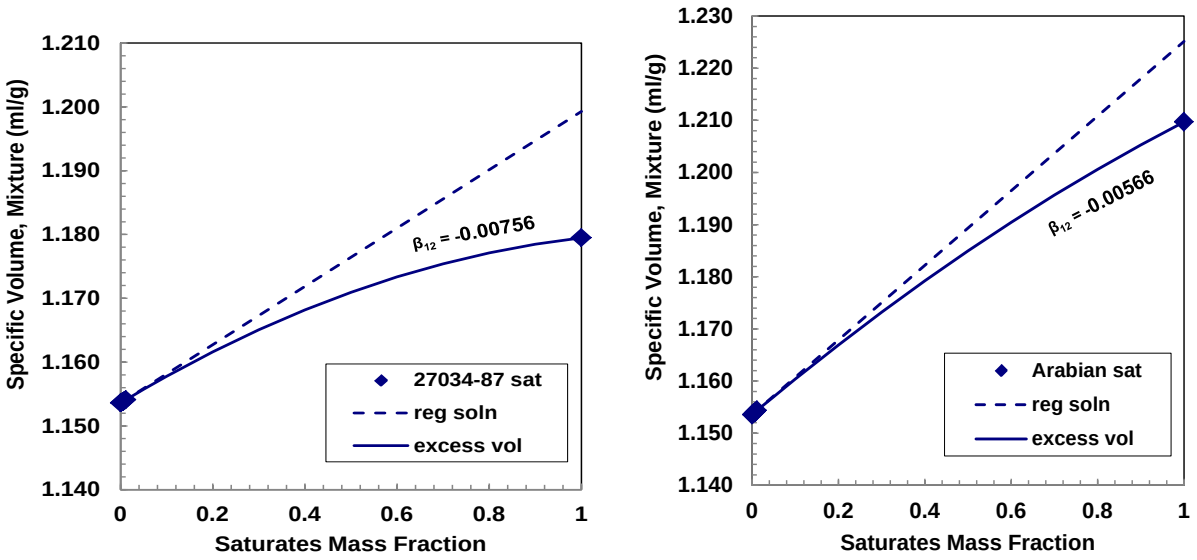

Figure B.21. Density measurements of 27034-87 & Arabian saturates in toluene

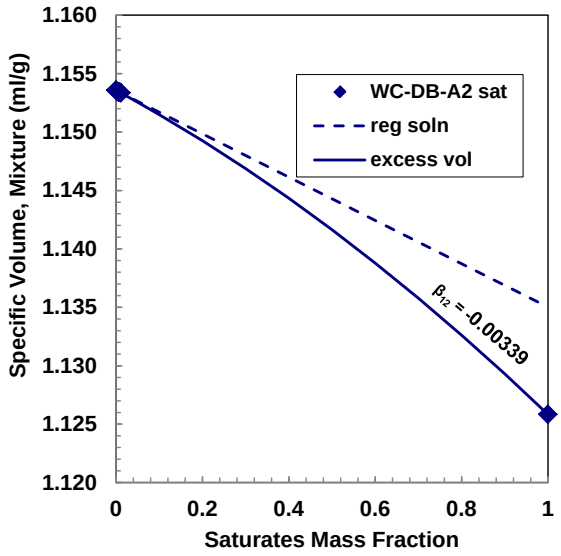

Figure B.22. Density measurements of WC-DB-A2 saturates in toluene

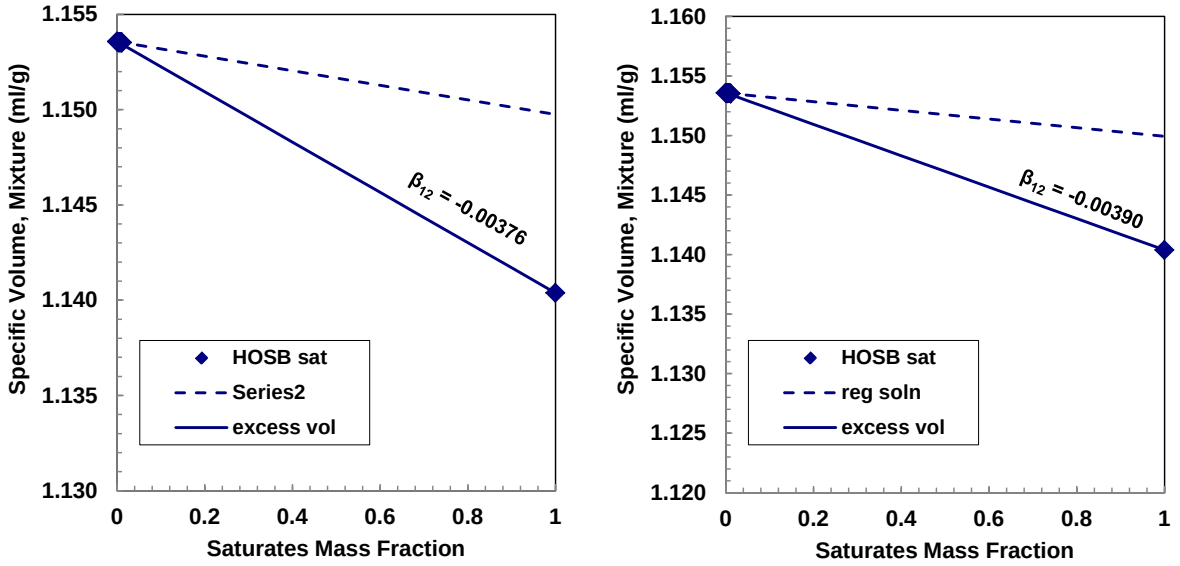

Figure B.23. Density measurements of HOSB saturates in toluene

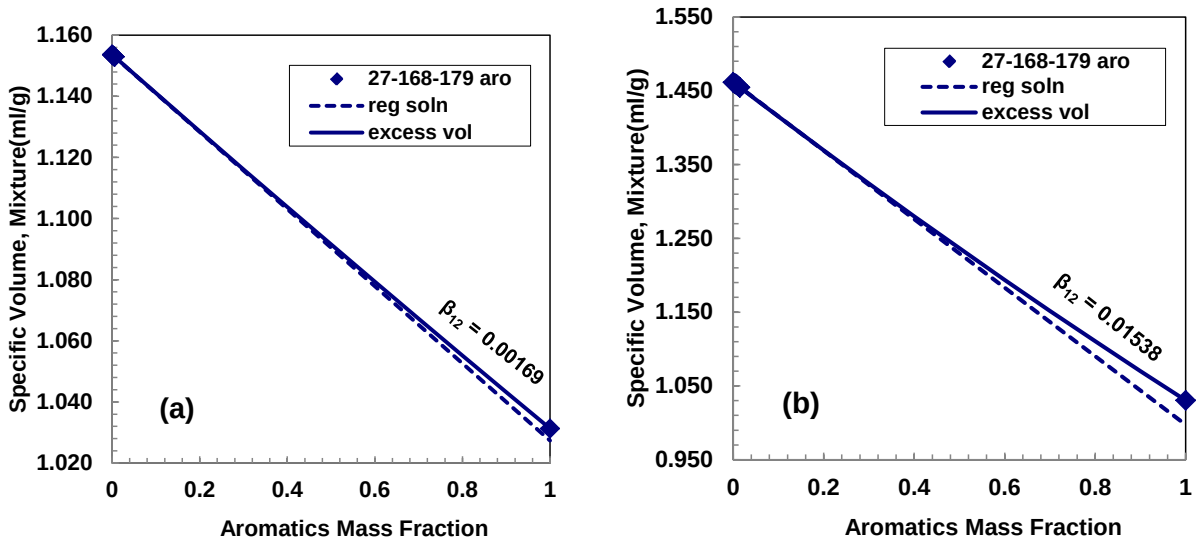

Figure B.24. Density measurements of 27-168-179 aromatics in: a) toluene b) heptane

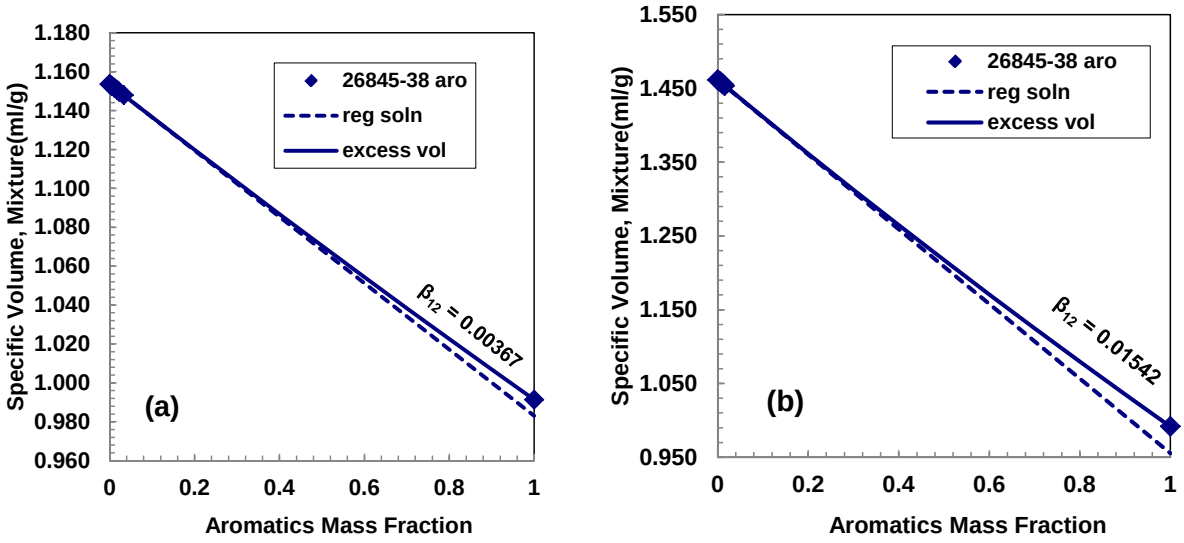

Figure B.25. Density measurements of 26845-38 aromatics in: a) toluene b) heptane

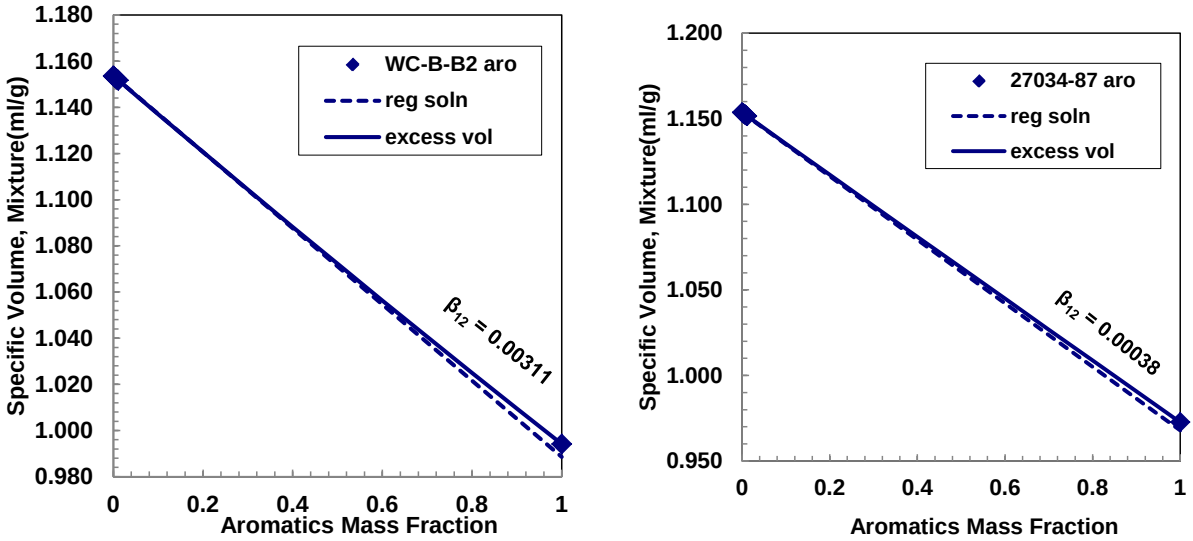

Figure B.26. Density measurements WC-B-B2 & 27034-87 aromatics in toluene

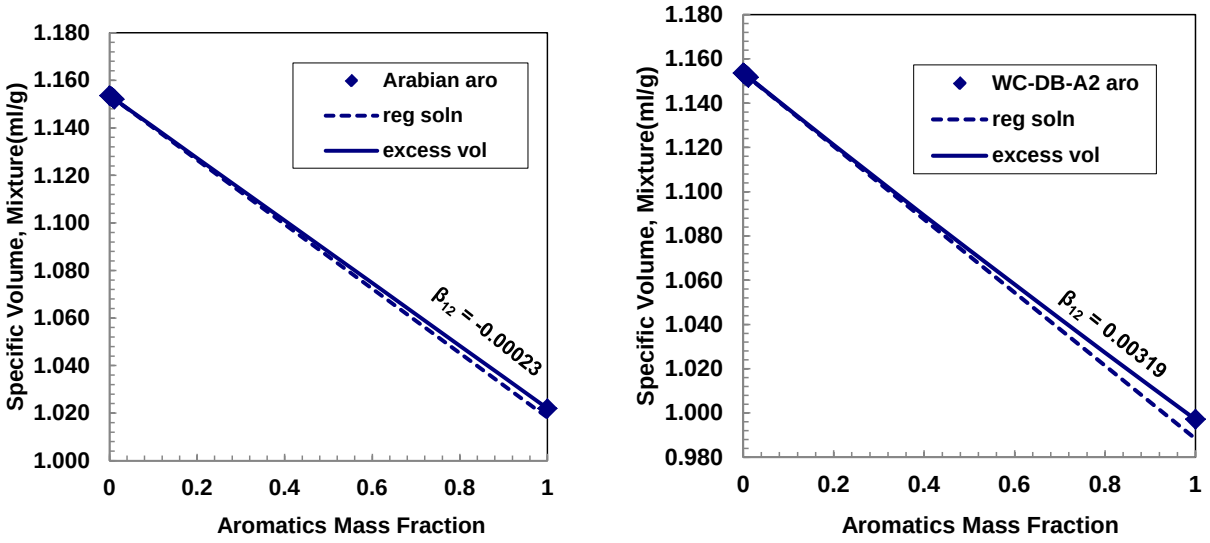

Figure B.27. Density measurements Arabian & WC-DB-A2 aromatics in toluene

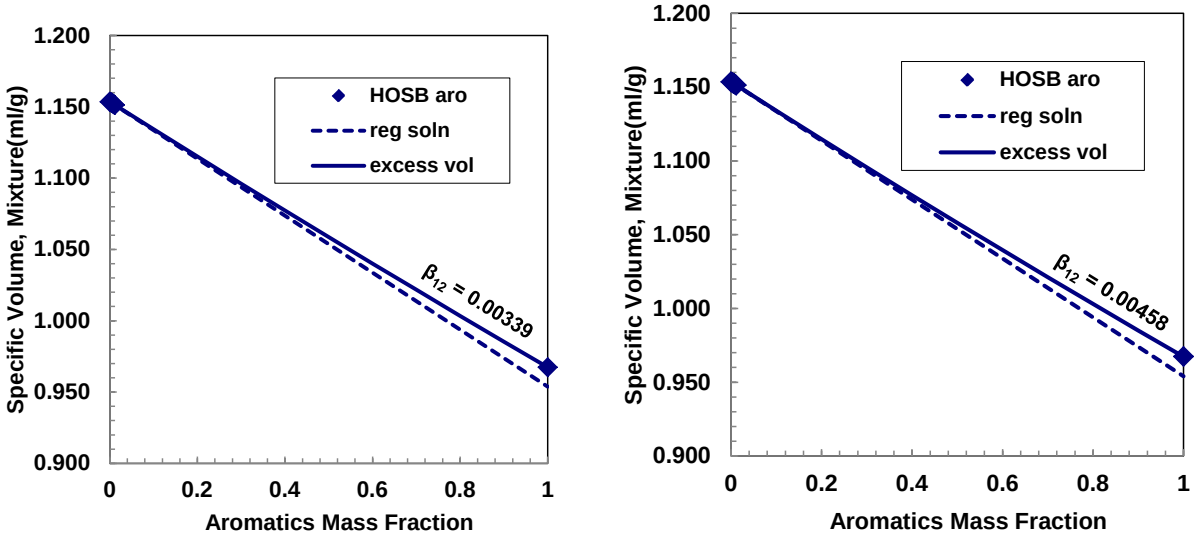

Figure B.28. Density measurements HOSB aromatics in toluene

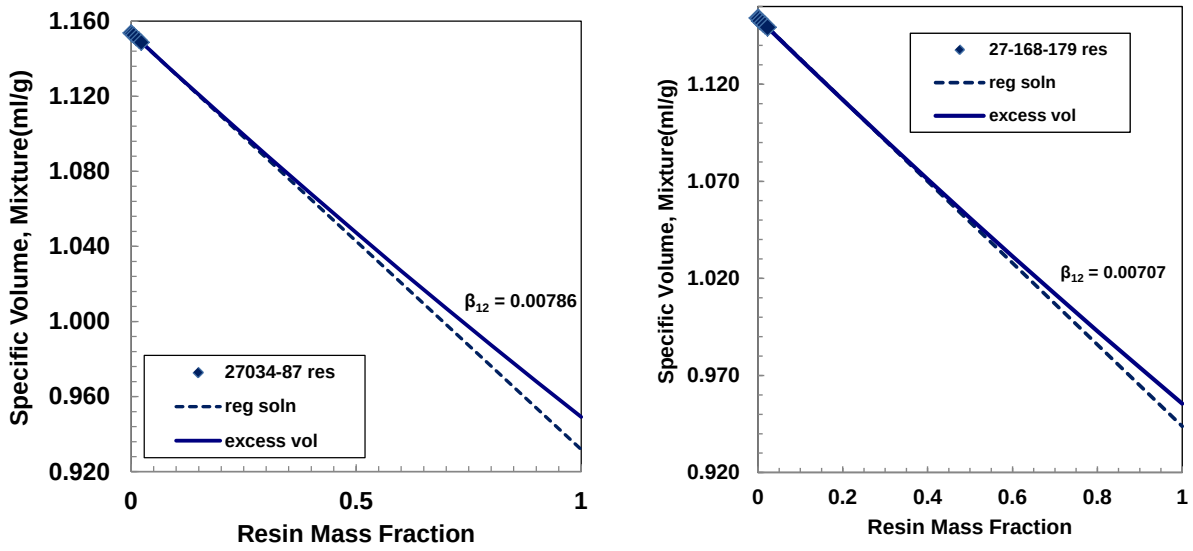

Figure B.29. Density measurements 27034-87 &27-168-179 resins in toluene

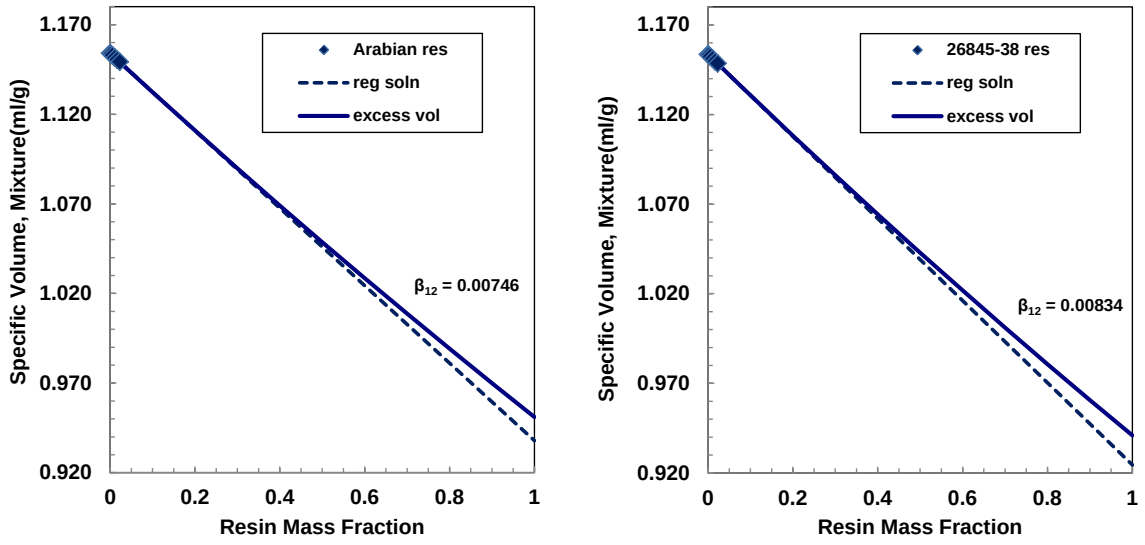

Figure B.30. Density measurements Arabian & 26845-38 resins in toluene

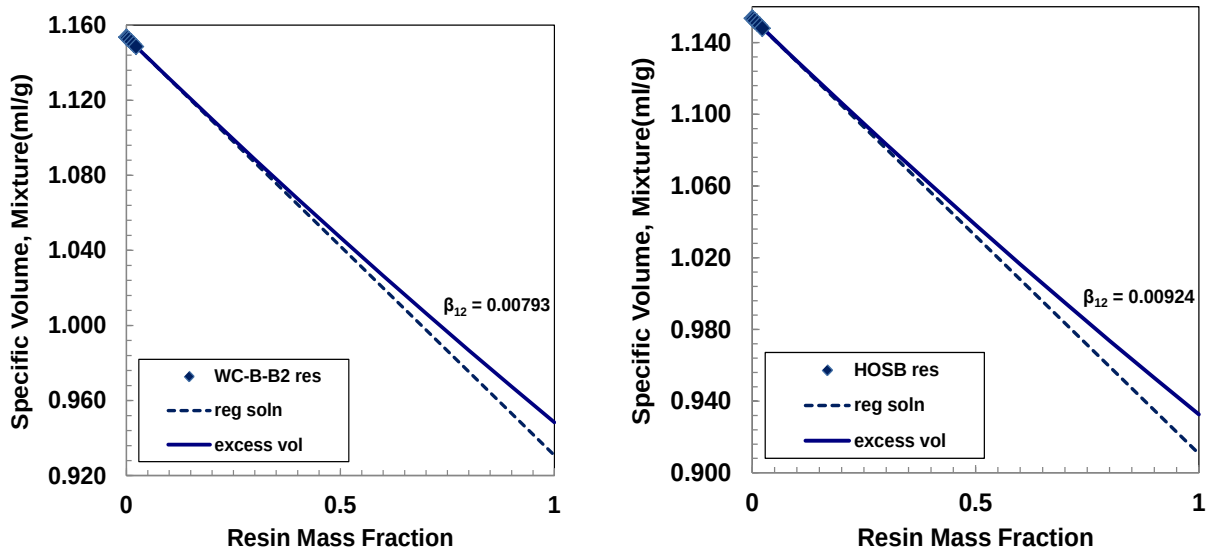

Figure B.31. Density measurements WC-B-B2 & HOSB resins in toluene

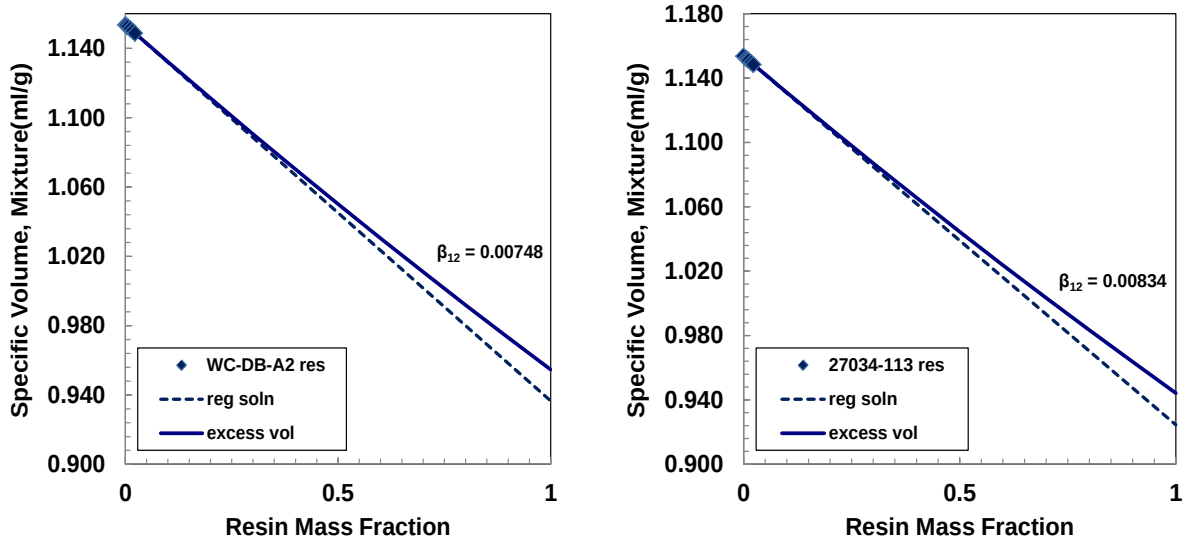

Figure B.32. Density measurements WC-DB-A2 & 27034-113 resins in toluene

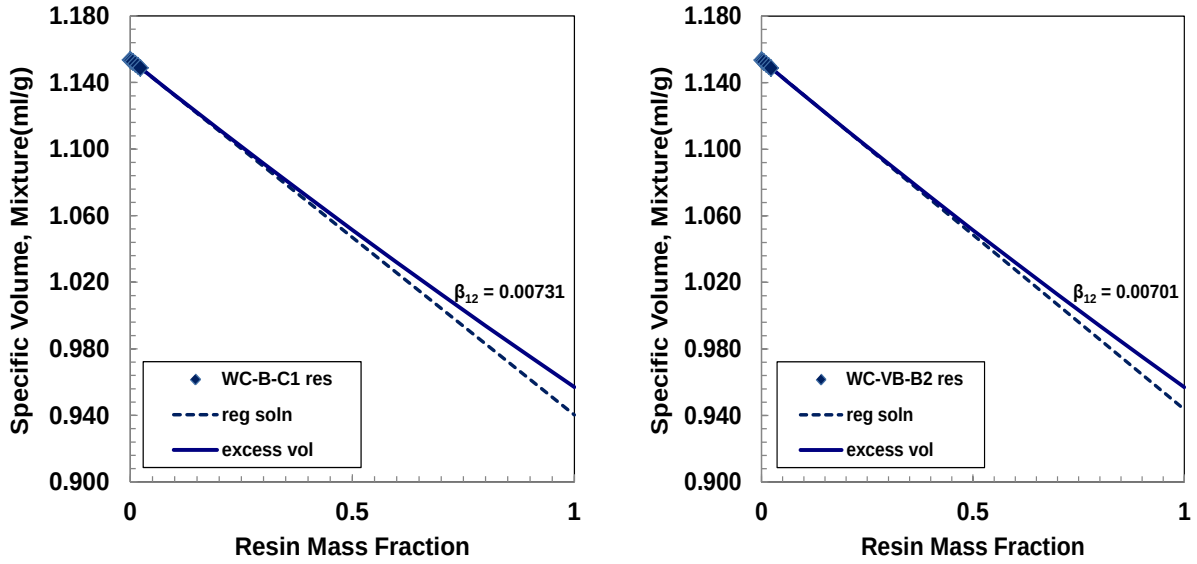

Figure B.33. Density measurements WC-B-C1 & WC-VB-B2 resins in toluene

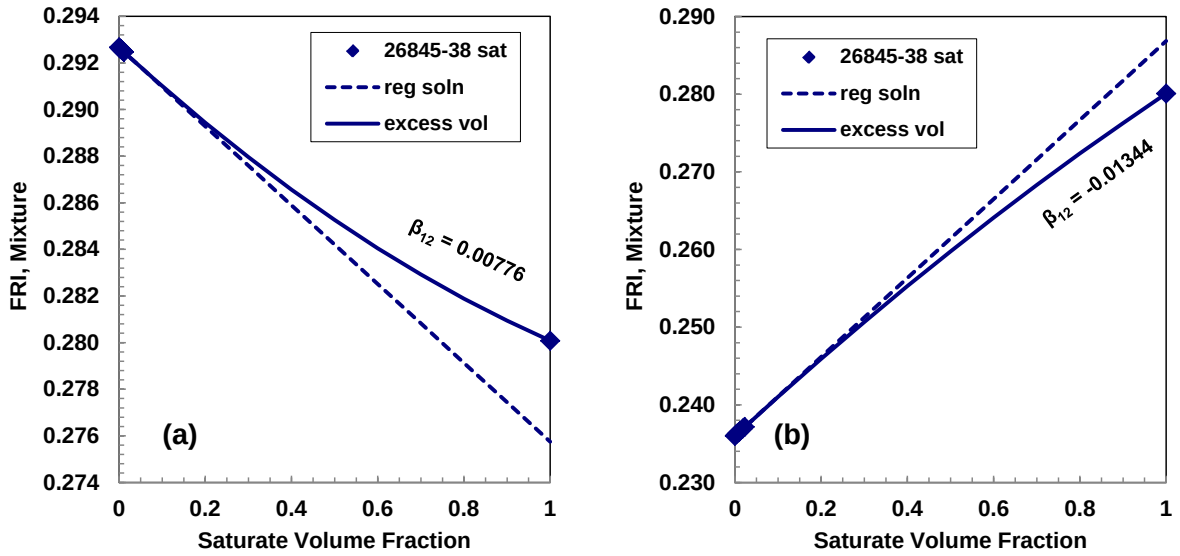

Figure B.34. FRI at 20°C of mixtures of: 26845-8 saturate a) in toluene and b) s in heptane.

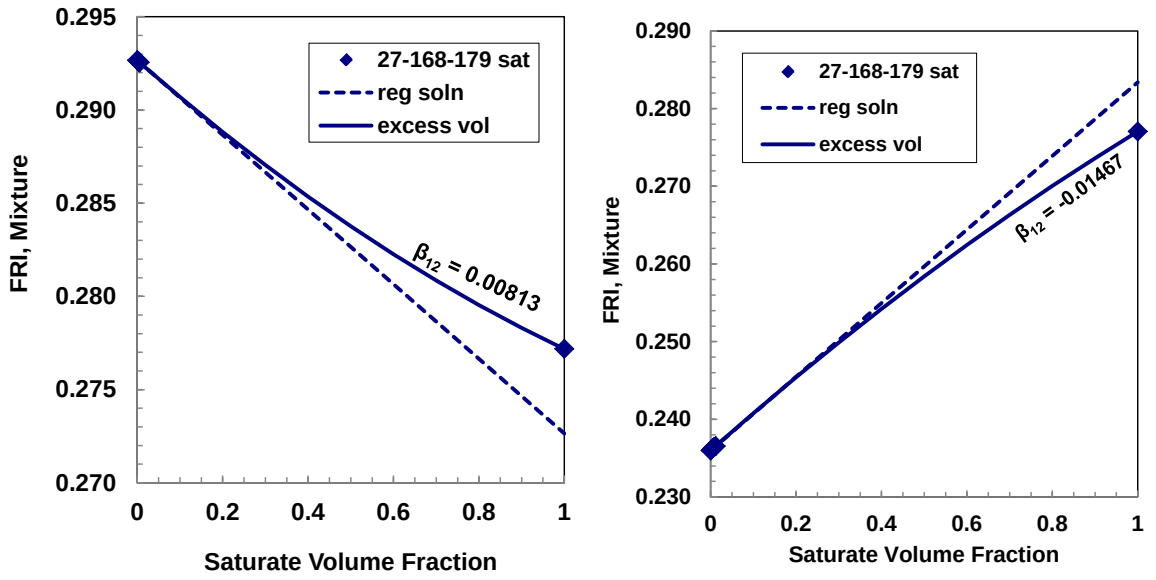

Figure B.35. FRI at 20°C of mixtures of: 27-168-179 saturate a) in toluene and b) in heptane.

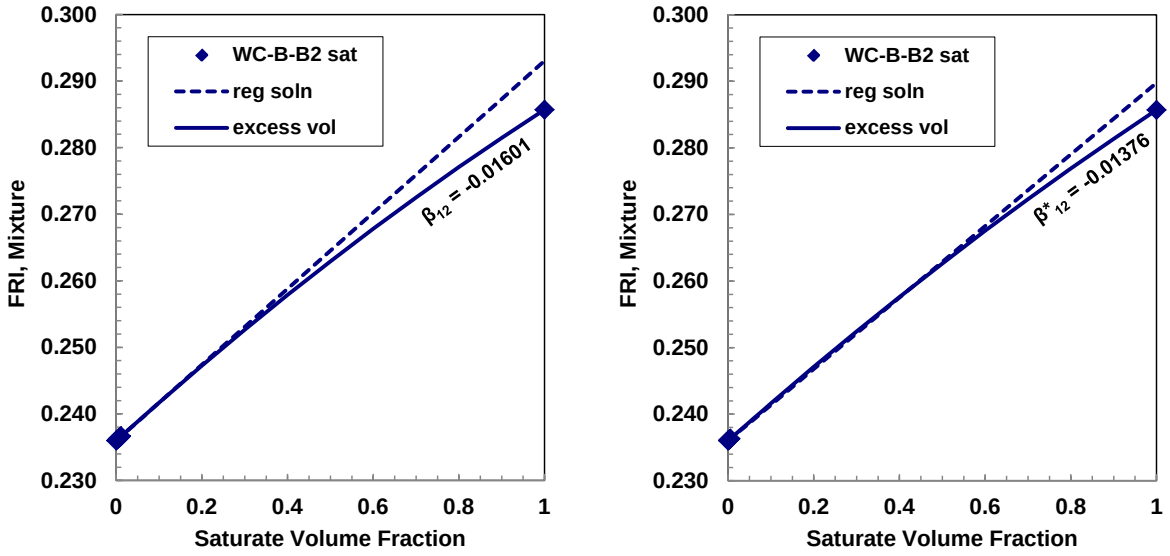

Figure B.35. FRI at 20°C of mixtures of: WC-B-B2 saturate in heptane

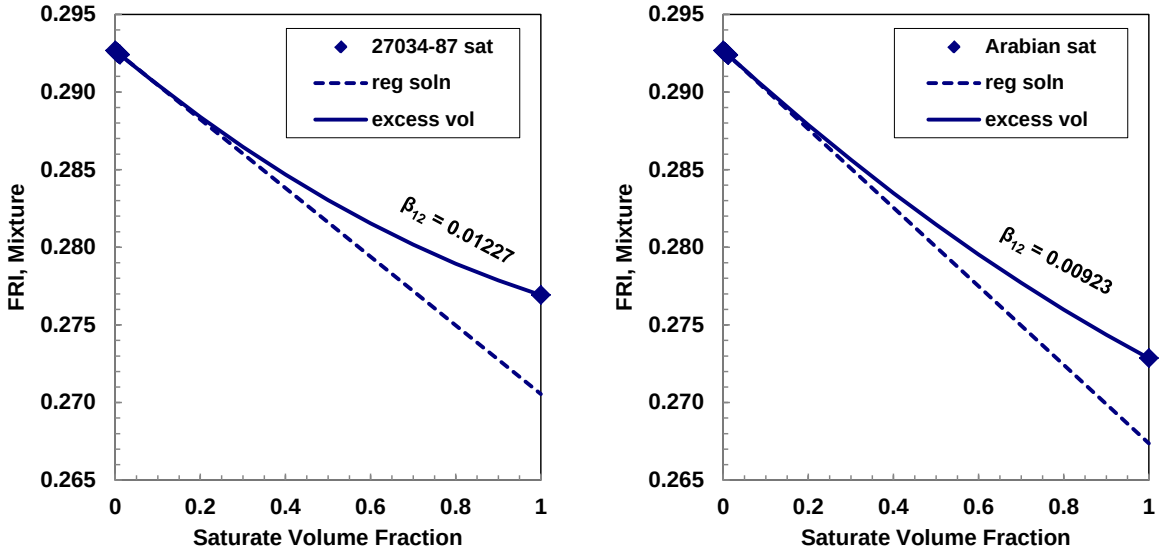

Figure B.36. FRI at 20°C of mixtures of a) 27034-87 b) Arabian saturate in toluene

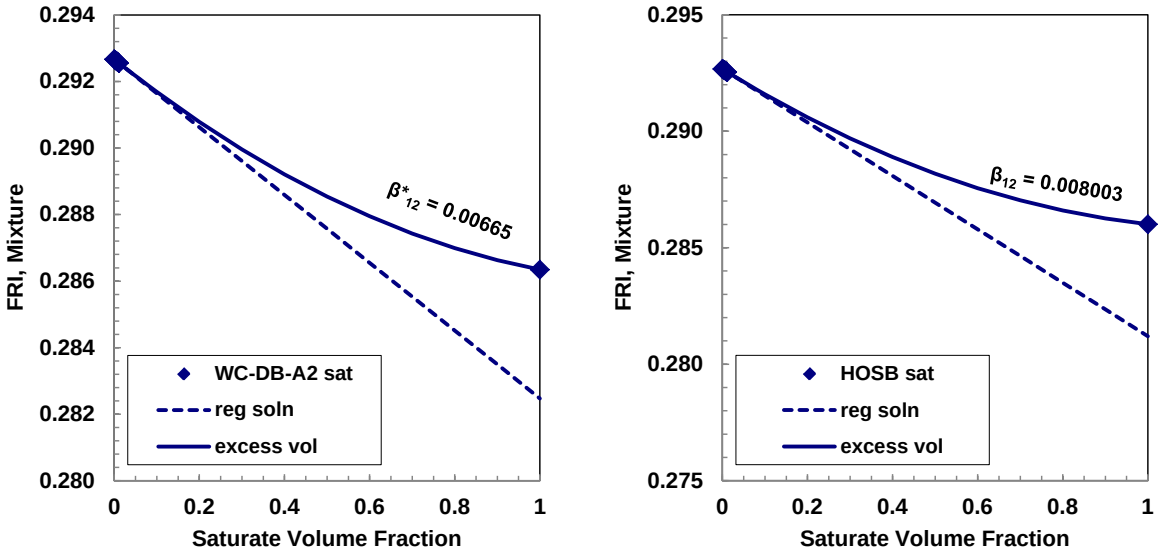

Figure B.37. FRI at 20°C of mixtures of a) WC-DB-A2 b) HOSB saturate in toluene

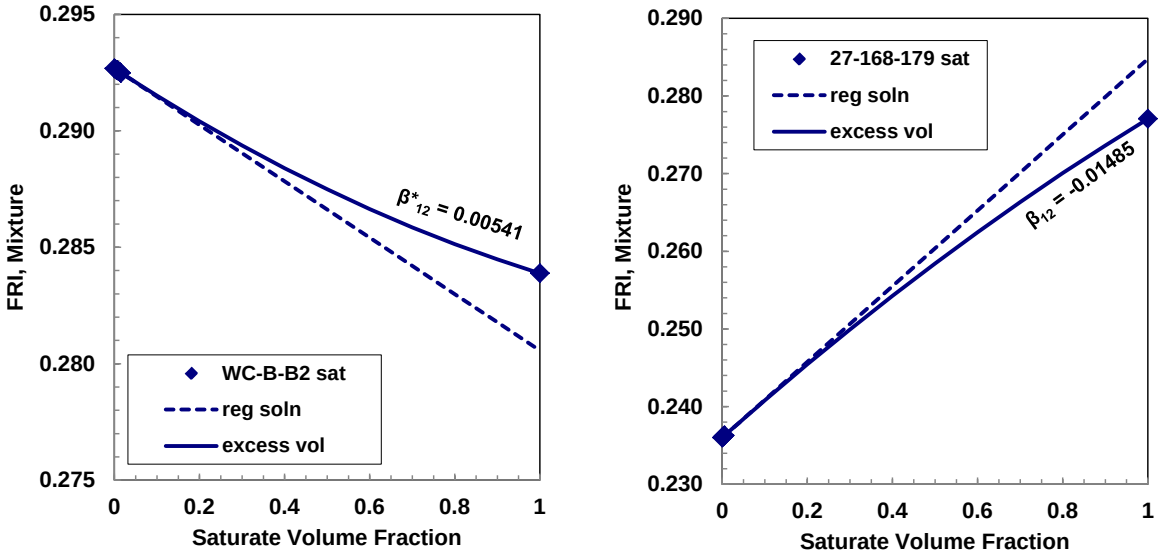

Figure B.38. FRI at 20°C of mixtures of a) WC-B-B2 saturates in toluene b) 27-168-179 saturate in heptane

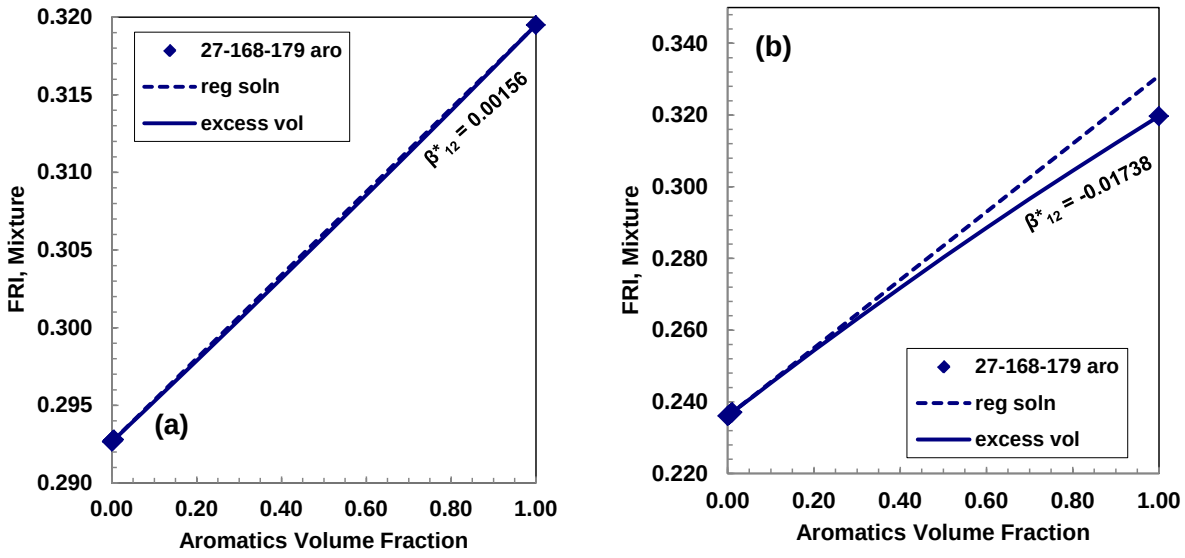

Figure B.39. FRI at 20°C of mixtures of a) 27-168-179 aromatics in a) in toluene b) heptane

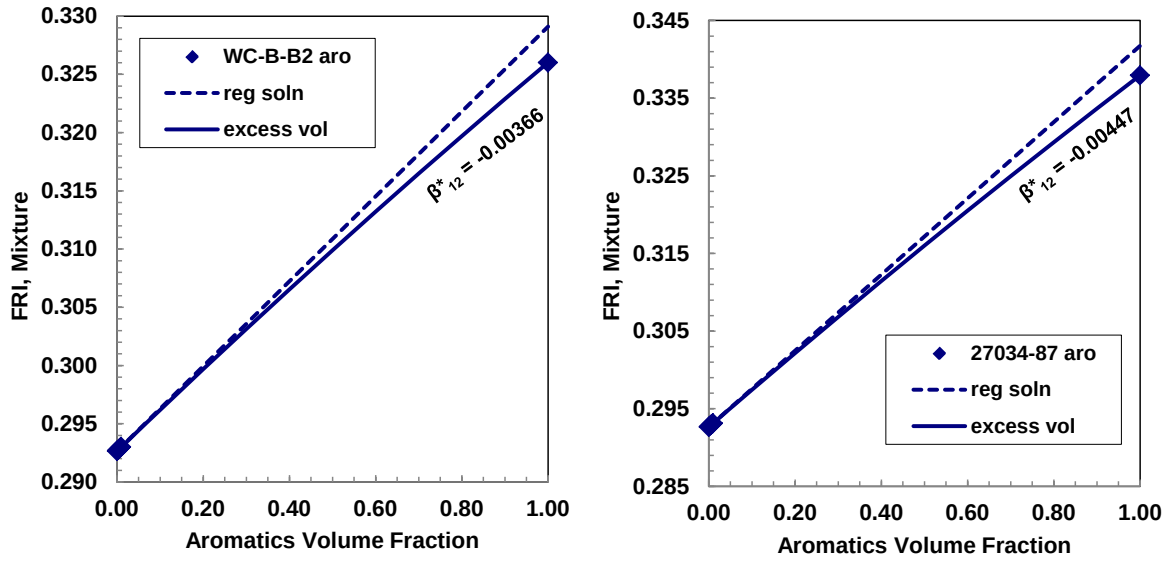

Figure B.40. FRI at 20°C of mixtures of a) WC-B-B2 aromatics b) 27034-87 aromatics in toluene

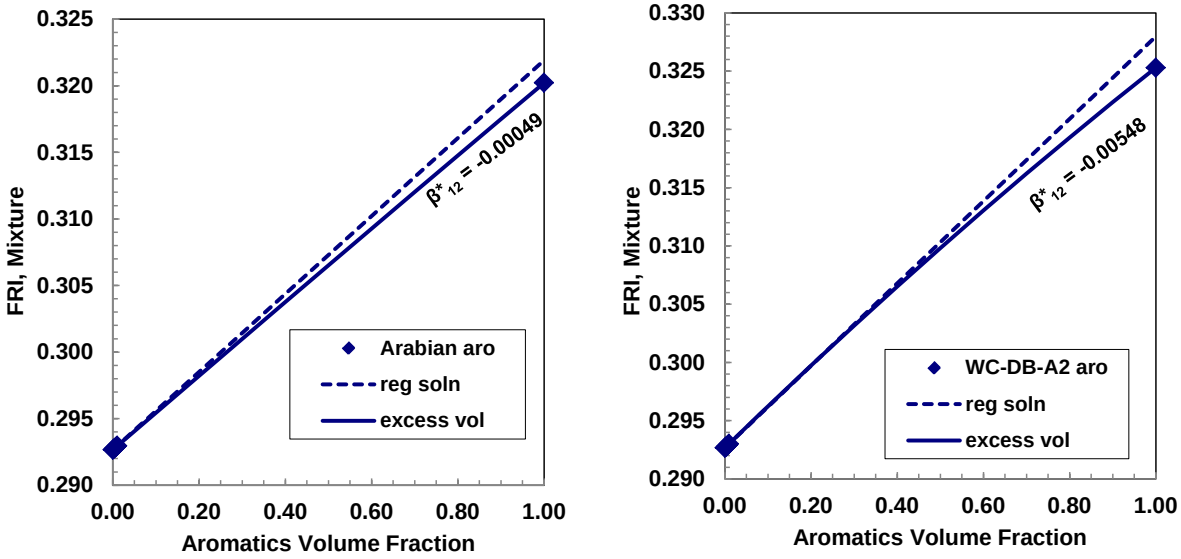

Figure B.41. FRI at 20°C of mixtures of a) Arabian aromatics b) WC-DB-A2 aromatics in toluene

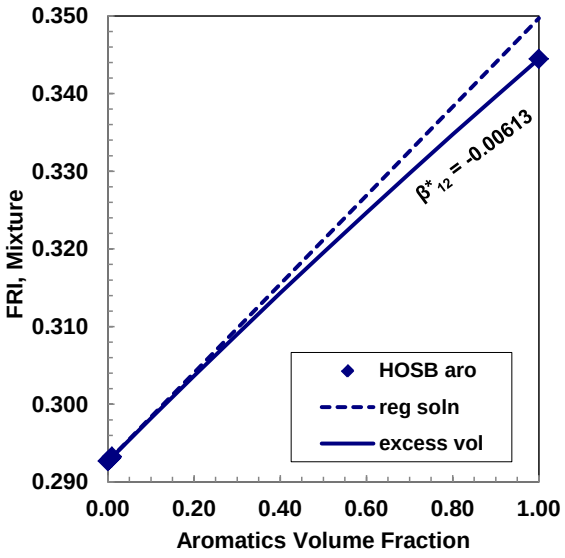

Figure B.42. FRI at 20°C of mixtures of HOSB aromatics in toluene

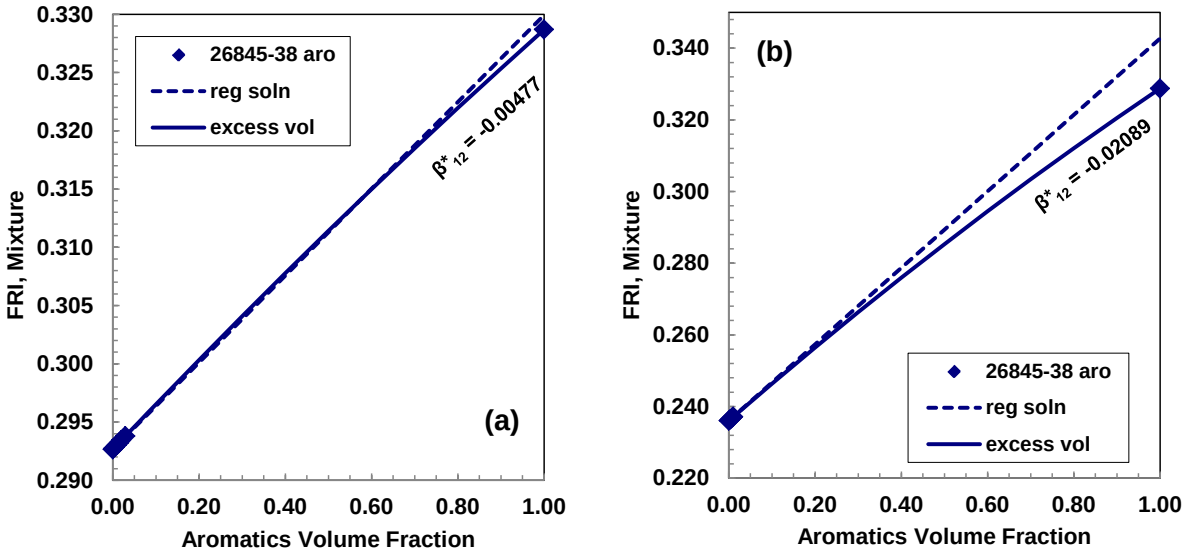

Figure B.43. FRI at 20°C of mixtures of 26845-38 aromatics in a) toluene b) heptane

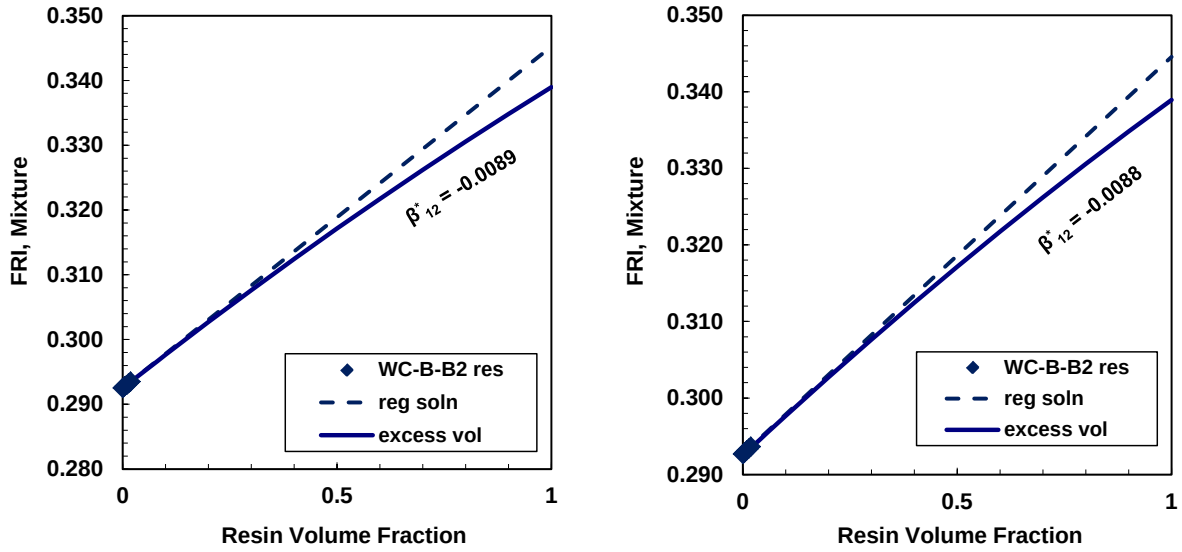

Figure B.44. FRI at 20°C of mixtures of WC-B-B2 resins in toluene

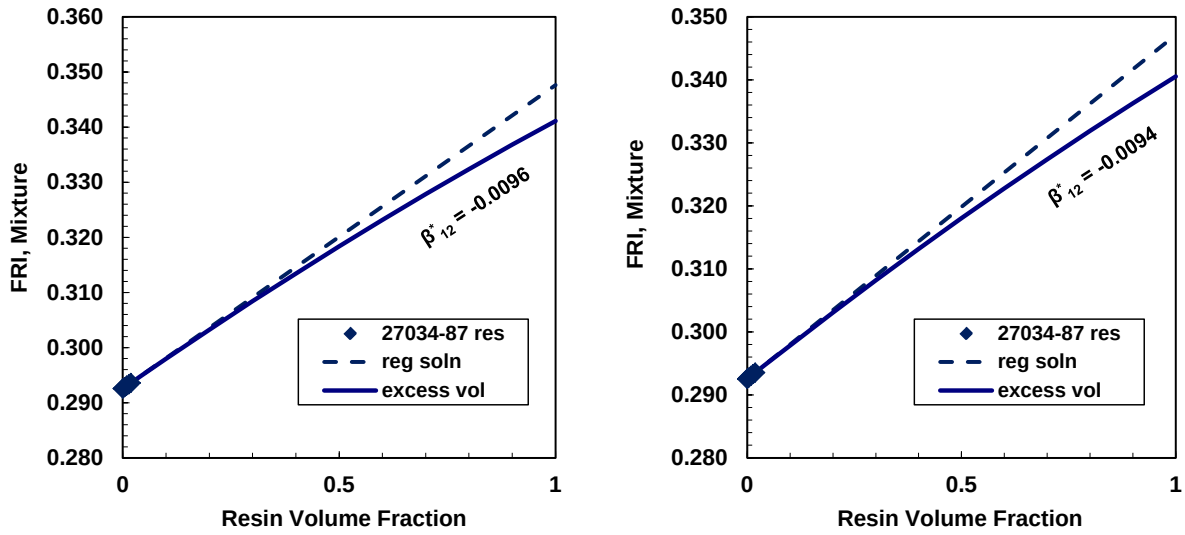

Figure B.45. FRI at 20°C of mixtures of 27034-87 resins in toluene

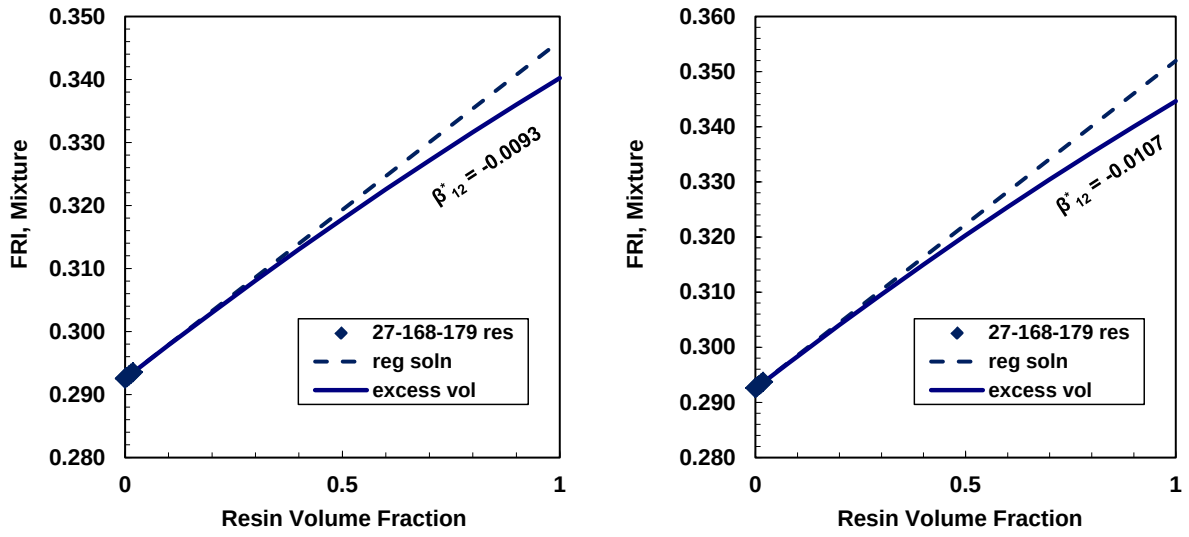

Figure B.46. FRI at 20°C of mixtures of 27-168-179 resins in toluene

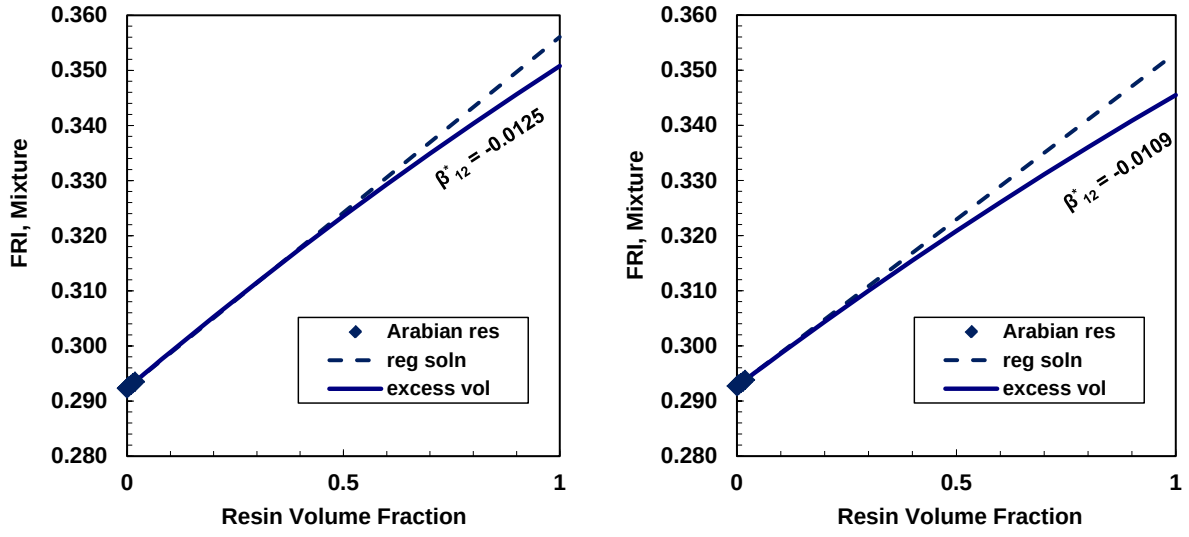

Figure B.47. FRI at 20°C of mixtures of Arabian resins in toluene

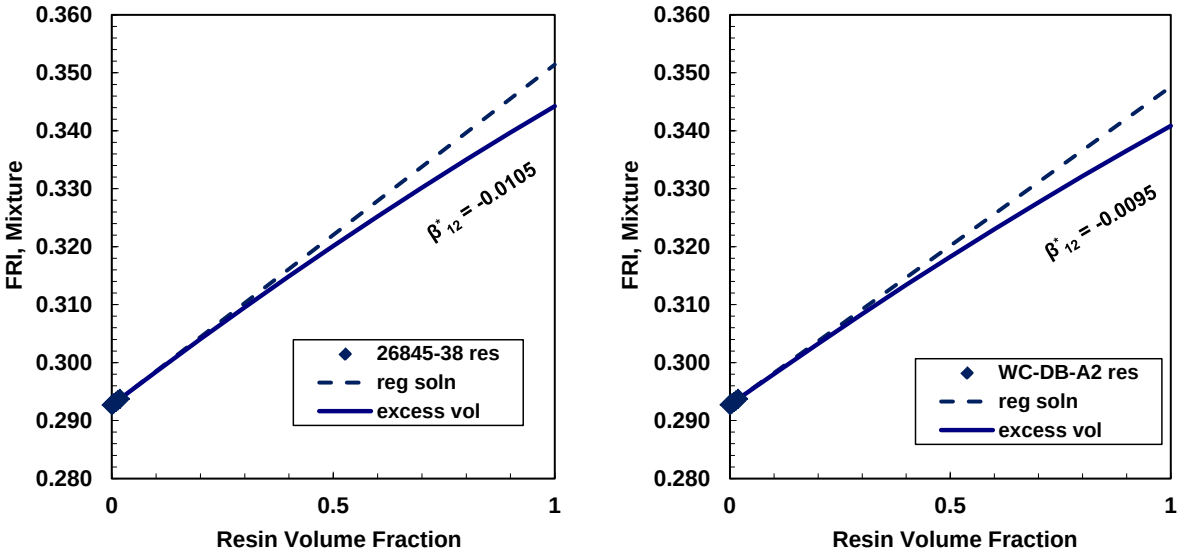

Figure B.48. FRI at 20°C of mixtures of a) 26845-38 and b) WC-DB-A2 resins in toluene

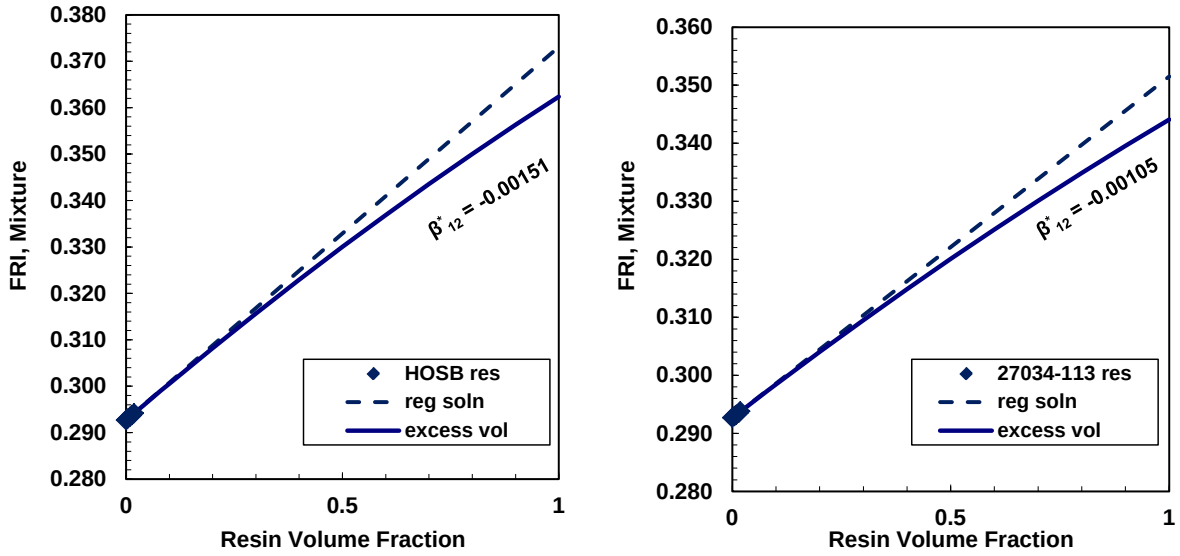

Figure B.48. FRI at 20°C of mixtures of a) HOSB and b) 27034-113 resins in toluene

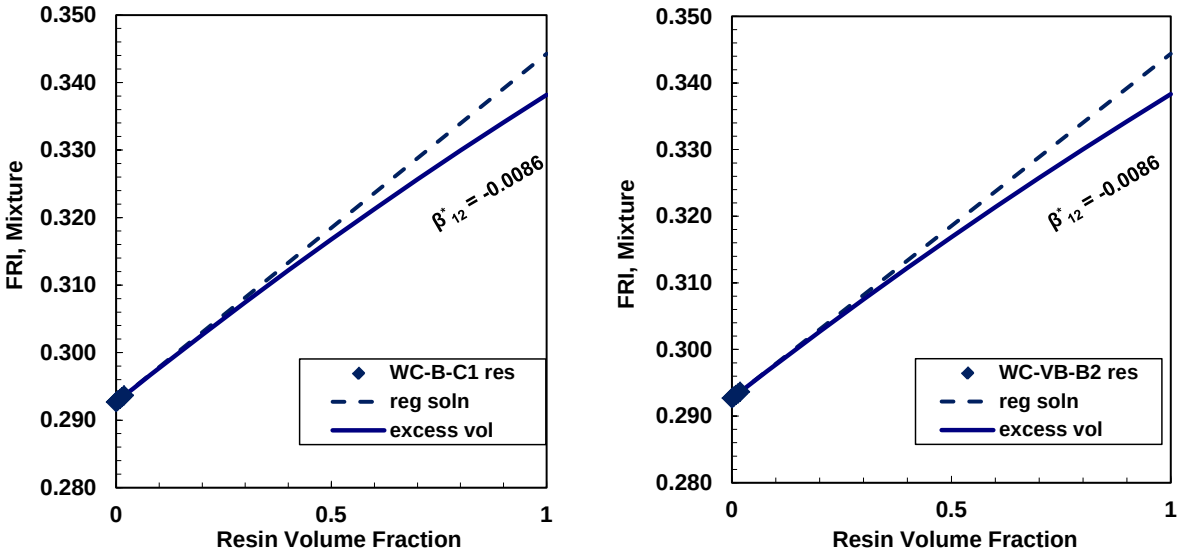

Figure B.49. FRI at 20°C of mixtures of a) WC-B-C1 and b) WC-VB-B2 resins in toluene

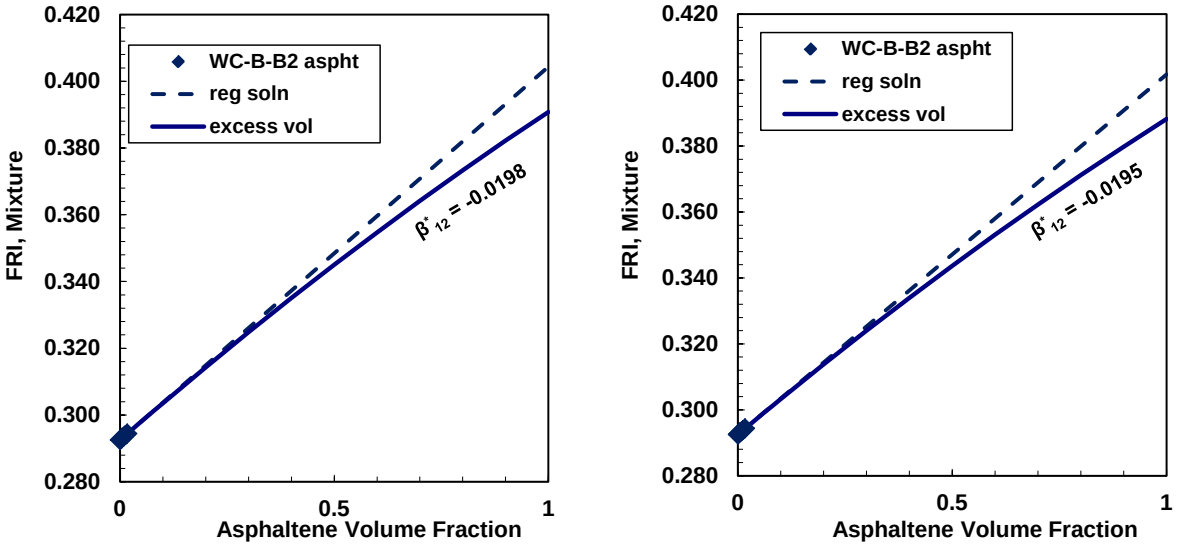

Figure B.50. FRI at 20°C of mixtures of WC-B-B2 asphaltenes in toluene

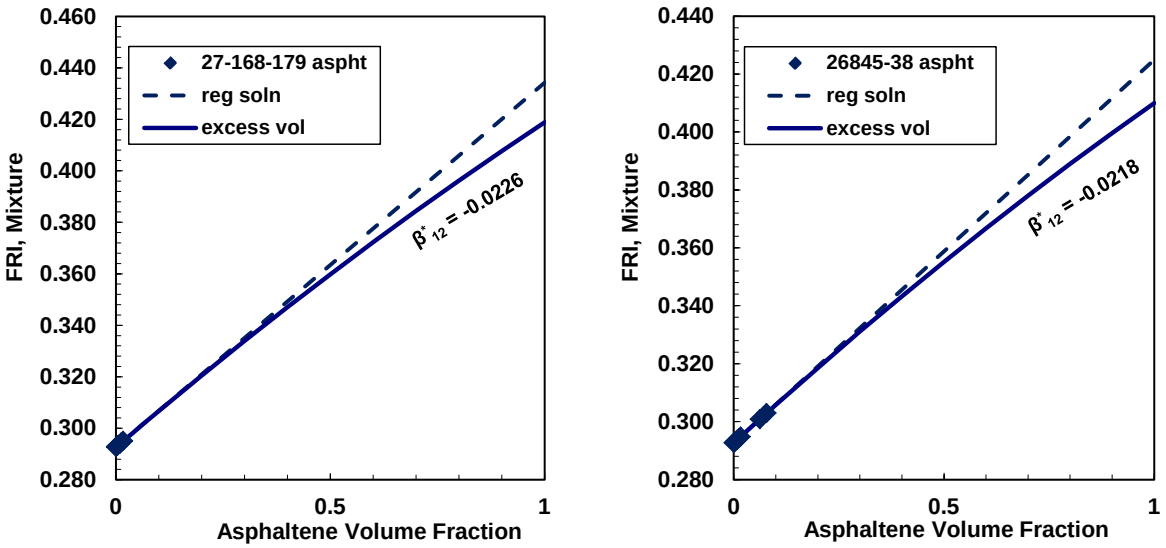

Figure B.51. FRI at 20°C of mixtures of: a) 27-168-179 b) 26845-38 asphaltenes in toluene

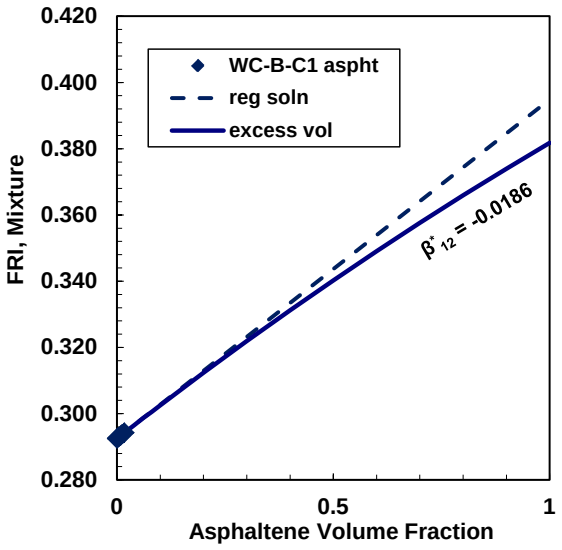

Figure B.52. FRI at 20°C of mixtures of WC-B-C1asphaltenes in toluene

Table B.1: Summary of the thermal expansion coefficients of saturates and aromatic from the individual plots given in Figures B.53 – B60

	Saturates			*Aromatics*		
Sample	v_{20}	**slope**	α_v	v_{20}	**slope**	α_v
WC-B-B2	1.1273	0.00082	0.00073	0.9944	0.00067	0.00068
Arabian	1.2097	0.00102	0.00084	1.0219	0.00071	0.00069
WC-B-C1	1.1398	0.00085	0.00075	0.9984	0.00067	0.00067
WC-DB-A2	1.1258	0.00082	0.00072	0.9971	0.00065	0.00066
WC-VB-B2	-	-	-	0.9838	0.00063	0.00064
27-168-179	1.1829	0.00096	0.00081	-	-	-
27034-113	1.1883	0.00096	0.00080	0.9917	0.00069	0.00070
27034-87	1.1795	0.00094	0.00080	0.9726	0.00067	0.00069
HOSB	1.1404	0.00082	0.00072	0.9673	0.00061	0.00063

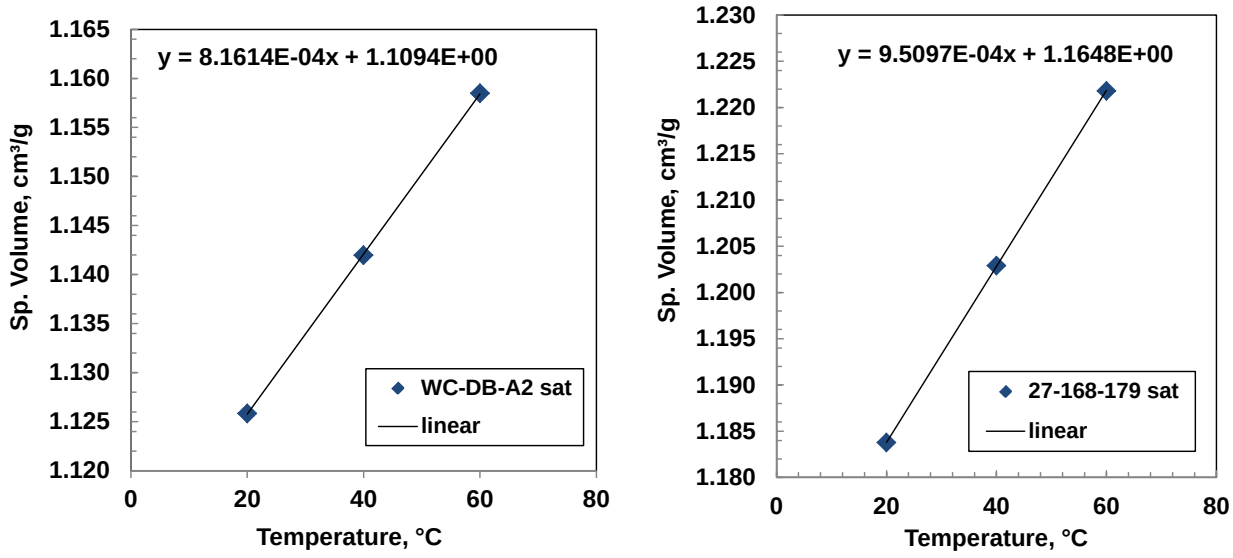

Figure B.53: Temperature is linearly related to the specific volume of a) WC-DB-A2 b) 27-168-179 saturates

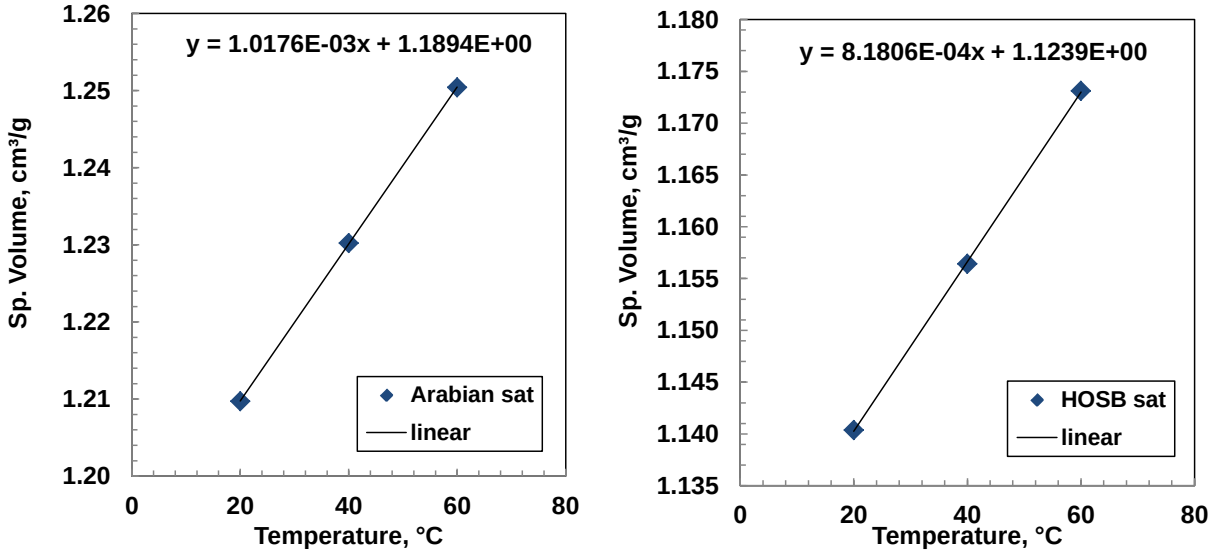

Figure B.54: Temperature is linearly related to the specific volume of a) Arabian b) HOSB saturates

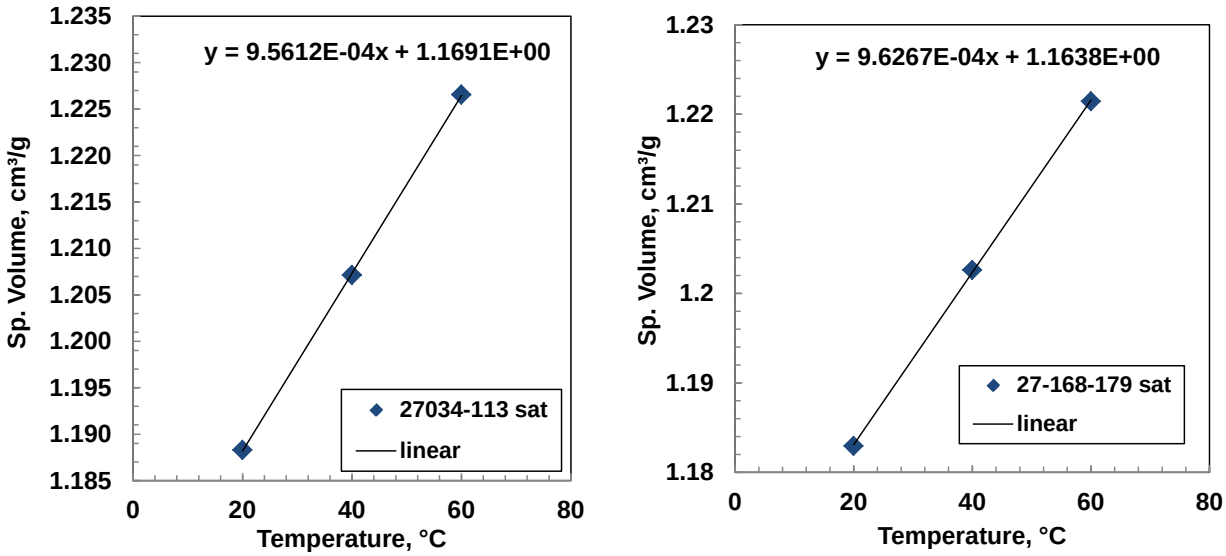

Figure B.55: Temperature is linearly related to the specific volume of: a) 27034-113 b) 27-168-179 saturates

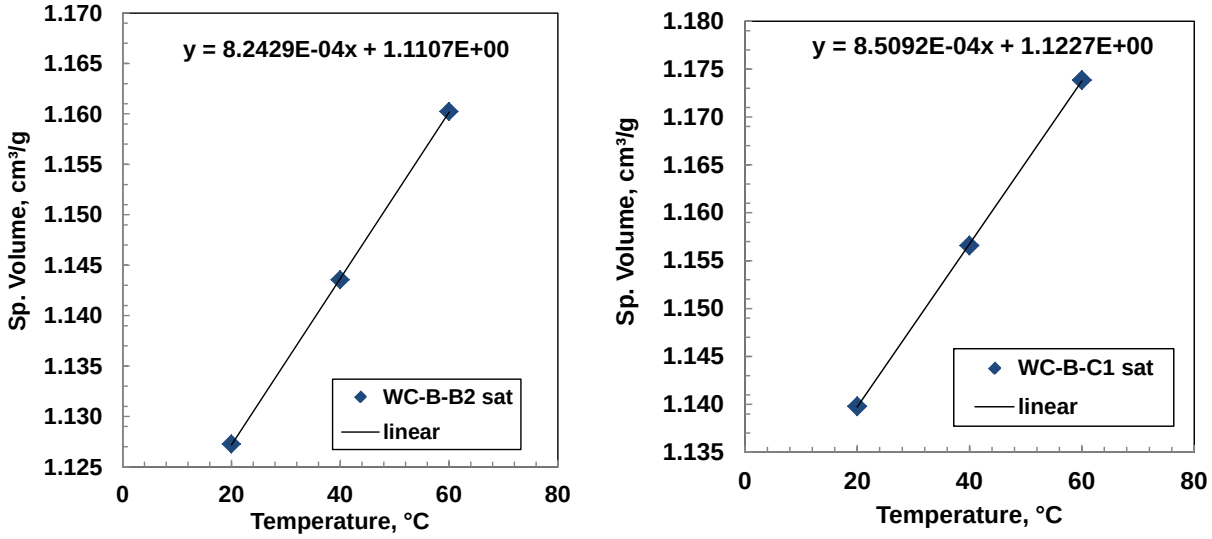

Figure B.56: Temperature is linearly related to the specific volume of: a) WC-B-B2 b) WC-B-C1 saturates

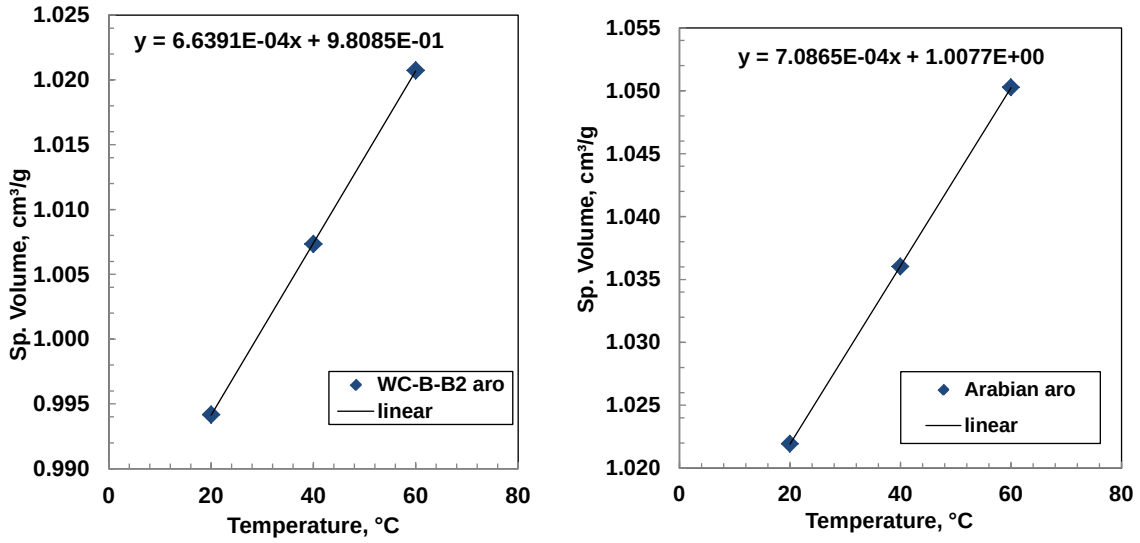

Figure B.57: Temperature is linearly related to the specific volume of: a) WC-B-B2 b) Arabian aromatics

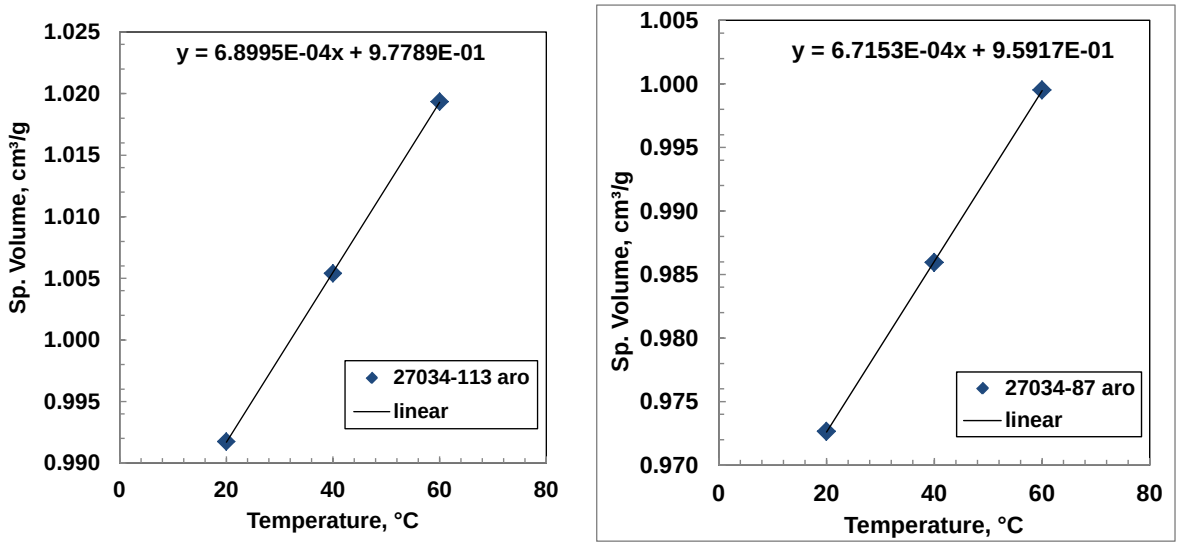

Figure B.58: Temperature is linearly related to the specific volume of: a) 27034-113 b) 27034-87 aromatics

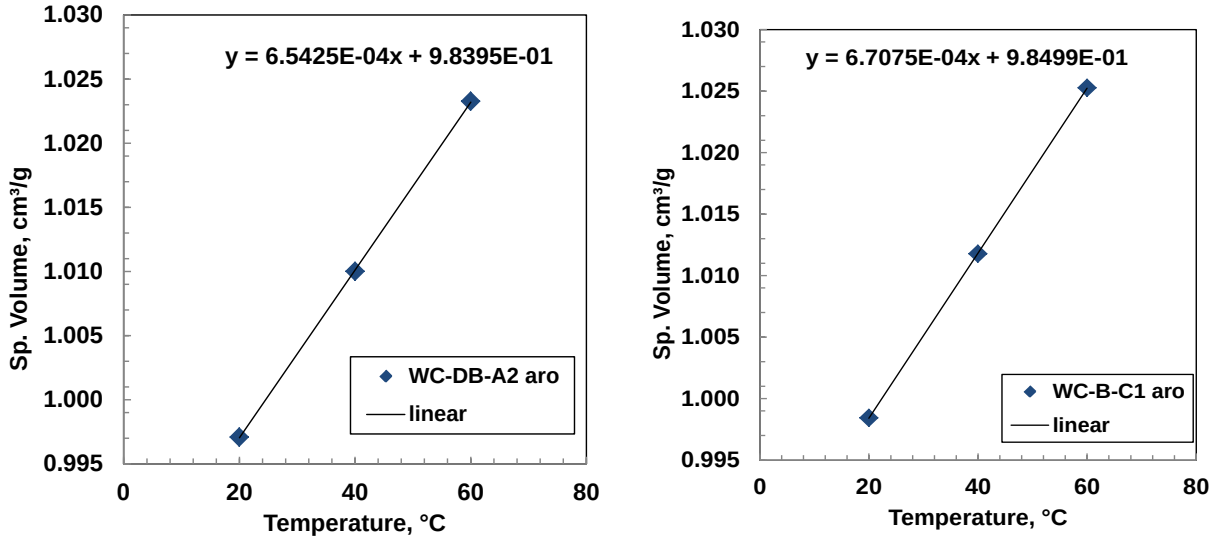

Figure B.59: Temperature is linearly related to the specific volume of: a) WC-DB-A2 b) WC-B-C1 aromatics

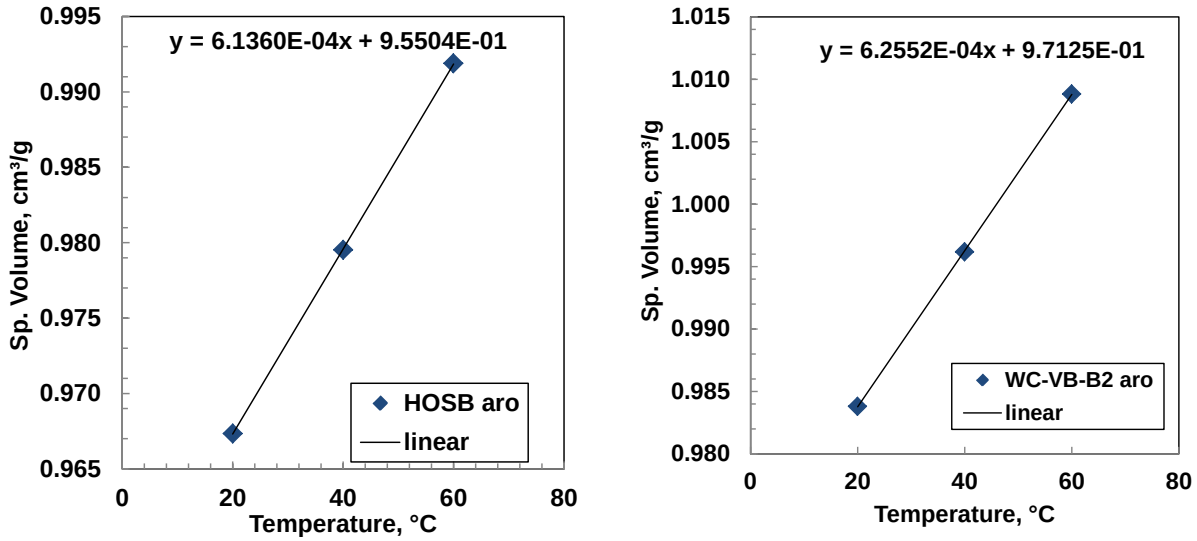

Figure B.60: Temperature is linearly related to the specific volume of: a) HOSB b) WC-VB-B2 aromatics

Table B.2: Summary of the thermal FRI coefficients of saturates and aromatic from the individual plots given in Figures B.61 – B.69

	Saturates			***Aromatics***		
Sample	FRI_{20}	**slope**	α_{FRI}	FRI_{20}	**slope**	α_{FRI}
WC-B-B2	0.28579	-0.00019	-0.00065	0.32602	-0.00019	-0.00057
Arabian	0.27286	-0.00020	-0.00074	0.32022	-0.00019	-0.00060
WC-B-C1	0.28381	-0.00019	-0.00067	0.32475	-0.00019	-0.00058
WC-DB-A2	0.28635	-0.00018	-0.00065	0.32529	-0.00018	-0.00056
WC-VB-B2	-	-	-	0.32999	-0.00019	-0.00058
27-168-179	0.27708	-0.00020	-0.00074	-	-	-
27034-113	0.27563	-0.00020	-0.00073	0.33070	-0.00020	-0.00059
27034-87	0.27692	-0.00020	-0.00072	0.33794	-0.00020	-0.00058
HOSB	0.28600	-0.00022	-0.00075	0.34448	-0.00018	-0.00053

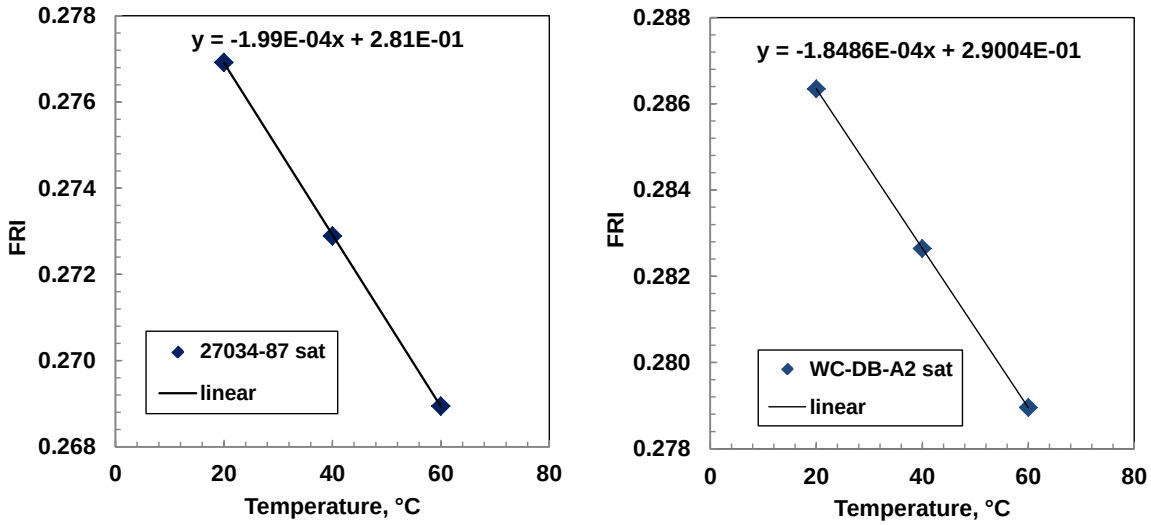

Figure B.61: Temperature is linearly related to FRI of: a) 27034-87 b) WC-DB-A2 saturates

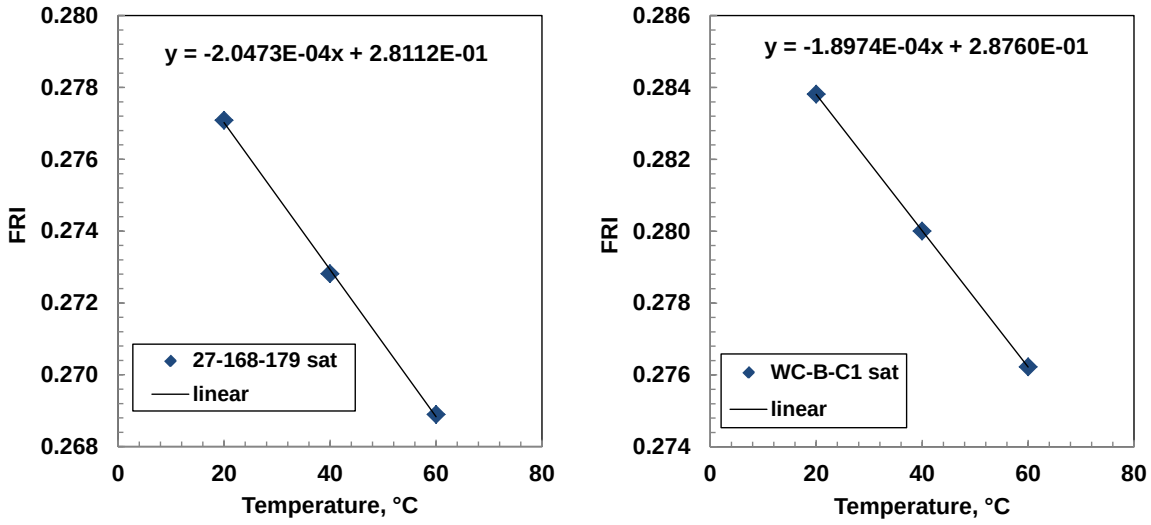

Figure B.62: Temperature is linearly related to FRI of: a) 27-168-179 b) WC-B-C1 saturates

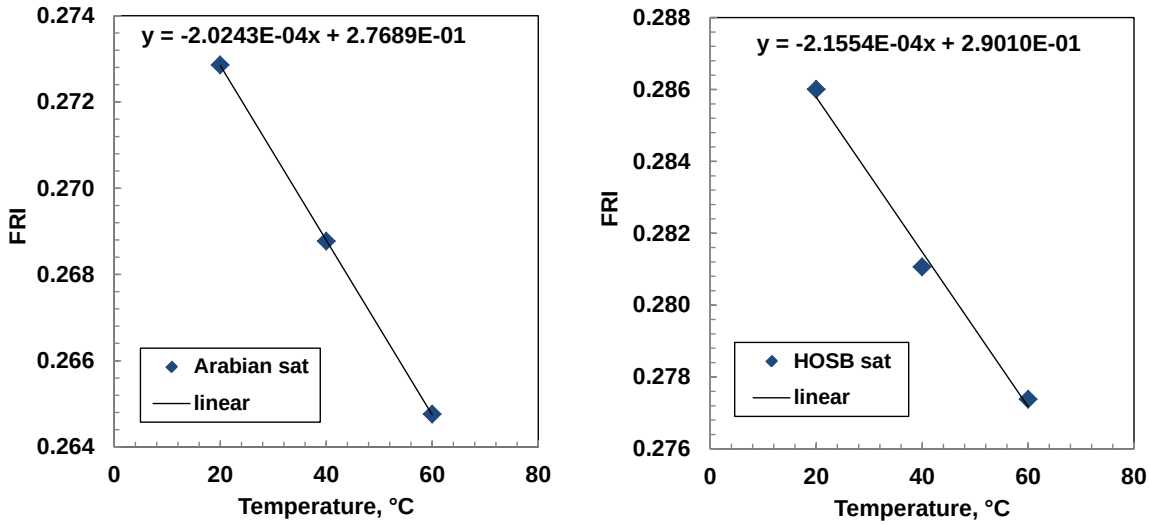

Figure B.63: Temperature is linearly related to FRI of: a) Arabian b) HOSB saturates

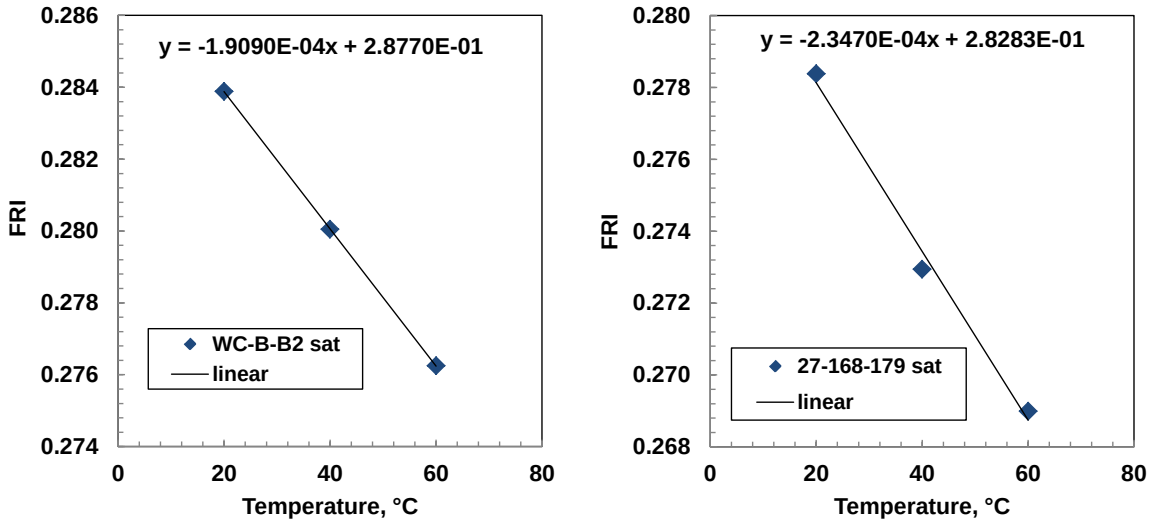

Figure B.64: Temperature is linearly related to FRI of: a) WC-B-B2 b) 27-168-179 saturates

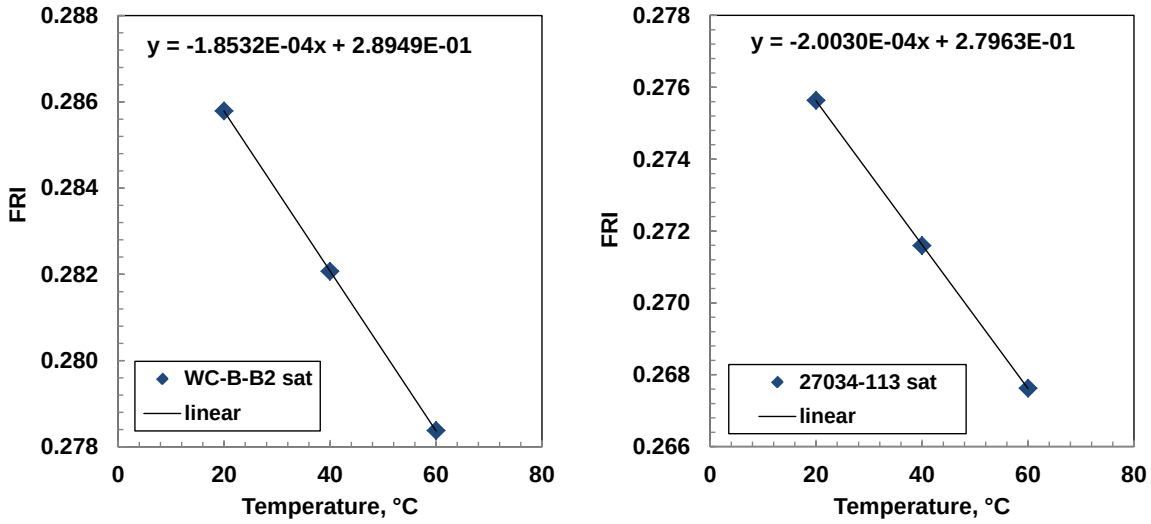

Figure B.65: Temperature is linearly related to FRI of: a) WC-B-B2 b) 27034-113 saturates

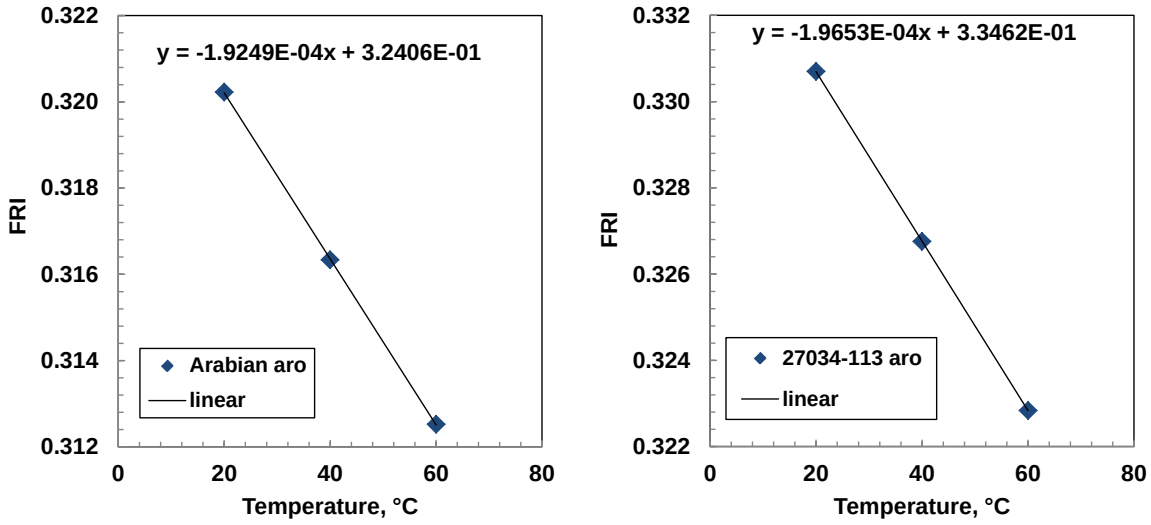

Figure B.66: Temperature is linearly related to FRI of: a) Arabain b) 27034-113 aromatics

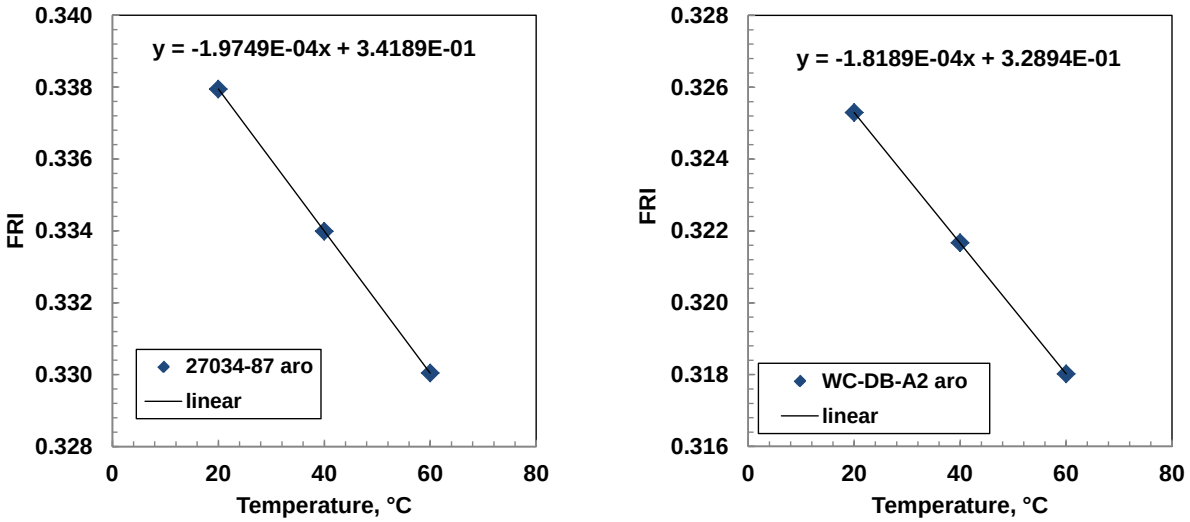

Figure B.67: Temperature is linearly related to FRI of: a) 27034-87 b) WC-DB-A2 aromatics

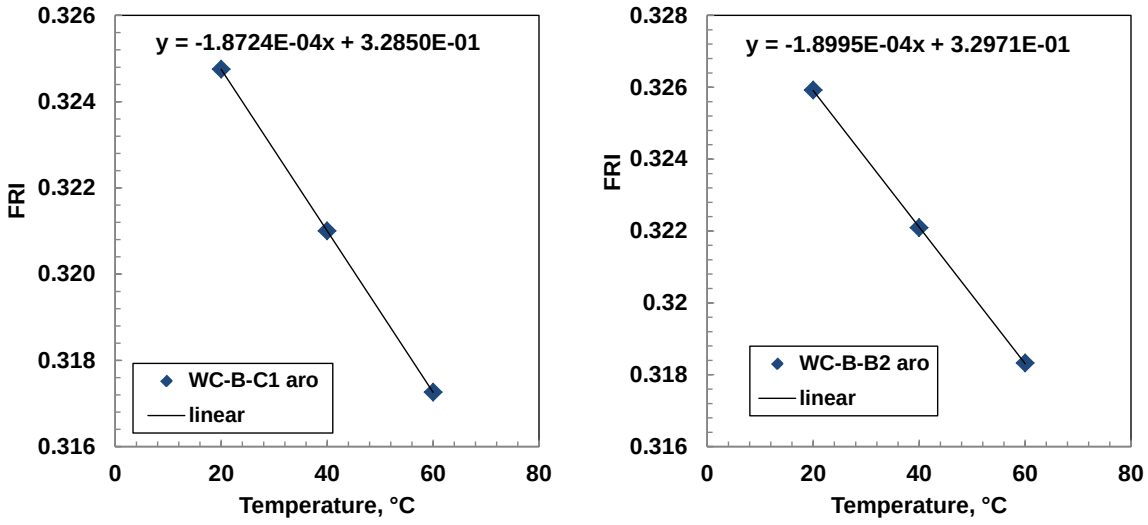

Figure B.68: Temperature is linearly related to FRI of: a) WC-B-C1 b) WC-B-B2 aromatics

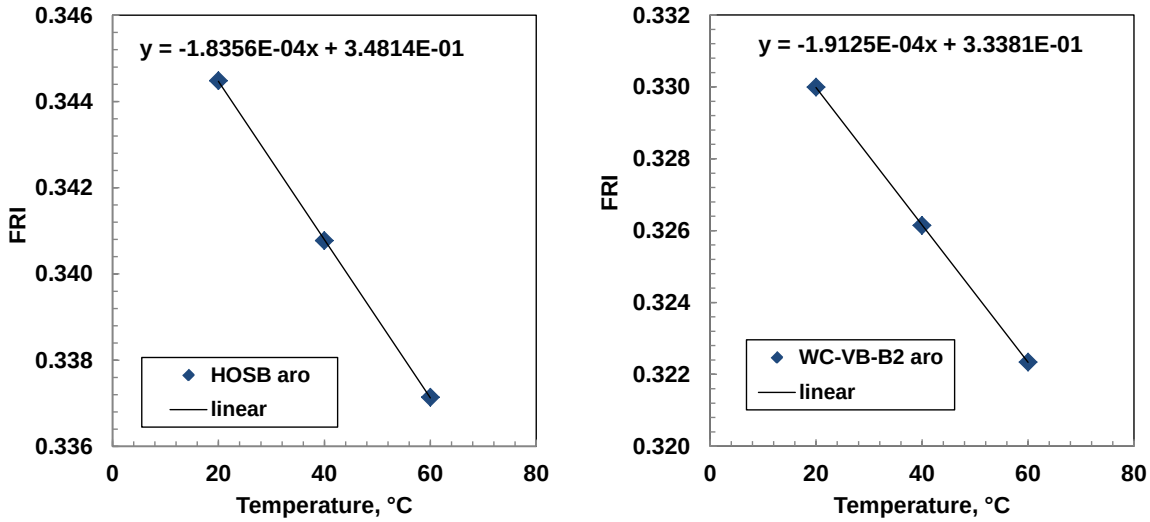

Figure B.69: Temperature is linearly related to FRI of: a) HOSB b) WC-VB-B2 aromatics

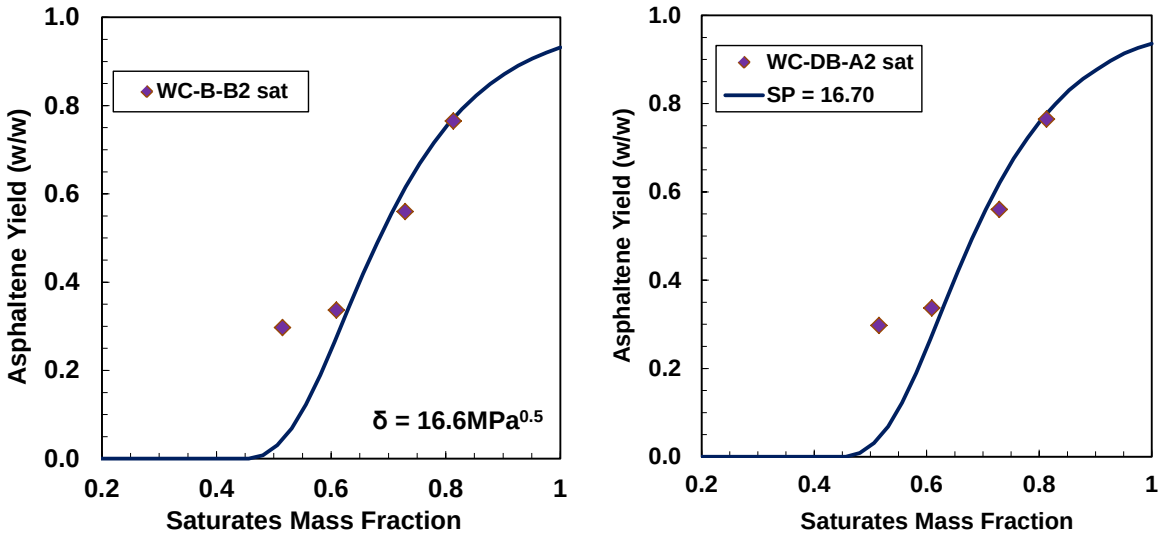

Figure B.70: Asphaltene precipitation from solutions of asphaltenes in toluene/saturates at 21°C fit with regular solution model for; a) WC-B-B2 b) WC-DB-A2 saturates

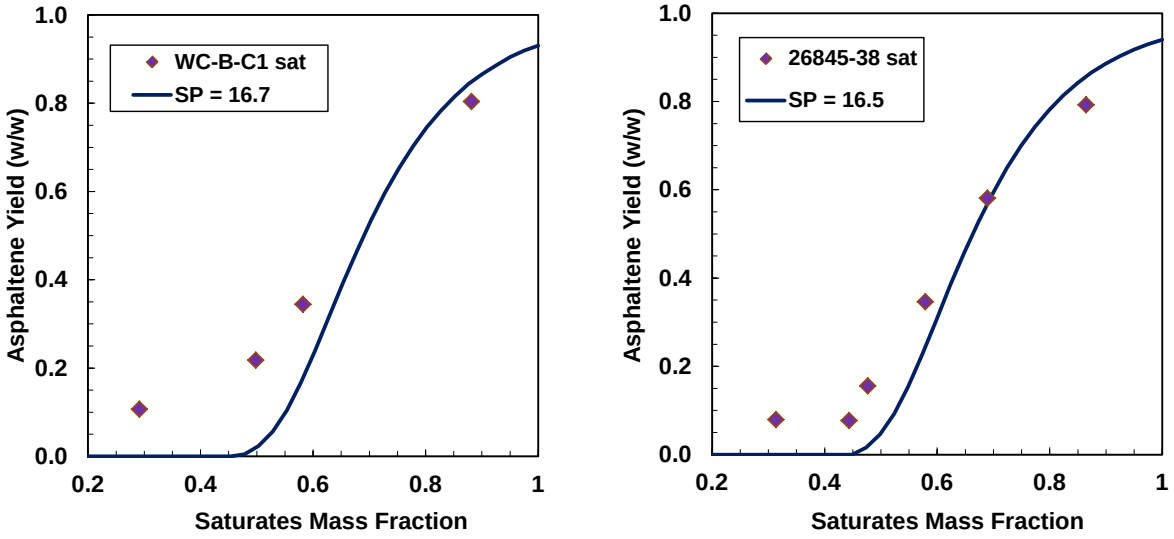

Figure B.71: Asphaltene precipitation from solutions of asphaltenes in toluene/saturates at 21°C fit with regular solution model for; a) WC-B-C1 b) 26845-38 saturates

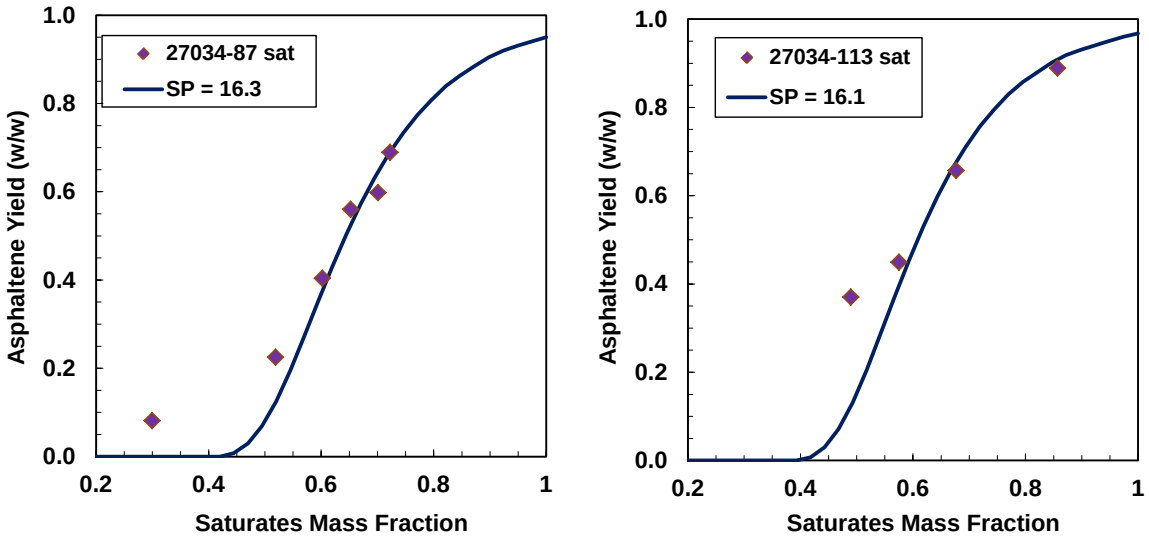

Figure B.72: Asphaltene precipitation from solutions of asphaltenes in toluene/saturates at 21°C fit with regular solution model for; a) 27034-87 b) 27034-113 saturates

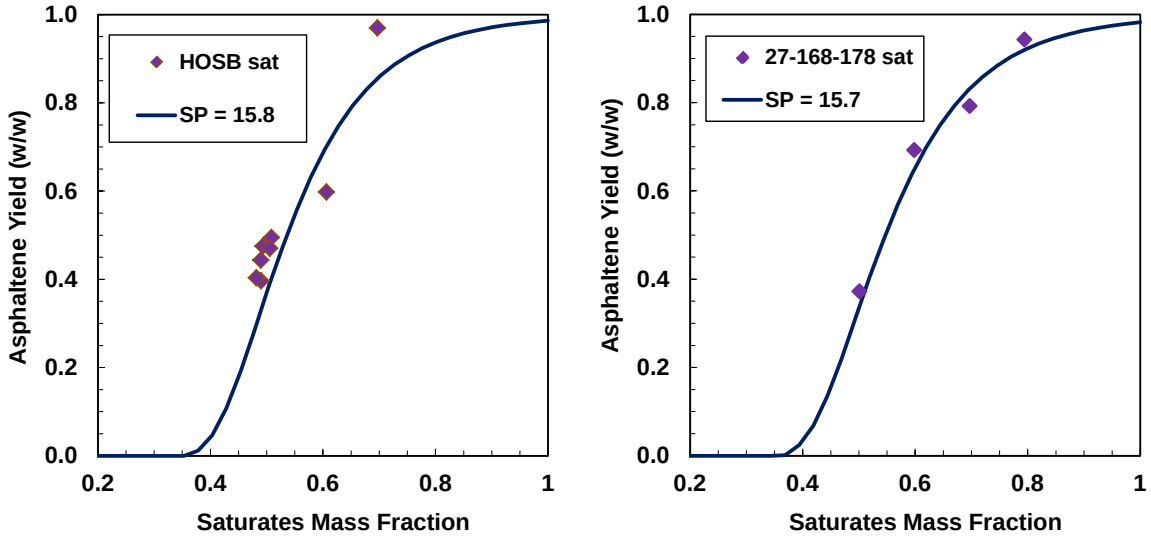

Figure B.73: Asphaltene precipitation from solutions of asphaltenes in toluene/saturates at 21°C fit with regular solution model for; a) HOSB b) 27-168-179 saturates

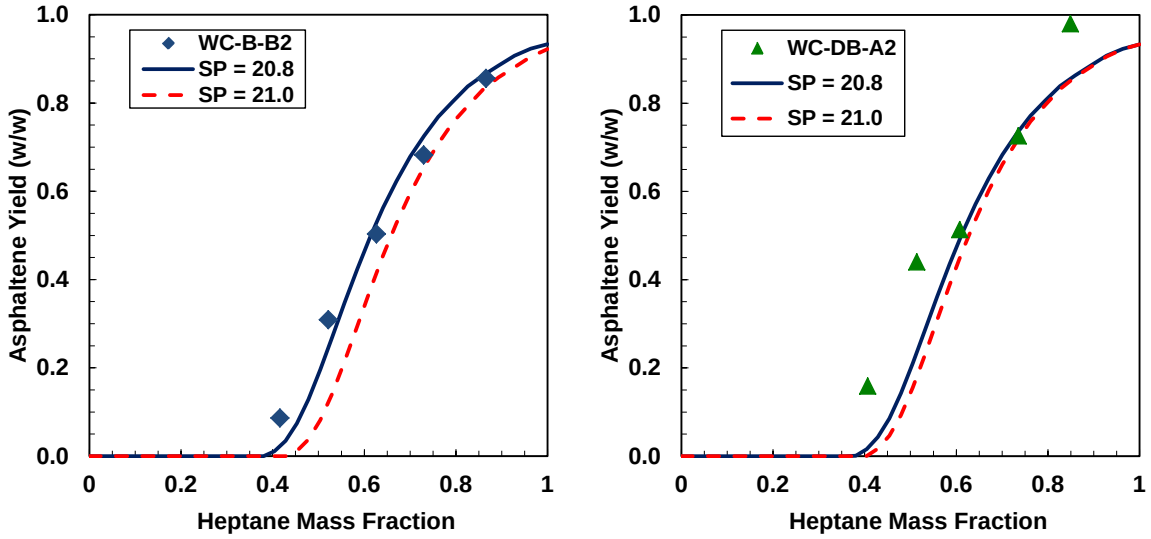

Figure B.74: Asphaltene precipitation from solutions of asphaltenes in aromatics/heptane at 21°C fit with regular solution model for; a) WC-B-B2 b) WC-DB-A2 aromatics precise to ±0.2

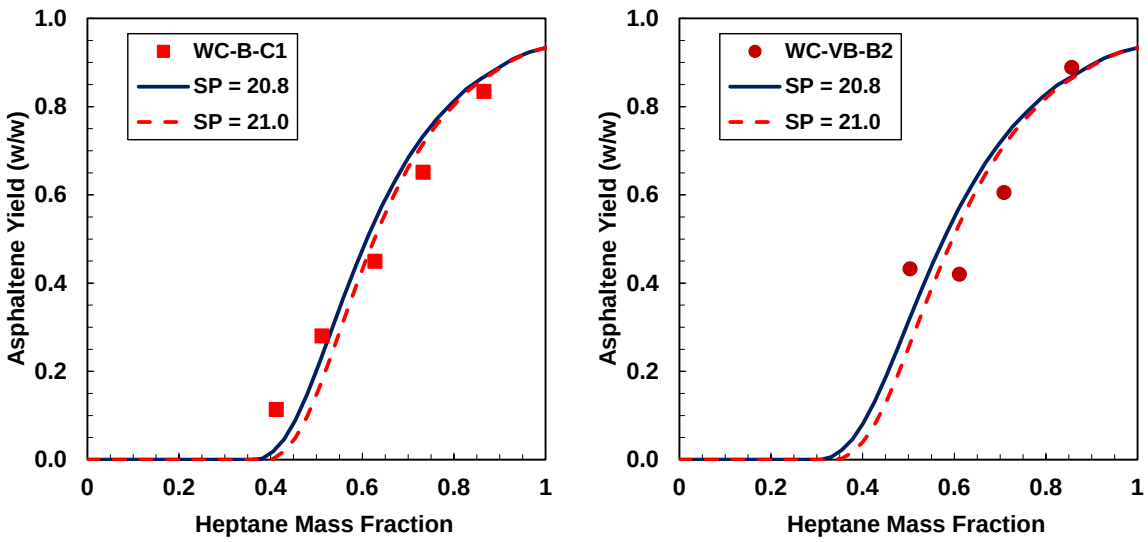

Figure B.75: Asphaltene precipitation from solutions of asphaltenes in aromatics/heptane at 21°C fit with regular solution model for; a) WC-B-C1 b) WC-VB-B2 aromatics precise to ±0.2

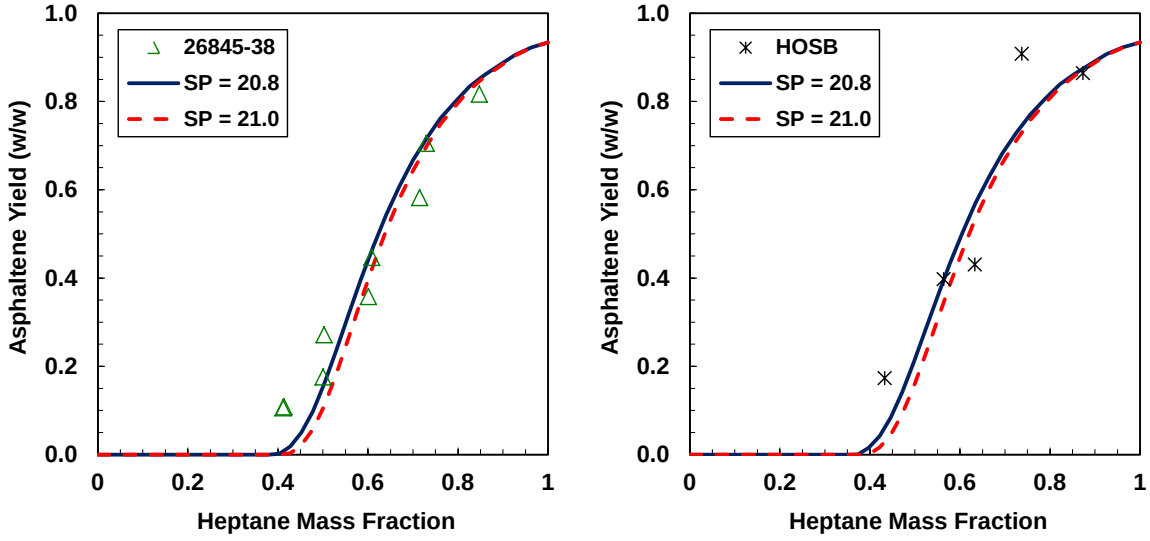

Figure B.76: Asphaltene precipitation from solutions of asphaltenes in aromatics/heptane at 21°C fit with regular solution model for; a) 26845-38 b) HOSB aromatics precise to ±0.2

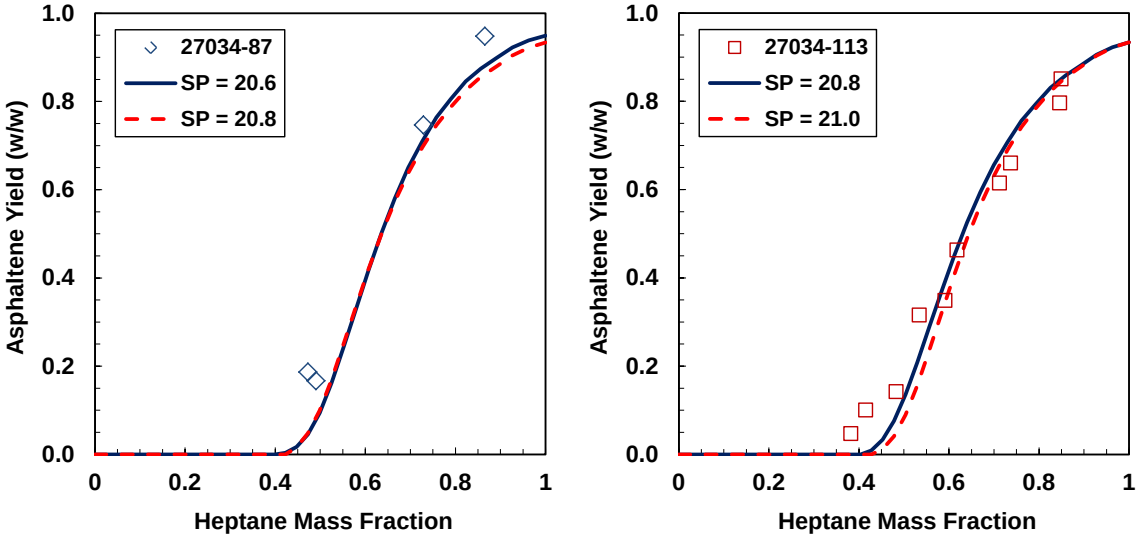

Figure B.77: Asphaltene precipitation from solutions of asphaltenes in aromatics/heptane at 21°C fit with regular solution model for; a) 27034-87 b) 27034-113 aromatics precise to ±0.2

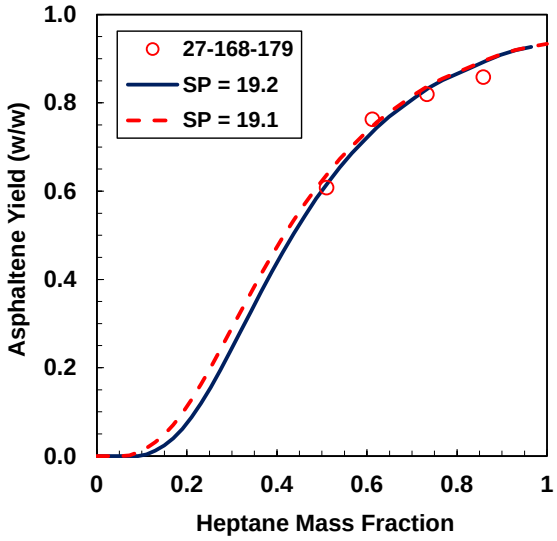

Figure B.78: Asphaltene precipitation from solutions of asphaltenes in aromatics/heptane at 21°C fit with regular solution model for; 27-168-179 aromatics precise to ±0.1